

Technical Report Documentation Page

| | | | | | |
|--|--|-----------------------------|-------------------------|---|-----------|
| 1. Report No. FHWA/TX-07/0-4823-CT-1 | | 2. Government Accession No. | | 3. Recipient's Catalog No. | |
| 4. Title and Subtitle Design of Retrofit Vehicular Barriers Using Mechanical Anchors | | | | 5. Report Date October 2006 | |
| | | | | 6. Performing Organization Code | |
| 7. Author(s) G. Mitchell, M. Tolnai, V. Gokani, R. Picón, S. Yang, R. E. Klingner, E. B. Williamson | | | | 8. Performing Organization Report No. 0-4823-CT-1 | |
| 9. Performing Organization Name and Address Center for Transportation Research The University of Texas at Austin 3208 Red River, Suite 200 Austin, TX 78705-2650 | | | | 10. Work Unit No. (TRAIS) | |
| | | | | 11. Contract or Grant No. 0-4823 | |
| 12. Sponsoring Agency Name and Address Texas Department of Transportation Research and Technology Implementation Office P.O. Box 5080 Austin, TX 78763-5080 | | | | 13. Type of Report and Period Covered Technical Report September 2003–August 2006 | |
| | | | | 14. Sponsoring Agency Code | |
| 15. Supplementary Notes Project performed in cooperation with the Texas Department of Transportation and the Federal Highway Administration. Project title: Mechanical Anchors for Retrofit/Repair of Bridge Rails | | | | | |
| 16. Abstract Retrofit barriers can be used to replace highway barriers damaged by vehicular collisions. The purpose of TxDOT Research Project 0-4823 is to develop retrofit designs of current TxDOT highway barriers using mechanical anchors. The retrofit designs should meet the TxDOT performance criteria for retrofit barriers as well as <i>NCHRP Report 350</i> requirements. Investigators for this project developed an impact pendulum test setup to represent a surrogate vehicle for Test Level 3 of <i>NCHRP Report 350</i> . They also developed retrofit designs for T203 and T501 barriers using mechanical anchors. Using the impact pendulum, tests were conducted on stand-alone cast-in-place and retrofit T203 and T501 barrier specimens. A quasi-static test was also conducted on the retrofit T203 barrier design. These designs met TxDOT performance criteria and <i>NCHRP Report 350</i> requirements for Test Level-3. Finite element models of the cast-in-place and retrofit T203 and T501 barrier specimens were developed using LS-DYNA, and they were validated using the pendulum impact tests. Using those models, vehicular crash simulations were conducted to <i>NCHRP Report 350</i> Test Level-3 and Test Level-4 standards to predict the performance and robustness of the retrofit T203 and T501 barrier designs when subjected to large impact forces. The retrofit barriers with mechanical anchors, while slightly inferior in performance to the cast-in-place barriers, did meet AASHTO and TxDOT requirements for new construction and are suitable for implementation by TxDOT. | | | | | |
| 17. Key Words Anchors, Finite Element Analysis, Crash Simulation | | | | 18. Distribution Statement No restrictions. This document is available to the public through the National Technical Information Service, Springfield, Virginia 22161; www.ntis.gov . | |
| 19. Security Classif. (of report) Unclassified | 20. Security Classif. (of this page) Unclassified | | 21. No. of pages 250 | | 22. Price |



Design of Retrofit Vehicular Barriers Using Mechanical Anchors

G. Mitchell
M. Tolnai
V. Gokani
R. Picón
S. Yang
R. E. Klingner
E. B. Williamson

| | |
|-----------------------|---|
| CTR Technical Report: | 0-4823-CT-1 |
| Report Date: | October 2006 |
| Project: | 0-4823 |
| Project Title: | Mechanical Anchors for Retrofit/Repair of Bridge Rails |
| Sponsoring Agency: | Texas Department of Transportation |
| Performing Agency: | Center for Transportation Research at The University of Texas at Austin |

Project performed in cooperation with the Texas Department of Transportation and the Federal Highway Administration.

Center for Transportation Research
The University of Texas at Austin
3208 Red River
Austin, TX 78705
www.utexas.edu/research/ctr
Copyright (c) 2007
Center for Transportation Research
The University of Texas at Austin
All rights reserved
Printed in the United States of America

Disclaimers

Author's Disclaimer: The contents of this report reflect the views of the authors, who are responsible for the facts and the accuracy of the data presented herein. The contents do not necessarily reflect the official view or policies of the Federal Highway Administration or the Texas Department of Transportation (TxDOT). This report does not constitute a standard, specification, or regulation.

Patent Disclaimer: There was no invention or discovery conceived or first actually reduced to practice in the course of or under this contract, including any art, method, process, machine manufacture, design or composition of matter, or any new useful improvement thereof, or any variety of plant, which is or may be patentable under the patent laws of the United States of America or any foreign country.

Notice: The United States Government and the State of Texas do not endorse products or manufacturers. If trade or manufacturers' names appear herein, it is solely because they are considered essential to the object of this report.

This report describes the use of retrofit (post-installed) mechanical anchors to attach highway barriers to existing bridge decks. Many classes of such anchors are commercially available. Of those classes, the authors selected undercut anchors, because that class of anchors generally has low splitting forces and has been demonstrated to perform well under dynamic loads. Of that class of undercut mechanical anchors, the authors selected one particular anchor, the Drillco Maxi-bolt®. That selection should not be interpreted as an endorsement of that particular anchor, either in the context of this research study or in other contexts. Additional information on the particular anchor used in this study is available at www.drillcogroup.com. Additional information on other post-installed mechanical anchors is widely available through the technical publications of the American Concrete Institute (www.aci-int.org).

Engineering Disclaimer

NOT INTENDED FOR CONSTRUCTION, BIDDING, OR PERMIT PURPOSES.

Project Engineer: Richard E. Klingner
Professional Engineer License State and Number: Texas No. 42483
P. E. Designation: Research Co-Supervisor

Project Engineer: Eric B. Williamson
Professional Engineer License State and Number: Texas No. 94410
P. E. Designation: Research Co-Supervisor

Acknowledgments

The authors would like to express their appreciation to Michael Hyzak (the TxDOT Project Director) and to the members of the Project Monitoring Committee, whose efforts were invaluable in ensuring that the work described here was relevant to the evolving, real-world needs of the Texas Department of Transportation. We would also like to acknowledge the support of the many Undergraduate Research Assistants whose work enriched this project, the Ferguson Laboratory staff whose ingenuity made it possible, and the CTR staff whose skill help shape this report.

Table of Contents

| | |
|--|-----------|
| Chapter 1. Introduction, Objectives and Scope | 1 |
| 1.1 Introduction..... | 1 |
| 1.2 Objectives of Project 0-4823 | 1 |
| 1.3 Basic Approach of this Study | 1 |
| Chapter 2. Background | 5 |
| 2.1 Motivation for Background Research..... | 5 |
| 2.2 Standard TxDOT Bridge Barriers..... | 5 |
| 2.3 Design of Retrofit Barriers Using Mechanical Anchors..... | 6 |
| 2.4 FHWA Requirements for Bridge Barrier Testing..... | 6 |
| 2.5 Finite Element Modeling in LS-DYNA..... | 8 |
| Chapter 3. Design of T203 Bridge Deck and Barrier Test Specimen | 11 |
| 3.1 Introduction..... | 11 |
| 3.2 Design Criteria for T203 Test Specimen | 11 |
| 3.3 Instrumentation of Specimen | 15 |
| 3.4 Concluding Remarks on Development of T203 Bridge Deck and Barrier Specimen | 16 |
| Chapter 4. Experimental Testing Program for T203 Bridge Barriers | 17 |
| 4.1 Introduction..... | 17 |
| 4.2 Impact Test Pendulum Setup for Project 0-4823..... | 17 |
| 4.3 Static Test Setup for Testing of T203 Retrofit Barriers..... | 23 |
| 4.4 Cast-in-Place and Retrofit Test Specimens of T203 Barriers..... | 24 |
| 4.5 Design of T203 Retrofit Barrier Specimen..... | 27 |
| 4.6 Instrumentation, Data Acquisition, and Processing..... | 33 |
| Chapter 5. Using LS-DYNA for Analysis | 39 |
| 5.1 Finite Element Computer Programs | 39 |
| 5.2 Selection of LS-DYNA for Use in this Study..... | 39 |
| 5.3 LS-DYNA Program Manager..... | 39 |
| 5.4 Before Beginning to Use LS-DYNA | 43 |
| 5.5 Overview of Major Steps Involved in Using LS-DYNA | 44 |
| 5.6 Create a File and Folder for the Model..... | 44 |
| 5.7 Define Each PART Comprising the Model | 45 |
| 5.8 Create Nodes and Lines for Each PART | 45 |
| 5.9 Create Elements and a Mesh for Each PART..... | 48 |
| 5.10 Define Element Properties for Each PART | 49 |
| 5.11 Select and Modify Materials for Each Part..... | 50 |
| 5.12 Set Up Initial Conditions and Boundary Conditions | 51 |
| 5.13 Create Contact Surfaces..... | 56 |
| 5.14 Select Information for Output..... | 59 |
| 5.15 Run the Defined LS-DYNA Model..... | 61 |
| Chapter 6. Developing LS-DYNA Models for Study 4823..... | 65 |
| 6.1 Overview of Project 4823 Models | 65 |
| 6.2 Development of LS-DYNA Model for Cast-in-Place Barrier | 65 |

| | |
|--|------------|
| 6.3 Analytical Modeling of Retrofit Barrier | 71 |
| 6.4 Overall Considerations in Modeling Barriers | 76 |
| 6.5 Development of Analytical Model for Impact Pendulum | 78 |
| 6.6 Design of Crush Package | 80 |
| 6.7 Incorporation of FHWA Vehicle Models into LS-DYNA Models | 86 |
| 6.8 Output Considerations for LS-DYNA Impact Simulations | 86 |
| Chapter 7. Design of Crush Package, Validation of Test Methods, and Significance of Results..... | 87 |
| 7.1 Preliminary Design of Crush Package for Impact Pendulum | 87 |
| 7.2 Testing and Simulation of Preliminary Design of Crush Package | 90 |
| 7.3 Modified Design of Crush Package for Laboratory Pendulum | 94 |
| 7.4 Validity of Testing Methods and Significance of Results | 99 |
| 7.5 Later Refinements to Current LS-DYNA Models | 100 |
| Chapter 8. Results from Experimental Testing of T203 Bridge Barriers | 103 |
| 8.1 Introduction..... | 103 |
| 8.2 Results of Pendulum Impact Tests on Cast-in-Place T203 Barriers..... | 103 |
| 8.3 Test Results for Retrofit T203 Barriers with Through-Anchor Configuration..... | 106 |
| 8.4 Results from Quasi-Static Test on Retrofit T203 Barrier | 108 |
| Chapter 9. Significance of Test Results for T203 Barriers | 109 |
| 9.1 Introduction..... | 109 |
| 9.2 Significance of Test Results in Terms of NCHRP Test Criteria | 109 |
| 9.3 Significance of Test Results in Terms of TxDOT Performance Criteria | 111 |
| 9.4 Final Design of Retrofit T203 Barrier | 114 |
| Chapter 10. Preliminary Design and Testing of Retrofit T501 Bridge Barrier | 117 |
| 10.1 Introduction..... | 117 |
| 10.2 T501 Bridge Barrier and Deck Test Specimens | 118 |
| 10.3 Probable Capacities of Retrofit T501 Barrier System | 120 |
| Chapter 11. Analytical Simulations of Bridge Barrier Performance Using LS-DYNA | 125 |
| 11.1 Introduction..... | 125 |
| 11.2 Simulation of Pendulum Mass and Crush Package | 125 |
| 11.3 Basic LS-DYNA Model of T203 Barrier and Bridge Deck | 129 |
| 11.4 Simulation of Pendulum Impact Test on Cast-in-Place T203 Barrier and Deck Using Effective Elastic Properties | 130 |
| 11.5 Reinforced Concrete Model of T203 Barrier and Bridge Deck..... | 134 |
| 11.6 Validation of Reinforced Concrete Models of T203 Barrier and Bridge Deck..... | 141 |
| 11.7 Vehicular Crash Simulations on Reinforced Concrete LS-DYNA Models of T203 Barrier and Bridge Deck | 144 |
| 11.8 Evaluation of Retrofit T203 Barrier and Bridge Deck Using LS-DYNA Simulations | 147 |
| 11.9 Development of Reinforced Concrete LS-DYNA Models of T501 Barrier and Bridge Deck | 151 |
| 11.10 Pendulum Impact Test Simulations on T501 Barrier and Bridge Deck Using LS- DYNA | 157 |

| | |
|---|------------|
| 11.11 Evaluation of Retrofit T501 Barrier and Bridge Deck Using Vehicular Crash Simulations with LS-DYNA..... | 159 |
| Chapter 12. Results from Experimental Testing of T501 Bridge Barriers | 163 |
| 12.1 Introduction..... | 163 |
| 12.2 Test Results for Retrofit T501 Barriers with Seven Anchors..... | 163 |
| 12.3 Results of the First Test for Retrofit T501 Barrier with Four Anchors | 167 |
| 12.4 Results of the Second Test on Retrofit T501 Barrier with Four Anchors | 170 |
| Chapter 13. Significance of Test Results for T501 Barriers | 175 |
| 13.1 Introduction..... | 175 |
| 13.2 Load-Related Information..... | 176 |
| 13.3 Dynamic Resistance-Related Information | 177 |
| 13.4 Static Resistance-Related Information..... | 180 |
| 13.5 Significance of Results | 181 |
| Chapter 14. Summary, Conclusions, and Recommendations..... | 183 |
| 14.1 Summary..... | 183 |
| 14.2 Conclusions..... | 184 |
| 14.3 Recommendations..... | 184 |
| References..... | 187 |
| Appendix A: Standard TxDOT Bridge Barrier and Deck Details..... | 191 |
| Appendix B: Comparison of Results from Tests and Simulations on T203 Barrier Specimens..... | 195 |
| Appendix C: Estimated Capacities of Retrofit Barriers | 203 |
| Appendix D: Concrete Breakout Capacity of Retrofit T501 Barrier (Yang)..... | 209 |
| Appendix E: Conversions from Standalone to Continuous Barrier Models..... | 213 |
| Appendix F: Continuous Barrier System Tested by TTI..... | 217 |
| Appendix G: Initial Studies on Modeling Barrier with ABAQUS | 219 |

List of Tables

| | |
|---|-----|
| Table 2.1: Crash test criteria of <i>NCHRP Report 350</i> | 7 |
| Table 4.1: Comparison between impact pendulum test setup and the 1997 Geo Metro for <i>NCHRP Report 350</i> TL-3 | 23 |
| Table 4.2: Steps to obtain static capacities of retrofit T203 barrier system..... | 32 |
| Table 4.3: Static capacity estimates of T203 barrier systems | 32 |
| Table 6.1: Dimensions (mm) of cast-in-place T203 barrier | 68 |
| Table 6.2: CARD 1 for concrete, modeled as Isotropic Elastic Failure Material | 69 |
| Table 6.3: CARD 2 for concrete, modeled as Isotropic Elastic Failure Material | 70 |
| Table 6.4: CARD 1 for Reinforcing Bars, modeled as Elastic Spring Material | 71 |
| Table 6.5: CARD 1 for reinforcement, modeled as SECTION_BEAM..... | 75 |
| Table 6.6: CARD 4 for preliminary reinforcement, modeled as SECTION_BEAM..... | 75 |
| Table 6.7: CARD 1 for preliminary modeling of reinforcement as a Plastic Kinematic Material..... | 75 |
| Table 6.8: CARD 1 for pendulum mass, modeled as an Isotropic Elastic Plastic material..... | 80 |
| Table 6.9: CARD 1 for Honeycomb Material | 83 |
| Table 6.10: CARD 2 for Honeycomb Material | 84 |
| Table 6.11: CARD 3 for Honeycomb Material | 84 |
| Table 6.12: Load curve definition CARD..... | 85 |
| Table 9.1: Comparison of cast-in-place and retrofit T203 barrier for NCHRP TL-3 criteria | 110 |
| Table 9.2: Capacities of T203 barrier systems..... | 113 |
| Table 10.1: Steps to obtain dynamic capacity of retrofit T501 barrier system..... | 121 |
| Table 10.2: Steps to obtain 50-msec dynamic capacity of retrofit T501 barrier system | 122 |
| Table 10.3: Steps to obtain static capacity of retrofit T501 barrier system | 123 |
| Table 10.4: Summary of estimated probable of T501 barrier systems | 123 |
| Table 11.1: Comparison between impact pendulum test on a steel barrier and its LS-DYNA simulation..... | 128 |
| Table 11.2: CARD 1 for T203 barrier modeled as elastic material | 131 |
| Table 11.3: CARD 1 for bridge deck, modeled as elastic material | 131 |
| Table 11.4: Comparison of results of pendulum impact test on cast-in-place T203 barrier and bridge deck and its elastic simulation in LS-DYNA. | 133 |
| Table 11.5: CARD 1 for T203 bridge barrier and deck modeled with MAT_SOIL_AND_FOAM | 136 |

| | |
|---|-----|
| Table 11.6: CARD 2 for T203 bridge barrier and deck modeled with MAT_SOIL_AND_FOAM | 137 |
| Table 11.7: CARD 3 for T203 bridge barrier and deck modeled with MAT_SOIL_AND_FOAM | 137 |
| Table 11.8: CARD 4 for T203 bridge barrier and deck modeled with MAT_SOIL_AND_FOAM | 137 |
| Table 11.9: CARD 5 for T203 bridge barrier and deck modeled with MAT_SOIL_AND_FOAM | 137 |
| Table 11.10: CARD 6 for T203 bridge barrier and deck modeled with MAT_SOIL_AND_FOAM..... | 138 |
| Table 11.11: CARD 1 for modeling rebars with MAT_PLASTIC_KINEMATIC | 139 |
| Table 11.12: Comparison of results of pendulum impact test on cast-in-place T203 barrier and bridge deck and its reinforced concrete simulation in LS-DYNA..... | 142 |
| Table 11.13: Comparison of results of pendulum impact test on retrofit T203 barrier and bridge deck and its reinforced concrete simulation in LS-DYNA..... | 144 |
| Table 11.14: Comparison between cast-in-place and retrofit T203 barriers for NCHRP TL-3 (Test Designation 3-10) | 147 |
| Table 11.15: Comparison between cast-in-place and retrofit T203 barriers for NCHRP TL-3 (Test Designation 3-11) using LS-DYNA simulations..... | 148 |
| Table 11.16: Comparison between cast-in-place and retrofit T203 barriers for NCHRP TL-4 (Test Designation 4-12) using LS-DYNA simulations..... | 150 |
| Table 11.17: Comparison between cast-in-place and retrofit T501 barriers for NCHRP TL-3 (Test Designation 3-10) | 159 |
| Table 11.18: Comparison between cast-in-place and retrofit T501 barriers for NCHRP TL-3 (Test Designation 3-11) | 160 |
| Table 11.19: Comparison between cast-in-place and retrofit T501 barriers for NCHRP TL-4 (Test Designation 4-12) | 161 |
| Table 13.1: Summary of pendulum-test data for T501 retrofit barrier specimens | 182 |

List of Figures

| | |
|---|----|
| Figure 1.1: Basic approach of Project 4823..... | 2 |
| Figure 2.1: Transverse sections of the (a) T203 and (b) T501 bridge barriers | 5 |
| Figure 2.2: Crash test criteria of NCHRP Report 350 TL-3, Test Designation 3-10 | 7 |
| Figure 3.1: T203 bridge deck and barrier specimen at FSEL | 11 |
| Figure 3.2: Reinforcement layout of the T203 bridge deck and cast-in-place barrier test specimens | 12 |
| Figure 3.3: (a) Schematic of T203 bridge barrier in a typical highway configuration, and (b) bridge deck and barrier specimen at FSEL | 13 |
| Figure 3.4: Impact test pendulum with T203 test specimen in place..... | 13 |
| Figure 3.5: Tensile breakout capacity of concrete bridge deck as a function of anchors used to connect T203 retrofit bridge barrier to overhang | 14 |
| Figure 3.6: (a) Schematic of T203 retrofit specimen and (b) T203 retrofit bridge barrier with PVC ducts for anchors | 15 |
| Figure 4.1: Impact test pendulum setup..... | 18 |
| Figure 4.2: (a) Schematic diagram of a T203 barrier and bridge deck specimen, the pendulum mass installed with a crush package and (b) the position of the bridge deck within the support frame | 19 |
| Figure 4.3: Impact test pendulum support frame | 20 |
| Figure 4.4: (a) Pendulum mass and (b) pneumatic release latch | 20 |
| Figure 4.5: Pendulum mass lifting frame..... | 21 |
| Figure 4.6: (a) and (b) Crush package used in this research | 21 |
| Figure 4.7: Geo Metro NCHRP Report 350 TL-3 crash test (a) acceleration history and (b) photograph of impact with steel bridge barrier | 22 |
| Figure 4.8: (a) Acceleration history of impact pendulum test setup and (b) photo of test | 23 |
| Figure 4.9: Static test setup for retrofit T203 barrier | 24 |
| Figure 4.10: Cast-in-place and retrofit T203 bridge barrier specimens..... | 25 |
| Figure 4.11: Schematic of T203 barrier and bridge deck specimen within impact test pendulum frame | 26 |
| Figure 4.12: (a) Schematic of T203 bridge barrier in a typical highway configuration and (b) barrier and bridge deck specimen at FSEL | 26 |
| Figure 4.13: (a) Side view and (b) front view T203 retrofit bridge barrier with PVC ducts to accommodate anchors..... | 27 |
| Figure 4.14: (a) Side view and (b) front view of retrofit T203 barrier with through-anchor configuration | 29 |
| Figure 4.15: Schematic of retrofit T203 barrier with undercut anchor configuration | 30 |
| Figure 4.16: Steps to find T203 barrier system capacity from stand-alone T203 barrier capacity | 31 |
| Figure 4.17: Location of string potentiometers in barriers | 34 |

| | |
|--|----|
| Figure 4.18: Location of strain gages in bridge deck..... | 35 |
| Figure 4.19: Location of strain gages in (a) cast-in-place and (b) retrofit T203 bridge barriers | 35 |
| Figure 4.20: Frequency characteristics of Butterworth low-pass filter..... | 36 |
| Figure 4.21: Impulse values of accelerometer signal as a function of low-pass corner frequency..... | 37 |
| Figure 5.1: “Program Manager” screen of LS-DYNA | 40 |
| Figure 5.2: Example of three-dimensional input geometry created using the pre-processor (eta/FEMB-PC) | 41 |
| Figure 5.3: Sample model crash animation using the post-processor (PostGL)..... | 42 |
| Figure 5.4: Example force-time graph using post-processor (eta Graph)..... | 43 |
| Figure 5.5: Typical PART menu and card..... | 45 |
| Figure 5.6: Typical node-creation menu | 46 |
| Figure 5.7: Examples of proper and improper node-selection techniques..... | 47 |
| Figure 5.8: Example of geometric line framework..... | 48 |
| Figure 5.9: Order of line selection in mesh creation..... | 49 |
| Figure 5.10: Example of element property selection..... | 50 |
| Figure 5.11: Sample menu for material selection | 51 |
| Figure 5.12: Sample material input card..... | 51 |
| Figure 5.13: Sample menu for creating a node set..... | 52 |
| Figure 5.14: Initial Condition menu..... | 53 |
| Figure 5.15: Example of how to create an Initial Velocity CARD..... | 53 |
| Figure 5.16: Sample display of Initial Velocity..... | 54 |
| Figure 5.17: Boundary condition menu | 55 |
| Figure 5.18: Example of assigning SPC boundary conditions | 56 |
| Figure 5.19: Menu of types of contact surface | 57 |
| Figure 5.20: List of three-dimensional contact types | 58 |
| Figure 5.21: AUTOMATIC_SURFACE_TO_SURFACE CARD..... | 59 |
| Figure 5.22: “DYNA Miscellaneous” Output Control Menus..... | 60 |
| Figure 5.23: Output-control menus for Contact Forces (RCFORC)..... | 61 |
| Figure 5.24: Starting the LS-DYNA Solver | 62 |
| Figure 5.25: Menu with Solver settings..... | 63 |
| Figure 5.26: Example Solver screen during an analysis | 64 |
| Figure 6.1: TxDOT T203 bridge barrier with intermittent base and concrete parapet..... | 65 |
| Figure 6.2: Cast-in-place laboratory specimen representing a segment of a TxDOT T203 barrier with continuous base and concrete parapet..... | 66 |
| Figure 6.3: TxDOT Details of Type T203 Traffic Rail (TxDOT 2004)..... | 67 |
| Figure 6.4: DYNA model of cast-in-place concrete barrier | 69 |
| Figure 6.5: Placement of reinforcing bars in cast-in-place barrier | 70 |

| | |
|---|----|
| Figure 6.6: Schematic of proposed retrofit barrier design | 71 |
| Figure 6.7: Selection of elements to be deleted to form ducts for reinforcement or anchors | 72 |
| Figure 6.8: Re-creation of element at top of hollow duct | 73 |
| Figure 6.9: Division of LS-DYNA element for attachment of reinforcing bar | 73 |
| Figure 6.10: Analytical representation of post-installed reinforcement as a line element inside a hollow duct | 74 |
| Figure 6.11: Spring elements added at ends of barrier segments to simulate the restraining effects of infinitely long barriers..... | 76 |
| Figure 6.12: Assumptions used in developing stiffnesses of equivalent springs to represent an infinitely long barrier..... | 77 |
| Figure 6.13: Assumptions used in developing equivalent beam stiffness for finite-length section | 77 |
| Figure 6.14: Laboratory pendulum mass | 78 |
| Figure 6.15: Creating initial mesh for DYNA model of laboratory pendulum | 79 |
| Figure 6.16: Simplified DYNA model of laboratory pendulum mass..... | 80 |
| Figure 6.17: Preliminary design of tubular steel crush package..... | 81 |
| Figure 6.18: Crush package in position on pendulum during a crash test..... | 82 |
| Figure 6.19: DYNA model of preliminary crush package..... | 83 |
| Figure 6.20: Stress-strain curve for honeycomb material | 85 |
| Figure 7.1: Acceleration-time history for full-scale vehicular crash test of Geo Metro under TL-3 of NCHRP Report 350..... | 87 |
| Figure 7.2: Arrangement of steel tubes for static crush test | 88 |
| Figure 7.3: Force-deformation curve obtained from static test of first arrangement of steel tubing | 89 |
| Figure 7.4: Geometry of preliminary design for crush package for laboratory pendulum and corresponding DYNA model | 90 |
| Figure 7.5: Acceleration-time curve for preliminary design of crush package (pendulum testing)..... | 91 |
| Figure 7.6: Acceleration-time curve for preliminary design of crush package (LS-DYNA simulation) | 92 |
| Figure 7.7: Comparison of acceleration-time curves for preliminary design of crush package (LS-DYNA simulation of laboratory pendulum; Geo Metro test; and laboratory pendulum)..... | 93 |
| Figure 7.8: Comparison of impulses for real and surrogate tests to NCHRP TL-3 (pendulum tests with preliminary crush package; Geo Metro test; and LS- DYNA simulation of pendulum test with preliminary crush package) | 93 |
| Figure 7.9: Comparison of peak forces for real and surrogate tests to NCHRP TL-3 (pendulum tests with preliminary crush package; Geo Metro test; and LS- DYNA simulation of pendulum test with preliminary crush package) | 94 |
| Figure 7.10: Geometry of modified design for crush package, and corresponding LS- DYNA model | 95 |

| | |
|--|-----|
| Figure 7.11: Acceleration-time curve from laboratory pendulum testing (modified design of crush package) | 96 |
| Figure 7.12: Acceleration-time curve from LS-DYNA simulation (laboratory test pendulum with modified design of crush package) | 97 |
| Figure 7.13: Comparison of acceleration-time curves (laboratory pendulum testing with modified design of crush package; LS-DYNA simulation of that testing; and Geo Metro test) | 98 |
| Figure 7.14: Comparison of impulses (laboratory pendulum testing with modified design of crush package; Geo Metro test; and LS-DYNA simulation of pendulum test)..... | 98 |
| Figure 7.15: Comparison of impulses from different tests and simulations to TL- 3 of NCHRP 350 | 100 |
| Figure 8.1: Still image from impact pendulum test on stand-alone, cast-in-place T203 bridge barrier and deck specimen | 104 |
| Figure 8.2: Force versus time from pendulum impact test on stand-alone cast-in-place T203 bridge barrier and deck specimen..... | 105 |
| Figure 8.3: Barrier displacement-versus-time graph from pendulum impact test on standalone cast-in-place T203 bridge barrier and deck specimen | 105 |
| Figure 8.4: Still image from impact pendulum test on stand-alone retrofit T203 bridge barrier and deck specimen | 106 |
| Figure 8.5: Force-versus-time graph from pendulum impact test on standalone retrofit T203 bridge barrier and deck specimen..... | 107 |
| Figure 8.6: Barrier displacement-versus-time graph from pendulum impact test on standalone retrofit T203 bridge barrier and deck specimen..... | 107 |
| Figure 8.7: Force-versus-displacement graph from quasi-static test on stand-alone retrofit T203 bridge barrier and deck specimen..... | 108 |
| Figure 9.1: Force-versus-time graphs from pendulum impact test on standalone cast-in-place and retrofit T203 bridge barrier and deck specimens | 110 |
| Figure 9.2: Recommended design of retrofit T203 barrier (a) side view and (b) front view | 115 |
| Figure 10.1: (a) Typical TxDOT T501 bridge barrier system and (b) its cross-section (TxDOT 2003) | 117 |
| Figure 10.2: Schematic of cross-section of retrofit T501 barrier using Drillco flush-mount undercut anchors | 119 |
| Figure 10.3: Steps to find capacity of T501 barrier system from capacity of 5 ft. section of T501 barrier | 120 |
| Figure 11.1: LS-DYNA Model of the laboratory pendulum mass (Tolnai 2005) | 126 |
| Figure 11.2: LS-DYNA simulation of pendulum mass and crush package impacting a rigid barrier (Tolnai) | 127 |
| Figure 11.3: Comparison of acceleration versus time graphs from laboratory test of impact pendulum on steel barrier in laboratory and simulation of the same test using LS-DYNA (Tolnai) | 128 |

| | |
|--|-----|
| Figure 11.4: Basic LS-DYNA model of the T203 barrier and bridge deck with support conditions | 129 |
| Figure 11.5: Moment-curvature relationship of (a) T203 barrier and (b) bridge deck from RECONASANCE | 131 |
| Figure 11.6: LS-DYNA model of pendulum impact test simulation on T203 barrier and deck | 132 |
| Figure 11.7: Acceleration-time histories from pendulum impact test on cast-in-place T203 barrier and deck, and its effective elastic simulation in LS-DYNA | 133 |
| Figure 11.8: Graph of pressure (p) versus logarithmic relative volume curve for 27.6-MPa concrete | 135 |
| Figure 11.9: Graph of second stress invariant (J_2) versus pressure (p) for 27.6-MPa concrete | 136 |
| Figure 11.10: (a) Side view and (b) back view of the reinforced concrete LS-DYNA model of cast-in-place T203 barrier and bridge deck | 140 |
| Figure 11.11: (a) Side view and (b) back view of the reinforced concrete LS-DYNA model of retrofit T203 barrier and bridge deck | 141 |
| Figure 11.12: (a) Acceleration-versus-time graphs and (b) displacement-versus-time graphs from pendulum impact test on cast-in-place T203 barrier and bridge deck and its reinforced concrete LS-DYNA simulation | 142 |
| Figure 11.13: (a) Acceleration-versus-time graphs and (b) displacement-versus-time graphs from pendulum impact test on retrofit T203 barrier and bridge deck and its reinforced concrete LS-DYNA simulation | 143 |
| Figure 11.14: LS-DYNA models of T203 barrier crash simulations with (a) 1997 Geo Metro (b) Chevrolet C2500 Truck and (c) Ford Single Unit Truck | 146 |
| Figure 11.15: (a) Force-time histories and (b) displacement-time histories for NCHRP TL-3 (Test Designation 3-10) crash simulation using 1997 Geo Metro | 147 |
| Figure 11.16: (a) Force-time histories and (b) displacement-time histories for NCHRP TL-3 (Test Designation 3-11) crash simulation using Chevrolet C2500 truck | 148 |
| Figure 11.17: (a) Force-time histories and (b) displacement-time histories for NCHRP TL-4 (Test Designation 4-12) crash simulation using Ford Single Unit Truck | 150 |
| Figure 11.18: Cross-sectional geometry of LS-DYNA model of T501 barrier in LS-DYNA compatible units (mm) | 151 |
| Figure 11.19: Steps for creating basic LS-DYNA model of T501 barrier using SOLID elements | 153 |
| Figure 11.20: Basic LS-DYNA model of T501 barrier and bridge deck | 154 |
| Figure 11.21: (a) Side view and (b) back view of reinforced concrete LS-DYNA model of cast-in-place T501 barrier and bridge deck | 155 |
| Figure 11.22: (a) Side view and (b) back view of reinforced concrete LS-DYNA model of retrofit T501 bridge barrier and deck | 156 |
| Figure 11.23: Pendulum impact test simulation on T501 barrier and bridge deck using LS-DYNA model | 157 |

| | |
|--|-----|
| Figure 11.24: (a) Force-versus-time and (b) displacement-versus-time graphs from pendulum impact test simulation on cast-in-place T501 barrier and bridge deck | 158 |
| Figure 11.25: (a) Force-versus-time and (b) displacement-versus-time graphs from pendulum impact test simulation on retrofit T501 barrier and bridge deck | 158 |
| Figure 11.26: (a) Force-time histories and (b) displacement-time histories for NCHRP TL-3 (Test Designation 3-10) crash simulation using 1997 Geo Metro..... | 159 |
| Figure 11.27: (a) Force-time histories and (b) displacement-time histories for NCHRP TL-3 (Test Designation 3-11) crash simulation using Chevrolet C2500 truck | 160 |
| Figure 11.28: (a) Force-time histories and (b) displacement-time histories for NCHRP TL-4 (Test Designation 4-12) crash simulation using Ford Single Unit Truck..... | 161 |
| Figure 12.1: Still image from impact pendulum test on stand-alone retrofit T501 bridge barrier with seven anchors and deck specimen..... | 164 |
| Figure 12.2: Force-versus-time graph from pendulum impact test on standalone retrofit T501 bridge barrier with seven anchors and deck specimen | 164 |
| Figure 12.3: Barrier displacement-versus-time graph from pendulum impact test on standalone retrofit T501 bridge barrier with seven anchors and deck specimen..... | 165 |
| Figure 12.4: Strain values of steel rods from pendulum impact test on standalone retrofit T501 bridge barrier with seven anchors and deck specimen | 166 |
| Figure 12.5: Force-versus-displacement graph from quasi-static test on stand-alone retrofit T501 bridge barrier with seven anchors and deck specimen | 167 |
| Figure 12.6: Still image from impact pendulum test on stand-alone retrofit T501 bridge barrier with four anchors and deck specimen for a drop height of 16 feet | 168 |
| Figure 12.7: Force-versus-time graph from pendulum impact test on standalone retrofit T501 bridge barrier with four anchors and deck specimen for a drop height of 16 feet..... | 169 |
| Figure 12.8: Barrier displacement versus time from pendulum test on standalone retrofit T501 bridge barrier specimen with four anchors, drop height of 16 ft..... | 169 |
| Figure 12.9: Strain values of steel rods from pendulum impact test on standalone retrofit T501 bridge barrier with four anchors and deck specimen for a drop height of 16 feet..... | 170 |
| Figure 12.10: Still image from impact pendulum test on stand-alone retrofit T501 bridge barrier with four anchors and deck specimen for a drop height of 19.5 feet | 171 |
| Figure 12.11: Force-versus-time graph from pendulum impact test on standalone retrofit T501 bridge barrier with four anchors and deck specimen for a drop height of 19.5 feet..... | 172 |
| Figure 12.12: Barrier displacement versus time from pendulum test on standalone retrofit T501 bridge barrier specimen with four anchors (drop height of 19.5 ft) | 173 |
| Figure 12.13: Strain values of steel rods from pendulum impact test on standalone retrofit T501 bridge barrier with four anchors and deck specimen for a drop height of 19.5 feet..... | 174 |

| | |
|---|-----|
| Figure A.1. Side sectional view of standard TxDOT T203 barrier and bridge deck (TTI 2003) | 191 |
| Figure A.2. Front sectional view of standard TxDOT T203 barrier and bridge deck (TTI 2003) | 192 |
| Figure A.3. Side sectional view of standard TxDOT T501 barrier and bridge deck (TTI 2003) | 193 |
| Figure A.4. Front sectional view of standard TxDOT T501 barrier and bridge deck (TTI 2003) | 194 |
| Figure B.1. Strain histories in row R1 of cast-in-place T203 bridge deck | 195 |
| Figure B.2. Strain histories in row R3 of cast-in-place T203 bridge deck | 195 |
| Figure B.3. Strain histories in row R5 of cast-in-place T203 bridge deck | 196 |
| Figure B.4. Strain histories in row B of cast-in-place T203 bridge barrier | 196 |
| Figure B.5. Strain histories in row R1 of cast-in-place T203 bridge deck DYNA model..... | 197 |
| Figure B.6. Strain histories in row R3 of cast-in-place T203 bridge deck DYNA model..... | 197 |
| Figure B.7. Strain histories in row R5 of cast-in-place T203 bridge deck DYNA model..... | 198 |
| Figure B.8. Strain histories in row B of cast-in-place T203 bridge barrier DYNA model..... | 198 |
| Figure B.9. Strain histories in row R1 of retrofit T203 bridge deck..... | 199 |
| Figure B.10. Strain histories in row R3 of retrofit T203 bridge deck..... | 199 |
| Figure B.11. Strain histories in row R5 of retrofit T203 bridge deck..... | 200 |
| Figure B.12. Strain histories in row B of retrofit T203 bridge barrier..... | 200 |
| Figure B.13. Strain histories in row R1 of retrofit T203 bridge deck DYNA model | 201 |
| Figure B.14. Strain histories in row R3 of retrofit T203 bridge deck DYNA model | 201 |
| Figure B.15. Strain histories in row R5 of retrofit T203 bridge deck DYNA model | 202 |
| Figure B.16. Strain histories in row B of retrofit T203 bridge barrier DYNA model | 202 |
| Figure C1. Forces in undercut anchors of retrofit T501 barrier and bridge deck and their anticipated failure surface | 207 |
| Figure D.1. Geometric configuration of inclined anchors used in T501 retrofit specimens | 209 |
| Figure D.2. Geometry of projected breakout areas by ACI 318-05 Appendix D for Retrofit T501 Specimen 1 (7 anchors)..... | 209 |
| Figure D.3. Geometry of projected breakout areas by ACI 318-05 Appendix D for Retrofit T501 Specimen 2 (4 anchors)..... | 211 |
| Figure E.1. Details of SAP analysis on cast-in-place T203 barrier system using TTI static test results..... | 213 |
| Figure E.2. Details of SAP analysis on cast-in-place T203 barrier system using TTI dynamic test results..... | 214 |
| Figure E.3. Details of SAP analysis on cast-in-place T203 barrier system using TTI dynamic test results (50-msec window)..... | 215 |
| Figure E.4. Details of SAP analysis on cast-in-place T501 barrier system using TTI static test results..... | 216 |
| Figure F.1. TTI T501 and T203 barrier and bridge deck systems | 217 |

Chapter 1. Introduction, Objectives and Scope

1.1 Introduction

Bridge rails (also referred to as “barriers”) are very important structural components for ensuring highway safety. They should contain and redirect impacting vehicles back onto the roadway, while deforming so as to limit the forces on the occupants of the vehicle, and they should resist impact from a collision. To meet these demands, the Federal Highway Administration (FHWA) requires that barriers meet the testing and performance requirements established in the National Highway Cooperative Research Program (NCHRP) *Report 350* (1993). Those requirements are discussed later in this report.

If an original cast-in-place barrier is slightly damaged by vehicular impact, it can be repaired. More severe damage, however, may require that the original barrier be replaced with a retrofit barrier. Existing barriers that are substandard by current requirements may also be replaced by retrofit barriers. Post-installed mechanical anchors are widely used to connect structural components to hardened concrete. The use of these anchors can be extended to retrofit barriers. The purpose of Texas Department of Transportation (TxDOT) Research Project 0-4823 (“*Performance Testing of Anchors for Retrofitting and Repair of Bridge Barriers*”) is to develop designs of retrofit barriers using mechanical anchors that satisfy stated performance criteria. As this project was originally conceived by TxDOT, these barriers should conform to the standards of the National Cooperative Highway Research Program (NCHRP), specifically those of *NCHRP Report 350* (1993) and perform at least as well as the current cast-in-place design under vehicular impact. As is discussed later in this report, these criteria were subsequently relaxed to require only compliance with TxDOT requirements for new construction.

1.2 Objectives of Project 0-4823

The objectives of this project are as follows:

- develop preliminary patterns and spacing of mechanical anchors for bridge retrofit barriers based on constructability, structural performance and behavior, including clearly defined field installation procedures;
- evaluate performance of retrofit barriers based on TxDOT performance criteria for retrofit barriers using pendulum impact testing and quasi-static testing, and also compare that performance with that of cast-in-place barriers;
- use finite element analysis in a general way to evaluate, develop, and refine barriers and their connection to the bridge slab prior to NCHRP crash testing; and
- verify the performance of refined retrofit barriers under pendulum testing.

1.3 Basic Approach of this Study

The basic approach of Study 4823 involves the following steps (Figure 1.1):

- 1) Because vehicular barriers are required by the Federal Highway Administration (FHWA) to be tested according to the criteria of *NCHRP Report 350*, the barrier-

testing equipment and procedures used in this study had to meet those criteria. Investigators decided to use a pendulum as a “surrogate vehicle” to develop the prescribed impact force. The pendulum was designed, constructed, and verified to meet the test criteria of *NCHRP Report 350*. This process is described in Mitchell (2005) and in this report.

Work Plan in a Nutshell

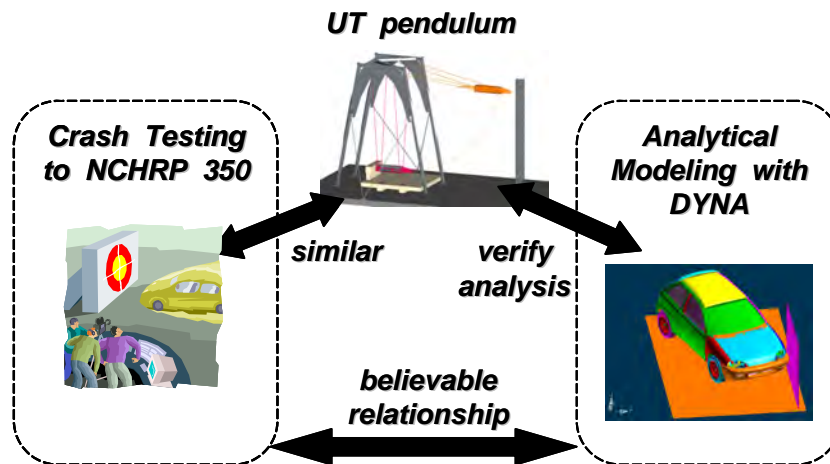


Figure 1.1: Basic approach of Project 4823

- 2) To permit the extrapolation of pendulum-test results to additional cases (such as different levels of impact, or changes in barrier configuration or anchorage), it was necessary to develop reliable numerical models. Using LS-DYNA (Livermore 2003, 2005, 2006), a sophisticated nonlinear finite-element package widely used to simulate vehicular impact, models were developed for the pendulum, its associated crush nose, and a flexible steel test barrier. This process is described in Tolnai (2005) and in this report.
- 3) After discussion with TxDOT personnel, investigators decided to concentrate on retrofit designs for two TxDOT barriers: the T203 barrier (an intermittent concrete barrier) and the T501 barrier (a continuous concrete barrier). The T203 barrier was selected because it is often used when an intermittent barrier is required, and intermittent barriers are more difficult to attach and to model. The T501 barrier was selected because it is the most common continuous barrier, is commonly used in retrofit applications, and has the favorable geometric characteristic of a wide base. A basic configuration was proposed for the retrofit T203 barrier, using mechanical anchors. Reference cast-in-place T203 barriers were designed, constructed and tested using the pendulum; and techniques were developed and refined for processing the data obtained from pendulum testing. This process is described in Mitchell (2005) and in this report.

- 4) The retrofit T203 barrier was tested under pendulum impact. Its response was compared with that of the original cast-in-place T203 barrier and was evaluated using TxDOT criteria. LS-DYNA models were refined to include the original and the retrofit T203 barrier, and results of analytical modeling were calibrated against test results. Analytical simulation was first conducted at Test Level 3 of *NCHRP Report 350*, and was then extended to cases involving higher test levels and more complex vehicles to demonstrate how LS-DYNA could be used to predict the behavior of cast-in-place and retrofit T203 barriers under a wide range of possible crash conditions as a cost-effective adjunct to crash testing. This process is described in Gokani (2006) and later in this report. Analytical models less complex than those developed with LS-DYNA can also give useful results, as analyses using ABAQUS (ABAQUS 2006) are described in this report.
- 5) A basic configuration was proposed for the retrofit T501 barrier, using mechanical anchors. Reference cast-in-place T501 barriers were designed, constructed, and tested using the pendulum, and the test results were compared with the results of LS-DYNA modeling. This process is described in Gokani (2006) and in this report.
- 6) The retrofit T501 barrier was tested under pendulum impact. Its response was compared with that of the original cast-in-place T501 barrier and was evaluated using TxDOT criteria. This process is described in this report.
- 7) Predict the behavior of cast-in-place and retrofit T501 barriers using impact pendulum test and crash simulations and evaluate their behavior based on those predictions. The crash simulations are conducted primarily to TL-3 to verify equivalence with the pendulum. They are also used to demonstrate the potential usefulness of simulations as a cost-effective adjunct to crash testing under a wide range of possible crash conditions.

Chapter 2. Background

2.1 Motivation for Background Research

One of the objectives of TxDOT Project 0-4823 is to develop standard procedures for retrofitting TxDOT T203 and T501 bridge barriers damaged by vehicular impact. Another objective of the project is to evaluate the behavior of the designed retrofit barriers under a variety of standard vehicular impacts. These objectives presented the investigators with the following challenges:

- develop preliminary designs for T203 and T501 bridge barriers using mechanical anchors to connect the barriers to a reinforced concrete bridge deck;
- test these barriers using a pendulum as a surrogate vehicle;
- conduct nonlinear finite element analyses on these barriers using LS-DYNA; and
- use the results of analysis and pendulum testing to develop final retrofit designs for the T203 and T501 bridge barriers.

To develop sufficient knowledge to address these issues, the investigators conducted extensive background research, which is summarized in this chapter.

2.2 Standard TxDOT Bridge Barriers

To develop retrofit designs for TxDOT T203 and T501 barriers using mechanical anchors, it is necessary to study existing TxDOT standards for these barriers. Figure 2.1 shows the transverse sections of standard T203 and T501 bridge barriers. The purpose of the figure is only to show each barrier schematically. Dimensions and details are provided in subsequent sections of this report.

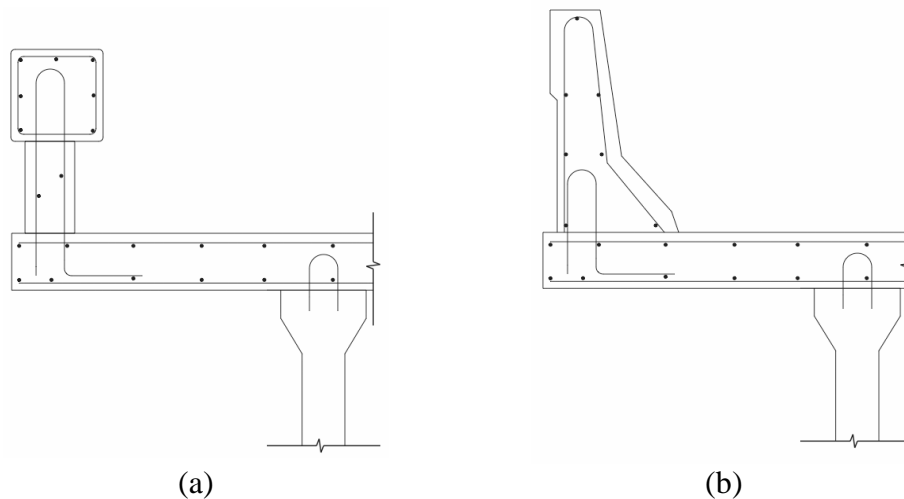


Figure 2.1: Transverse sections of the (a) T203 and (b) T501 bridge barriers (TxDOT 2003)

Using the standard design of the T203 barrier, previous researchers at The University of Texas at Austin developed test specimens incorporating a standard TxDOT bridge deck and a cast-in-place T203 barrier conventionally anchored to that bridge deck with reinforcing steel. The development of these test specimens is discussed in detail by Mitchell (2005) and is also summarized in Chapter 4 of this report.

2.3 Design of Retrofit Barriers Using Mechanical Anchors

The design of retrofit barriers using mechanical anchors requires an understanding of the behavior of mechanical anchors under direct tension and shear. The behavior of these anchors is discussed in detail in the class notes on *Behavior and Design of Fastening to Concrete*¹. Design guidelines for mechanical anchors are given in ACI 318-05 (2005) Appendix D.

Using the standard design of the T203 barrier and using the mechanical anchor design provisions of ACI 318-05 Appendix D, researchers at The University of Texas at Austin developed test specimens for the retrofit T203 barrier and bridge deck. The development of these test specimens is discussed in detail in Mitchell (2005) and is also summarized in Chapter 4 of this report.

Using the standard TxDOT design of T501 barriers and the mechanical anchor design provisions of ACI 318-05 Appendix D, project researchers developed a preliminary retrofit design for the T501 bridge barrier. This design is discussed in Chapter 10 and was verified in the final phases of this project.

2.4 FHWA Requirements for Bridge Barrier Testing

Under the jurisdiction of the Federal Highway Administration, the testing procedures and evaluation criteria developed by the National Cooperative Highway Research Program (NCHRP) govern the testing of highway bridge barriers throughout the United States. *NCHRP Report 350* (1993) prescribes testing procedures and evaluation criteria for highway barriers. Bridge barrier designs to be installed must be crash-tested in accordance with *NCHRP Report 350* and must pass that document's performance criteria. *NCHRP Report 350* applies to all longitudinal barriers, including the original and retrofit T203 and T501 barriers addressed by Project 0-4823.

2.4.1 Test Criteria of *NCHRP Report 350*

A longitudinal barrier has two functions: 1) prevent penetration of the barrier by a vehicle; and 2) redirect a vehicle without causing it to flip, vault, or snag on the barrier. For any longitudinal barrier to pass an NCHRP test, it must satisfy criteria based on both of those functions.

NCHRP Report 350 prescribes six test levels for evaluating longitudinal barriers against vehicular impact (Table 2.1). In this research, the original and retrofit T203 and T501 barriers are evaluated under NCHRP Test Level 3 (TL-3) and Test Level 4 (TL-4). Vehicle designations are described in *NCHRP Report 350*.

¹ Klingner, R. E., class notes, The University of Texas at Austin, 2003.

Table 2.1: Crash test criteria of NCHRP Report 350

| <i>Test Level</i> | <i>Test Designation</i> | <i>Impact Conditions</i> | | | <i>Weight of Vehicle (kg)</i> |
|-------------------|-------------------------|--------------------------|------------------------------|--|-------------------------------|
| | | <i>Vehicle</i> | <i>Nominal Speed (km/hr)</i> | <i>Angle of Impact θ (deg)</i> | |
| 3 | 3-10 | 820C | 100 | 20 | 820 ± 25 |
| | 3-11 | 2000P | 100 | 25 | 2000 ± 45 |
| 4 | 4-10 | 820C | 100 | 20 | 820 ± 25 |
| | 4-12 | 8000S | 80 | 15 | 8000 ± 200 |

2.4.2 Use of Surrogate Vehicle in NCHRP 350 Testing

NCHRP Report 350 permits the use of surrogate vehicles to simulate vehicular impact loads when only the strength and stiffness of the barrier are to be evaluated. Because the T203 and T501 bridge barriers have been designed, tested and validated to TL-3, Test Designation 3-10 test criteria using actual vehicle impact, it is sufficient to develop and test the retrofit design of these barriers using a surrogate vehicle designed for TL-3, Test Designation 3-10.

To be an acceptable surrogate vehicle for TL-3, Test Designation 3-10, the surrogate must deliver an impact energy equivalent to that associated with the component perpendicular to the plane of the bridge barrier from a crash test meeting NCHRP TL-3, Test Designation 3-10 (Figure 2.2). Impact energy is calculated as the product of the vehicle's mass and the square of its impact velocity perpendicular to the barrier, divided by 2 (kinetic energy).

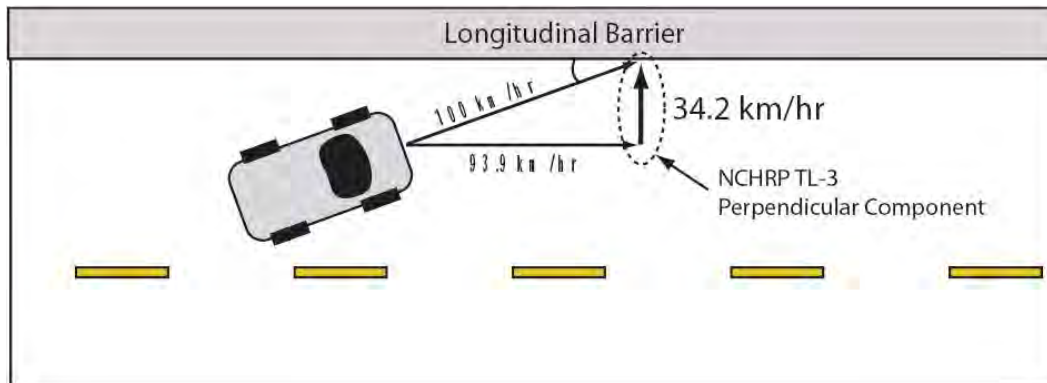


Figure 2.2: Crash test criteria of NCHRP Report 350 TL-3, Test Designation 3-10

Acceptable surrogate vehicles include impact pendulums and four-wheeled bogies. Researchers at The University of Texas at Austin developed and validated an impact pendulum test setup to simulate crash tests meeting NCHRP TL-3, Test Designation 3-10. The design, development and validation of this setup are discussed in Mitchell (2005), and the impact pendulum test setup is briefly reviewed in Chapter 4. of this report.

2.5 Finite Element Modeling in LS-DYNA

Although finite-element modeling is not required by FHWA criteria, it was used in this study to enhance the application and thereby the cost-effectiveness of the experimental results. Finite element analysis is increasingly used to study the crash-worthiness of vehicles as well as the behavior of highway structures during collisions. Due to its capabilities, LS-DYNA (LSTC 2006) was selected for use in this study.

2.5.1 Background of Initial Finite Element Modeling by Tolnai (2005)

The thesis of Tolnai (2005), in the first phase of the Project 0-4823, addresses the following aspects of finite-element modeling using LS-DYNA, using linear elastic materials for concrete and steel, and including material nonlinearity in the crush package only:

- creation and processing of finite-element models in LS-DYNA to serve as a user guide for future researchers working on this project;
- simulation of the pendulum mass and crush package, used for the pendulum impact testing of barriers, in LS-DYNA;
- creation of some basic models in LS-DYNA to simulate the pendulum impact testing of barriers; and
- use of LS-DYNA models of test vehicles, developed by the National Crash Analysis Center (FHWA 2006), to simulate vehicular impact on TxDOT barriers. That material is presented in more detail in Chapters 5 and 6 of this report.

2.5.2 Background of Nonlinear Material Modeling for this Report

The preliminary models of Tolnai (2005) served as a basis for developing more complex models to simulate impact tests on TxDOT T203 and T501 barriers. One aspect of those more complex models, which required literature review, was the representation of concrete material in finite element analysis programs and LS-DYNA in particular. This literature review is summarized here.

LS-DYNA contains a wide variety of material models that conceivably could be used to model concrete. These include the following:

- *MAT_SOIL_AND_FOAM* (Model 5 in *LS-DYNA User's Manual*);
- *MAT_PSEUDO_TENSOR* (Model 16 in *LS-DYNA User's Manual*);
- *MAT_CONCRETE_DAMAGE* (Model 72 in *LS-DYNA User's Manual*);
- *MAT_SOIL_CONCRETE* (Model 78 in *LS-DYNA User's Manual*);
- *MAT_WINFRITH_CONCRETE_REINFORCEMENT* (Model 85 in *LS-DYNA User's Manual*); and
- *MAT_BRITTLE_DAMAGE* (Model 96 in *LS-DYNA User's Manual*).

The criteria for choosing among these available models are briefly discussed here and are addressed in more detail in Chapter 11 of this report. The criteria for choosing one of the described material models for this research are:

- the material model should be able to represent non-linearity and cracking in concrete under impact; and
- the material model should be able to be calibrated without conducting laboratory tests on concrete.

Previous published research using LS-DYNA was helpful in making this selection. Uddin *et al.* (2005) report the behavior of composite panels under ballistic impact tests. The composite panels were made of concrete plates ($8 \times 11 \times 0.5$ in.), reinforced with glass-infused polypropylene thermo-plastic tape. Glass-infused polypropylene thermo-plastic is a composite material composed of a thermoplastic matrix and reinforcing fibers. It is used to improve strength of structural components (Uddin *et al.* 2005). These composite panels were subjected to impact loads in the laboratory using projectiles with varying velocities. LS-DYNA models were created to simulate these laboratory ballistic impact tests on composite panels. *MAT_SOIL_AND_FOAM* was used to model the concrete plates. According to Uddin *et al.* (2005), *MAT_SOIL_AND_FOAM* is a robust material model which produces good results with minimum amount of input data. The results obtained from the simulation indicated that the failure mode, cracking patterns and energy absorption of the concrete plates modeled using that material were similar to that observed in laboratory tests. Therefore, they concluded that the *MAT_SOIL_AND_FOAM* can satisfactorily represent non-linearity and cracking in concrete.

This model requires some calibration of input parameters using laboratory tests, as discussed by Schwer (2001). These laboratory tests are:

- hydrostatic compression test;
- triaxial compression/extension test; and
- uniaxial strain test.

The calibration of the input parameters of *MAT_SOIL_AND_FOAM* from these laboratory tests is briefly discussed by Schwer. Such tests are not always necessary, however. Chen (1982) gives dimensionless curves obtained from these laboratory tests on typical concrete, which can be used to calibrate the necessary input parameters of the *MAT_SOIL_AND_FOAM* model. These dimensionless curves are discussed in Chapter 11 along with ways of obtaining the necessary input parameters from the curves.

Other LS-DYNA models were investigated but not used. The *MAT_PSEUDO_TENSOR* model, for example, requires the input of just the unconfined compressive strength of concrete. Simulations of laboratory impact pendulum tests on barrier specimens using this model to represent concrete did not give appropriate results. The project researchers were not able to derive input parameters for the other concrete material models in LS-DYNA discussed earlier without conducting laboratory tests on concrete.

Because *MAT_SOIL_AND_FOAM* meets both criteria used to select material models to represent concrete in LS-DYNA, it is used in the nonlinear concrete modeling of this report.

Chapter 3. Design of T203 Bridge Deck and Barrier Test Specimen

3.1 Introduction

In this report, a test specimen consisting of a TxDOT bridge deck with a T203 bridge barrier is referred to, for convenience, as a “T203 bridge deck and barrier test specimen,” whose purpose is to allow researchers at UT Austin to observe the behavior of cast-in-place and retrofit TxDOT T203 bridge barriers subjected to a NCHRP TL-3 impact. To achieve the best possible simulation of actual bridge deck and barrier construction, researchers used TxDOT design drawings and design standards to design a test specimen incorporating a full-scale T203 barrier mounted on a reinforced concrete deck (Figure 3.1).



Figure 3.1: T203 bridge deck and barrier specimen at FSEL

3.2 Design Criteria for T203 Test Specimen

Design criteria for the development of the T203 bridge deck and barrier specimen include the following:

- the specimen must be capable of representing retrofit as well as cast-in-place barriers,
- the specimen must include relevant details of the T203 barrier and the standard TxDOT 8-in. bridge deck with a 3-ft (0.9-m) overhang;
- the specimen must fit into the impact test pendulum setup whose design is described in Chapter 4 of this report; and
- the specimen must incorporate details permitting the retrofit barrier to be attached to the bridge deck.

3.2.1 Relevance of Test Specimen for Retrofit and Cast-in-Place Bridge Barriers

The bridge barrier specimen is designed to accommodate both cast-in-place and retrofit bridge barriers. Cast-in-place T203 barrier specimens are constructed by casting stirrups into the T203 bridge deck specimen (Figure 3.2), and then later casting the T203 bridge barrier specimen over the stirrups. Retrofit bridge barrier specimens are attached by drilling or coring into the bridge deck specimen and installing mechanical anchors, either into the deck or through it.



Figure 3.2: Reinforcement layout of the T203 bridge deck and cast-in-place barrier test specimens

3.2.2 Relevant Details of T203 Barrier and Deck Overhang

The reinforcing details of the T203 bridge deck and barrier test specimen were taken directly from TxDOT design documentation (TxDOT 2003). An important criterion for the T203 bridge deck and barrier specimen is that it include the standard TxDOT overhang usually used on TxDOT bridges. In this case, this overhang extends 3 ft (0.9 m) from the outside face of the outside bridge girder, which is connected (for the case of prestressed I-beams) to the bridge deck via U-bars (extensions of girder transverse reinforcement) during casting (Figure 3.3(a)). To reproduce those boundary conditions in the test setup, the T203 bridge deck and barrier test specimen incorporates a 3-ft (0.9-m) cantilever overhang whose base is tied to the laboratory strong floor with threaded steel rods (Figure 3.3(b)). Transverse reinforcement in the slab typically consists of #5 bars spaced at 6 in. (0.15 m). Vertical reinforcement in the barrier, which also anchors the barrier to the slab, typically consists of #4 bars spaced at 5 in. (0.13 m).

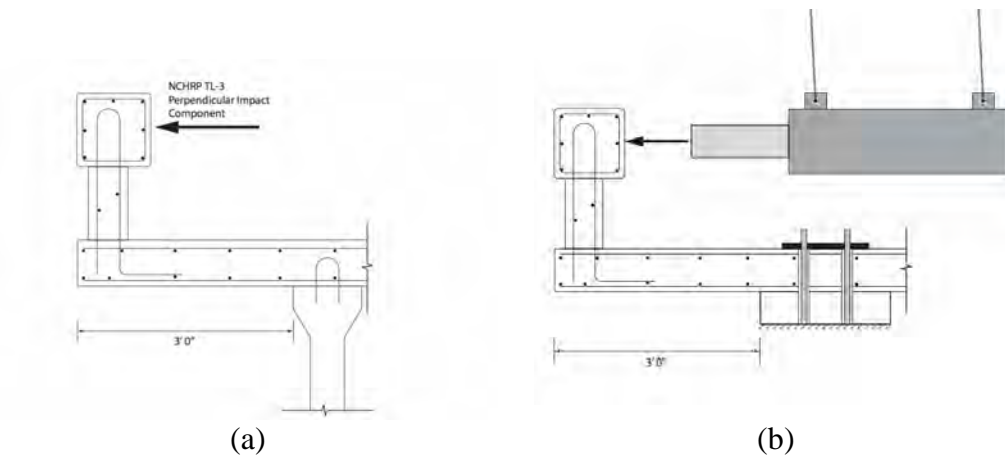


Figure 3.3: (a) Schematic of T203 bridge barrier in a typical highway configuration, and (b) bridge deck and barrier specimen at FSEL

3.2.3 Relevant Dimensional Compatibility between Specimen and Impact Test Pendulum

The T203 bridge deck and barrier specimen was also required to fit within the impact test pendulum setup at Ferguson Laboratory. Figure 3.4 shows a model of the specimen within the pendulum's support frame. Each specimen has two bridge barriers, one at each end. After the first barrier is tested (Figure 3.4), the specimen can be lifted with an overhead crane and rotated 180 degrees to test the barrier at the other end.

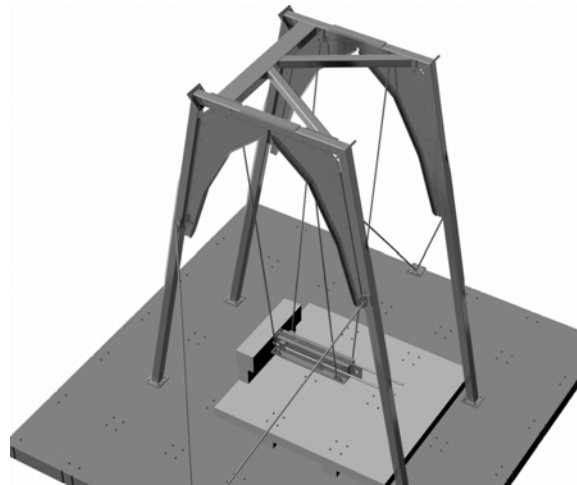


Figure 3.4: Impact test pendulum with T203 test specimen in place

3.2.4 Relevant Details for Attachment of T203 Retrofit Bridge Barrier to Deck of Specimen

In designing the T203 retrofit bridge barrier test specimen, special attention was paid to ensure that it could accommodate a wide variety of possible retrofit barrier connection details using mechanical post-installed anchors.

Using the anchor connection design provisions of ACI 318-05 Appendix D, the capacity of the bridge deck overhang as governed by concrete breakout around the anchors was estimated in terms of the number of anchors used to connect a T203 retrofit bridge barrier to the deck. The T203 bridge barrier has either a continuous lower portion 7-1/2 in. (0.19 m) thick or intermittent lower portions 5-ft (1.5-m) long with the same prescribed thickness. Based on the dimensions specified by TxDOT, the footprint of the barrier on the deck is prescribed in size. Breakout capacity of the anchor group does not increase much as more anchors are added because of increasing overlap among the concrete breakout bodies associated with each anchor (Appendix A). This observation is shown in Figure 3.5, which suggests that the tensile breakout capacity of the bridge deck is limited to about 78 kips (347 kN), regardless of the number of anchors used.

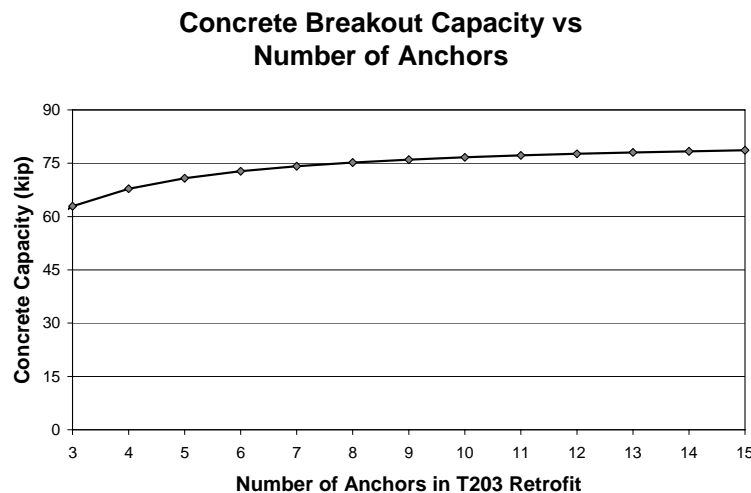


Figure 3.5: Tensile breakout capacity of concrete bridge deck as a function of anchors used to connect T203 retrofit bridge barrier to overhang

Based on this relationship, the researchers of Project 0-4823 concluded that eight anchors would be an appropriate upper bound for a T203 retrofit barrier connection design. The barrier of the T203 retrofit specimen (Figure 3.6(a)) was therefore designed with eight vertical PVC ducts, shown in Figure 3.6(b), to accommodate any reasonable combination of threaded rods, which would then be attached to the underlying deck, using either mechanical anchors or through-bolts. Figure 3.5 is independent of anchor diameter, provided that the diameter is large enough so that concrete breakout controls (about 3/8 in., or 9.5 mm). In Figure 3.6(a), the vertical ducts are centered at 2 in. (51 mm) from the inside face of the intermittent section, and 5 in. (127 mm) from the outside face. Complete dimensions are provided in Figure 4.12, Figure 4.13 and Figure 4.14.

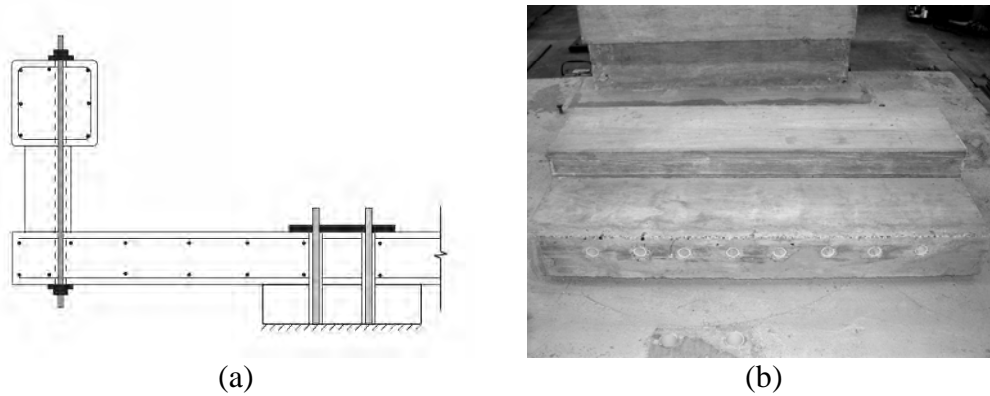


Figure 3.6: (a) Schematic of T203 retrofit specimen and (b) T203 retrofit bridge barrier with PVC ducts for anchors

3.3 Instrumentation of Specimen

The ability of UT Austin researchers to evaluate the performance of the T203 bridge barrier depends on the instrumentation scheme developed for the test specimen. To understand the impact performance of a T203 bridge barrier, the following must be known:

- impact force;
- bridge barrier and deck stresses; and
- bridge barrier and deck displacements.

Measurement of impact force is discussed in Chapter 4, and the measurement of displacements and stresses is briefly discussed in this section.

To measure stresses in the T203 bridge deck and barrier test specimen, a large number of electrical resistance strain gages were installed on steel reinforcing bars prior to casting concrete. For the bridge deck, strain gauges were installed on tension-side reinforcing bars near anticipated yield lines in the bridge deck near the interface with the T203 bridge barrier. These strain gages produced data regarding the propagation of stresses within the bridge deck during a pendulum impact test.

Strain gauges were also installed on reinforcing bars at the tension face of the T203 bridge barrier specimen. These gages helped researchers determine the stress level of the reinforcement at concrete breakout. This stress information was extremely valuable in confirming that the anchor design provisions of ACI 318-05 Appendix D accurately predict concrete breakout capacity under TL-3 impact loads.

Finally, linear variable differential transformers (LVDT) were installed underneath the bridge deck overhang of the test specimen to capture displacements and rotations of the bridge deck and barrier specimens during a pendulum impact test. The data obtained from the LVDTs were used to estimate impact energy absorption characteristics of the bridge deck and the T203 bridge barrier specimens.

3.4 Concluding Remarks on Development of T203 Bridge Deck and Barrier Specimen

The T203 bridge deck and barrier test specimen was designed to allow researchers at UT Austin to evaluate the behavior of cast-in-place and retrofit TxDOT T203 bridge barriers subjected to a NCHRP TL-3 impact. By consulting TxDOT design documentation and considering geometric compatibility with the impact test pendulum, the T203 bridge deck and barrier specimen was designed to permit an accurate and efficient testing program for retrofit bridge barriers.

Chapter 4. Experimental Testing Program for T203 Bridge Barriers

4.1 Introduction

This chapter discusses the development of an experimental test program for T203 bridge barriers. The objectives of the test program are as follows:

- to develop a surrogate vehicle to test highway barriers for *NCHRP Report 350 TL-3*;
- to design and develop test specimens of TxDOT standard bridge deck and cast-in-place and retrofit T203 bridge barrier (using mechanical anchors);
- to evaluate and compare the performance of the cast-in-place and retrofit T203 barriers for *NCHRP Report 350 TL-3* using the developed surrogate vehicle; and
- to determine if the retrofit T203 barrier design meets the TxDOT performance criteria for retrofit barriers (discussed later in this chapter).

A TxDOT T203 barrier and its associated standard bridge deck are referred to as “T203 barrier and bridge deck” in this report. The experimental test program developed at FSEL is presented in this chapter in the following order:

- an outline of the development and validation of an impact pendulum test setup as a surrogate vehicle by Mitchell (2005) for testing bridge barriers under *NCHRP Report 350 TL-3*, and the pendulum impact testing of bridge barriers;
- a quasi-static test setup for testing barriers;
- the development of cast-in-place T203 barrier specimens and the basic configuration of retrofit T203 barrier test specimens;
- the design of retrofit T203 barrier specimens using two different type of mechanical anchors, and the selection of one type of specimen for testing based on the TxDOT performance criteria for retrofit barriers; and
- the test instrumentation and the data acquisition system.

4.2 Impact Test Pendulum Setup for Project 0-4823

According to *NCHRP Report 350*, a validated surrogate vehicle can be used to study impact performance of highway safety features. Mitchell (2005) gives an in-depth description of the design, fabrication and validation of an impact test pendulum setup to test T203 barrier and bridge deck specimens under *NCHRP Report 350 TL-3*. In this section, the setup is briefly described, its operation is summarized, and its validation is addressed.

4.2.1 Overview of the Impact Test Pendulum Setup

The impact pendulum test setup developed at The University of Texas at Austin has a 22-ft (6.7-m) tall steel frame which supports an 855-kg pendulum mass on four cables (Figure 4.1).

The mass can be released from a maximum drop height of 16 ft (4.9 m). The pendulum mass and the drop height are designed to meet the *NCHRP Report 350* TL-3 criteria for barriers. The pendulum mass is lifted to the drop height with a steel lifting cable using an electric winch and pulley, attached to a pendulum mass lifting frame. The pendulum mass can be released from the desired height by actuating a pneumatic release latch attached at its top.

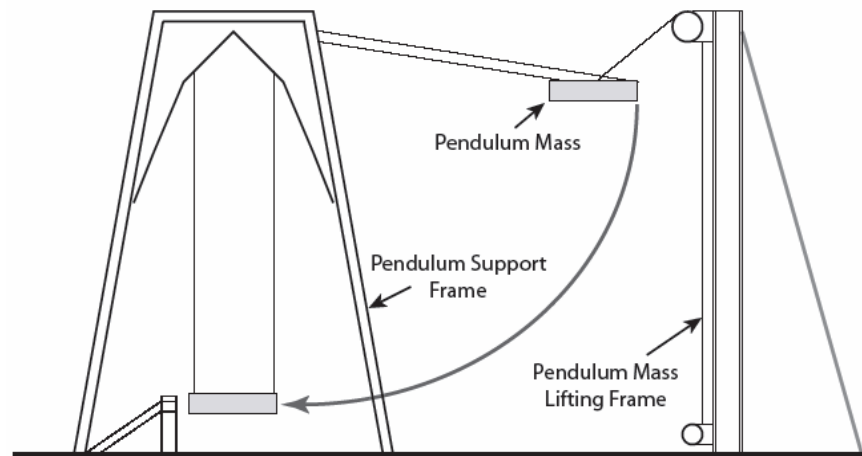


Figure 4.1: Impact test pendulum setup

A crush package made of bundled steel tubes is installed in front of the pendulum mass to simulate vehicle-specific impact characteristics. The steel crush package used in this research is described in Chapter 7. The pendulum test setup permits testing of barriers up to 10 ft (3-m) wide with a bridge deck overhang of 3 ft (0.9 m). Figure 4.2 shows the schematic diagram of a T203 barrier and bridge deck specimen, the pendulum mass with a crush package installed, and the position of a bridge-deck specimen within the support frame. This versatile setup can simulate any impact scenario to Test Level T-3 of *NCHRP Report 350*.

For the impact tests conducted by the project investigators on cast-in-place and retrofit T203 barrier and bridge deck specimens (Section 4.4 and 4.5), the pendulum mass (with crush package installed) was released from a height of 16 ft (4.9 m), representing *NCHRP Report 350* TL-3 (Test Designation 3-10).

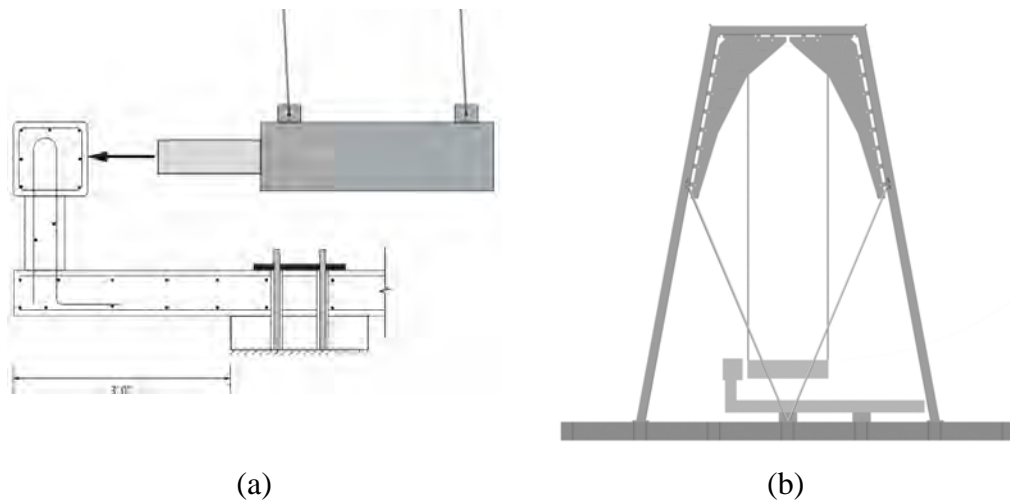


Figure 4.2: (a) Schematic diagram of a T203 barrier and bridge deck specimen, the pendulum mass installed with a crush package and (b) the position of the bridge deck within the support frame

4.2.2 Components of the Impact Test Pendulum Setup

Impact test pendulum support frame

The pendulum support frame is 22-ft (6.7-m) tall. Performance criteria for the design of this frame include sufficient resistance to design loads and sufficient stiffness to limit deflections at Test Level TL-3 of *NCHRP Report 350*. Mitchell (2005) reports that a deflection limit of 0.10 in. (2.5 mm) governs its design. Figure 4.3 shows the installed impact test pendulum support frame.



Figure 4.3: Impact test pendulum support frame

Pendulum mass

The pendulum mass used in this research has a mass of 855 kg and meets the *NCHRP Report 350* impact energy criterion for TL-3. To make the mass reusable for other research projects, it is created as a system of modular steel plates bolted together (Mitchell 2005). The pendulum mass hangs on the support frame with the help of support cables attached to plate anchors. The pendulum mass also has a pneumatic release latch at its center of gravity. Figure 4.4 shows the pendulum mass and the pneumatic release latch.



(a)



(b)

Figure 4.4: (a) Pendulum mass and (b) pneumatic release latch

Pendulum mass lifting frame

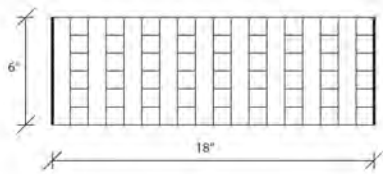
The pendulum mass lifting frame is made of a W-section (Figure 4.5), supported in the plane of the pendulum swing by a steel pipe backstay. An electric winch and pulley system is used as the lifting mechanism for the pendulum mass.



Figure 4.5: Pendulum mass lifting frame

Crush package

The crush package used in this research is fabricated using thin-walled square steel tubing ($1 \times 1 \times 0.049$ in., or $25.4 \times 25.4 \times 1.2$ mm). The axes of the tubes are oriented in planes normal to the direction of impact. Figure 4.6 (a) and (b), respectively, show a dimensional schematic and a photograph of the crush package. It has a uniform gross cross-sectional area of 36 in.^2 and a length of 18 in.



(a)



(b)

Figure 4.6: (a) and (b) Crush package used in this research

4.2.3 Validation of the Impact Test Pendulum Setup

For the impact test pendulum setup to be acceptable as a surrogate vehicle for the *NCHRP Report 350 TL-3*, it must impart sufficient impact energy, and must produce an impulse of impact similar to that of an actual vehicular collision. (Mitchell 2005). The surrogate vehicle should be modeled to simulate the behavior of a specific production vehicle.

The impact acceleration history data selected to evaluate the pendulum impact test setup was from an *NCHRP Report 350 TL-3* crash test conducted at the Texas Transportation Institute (TTI) in August 2002. That test measured the behavior of a 1997 Geo Metro colliding with a TxDOT T77 steel bridge barrier (TTI 2002). Figure 4.7 (a) shows the history of transverse acceleration (normal to the plane of the longitudinal barrier) during the Geo Metro collision against a steel bridge barrier.

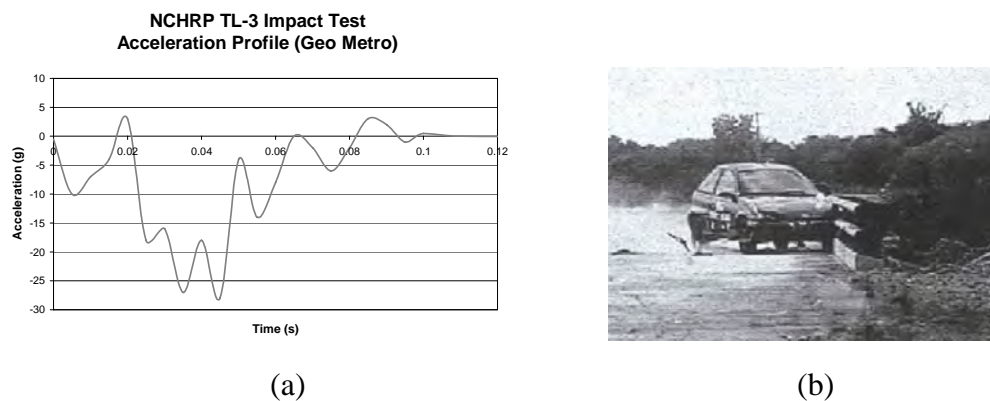


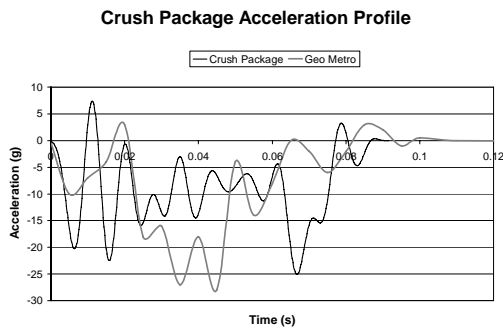
Figure 4.7: Geo Metro NCHRP Report 350 TL-3 crash test (a) acceleration history and (b) photograph of impact with steel bridge barrier

(TTI Research Report 4288-1)

In addition to the impulse of impact, the acceleration history contains the following information: 1) peak acceleration; and 2) duration of impact. Hence, in addition to the energy and impulse of impact criteria, the pendulum impact test setup was compared to Geo Metro crash test for the following criteria (Mitchell 2005):

- the acceleration history obtained from the pendulum impact test setup should produce a peak acceleration similar to that of the Geo Metro; and
- the duration of impact obtained from the pendulum impact test setup should be similar to that obtained from the Geo Metro.

Figure 4.8 shows the acceleration histories of the impact pendulum test setup impacting a steel barrier at FSEL and the 1997 Geo Metro.



(a)



(b)

Figure 4.8: (a) Acceleration history of impact pendulum test setup and (b) photo of test

Table 4.1 gives the comparison of results obtained from the pendulum test setup impacting a steel barrier and the 1997 Geo Metro for *NCHRP Report 350 TL-3*.

Table 4.1: Comparison between impact pendulum test setup and the 1997 Geo Metro for *NCHRP Report 350 TL-3*

| <i>Comparison Between:</i> | <i>Comparison Criterion</i> | | | |
|---------------------------------------|-----------------------------|------------------------------------|------------------------|---------------------------------|
| | <i>Impact Energy (kJ)</i> | <i>Impulse of Impact (kip-sec)</i> | <i>Peak Accel. (g)</i> | <i>Duration of impact (sec)</i> |
| 1997 Geo Metro | 38.5 | 1.54 | 25 | 0.09 |
| Pendulum Impact Test on Steel Barrier | 38.5 | 1.49 | 27 | 0.09 |

The impact energy imparted by the impact pendulum test setup was the same as that imparted by the 1997 Geo Metro, and it meets the *NCHRP Report 350 TL-3* energy criterion. The impulse of impact obtained from the impact pendulum setup was about 1.49 kip-sec (6625 N-sec), within 5% of the impulse obtained from the 1997 Geo Metro (1.54 kip-sec (6850 N-sec)). The peak acceleration value obtained from the impact pendulum (27g) was about 8% greater than the peak acceleration obtained from the 1997 Geo Metro (25g). The duration of the impact obtained from the impact pendulum setup was about the same as that obtained from the 1997 Geo Metro. Because the impact pendulum test setup met all the required criteria, it was considered an acceptable surrogate vehicle for *NCHRP Report 350 TL-3*.

4.3 Static Test Setup for Testing of T203 Retrofit Barriers

Static capacity is one of the TxDOT criteria (Section 4.5.4) to evaluate retrofit barriers. Hence, it was decided to conduct a quasi-static test on a retrofit T203 bridge barrier design. The test specimen is discussed in detail in Sections 4.4 and 4.5. Figure 4.9 shows the test setup used for the static testing of this barrier. A buttress was installed on the bridge deck specimen using

threaded rods running through holes in the deck and the underlying laboratory floor. A hydraulic jack having a capacity of 50 tons was installed horizontally on the buttress at a height of 21 in. above the bridge deck. Hence, the barrier was loaded by the jack at a height of 21 in. from its base. A hemispherical head was installed at the front of the hydraulic jack to provide a smooth loading surface and accommodate rotation of the barrier.

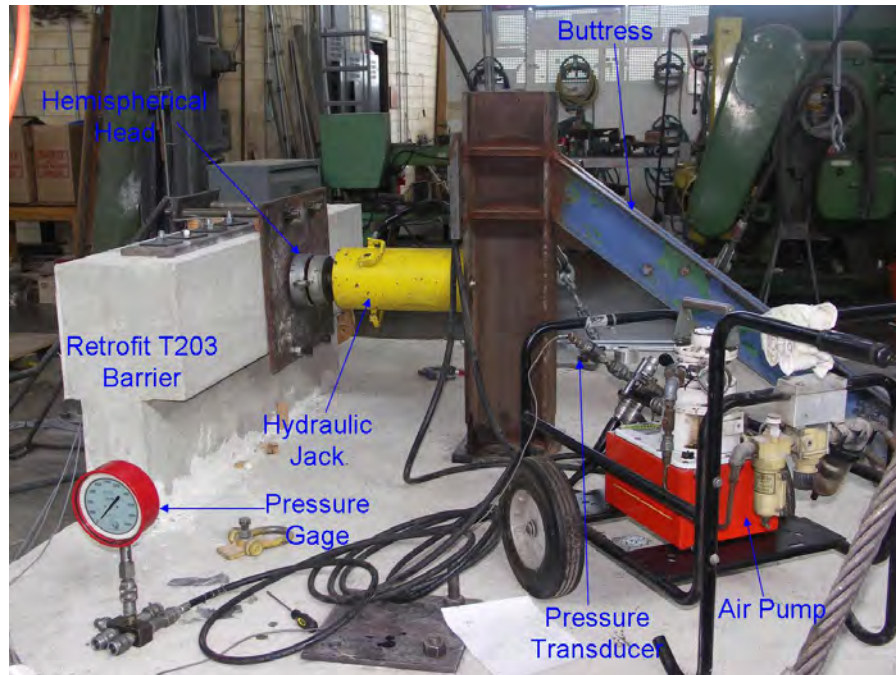


Figure 4.9: Static test setup for retrofit T203 barrier

The retrofit barrier specimen was loaded using an air pump connected to the hydraulic jack. The hydraulic jack was also connected to a calibrated pressure transducer, which was connected to the data acquisition system (discussed in Section 4.6) to record the test readings. The instrumentation of the retrofit T203 barrier and bridge deck specimen for the static test is discussed in Section 4.6.

4.4 Cast-in-Place and Retrofit Test Specimens of T203 Barriers

To understand the behavior of the cast-in-place and retrofit TxDOT T203 bridge barriers subjected to an *NCHRP Report 350* TL-3 impact, previous researchers at UT Austin designed test specimens by referring to TxDOT design documentation. Figure 4.10 shows the cast-in-place and retrofit barrier specimens and a standard TxDOT bridge deck.



Figure 4.10: Cast-in-place and retrofit T203 bridge barrier specimens

According to Mitchell (2005), the T203 test specimens, as designed, have the following characteristics:

- the specimens are capable of representing retrofit as well as cast-in-place barriers;
- the specimens include relevant details of the T203 barrier and the standard TxDOT 3-ft (0.9-m) bridge deck overhang;
- the specimens fit into the impact test pendulum setup; and
- the specimens incorporate details permitting the retrofit barrier to be attached to the bridge deck.

Figure 4.11 shows a model of the test specimen within the pendulum support frame. After a barrier is tested, the deck is rotated 180 degrees to attach and test a barrier at the other end. The test slab has length (perpendicular to the direction of pendulum swing), breadth (parallel to the direction of pendulum swing) and thickness of 120 in., 127 in. and 8 in. respectively. This slab has reinforcement similar to the TxDOT standard bridge deck. To produce the same boundary conditions as in TxDOT bridge deck, the slab specimen has a 3-ft (0.9-m) overhang and its base and is tied to the laboratory strong floor using high-strength steel rods (Figure 4.12).

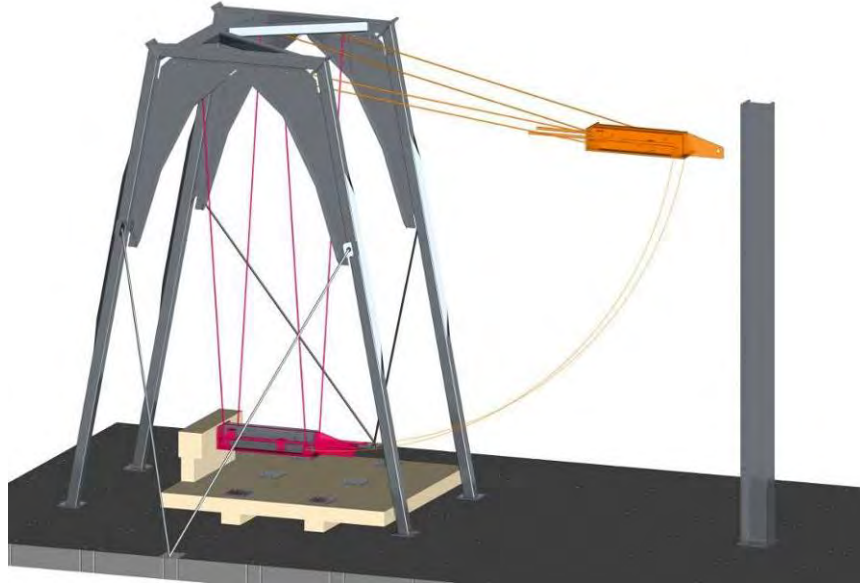


Figure 4.11: Schematic of T203 barrier and bridge deck specimen within impact test pendulum frame

4.4.2 Cast-in-Place T203 Barrier Specimen

A TxDOT cast-in-place T203 bridge barrier is conventionally anchored to a TxDOT bridge deck with a typical overhang of 3 ft (0.9 m) using U-bars, which are extensions of the deck transverse reinforcement and act as the primary flexural reinforcement of the barrier (Figure 4.12 (a)) when subjected to an impact. Those U-bars are typically #5 bars, spaced at 6 in. (152 mm), with an effective flexural depth (at the intermittent barrier section) of 5 in. (127 mm). To reproduce the same conditions, the cast-in-place T203 barrier test specimen has reinforcement similar to that of the typical TxDOT T203 bridge barrier (Figure 4.12 (b)). To understand their behavior, two of these specimens were tested at FSEL during the project, using the impact pendulum test setup for *NCHRP Report 350 TL-3*.

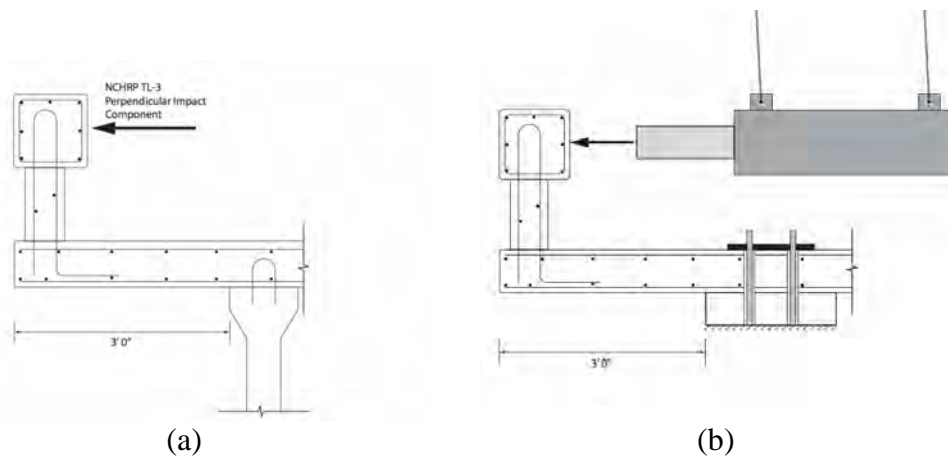


Figure 4.12: (a) Schematic of T203 bridge barrier in a typical highway configuration and (b) barrier and bridge deck specimen at FSEL

4.4.3 Retrofit TxDOT T203 Barrier Specimens

The concept of T203 retrofit barriers using mechanical anchors is proposed by Mitchell (2005). Using the anchorage design provisions of ACI 318-05 Appendix D, the capacity of the bridge deck overhang as governed by concrete breakout around the anchors was estimated in terms of the number of anchors used to connect a T203 retrofit barrier to the deck. Mitchell (2005) reports that the breakout capacity of the anchor group, as governed by tension, does not increase much if more than seven anchors are used. Based on this finding, and considering the layout of reinforcement in the barrier and the bridge deck, it was concluded that eight anchors would be an appropriate number for a T203 retrofit barrier connection design. The T203 retrofit barrier specimen was therefore designed with eight vertical PVC ducts, shown in Figure 4.13, to accommodate threaded rods, which would then be attached to the underlying deck using either mechanical anchors or through-bolts. The next section describes the design of T203 retrofit barriers.

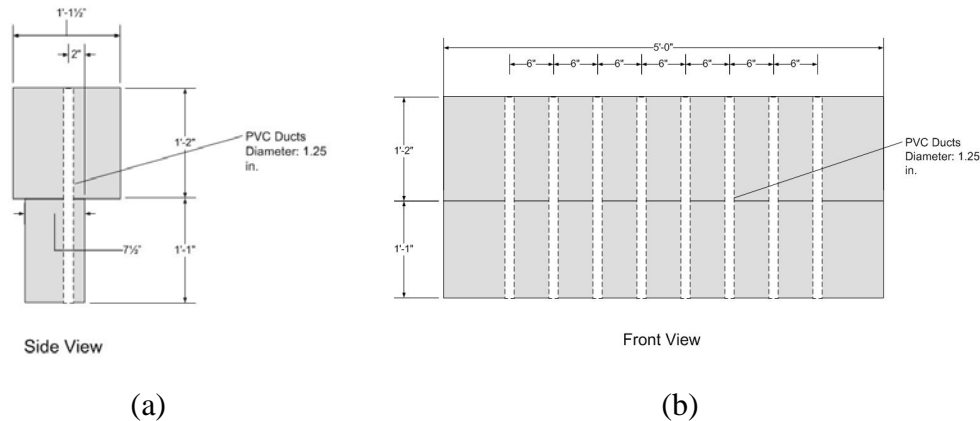


Figure 4.13: (a) Side view and (b) front view T203 retrofit bridge barrier with PVC ducts to accommodate anchors

4.5 Design of T203 Retrofit Barrier Specimen

The following is discussed in this section:

- preliminary performance criteria to evaluate retrofit barriers;
- preliminary design of retrofit T203 barrier specimens using through-anchor and under-cut anchor configurations, and estimated capacities of each configuration;
- comparison of estimated capacities of retrofit T203 barriers with capacity of cast-in-place T203 barrier obtained from Texas Transportation Institute (TTI) test results to evaluate the retrofit designs based on preliminary performance criteria;
- revised performance criteria to evaluate retrofit barriers; and
- selection of a retrofit T203 barrier configuration to be developed and tested at FSEL based on the revised performance criteria.

4.5.1 Preliminary Performance Criteria for T203 Retrofit Barrier Specimen

The preliminary performance criteria for retrofit barriers using mechanical anchors were as follows:

- they should (if possible) have the same ultimate capacity as their cast-in-place counterparts; and
- they should (if possible) reach their ultimate capacity and their reinforcement should yield before damaging the concrete deck by breakout of the mechanical anchors.

4.5.2 Estimated Capacities of Preliminary T203 Retrofit Barrier Designs

Two configurations of mechanical anchors were considered for the retrofit design of T203 bridge barriers: a through-anchor configuration and an undercut anchor configuration. The through-anchor configuration consisted of eight $\frac{3}{4}$ -in. ASTM A307 threaded rods (used as longitudinal reinforcement as well as mechanical anchors) running through the eight PVC ducts in the retrofit barrier and holes drilled through the slab (Figure 4.14). The rod spacing of 6 in. (152 mm) was selected to coincide with the spacing of transverse reinforcement in the slab. The spacing of 9 in. (229 mm) between the outermost rods and the ends of the intermittent sections of barrier base was used because the concrete breakout capacity would not have increased significantly if one more bar had been used. This rod diameter was selected so that the tensile capacity of the 8 threaded rods ($8 \times 0.70 \times 0.44 \text{ in.}^2 \times 0.7 \times 60 \text{ ksi} = 103 \text{ kips}$) would exceed the breakout capacity of about 75 kips noted in Figure 3.5. The rods were unbonded to maximize the length over which they could deform axially, thereby increasing the maximum displacement of the barrier. In field applications, such unbonded rods would have to be protected against corrosion. The rods were bolted to the bottom of the slab and top of the barrier using ASTM A572 Grade 50 steel plates measuring $50 \times 6 \times \frac{3}{4}$ in. The threaded rods are post-tensioned to approximately 20 ksi (6680 lbs.) to minimize any possible increase in flexibility for the retrofit barrier compared to the cast-in-place barrier. The expected long-term reduction in effective post-tensioning due to relaxation was expected not to exceed 50% of this value. The post-tensioning force in the threaded rod (F , lbs) can be related to an applied torque (T , ft-lbs) using the following empirical formula (Efunda 2006):

$$T = \frac{KDP}{12} \quad (4.1)$$

where:

T = Torque to be applied, ft-lbs

K = Friction Factor (for threaded rods used for retrofit barriers $K = 0.2$)

D = Threaded rod diameter, in.

P = Tension force required in threaded rod, lbs

A torque wrench can be used to apply the required torque (Efunda 2006). Using the formula 4.1, the torque required to post-tension the threaded rods to 20 ksi (6680 lbs) was calculated as 85 ft-lbs and was applied to the threaded rods using a torque wrench.

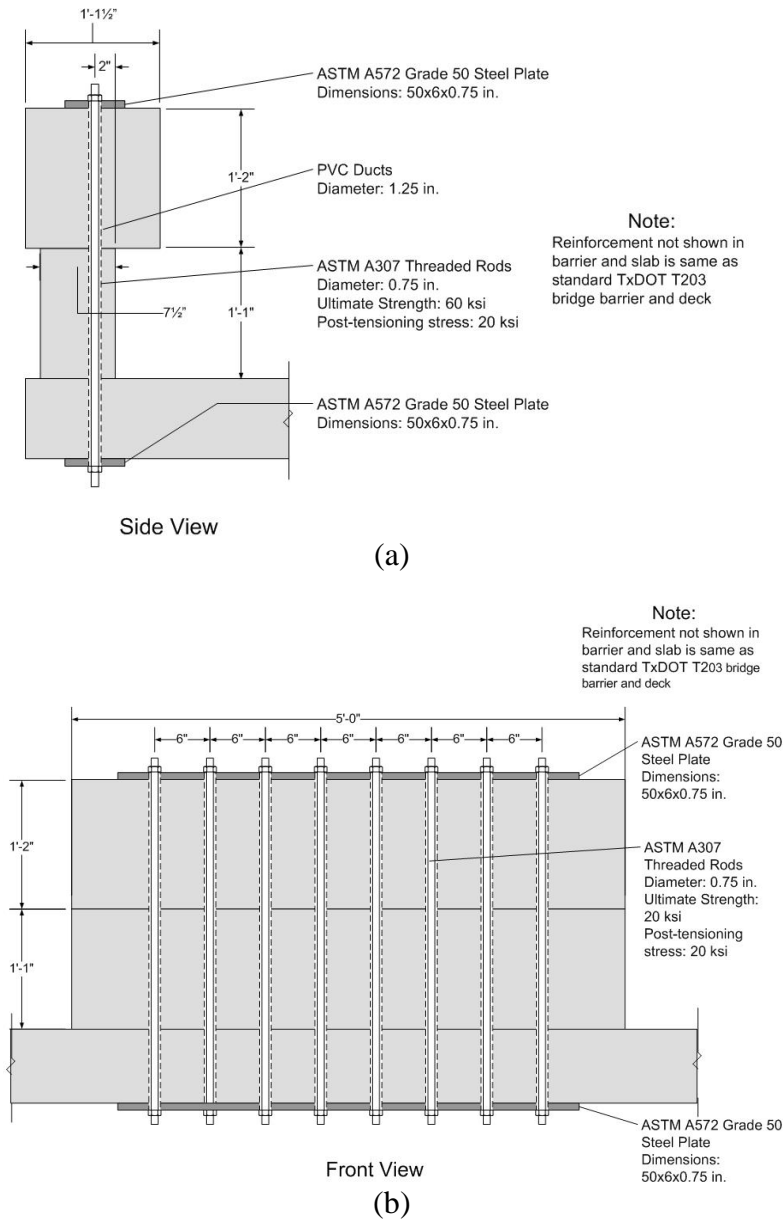


Figure 4.14: (a) Side view and (b) front view of retrofit T203 barrier with through-anchor configuration

The undercut anchor configuration consisted of eight $\frac{3}{4}$ -in. ASTM A307 threaded rods (used as longitudinal reinforcement) running through the PVC ducts in the barrier and connected to flush-mount undercut anchors installed in the bridge deck. The schematic of the retrofit T203 barrier with undercut anchors is shown in Figure 4.15. The effective embedment depth of the anchors was taken as 6.5 in. The anchors were left exposed in this first test specimen for convenience. In the final design, the heads would not be exposed.

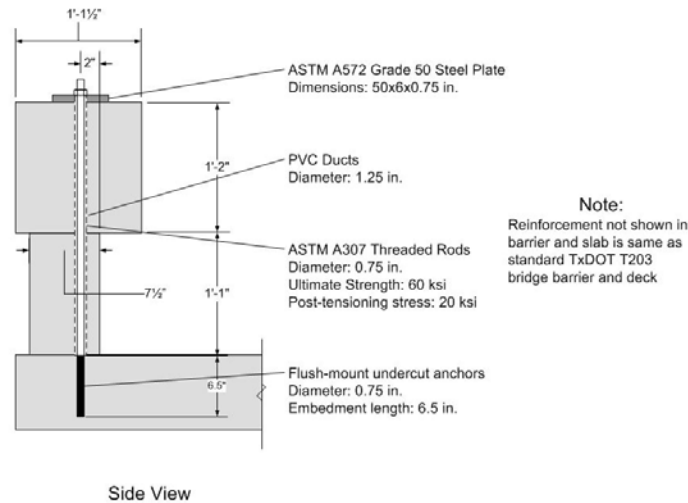


Figure 4.15: Schematic of retrofit T203 barrier with undercut anchor configuration

The capacities of the preliminary retrofit barrier designs were estimated in terms of the horizontal force acting on them at a height of 21 in. from their base. This height is approximately the height of the middle of the continuous upper portion of the barrier. Appendix D of ACI 318-05 was used to calculate their nominal capacities as described in Appendix B of this report. The nominal capacities of the T203 retrofit barrier using through-anchor and undercut anchor configuration are 17 kips and 8 kips, respectively. Those values represent lower 5% fractiles. For the coefficients of variation typical of concrete breakout with undercut or through anchors, mean nominal capacities are obtained by multiplying the lower 5% fractile capacities by a factor of 1.4, and these values are 24 kips and 11 kips for the retrofit T203 barriers with through-anchor and undercut anchor configurations, respectively. These values are lower than the required AASHTO LRFD capacity (A13.2) of 54 kips, because they as yet include no contribution for longitudinal continuity of the rail. This issue is addressed in the next section.

Dynamic capacity of structural elements can be obtained by multiplying the static capacity by a dynamic increase factor. The dynamic increase factor depends on the following factors: 1) shape of load versus time graph; 2) the state of the system (elastic or inelastic); 3) material model if the system doesn't remain elastic; and 4) ratio of the load duration to the natural period of the structure. The upper bound of the dynamic factor is 2 provided the structural element remains elastic. However, based on the irregular load versus time history, coupled with localized damage and non-linear response of the bridge barrier during an impact test, its dynamic increase factor can be within a range of 1.2 to 1.6. The dynamic increase factor for the bridge barriers (especially retrofit barriers with mechanical anchors) can be taken as roughly 1.3 based on the work by Rodriguez *et al.* (2001). Probable mean dynamic capacities of the two retrofit barrier configurations were obtained by multiplying their estimated mean static capacities by 1.3, giving 32 kips and 15 kips for the stand-alone retrofit T203 barrier with through-anchor and undercut anchor configurations, respectively.

4.5.3 Comparison of Estimated Capacities of T203 Retrofit Configurations with Capacity of Cast-in-Place T203 Bridge Barrier

The estimated static capacities of both retrofit T203 barrier configurations need to be compared to the static capacity of a standard cast-in-place barrier to check if they meet the

TxDOT criteria discussed. To do this, it is first necessary to estimate the capacity of a long length of barrier, as contrasted with the limited-length barriers tested here. For this purpose, researchers on this project used additional barrier test data from the Texas Transportation Institute (TTI).

TTI conducted static tests on cast-in-place T203 barrier specimens consisting of intermittent barriers connected together by beams providing continuity. Such a specimen, representing actual TxDOT highway practice, is called a “T203 barrier system.” The cast-in-place T203 barrier system tested by TTI is shown in Appendix E.

The capacities of the T203 retrofit configurations (discussed in Section 4.5.2) are for stand-alone T203 retrofit barriers. To compare the static capacities of the retrofit barriers with the cast-in-place T203 barrier TTI results, it is necessary to obtain the retrofit T203 system capacities from the stand-alone T203 retrofit barrier capacities. Figure 4.16 illustrates the 3 steps used to estimate the capacity of a T203 barrier system from the capacities of the corresponding stand-alone barrier.

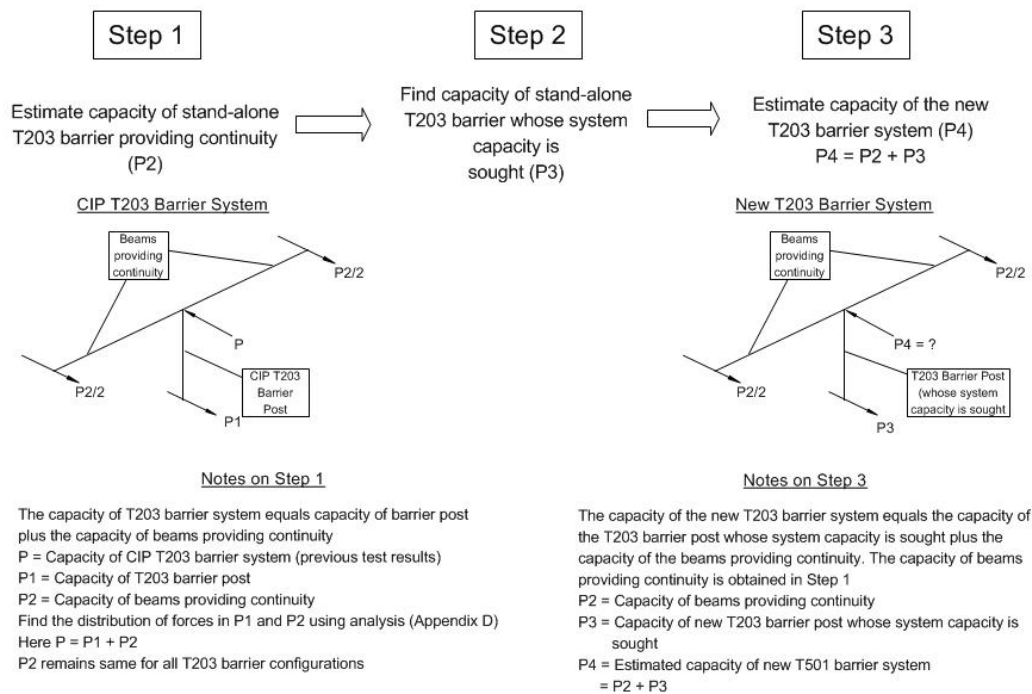


Figure 4.16: Steps to find T203 barrier system capacity from stand-alone T203 barrier capacity

The three steps to find the T203 barrier system capacity are:

- 1) Estimate the absolute increase in barrier capacity due to longitudinal continuity. The ultimate static capacity of the cast-in-place T203 barrier system, obtained from the TTI test results, is about 72 kips (force applied at 21 in. from the base of the barrier). As shown in the calculations of Appendix D of this report, about half of this capacity (35 kips) comes from the continuity provided by beams, and the other half from the capacity of the stand-alone barrier (Appendix D). This represents the first step given in Figure 4.16. The absolute value of the contribution due to barrier continuity is assumed to remain the same for both cast-in-place and retrofit T203 barrier systems.

- 2) Estimate the stand-alone retrofit barrier capacity as in Section 4.5.2.
- 3) Add the estimated capacity of the standalone retrofit T203 barrier to the estimated increase in capacity due to longitudinal continuity (35 kips) to give an estimate of the capacity of the retrofit T203 barrier system.

The values obtained from those three steps for the retrofit T203 barriers with through-anchor and undercut anchor configurations are given in Table 4.2.

Table 4.2: Steps to obtain static capacities of retrofit T203 barrier system

| <i>Version of Retrofit T203 Barrier</i> | <i>Values from:</i> | | |
|---|--|---|--|
| | <i>Step1 (kips)—Capacity from Barrier Continuity</i> | <i>Step2 (kips) – Capacity of Stand-alone Barrier</i> | <i>Step3 (kips)- System Capacity (Step1 + Step2)</i> |
| Retrofit with through-anchors | 35 | 24 | 59 |
| Retrofit with undercut anchors | 35 | 11 | 46 |

The static capacities of the retrofit T203 barrier system using through-anchor and undercut anchor configurations were estimated at 59 kips and 46 kips, respectively. These capacities are lower than the cast-in-place T203 barrier system static capacity of 72 kips. In Table 4.3, the estimated static capacity of the retrofit barrier system is compared to that of the cast-in-place barrier system. These estimates must be verified by tests on T203 barrier specimens.

Table 4.3: Static capacity estimates of T203 barrier systems

| <i>Version of T203 Barrier</i> | <i>Static Capacity of T203 Barrier System, kips</i> |
|---|---|
| Cast-in-Place | 72 |
| Retrofit with through-anchors (Estimate) | 59 |
| Retrofit with undercut anchors (Estimate) | 46 |

4.5.4 Revised Performance Criteria for Retrofit Barriers

According to Table 4.3, all retrofit T203 barriers have estimated static capacities less than that of the cast-in-place T203 barrier, all retrofit T203 barriers fail by concrete breakout, and hence all retrofit T203 barriers fail the ideal TxDOT criteria. Because the original performance criteria could not be met by any of the T203 retrofit configurations, TxDOT suggested in March

2006 that the UT Austin researchers use the following revised performance criteria to design retrofit T203 barriers:

- Barrier systems are required to have a dynamic capacity (50-msec window) of at least 60 kips;
- Barrier systems are required to have a static capacity of at least 54 kips; and
- Failure may be controlled by anchor breakout.

Dynamic capacity over a 50-msec window is obtained by taking a graph of force versus time (obtained from an impact test on the barrier) and obtaining a new curve whose ordinate at every time is obtained by averaging the ordinates of the original curve over a window extending from the given time minus 25 msec, to the given time plus 25 msec.

4.5.5 Selection of T203 Retrofit Barrier Configuration for Testing

Because of its estimated static capacity of only 46 kips, the retrofit T203 barrier system with undercut anchors does not meet the revised TxDOT static capacity criterion for barriers. In contrast, the retrofit T203 barrier system with through-anchor configuration does meet that criterion. Hence it was decided to test two retrofit T203 barriers with the through-anchor configuration. Figure 4.14 shows the test specimen of this barrier configuration, described in Section 4.5.3.

The dynamic capacities of the retrofit T203 barrier were obtained from impact pendulum tests, and the static capacity was obtained from the quasi-static test. Using the test results, the retrofit T203 barrier was evaluated based on the NCHRP TL-3 test criteria and the revised TxDOT criteria (Chapter 9.).

Because the estimated static capacity (46 kips) of the retrofit T203 barrier system with undercut anchors is close to the required capacity, it was judged premature to discard this configuration without testing. It should be tested by future researchers.

4.6 Instrumentation, Data Acquisition, and Processing

Data must be acquired from the static and impact pendulum tests to evaluate and compare the behavior cast-in-place and retrofit T203 barrier and bridge deck specimens. To capture the performance of the barrier specimens, it was decided to obtain the acceleration-time history of impact, the displacement at the top of the barrier and strains in the barrier and bridge deck reinforcement. The instrumentation to acquire these data from a test is discussed in Section 4.6.1.

The instrumentation was connected to a National Instruments 96-channel Signal Conditioning Chassis (Model No. NI SCXI-1001), which in turn was connected to a Windows®-based microcomputer. The data from the instrumentation generates signals in the chassis that are read using the Ferguson Laboratory's LabVIEW-based (LabVIEW 2006) high-speed data-acquisition program, converted from analog to digital format, and stored in the computer.

Some of the raw data acquired from pendulum tests must be processed to convert it to usable form. This section discusses that processing.

4.6.1 Instrumentation of Test Specimens

To obtain the acceleration-time history of impact, a Motorola 250-g accelerometer (Model No. MMA1200D) was mounted at the back of the pendulum mass. The data from the

accelerometer was sampled at 5000 Hz using the high-speed data acquisition system. The raw acceleration data are processed using a digital filter (Section 4.6.2).

String potentiometers were installed at the top of the barrier specimens, and are circled in Figure 4.17 (a). Figure 4.17 (b) shows a close-up of the string potentiometer installed on the barrier. They were used to capture the displacement history of the barriers during pendulum tests.



Figure 4.17: Location of string potentiometers in barriers

To measure stresses in the T203 barrier and bridge deck test specimens, electrical-resistance strain gages were installed on steel reinforcing bars. For the bridge deck, strain gages were installed on the tension-side bars near the interface with the T203 bridge barrier to give data regarding the propagation of stresses within the deck during pendulum testing. Figure 4.18 shows the location of the strain gages (Rows R1, R2, R3, R4 and R5) in the mat of reinforcement of the bridge deck.

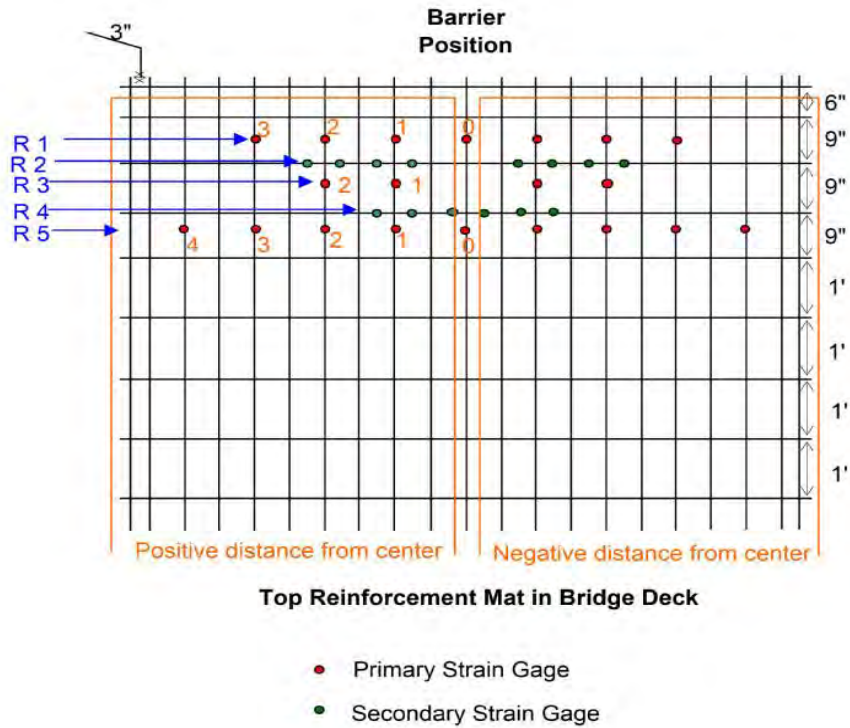
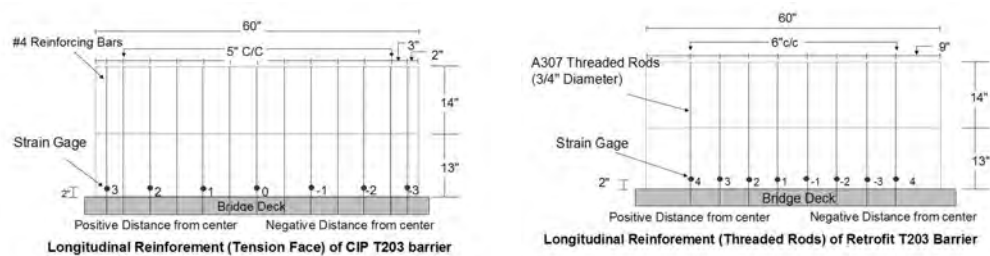


Figure 4.18: Location of strain gages in bridge deck

Strain gages were also installed on the tension-face reinforcement of the cast-in-place and retrofit T203 barriers. These strain gages were used to determine the stress level of the reinforcement during pendulum tests. Figure 4.19 (a) and (b) show the location of the strain gages (Row B) in the tension face reinforcement of the cast-in-place and retrofit T203 bridge barriers, respectively.



(a)

(b)

Figure 4.19: Location of strain gages in (a) cast-in-place and (b) retrofit T203 bridge barriers

4.6.2 Data Processing

During a pendulum test impact, the accelerometer mounted on the pendulum mass does not discriminate between accelerations generated from the pendulum impact with the concrete barrier and accelerations associated with subsequent axial vibrations of the pendulum mass induced by that impact. The result is raw accelerometer data that contain more information than necessary or desirable to determine the acceleration history for each crush package. Although the impact acceleration history of the crush package is embedded within those raw data, high-frequency axial vibration of the pendulum mass obscures that history and must be removed using digital post-processing. It was concluded that the axial vibrations of the pendulum mass could be filtered from the raw accelerometer data using a low-pass filter such as Butterworth filter (Mitchell 2005).

A detailed description of the development of the Butterworth filter is given in Mitchell (2005). It was designed by trial and error, using the *Signal Processing Toolbox* of Matlab 6 (MathWorks 2002). This program contains a platform to which the raw accelerometer data can be imported and also provides a graphical user interface for designing and applying various filtering algorithms. The filtering characteristics of the Butterworth filter are shown in Figure 4.20.

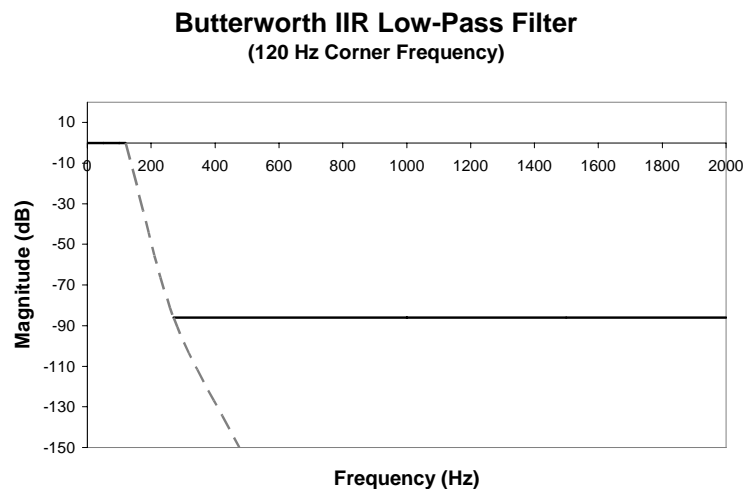


Figure 4.20: Frequency characteristics of Butterworth low-pass filter

The filter has three characteristics: 1) a low-frequency range in which data pass through; 2) a transition range; and 3) a high-frequency range in which data are greatly attenuated. The frequency at the low end of the transition range, known as the “corner frequency,” is shown as 120 Hz in Figure 4.20.

The corner frequency separates the frequencies of raw data that are permitted to pass through from those that are filtered. The final value of the corner frequency was determined by running the raw accelerometer data through several trial low-pass filters, each with a different corner frequency, and observing the sensitivity of the filtered data to the value of the corner frequency (Mitchell 2005).

Figure 4.21 shows the sensitivity of the impulse value of an impact acceleration history dataset to changes in the corner frequency.

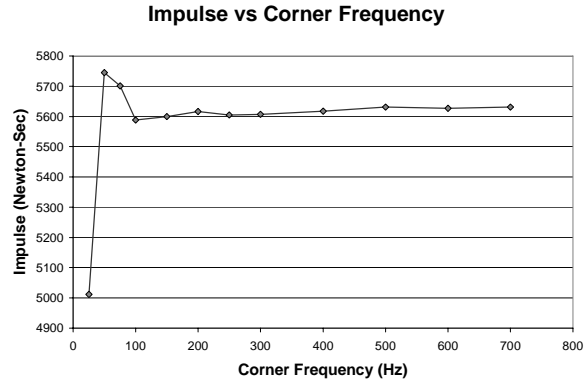


Figure 4.21: Impulse values of accelerometer signal as a function of low-pass corner frequency

Impulse is the primary criterion for evaluating the performance of a crush package. The impulse is constant through a large range of corner frequency values. The final value of 120 Hz for the corner frequency was determined as approximately the lowest value that preserved the impulse. This corner frequency also gave the same maximum acceleration of impact as that obtained from a 1997 Geo Metro colliding with a TxDOT T77 steel bridge barrier (Mitchell 2005).

Chapter 5. Using LS-DYNA for Analysis

5.1 Finite Element Computer Programs

Over the past 30 years, computer programs designed to analyze structures using the finite element method have become a mainstay of structural engineering design. As discussed in Chapter 2, such programs have also found a role in the development of vehicular crash barriers. Examples of commercially available software for finite element structural analysis include LS-DYNA, ANSYS, and ABAQUS. Such programs typically have three main components: a pre-processor, a solver, and a post-processor.

- The pre-processor is typically a graphical interface. With it, a user defines the structure's physical dimensions and geometry; specifies its materials, initial conditions, and boundary conditions; and indicates the desired output information.
- The solver carries out the computation associated with the problem as defined, without additional user interaction.
- The post-processor is used to display and interpret the analytical results, including such items as animated displacements, element stress and strain contours, and velocities. Possibly included may be a graphical processor, which can be used to display more detailed plots of desired information, such as forces and contact interfaces, or accelerations of various model parts.

5.2 Selection of LS-DYNA for Use in this Study

LS-DYNA is a three-dimensional finite element software package, developed in the late 1970s in nuclear weapons laboratories under US government contract, for the analysis of structures subjected to impact loads. Many subsequent updates have been released, with advances in features such as additional material models, element types, and integration techniques. In the late 1980s, significant advances were made to the software, including development of a commercial version, intended for application to vehicular impact problems (Livermore Software Technology Corporation 2003). LS-DYNA3D has since become an industry standard for crashworthiness studies involving vehicles and roadside appurtenances. Many analytical models of vehicles are available in the public domain for use with LS-DYNA. The Windows® version of LS-DYNA was selected for this project based upon its advanced modeling capabilities and current use in industry. The version of LS-DYNA used for analysis in this research project running on a dual-processor personal computer is PC-DYNA version 970 Rev 5434, June 2004, produced by Livermore Software Technology Corporation in Livermore, California.

5.3 LS-DYNA Program Manager

The main executable file for LS-DYNA is the *Program Manager*, whose screen window is shown in Figure 5.1.

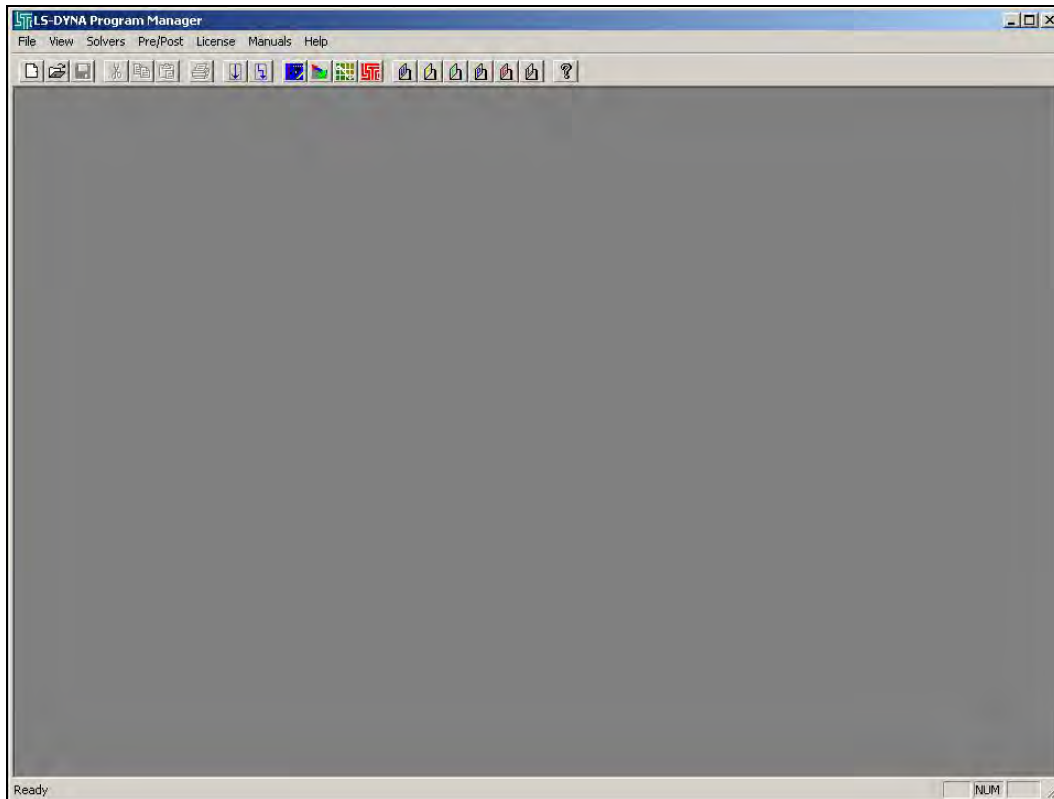


Figure 5.1: “Program Manager” screen of LS-DYNA

This window is used to run the finite element solver and launch LS-DYNA’s necessary sub-applications, including the pre-processor (*eta/FEMB-PC*), the solver, the post-processor (*PostGL*), and the graph processor (*eta Graph*). LS-DYNA user manuals for pre-processing, post-processing, graph processing and theory are available within the *Program Manager* in Adobe Acrobat (PDF) format.

5.3.2 Pre-processing

Within the pre-processor (*eta/FEMB-PC*), models are created and edited. The pre-processor can be launched either by selecting the appropriate icon from the *Program Manager* task bar, or by opening it through the *Pre/Post* menu located at the top of the *Program Manager* screen. As shown in Figure 5.2, the pre-processor can graphically display the three-dimensional geometry of the structure being modeled. The pre-processor also includes menu commands for creating an input file for the solver.

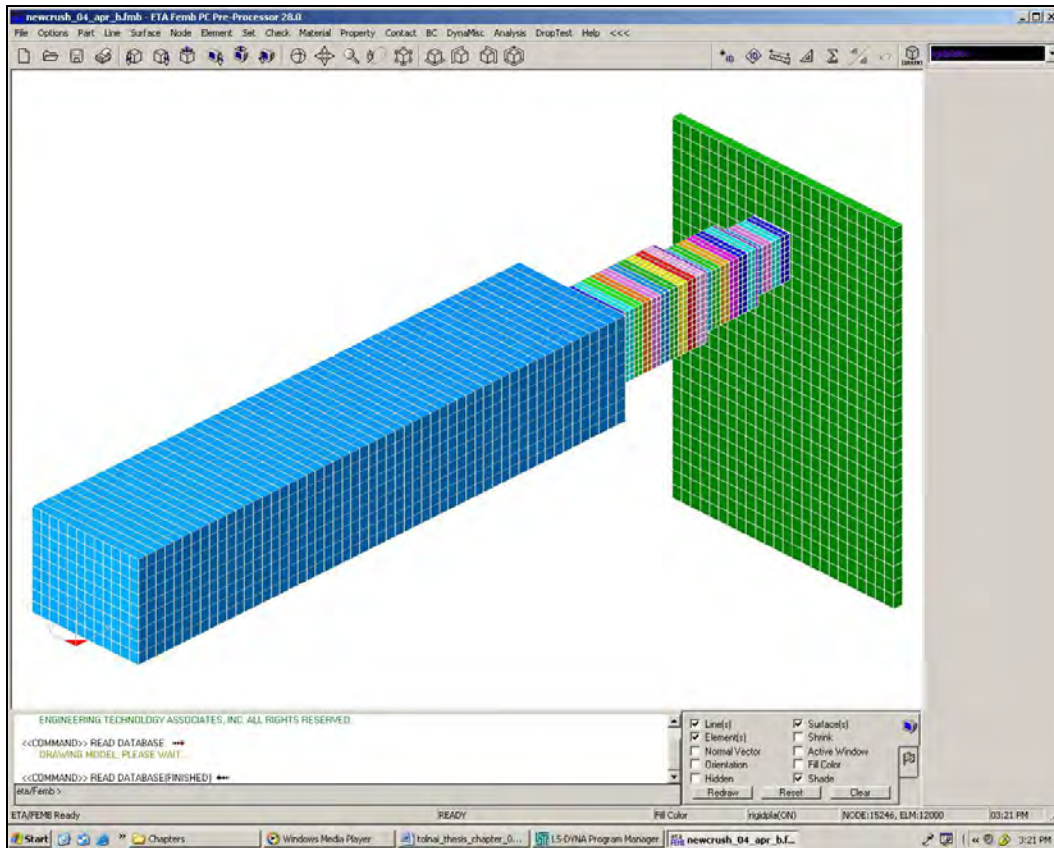


Figure 5.2: Example of three-dimensional input geometry created using the pre-processor (*eta/FEM-PC*)

5.3.3 Post-Processing

The post-processor (*PostGL*) allows the user to display many types of output, including the following: three-dimensional animations of model simulations; animated contour plots of stresses and strains within model elements; and the time variation of displacement or velocity of a specified node within the model. Figure 5.3 depicts one frame of a typical crash animation using the post-processor.

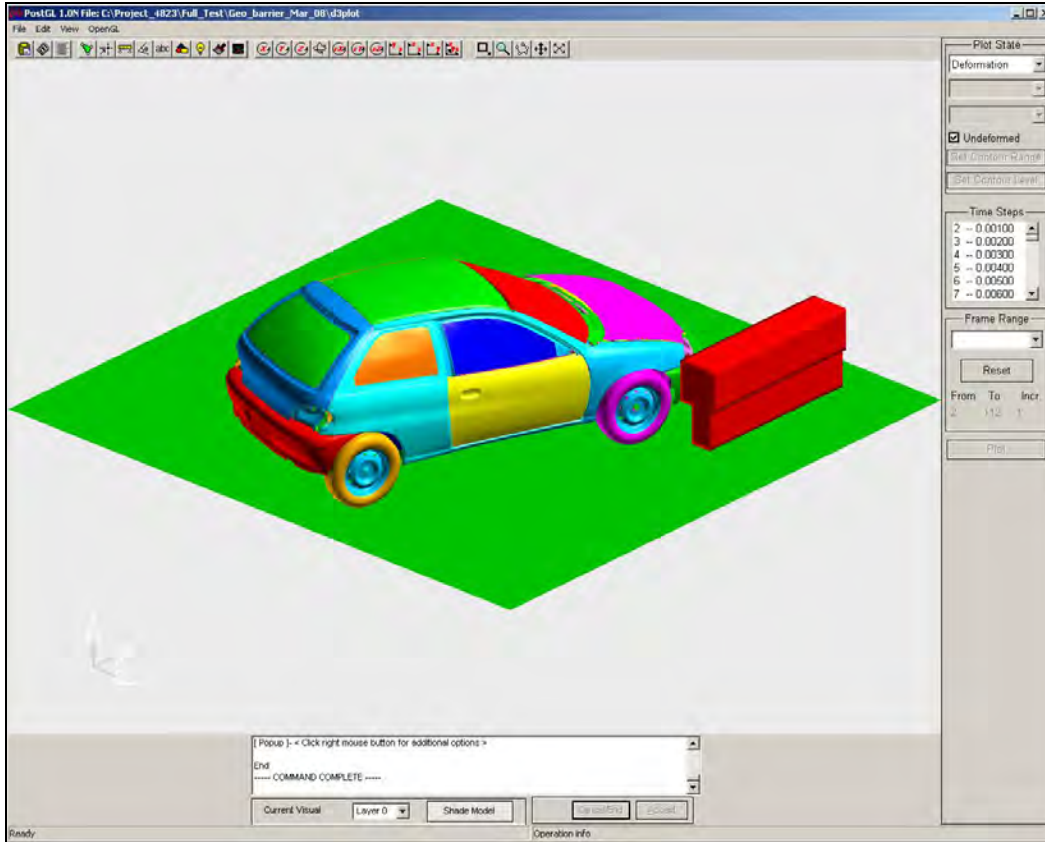


Figure 5.3: Sample model crash animation using the post-processor (PostGL)

5.3.4 Graph Processing

While the post-processor is capable of producing realistic animations of the crash simulations, the graph processor (*eta Graph*) offers additional graphing capabilities. Within a given model, using *eta Graph*, the user can define and then display the desired output information, including the time variations of forces at contact surfaces, displacements, velocities and accelerations of various nodes, and model energies. Figure 5.4 shows one such plot of contact forces with respect to time. In addition, several plots can be overlapped for comparison, and areas under curves can be calculated, which is useful in calculating the impulse of a given crash.

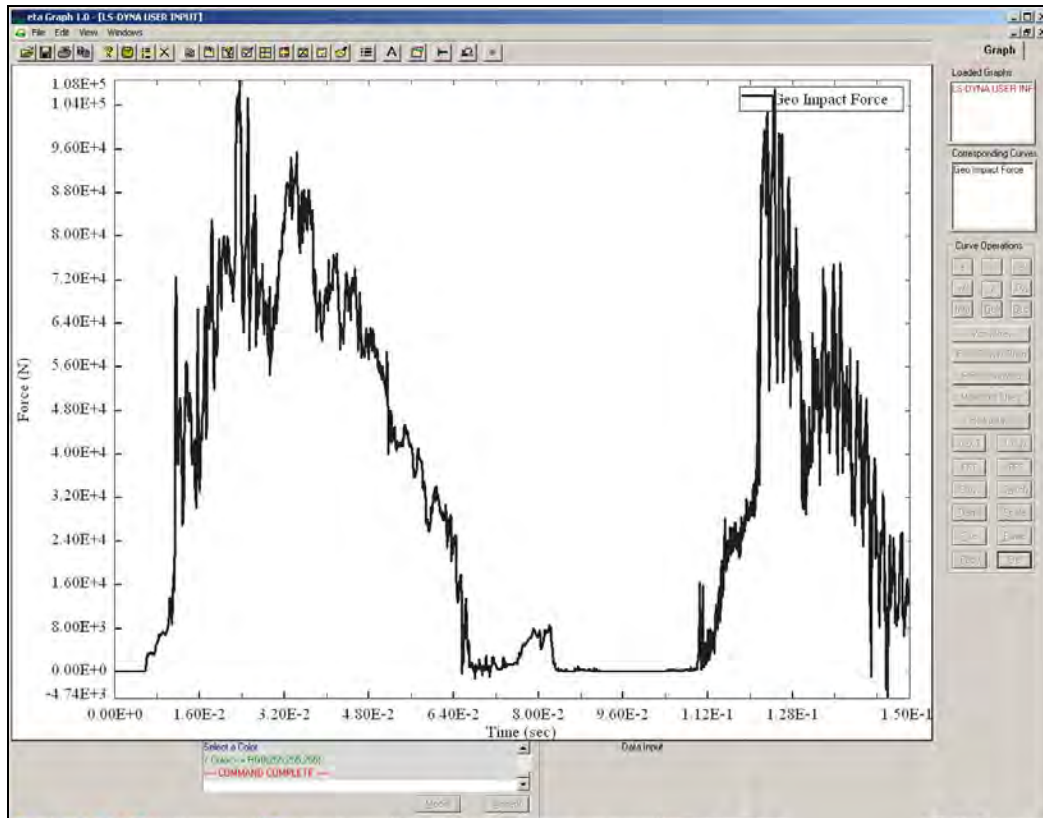


Figure 5.4: Example force-time graph using post-processor (*eta Graph*)

5.4 Before Beginning to Use LS-DYNA

A variety of existing LS-DYNA-compatible models is available for free download on established websites, such as that of the FHWA/NHTSA Crash Analysis Center (NCAC 2004). Downloaded models of approved crash vehicles and roadside hardware can be combined with user-defined barrier models to simulate complex crashes.

For a vehicle data file to be available for importing, it must be saved onto the hard drive of the same computer that will be used to perform the LS-DYNA analyses. From within the LS-DYNA pre-processor, the import command is given under the *File* menu. The user is then prompted to select the file to be imported. For FHWA vehicle models, appropriate files for importation are those with the file extension *.key*. The process by which a vehicle model is downloaded and used is explained in Chapter 4 of Tolnai (2005).

LS-DYNA has no fixed system of units, requiring only a consistent set of units. Establishing a consistent set of units before beginning is important for continuity of the model, and for interpreting the corresponding results. When importing models built by other users, one has the option to select the desired set of units, to ensure that imported models and user-generated models are compatible.

5.5 Overview of Major Steps Involved in Using LS-DYNA

A user can choose among many ways to generate finite element simulations for crashworthiness studies. The general steps used to simulate a crash simulation using LS-DYNA are the following:

- create a file and folder for the model;
- define each *PART* comprising the model;
- create nodes and lines for each part;
- create elements and a mesh for each part;
- define element properties for each *PART*;
- select and modify material models for each *PART*;
- set up initial conditions and boundary conditions;
- create contact surfaces;
- choose information for output; and
- run the defined model.

Each step is addressed further in the following sections. Generation of models specific to Project 4823 is discussed in Chapter 6.

5.6 Create a File and Folder for the Model

It is important to set up a file folder for each model. The program runs more quickly if the folders and files are stored on a local hard drive rather than a network fileserver. Each folder should contain the model file used in the pre-processor, the file used in the LS-DYNA solver, and all output files. LS-DYNA does not permit the user to run two model files from within the same folder, because output files for different models have the same names and cannot be overwritten. Because LS-DYNA does not have an “undo” button, it is vital to save each version of a model. It is best to create a completely new folder and re-save when making changes to existing models. In this way, if a particular change does not produce the desired result, or if a model should become corrupted, the previous version of the model still exists.

The files used by the LS-DYNA solver have the suffix *.dyn*. Each such file is a text file composed of a series of “*CARDS*” which are essentially blocks of input information relating to a single aspect of a model, such as nodal locations, selected materials, or boundary conditions. The required format of each *CARD* is given in the *LS-DYNA User’s Manual*, and a user could potentially create the text file and cards manually. It is easier, however, to use the pre-processor (*eta/FEMB-PC*), which automatically produces the *.dyn* file in the correct format when a built model is exported. Each *CARD* can also be defined in detail through the menu options within the pre-processor. Slight modifications to the *.dyn* file can then be made manually. A sample *.dyn* file is given in Appendix A.

5.7 Define Each PART Comprising the Model

The first step in creating a three-dimensional finite element model in LS-DYNA is to define the model geometry, including the size and shape of the objects to be analyzed, and the components comprising them. Within the LS-DYNA pre-processor, each component of the entire model must be designated as a separate “part.” For instance, a bridge railing model may consist of two parts: the concrete portion and the post-installed reinforcing bars. A laboratory pendulum may be composed of the steel body and a crush package mounted on the front of that body. Each *PART* can be assigned different properties and material definitions, but a *PART* may have at most one material and property. Though the *PART* menu, one may create, name, and edit various *PART* cards. The *PART* menu, along with an example card, is shown Figure 5.5.

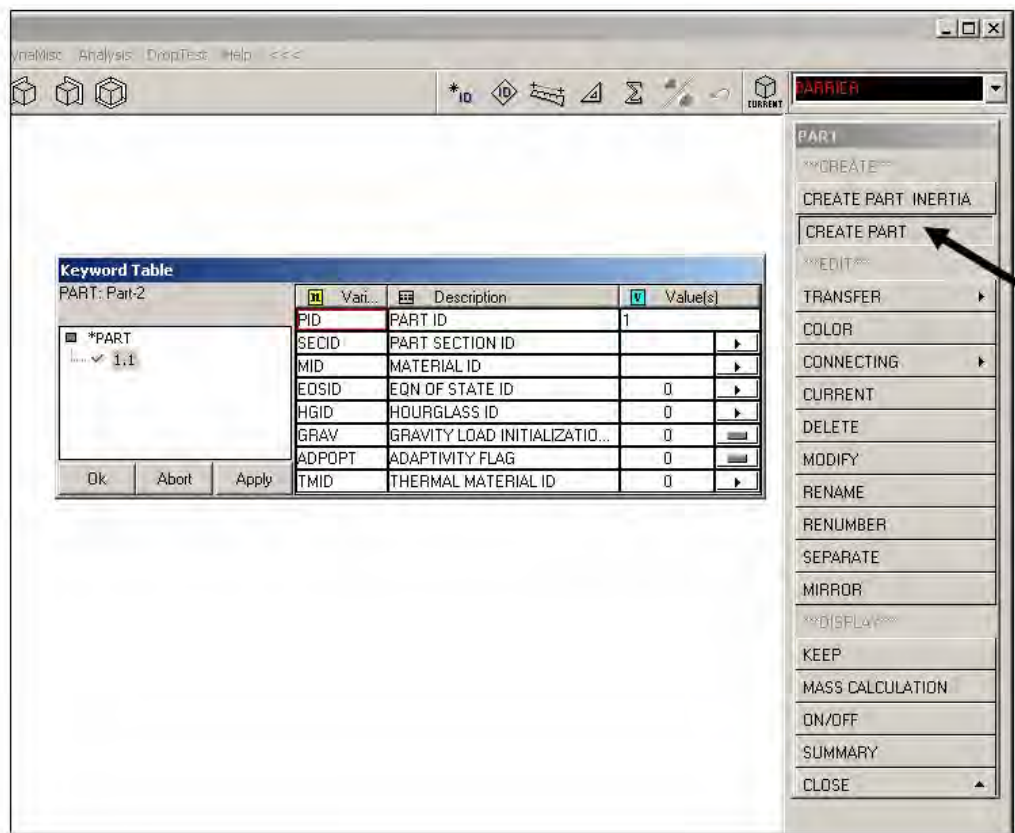


Figure 5.5: Typical PART menu and card

5.8 Create Nodes and Lines for Each PART

Once each *PART* has been created, the physical boundaries of each part must be established. In the case of geometrically regular, block-like objects, such as a barrier or a laboratory pendulum, the easiest way to establish boundaries is to create nodes in three-dimensional space that define the perimeter of the *PART*. Although a *PART* can theoretically be oriented in any direction, it is helpful to orient it in a meaningful manner. For instance, it may be beneficial to orient it so that the initial conditions (for example, initial velocity) occur predominantly in a single global direction, or so that the desired output forces occur in a global

direction. Commands for defining nodes by global coordinates are given under the *NODE* menu. Once a *PART* has been created using a convenient initial orientation, that orientation can be changed using the *TRANSFORM* command in the *NODES* menu.

5.8.1 Create Nodes for Each PART

To begin creating nodes, one must make sure that the desired *PART* is listed in the current window. After selecting *CREATE* under the *NODE* menu, the nodes can be defined by global coordinates using the *Key-In* command. Figure 5.6 depicts a typical node creation command window.

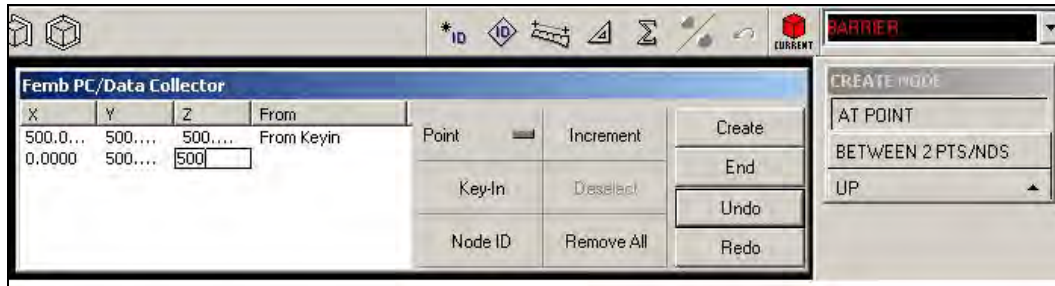


Figure 5.6: Typical node-creation menu

5.8.2 Create Lines for Each PART

Once all nodes are defined, they must be connected by lines to create a skeleton outline of the geometry of the *PART*. Using the *CREATE* command within the *LINE* menu, one creates lines by selecting two nodes with the cursor, and then selecting *CREATE*. To create lines between nodes, *NODE* (rather than *POINT*) must be active in the selection window. Each line between two nodes must be created separately; otherwise, it is possible that two line segments having two different axial orientations will be viewed by the solver as a single line. Examples of proper and improper node selection are shown in Figure 5.7.

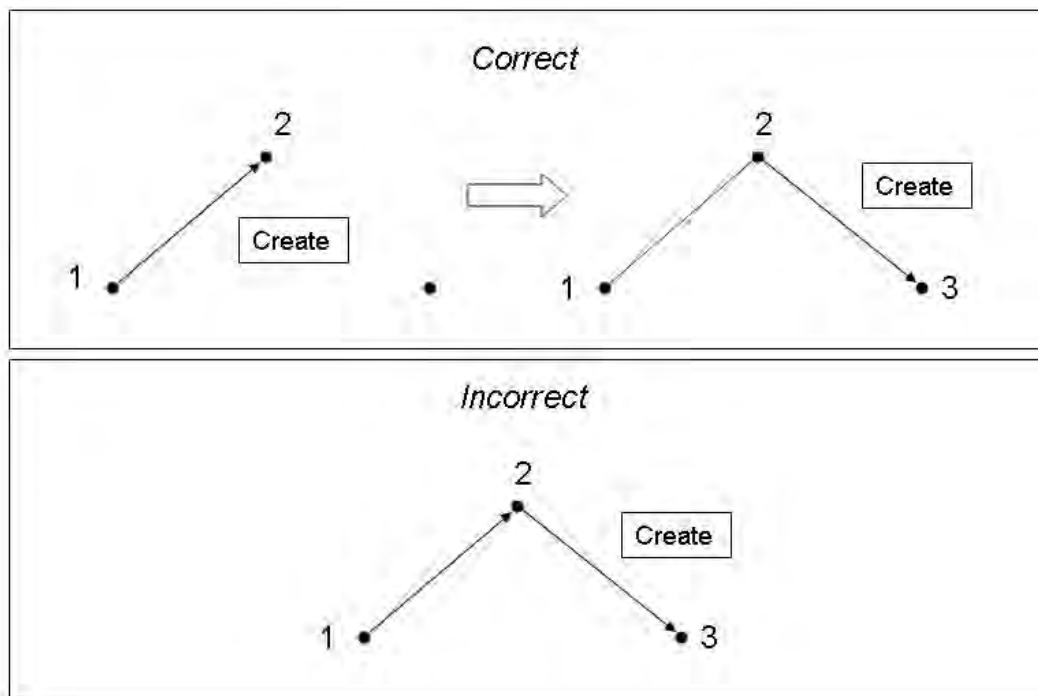


Figure 5.7: Examples of proper and improper node-selection techniques

Upon completion of line creation, each geometrically regular shape (such as a rectangular solid) consists of twelve lines, as shown in Figure 5.8. This framework of lines is then used to create the three-dimensional solid mesh of finite elements. If an object (like a T203 bridge rail), can be broken down into two simple component shapes, each shape should be created separately within the same *PART*. Thus, a single *PART* may consist of twenty-four lines instead of twelve.

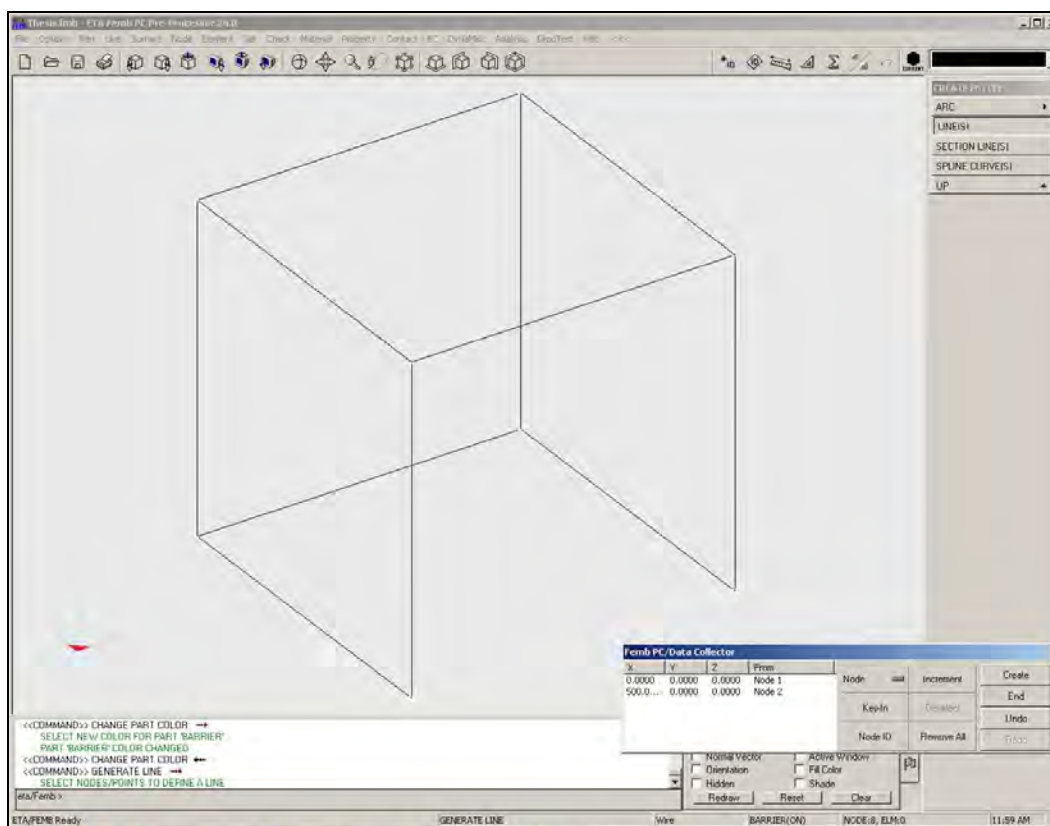


Figure 5.8: Example of geometric line framework

Commands for creating and editing lines are given under the *LINE* menu. All newly created nodes and lines are associated with whichever part is listed in the *CURRENT* field. Thus, when all nodes and lines for a particular *PART* are defined, the user must select a new *PART* in the *CURRENT PART* field before creating nodes and lines for a new part.

5.9 Create Elements and a Mesh for Each PART

The next step in creating a usable finite element model is to “mesh” the defined parts, including defining the density and arrangement of finite elements. There are many ways to create a solid mesh with LS-DYNA. A relatively easy way to create solid brick elements from the previously created lines is to use a 12-line plate/solid meshing tool. This tool requires the user to click on the twelve lines which define the part, and then allows the user to define the fineness of element size in each local direction. Options related to this task are given in the pre-processor under the *ELEMENT* menu.

One begins by selecting the four coplanar lines defining one face of the part to be meshed. Though the direction is irrelevant, the user must select these lines in a clockwise or counter-clockwise direction. Accordingly, once a line is selected, the next line chosen must be in contact with that first line, and so on. Lines must be selected in a consistent order—either clockwise or counterclockwise. The final four lines are then selected in order, with the first line connecting the corners formed by Lines 1 and 4, the second line connecting the corners formed by Lines 1 and 2, and so on (Figure 5.9).

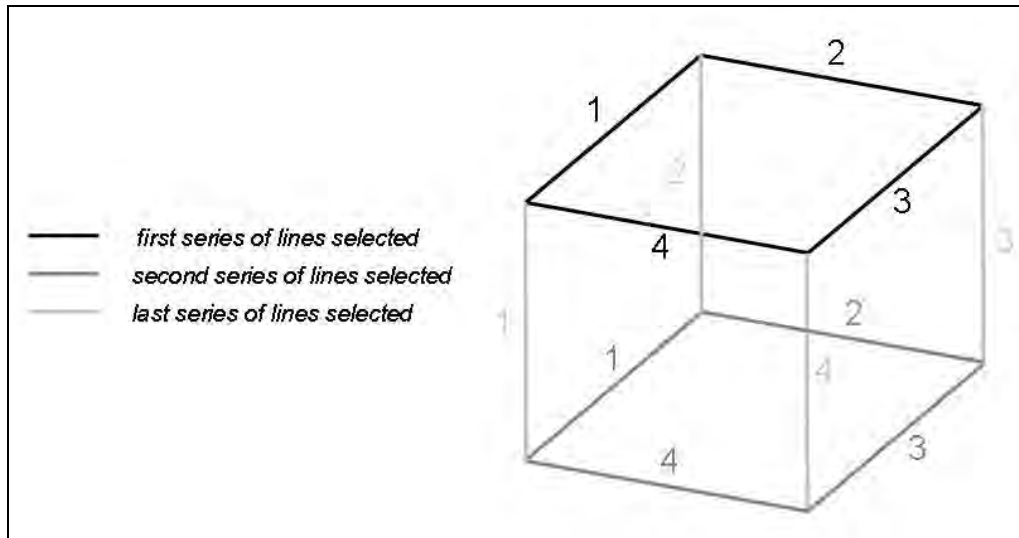


Figure 5.9: Order of line selection in mesh creation

Once all lines are selected, the user is prompted to enter the number of elements desired along each of the three local axes. The final result of meshing is a three-dimensional solid object consisting of smaller solid elements of the specified size. Once an object is meshed, a user has the option of modifying the size of individual elements using commands in the *ELEMENT* menu. Elements of arbitrary size and shape can also be created manually by selecting a series of eight nodes that outline the desired element shape.

The ratio of the longest dimension to the shortest dimension of an element is called its aspect ratio. Because of how finite element programs calculate displacements at the element boundaries, elements with smaller aspect ratios (that is, elements that are approximately cubical) are generally more accurate (Logan 1993). The National Crash Analysis Center (NCAC) at George Washington University recommends keeping aspect ratios between 1.0 and 5.0 (NCAC 2005). Another consideration in creating a mesh is the size of the elements relative to the size of the object that they comprise. In general, the smaller the elements (the denser the mesh), the more accurate the analysis, and also the greater the required computational effort.

5.10 Define Element Properties for Each PART

A *PART* can be assigned one of several types of element properties, including shells, solids, beams, and springs. Downloaded vehicle models typically consist of shell elements, which are three- and four-noded elements used to model three-dimensional plate-like surfaces and membranes (Livermore Software Technology Corporation 2003). To model solid, three-dimensional objects, the *SOLID* property is a logical choice. Beams are defined as two-noded elements used to represent members such as three-dimensional beams or truss members (Livermore Software Technology Corporation 2003). Beams can be used to create axially-loaded members such as concrete reinforcing bars. Other element properties also exist, such as spring/damper elements. *PART* properties are defined through the *PROPERTY* menu within LS-DYNA, as shown in Figure 5.10. Once a property is defined, it must be assigned to the desired *PART* using the *ASSIGN* command.

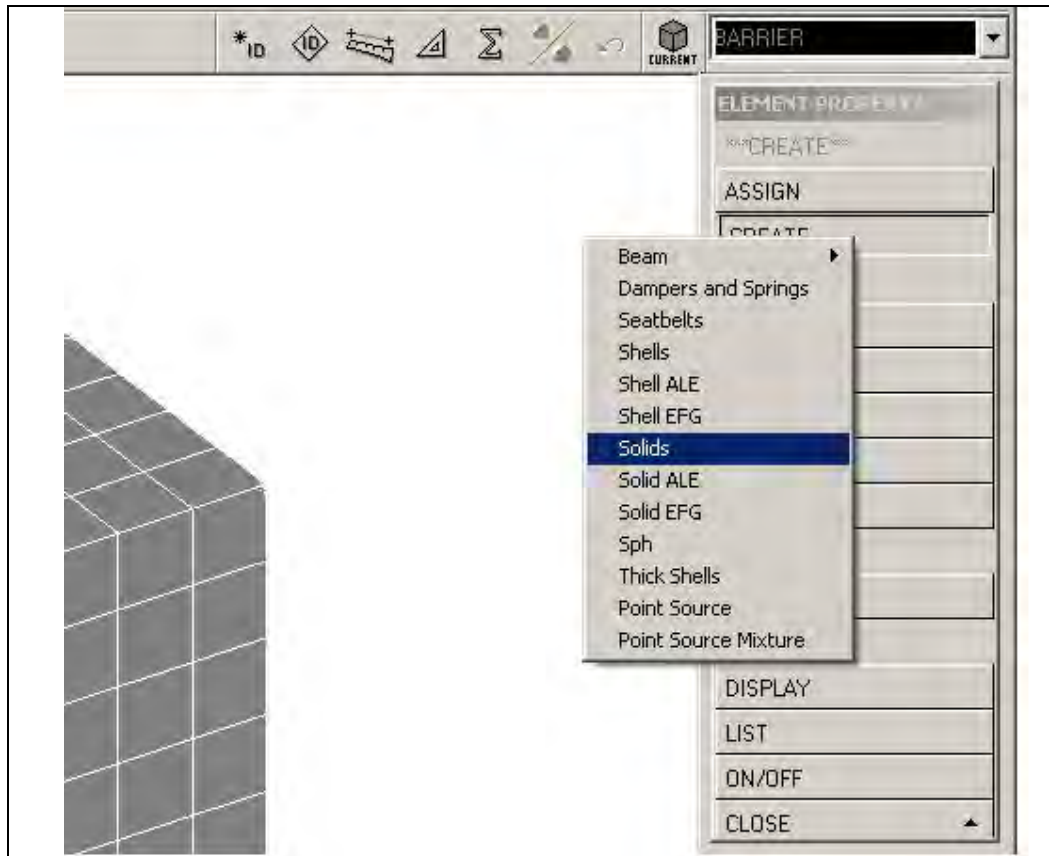


Figure 5.10: Example of element property selection

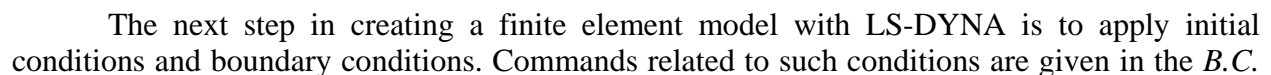
5.11 Select and Modify Materials for Each Part

Within the *MATERIAL* menu, the user can define, edit, and assign material properties to the created *PARTS*. Selecting an appropriate material model is perhaps the most significant part of creating a model. LS-DYNA has over two hundred predefined material models, some of which can be used only for specific element types, or to represent specific material properties. The elastic material model, for instance, can be used for all solid and shell elements and most beam elements, but does not address failure or strain-rate effects. A honeycomb material model, in contrast, can be used only for solid brick elements, but can address both failure and strain-rate effects (Livermore Software Technology Corporation 2003).

Each material model consists of one or more cards of input information, which are automatically produced when that material model is selected, and which contain the appropriate user prompts for that material. Material properties common to most predefined models are mass density, modulus of elasticity, and Poisson's ratio. Other properties, such as yield stress, failure strain, or tangent modulus, may be required for particular material models. Simpler material models, such as elastic or plastic with kinematic hardening, require a limited number of input values. Some more complex models also require the user to enter load-displacement or stress-strain curves, using the *LOAD CURVE* command in the *DYNA MISCELLANEOUS* menu.

To create a specific material in the pre-processor, the user selects the *CREATE* option in the *MATERIAL* menu, and is prompted to select either a structural or a spring/damper type

5.12 Set Up Initial Conditions and Boundary Conditions



51



51

51

51

menu. Initial conditions and boundary conditions can be assigned to an object or group of nodes either by individually selecting the nodes comprising the object, or by creating a *NODE SET* to which the conditions can be applied. The latter is discussed in the next subsection.

5.12.1 Create a Node Set for Initial Conditions or Boundary Conditions

Instead of selecting nodes individually, or even by a given region, a user can create a *NODE SET* to which boundary conditions can be applied. This process simplifies the application of boundary conditions, and also ensures that all desired nodes are included, as when an initial velocity is applied to all nodes in a specified *PART*. In addition, one *NODE SET* can be used to apply more than one type of boundary condition, making model creation more user-friendly. Various *NODE SETs* can be defined using the *SET* menu, selecting *NODE*, and then selecting the desired nodes by part, by region, or individually. The menu for creating a *NODE SET* is shown in Figure 5.13. To the same end, a user can create sets of parts or elements for applying various conditions in the model.

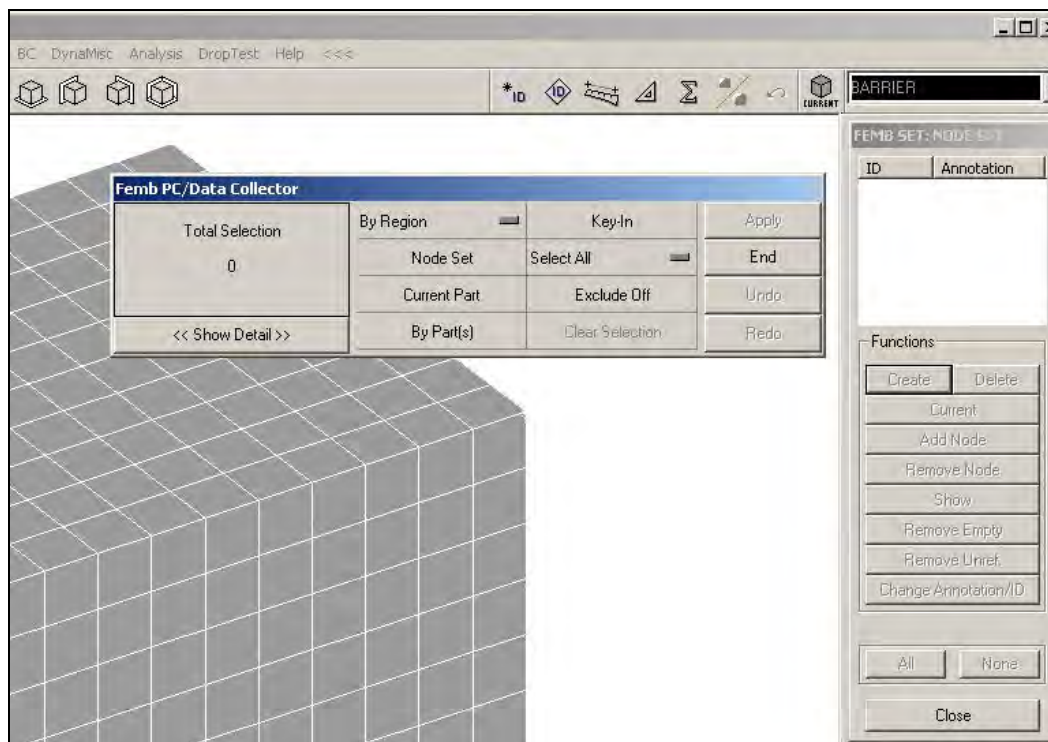


Figure 5.13: Sample menu for creating a node set

5.12.2 Apply Initial Conditions

Useful initial conditions for crash simulations include characteristics (such as velocities or accelerations) imposed on *PARTS* and *NODES*. For vehicle impact simulation, initial velocity is most useful. The *INITIAL CONDITION* menu (within *B.C.*) allows the user to select initial *VELOCITY*, as shown in Figure 5.14.

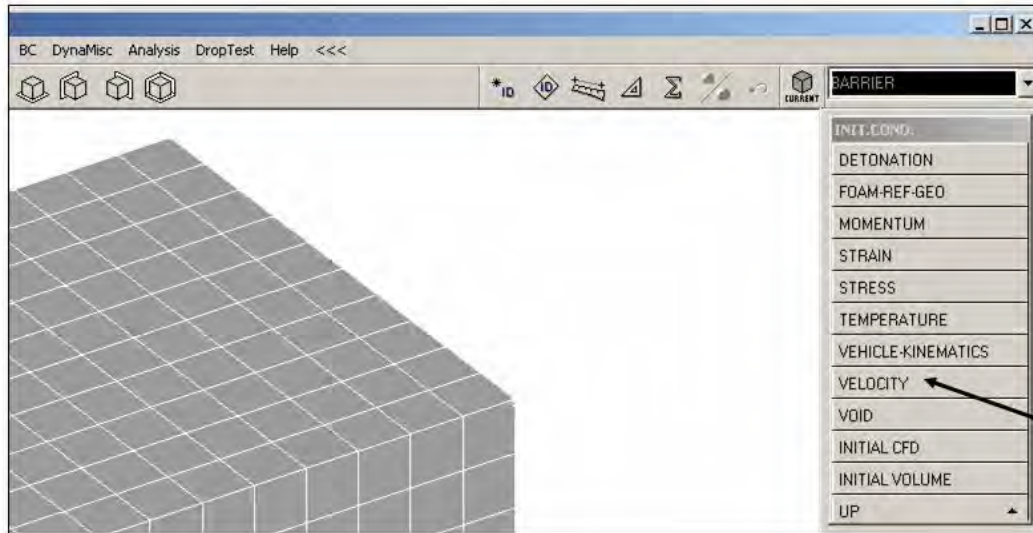


Figure 5.14: Initial Condition menu

When the user selects *VELOCITY*, an initial velocity card is created, using either individual nodes or a *NODE SET*. Initial translational or rotational velocities can be defined in global coordinates, using the input menu shown in Figure 5.15. Once initial velocities are defined, the resultant velocity vector at each node is displayed as in Figure 5.16.

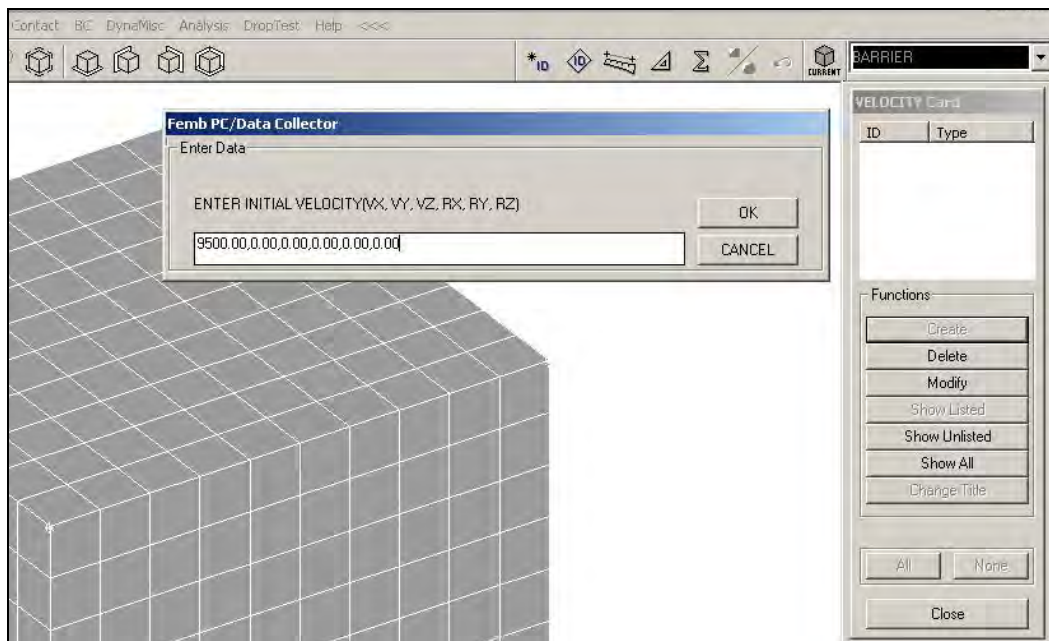


Figure 5.15: Example of how to create an Initial Velocity CARD

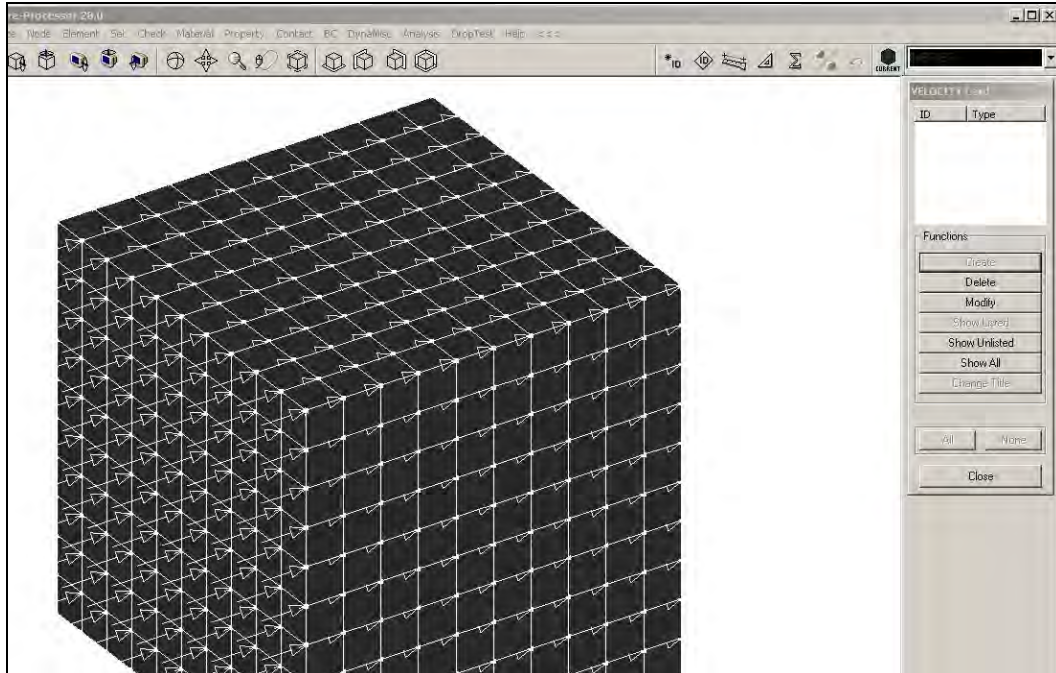


Figure 5.16: Sample display of Initial Velocity

5.12.3 Apply Boundary Conditions

Boundary conditions are applied by selecting, within the *B.C.* menu, the *BOUNDARY* option. As shown in Figure 5.17, many types of boundary conditions can be applied in many ways. The *SPC* (Single Point Constraint) option is often the most useful of these, and allows a user to apply any combination of translational or rotational restraint in global coordinates.

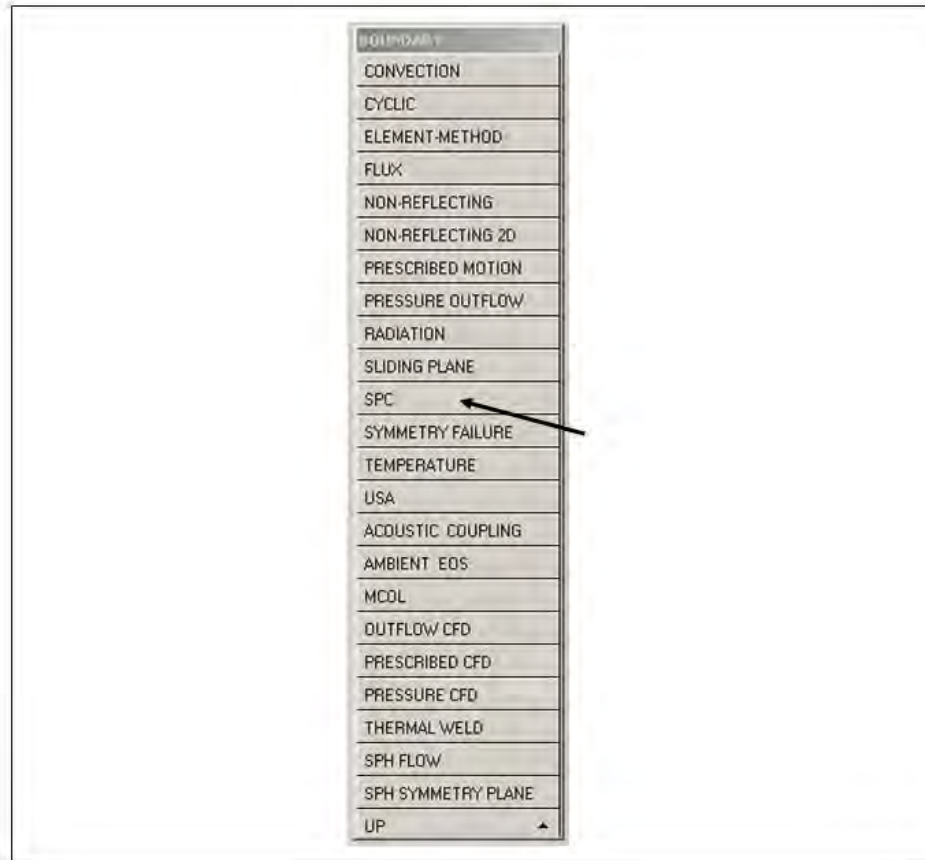


Figure 5.17: Boundary condition menu

Once a user opts to create an *SPC CARD*, a menu appears in which the restraints can be selected, after which they are displayed by number at the appropriate nodes. In the example shown in Figure 5.18, restraints 1 (x-translation), 2 (y-translation), and 6 (z-rotation) are applied to every node in a cube.

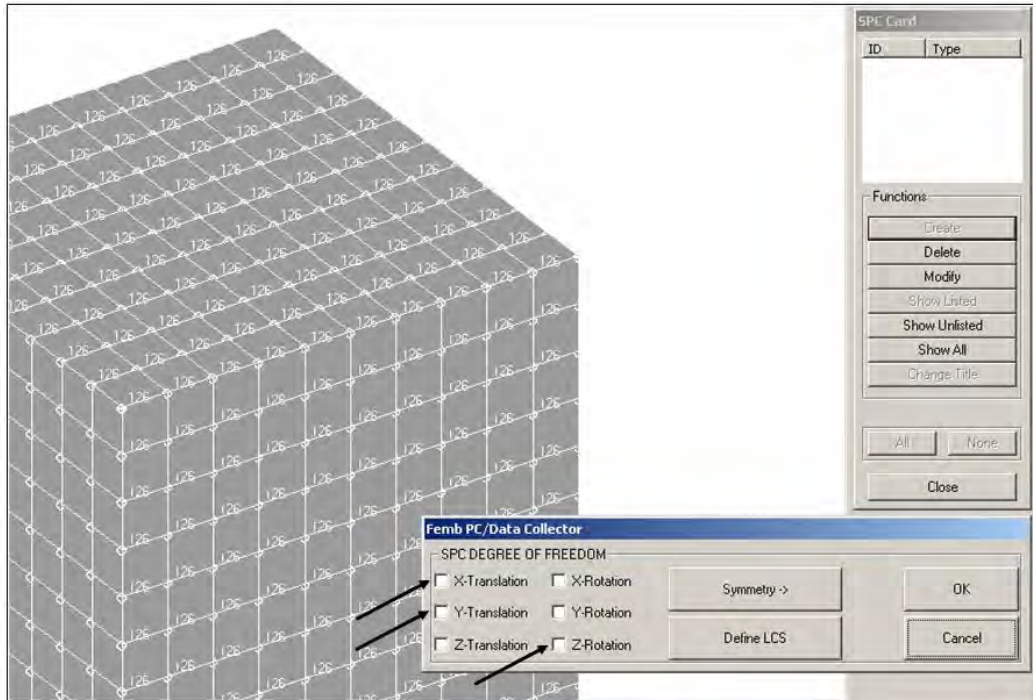


Figure 5.18: Example of assigning SPC boundary conditions

5.13 Create Contact Surfaces

After boundary conditions and initial velocities are applied to their respective *PARTS*, the fact that two *PARTS* may be in contact for the analysis must be explicitly declared in the model by creating a *CONTACT* card. To create a contact surface, the user must first select *CREATE*, and then *CONTACT*. Several types of contact surface options are then displayed (Figure 5.19). A three-dimensional contact option is appropriate for crash simulations, as most *PARTS* in these models are three-dimensional and their surfaces, rather than only their nodes, are anticipated to be in contact with each other.

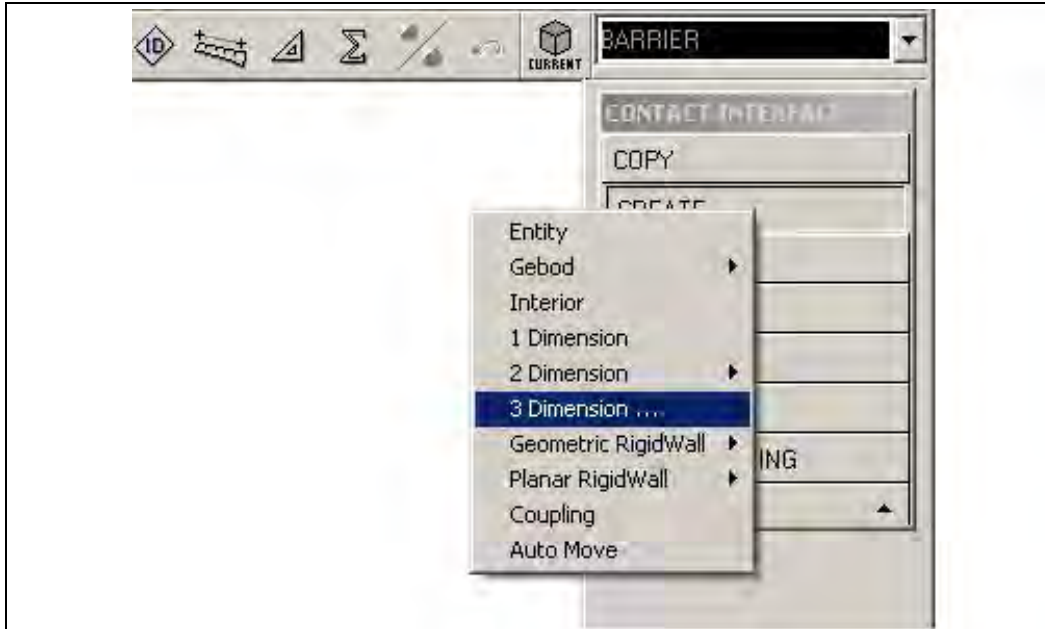


Figure 5.19: Menu of types of contact surface

Once the three-dimensional contact has been selected, a list of contact surface types appears (Figure 5.20). Of these, the most versatile and useful for impact analyses is the *AUTOMATIC_SURFACE_TO_SURFACE* contact, which can be used for almost all impact situations and requires little input information from the user. Contacts should be defined for all surfaces in the model where contact is anticipated. No default contact is defined in LS-DYNA. If a contact *CARD* is not created, objects that touch simply pass through each other, occupying the same space at the same time.

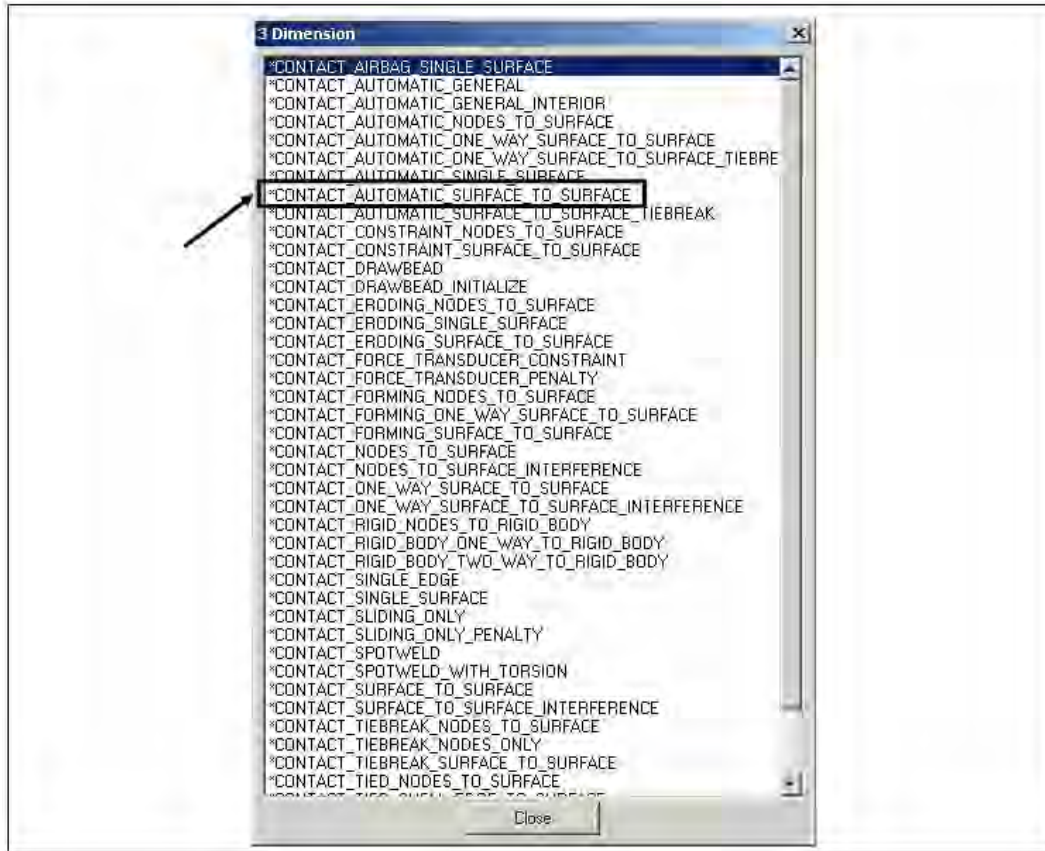


Figure 5.20: List of three-dimensional contact types

Once the *AUTOMATIC_SURFACE_TO_SURFACE* contact type is selected, the *AUTOMATIC_SURFACE_TO_SURFACE CARD* appears (Figure 5.21). Fields requiring user input are slave and master designations and slave and master IDs. When two objects are to be considered in potential contact, one must be selected as the master surface, and the other as the slave surface. Under most circumstances, the nodes of the slave surfaces cannot penetrate the geometry of the master surface. To minimize anomalies in applying this concept, the master surface should be the stiffer of the two materials in question or the larger surface with the coarser mesh (AC Engineering, Inc. 1996). The other surface should therefore be selected as the slave surface. LS-DYNA allows a user to define the master and slave surfaces in a variety of ways, the easiest of which is to select the surfaces by *PART*. Other options in the contact *CARD* include static and dynamic coefficients of friction for contact surfaces, and toggling checks for small penetrations between surfaces.

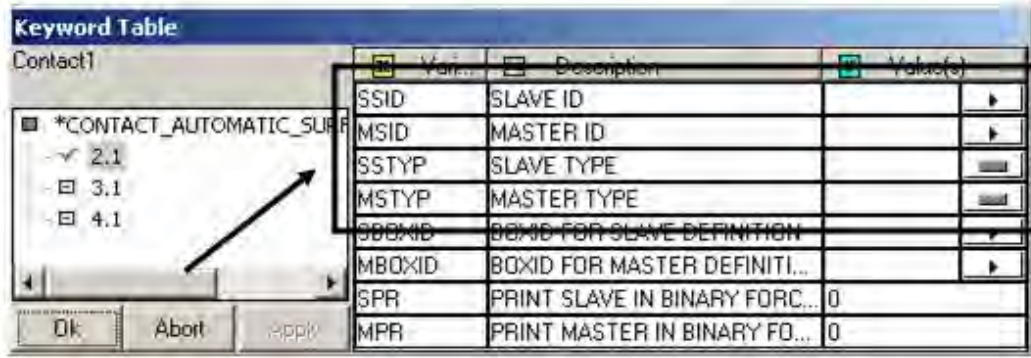


Figure 5.21: AUTOMATIC_SURFACE_TO_SURFACE CARD

5.14 Select Information for Output

When the geometric definition of the model is finished, output parameters must be selected through the *DYNA MISCELLANEOUS* menu, shown in *Column A* of Figure 5.22. From within that menu, *CONTROL* and *DATABASE*, shown respectively in *Columns B* and *C* of Figure 5.22, are the two most useful output categories. Within *CONTROL*, a user is permitted to define the termination time (time at which the analysis should end). To capture the period from 0.0 to 0.15 seconds in real time of a crash simulation, for instance, the termination time should be defined as 0.15 sec. This menu also permits the user to modify the time interval at which the solver integrates the solution, the way in which contact surfaces are calculated, and the energy equations on which the solutions are based.

The *DATABASE* menu contains two important sub-categories for specifying the desired output information: *ASCII* and *BINARY*. As shown in *Column C* of Figure 5.22, within those subcategories, *ELOUT*, *NODOUT* and *RCFORC* are useful for crash simulations. *ELOUT* and *NODOUT* refer to “element output” and “node output” respectively. By defining a time interval for these two output types, the user can obtain response histories for forces within beam elements, and displacement and acceleration histories for specified nodes. The beam elements and nodes for which output is desired must be selected within the *HISTORY* card, which is also given in the *DATABASE* menu. *RCFORC*, which stands for “resultant contact force,” is additional useful information from a crash simulation. By defining a time interval for output, the user can create force-time histories for any of the model’s contact surfaces, such as the surface between the barrier and vehicle. The menus for setting up *RCFORC* for output are given in Figure 5.23.

Finally, to create stress-contour plots or displacement animations, the *D3PLOT* command must be defined with a time interval for output, as shown in *Column D* of Figure 5.22.

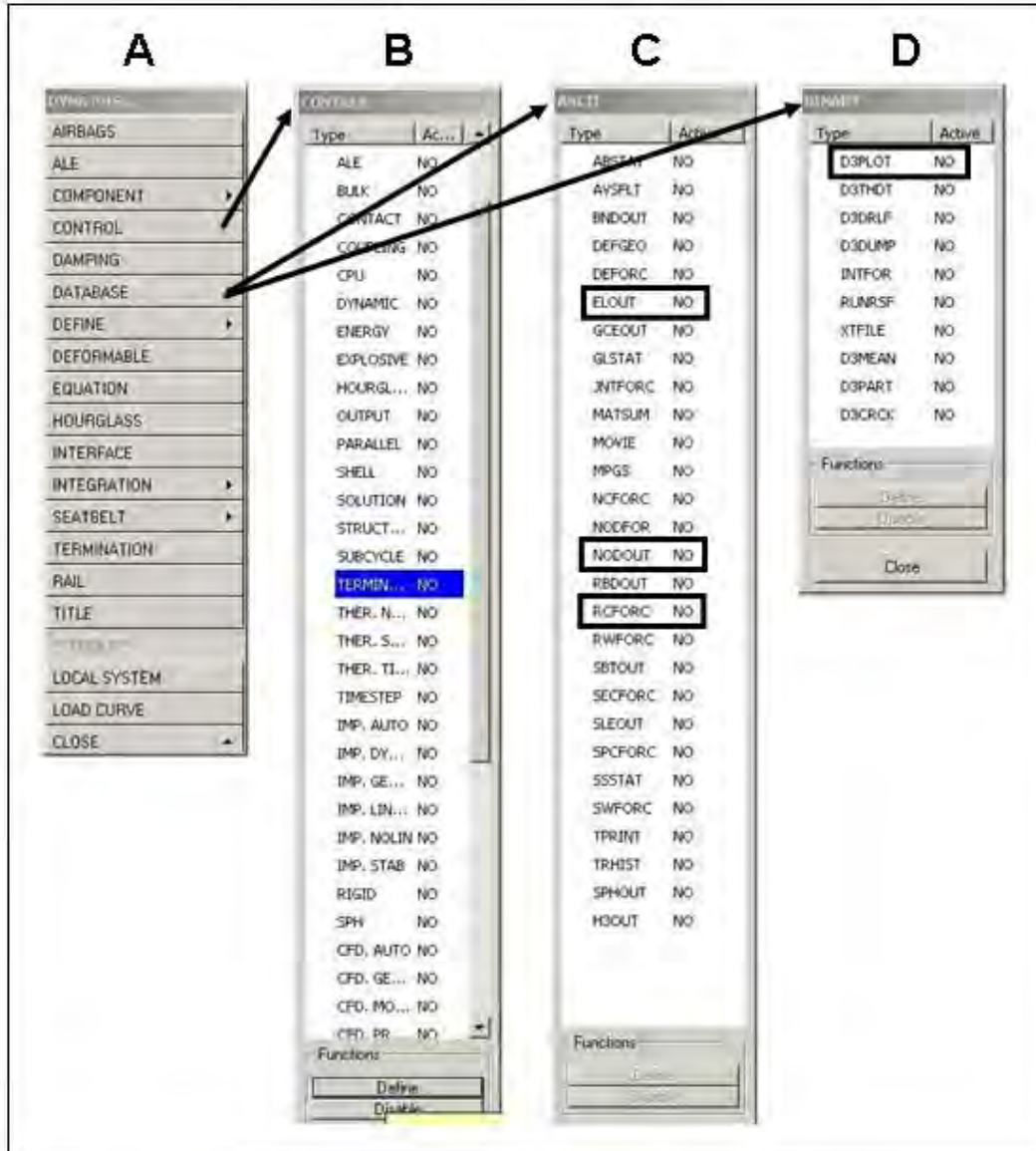


Figure 5.22: "DYNA Miscellaneous" Output Control Menus

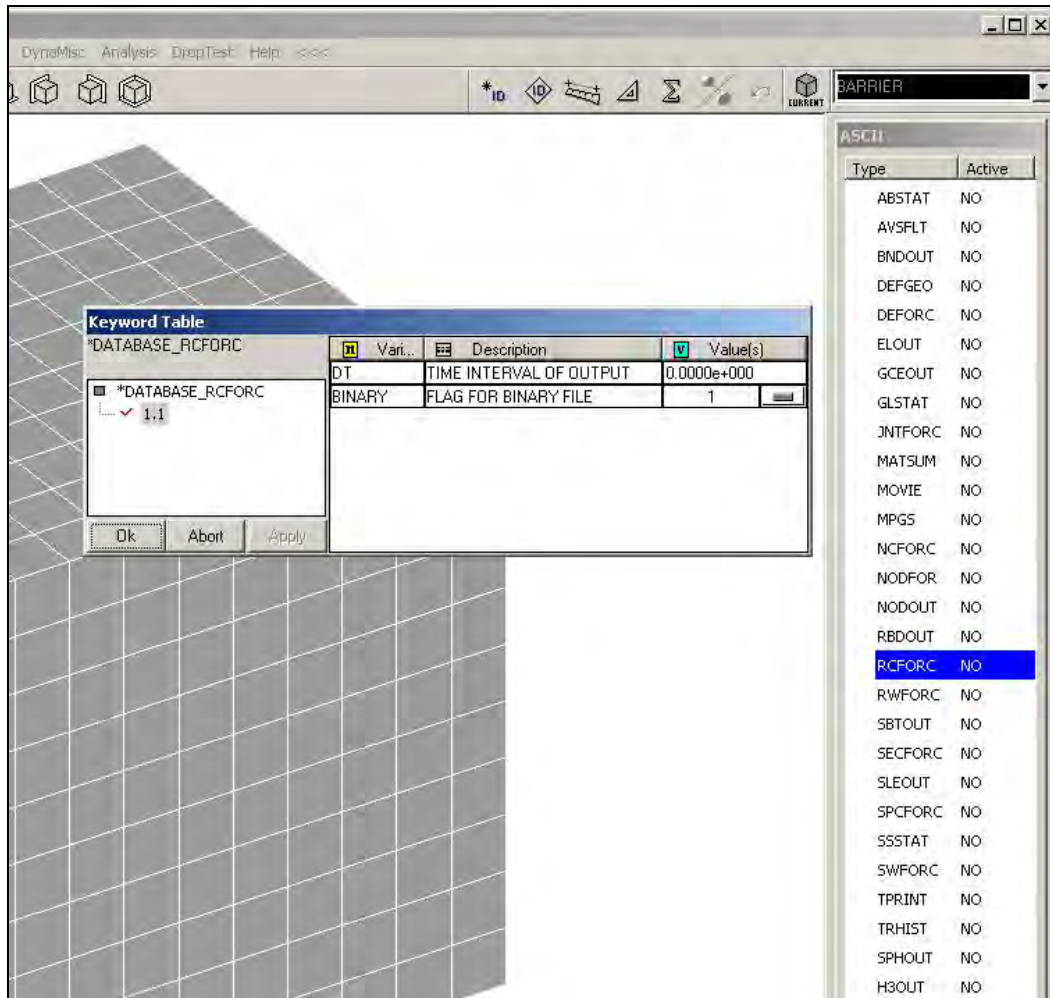


Figure 5.23: Output-control menus for Contact Forces (RCFORC)

5.15 Run the Defined LS-DYNA Model

Once all necessary *CARDs* are defined as described in the preceding sections, the model is ready to be analyzed. Previously created files have the file extension *.fmb*. The LS-DYNA solver, however, requires the file extension *.dyn*. To create this file, the model must be exported (menu heading *FILE*, *EXPORT* command), and assigned an appropriate file name. The preprocessor program is not needed for the model solution. As shown in Figure 5.24, the user must use the *SOLVERS* command in the *LS-DYNA Program Manager* to run an analysis.

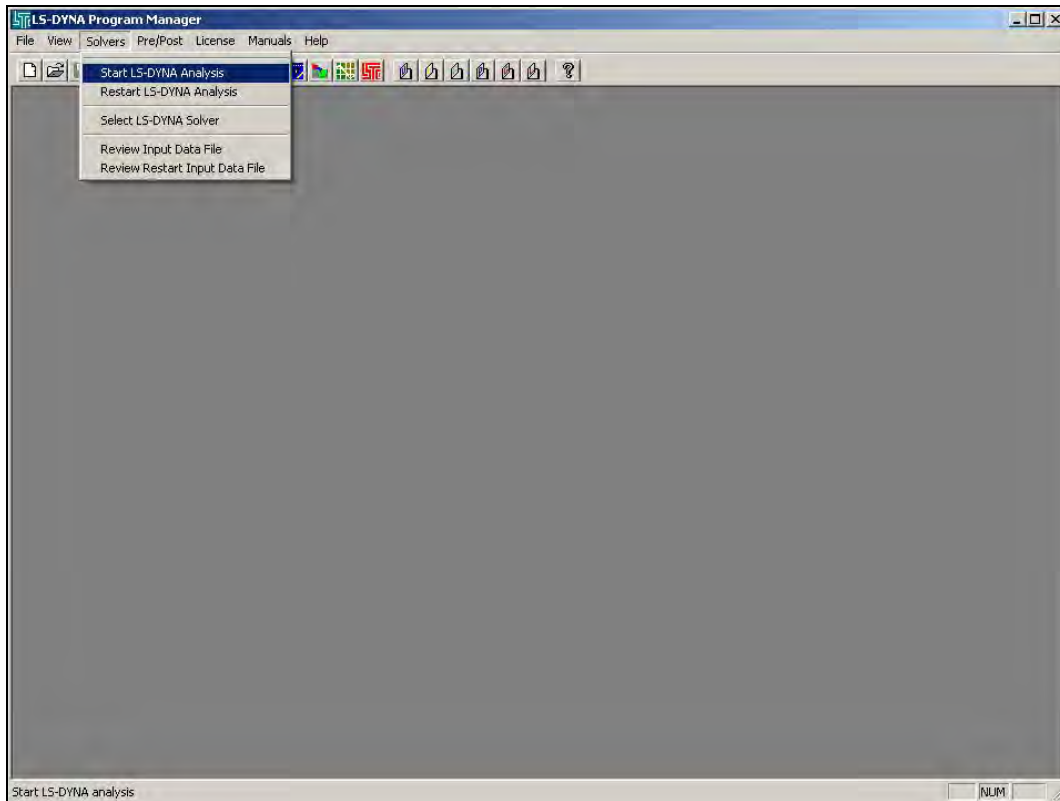


Figure 5.24: Starting the LS-DYNA Solver

Upon selecting “Start LS-DYNA Analysis,” the menu commands for setting up the analysis run are displayed (Figure 5.25). The desired analysis file can be selected using the *BROWSE* command within the *INPUT FILE* field. The *OUTPUT FILE* field should be filled in automatically by the program, because the output file destinations have already been specified indirectly within the pre-processor by selecting output information categories. If the analysis is run on a dual-processor micro-computer, the *NCPU* field, under the heading “Set Command Line Parameters,” should be changed to “2,” indicating two processors. If the input file is extremely large, the user may have to manually increase the number in the *MEMORY* field, under the heading “Set Command Line Parameters,” also shown in Figure 5.25. Once the input and output parameters are specified, clicking “OK” starts the analysis. While the analysis is running, a progress window automatically displays total input energies, and also updates the analysis time steps and eroded elements if erosion (i.e., failure and removal from the model) criteria have been specified. A typical progress window is shown in Figure 5.26.

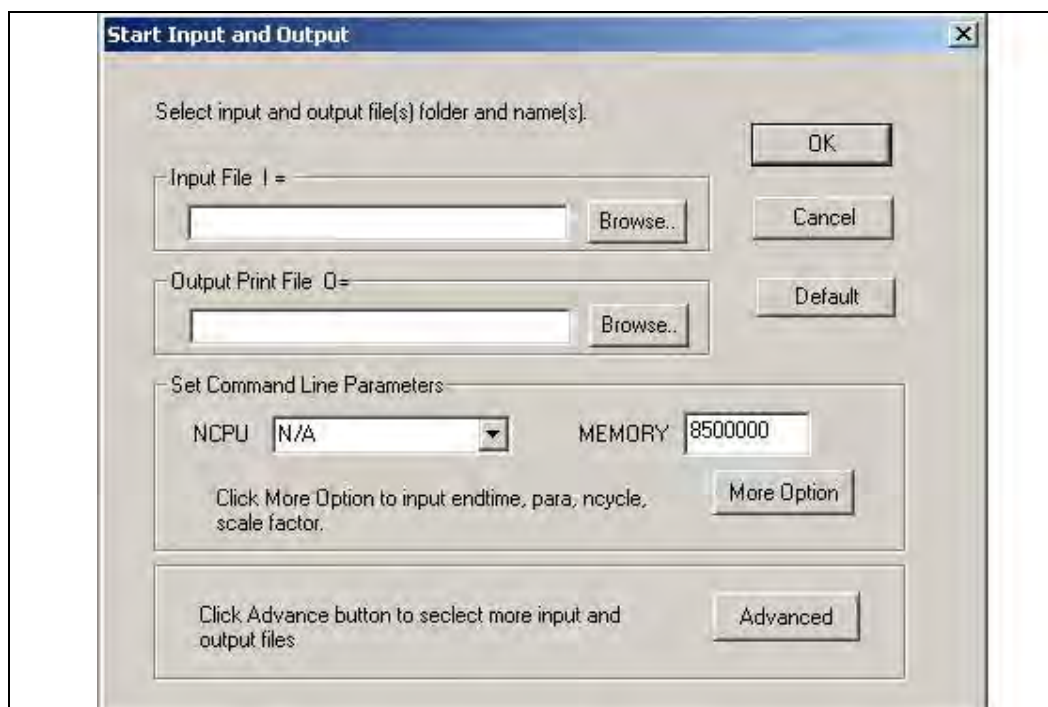


Figure 5.25: Menu with Solver settings

```

C:\I=PROJECT\1\HONEYC\1\H0AEB4\1\HONEYC\1.DYN O=C:\PROJECT\1\HONEYC\1\H0AEB4\1\d3hsp NCPU=2
Unauthorized use infringes LSTC copyrights

Input file: C:\PROJECT\1\HONEYC\1\H0AEB4\1\HONEYC\1.DYN

The native file format      : 32-bit small endian
Memory size from default   : 8500000

on UNIX computers note the following change:

ctrl-c interrupts ls-dyna and prompts for a sense switch.
type the desired sense switch: sw1., sw2., etc. to continue
the execution. ls-dyna will respond as explained in the users manual

type      response
-----
sw1.      a restart file is written and ls-dyna terminates.
sw2.      ls-dyna responds with time and cycle numbers.
sw3.      a restart file is written and ls-dyna continues calculations.
sw4.      a plot state is written and ls-dyna continues calculations.

***** notice ***** notice ***** notice *****
* This is the LS-DYNA Explicit Finite Element code. *
* Neither LSTC nor the authors assume any responsibility for *
* the validity, accuracy, or applicability of any results *
* obtained from this system. The user must verify his own *
* results. *
* LSTC endeavors to make the LS-DYNA code as complete, *
* accurate and easy to use as possible. *
* Suggestions and comments are welcomed. Please report any *
* errors encountered in either the documentation or results *
* immediately to LSTC through your site focus. *
* Copyright (C) 1990-2003 *
* by Livermore Software Technology Corp. (LSTC) *
* All rights reserved *
***** notice ***** notice ***** notice *****

input of data is completed

initial kinetic energy = 0.39704668E+08

The LS-DYNA time step size should not exceed 0.172E-05
to avoid contact instabilities. If the step size is
bigger then scale the penalty of the offending surface.

initialization completed

dt of cycle      1 is controlled by solid      element      84137

time..... 0.00000E+00
time step..... 1.41640E-06
kinetic energy..... 3.97027E+07
internal energy..... 1.00000E-20
spring and damper energy..... 1.00000E-20
system damping energy..... 0.00000E+00
sliding interface energy..... 0.00000E+00
external work..... 0.00000E+00
eroded kinetic energy..... 0.00000E+00
eroded internal energy..... 0.00000E+00
total energy..... 3.97027E+07
total energy / initial energy.. 1.00000E+00
energy ratio w/o eroded energy.. 1.00000E+00
global x velocity..... 1.99332E+03
global y velocity..... 0.00000E+00
global z velocity..... 0.00000E+00
cpu time..... 0 nanoseconds
average cpu time per zone cycle... 0 nanoseconds
average clock time per zone cycle.. 4159 nanoseconds

estimated total cpu time      =      0 sec <      0 hrs 0 mins>
estimated cpu time to complete =      0 sec <      0 hrs 0 mins>
estimated total clock time    =    3282 sec <      0 hrs 54 mins>

```

Figure 5.26: Example Solver screen during an analysis

Chapter 6. Developing LS-DYNA Models for Study 4823

6.1 Overview of Project 4823 Models

To create LS-DYNA models for barrier crashworthiness studies, four components must be modeled: the cast-in-place barrier to be studied, the retrofit barrier intended to replace that cast-in-place barrier, the pendulum intended for laboratory use in evaluating that barrier's performance, and the specific crush package attached to the nose of that pendulum. Each component must be modeled analytically, using appropriate dimensions and materials. In this chapter, the development of LS-DYNA analytical models for each component is presented. In addition, because those LS-DYNA models can be used with pre-existing finite element models of various test vehicles, the process of incorporating pre-existing models is also presented.

6.2 Development of LS-DYNA Model for Cast-in-Place Barrier

Development of an LS-DYNA model for the cast-in-place bridge barrier is essential for studying the behavior of such barriers, and for determining a suitable retrofit design with similar behavior. A typical field installation of a TxDOT T203 cast-in-place barrier is shown in Figure 6.1. Figure 6.2 shows photos of a laboratory specimen representing a segment of that same type of barrier (TxDOT 2004). An appropriate LS-DYNA analytical model was created for the same barrier, considering its geometry, element size, materials, and treatment of the steel reinforcement.



Figure 6.1: TxDOT T203 bridge barrier with intermittent base and concrete parapet



Figure 6.2: Cast-in-place laboratory specimen representing a segment of a TxDOT T203 barrier with continuous base and concrete parapet

6.2.2 Geometry of Cast-in-Place Barrier

The geometry of the Type T203 bridge barrier, based on TxDOT standards, is shown in Figure 6.3. Though some characteristics must be modified slightly for ease of modeling, the geometry of the analytical model must still be consistent with those standards. The outer dimensions of that geometry were used to create the finite element model. Modeling of the steel reinforcement in the cast-in-place barrier is discussed in Section 6.2.6, and modeling of the deck slab is discussed in Section 6.4.3.

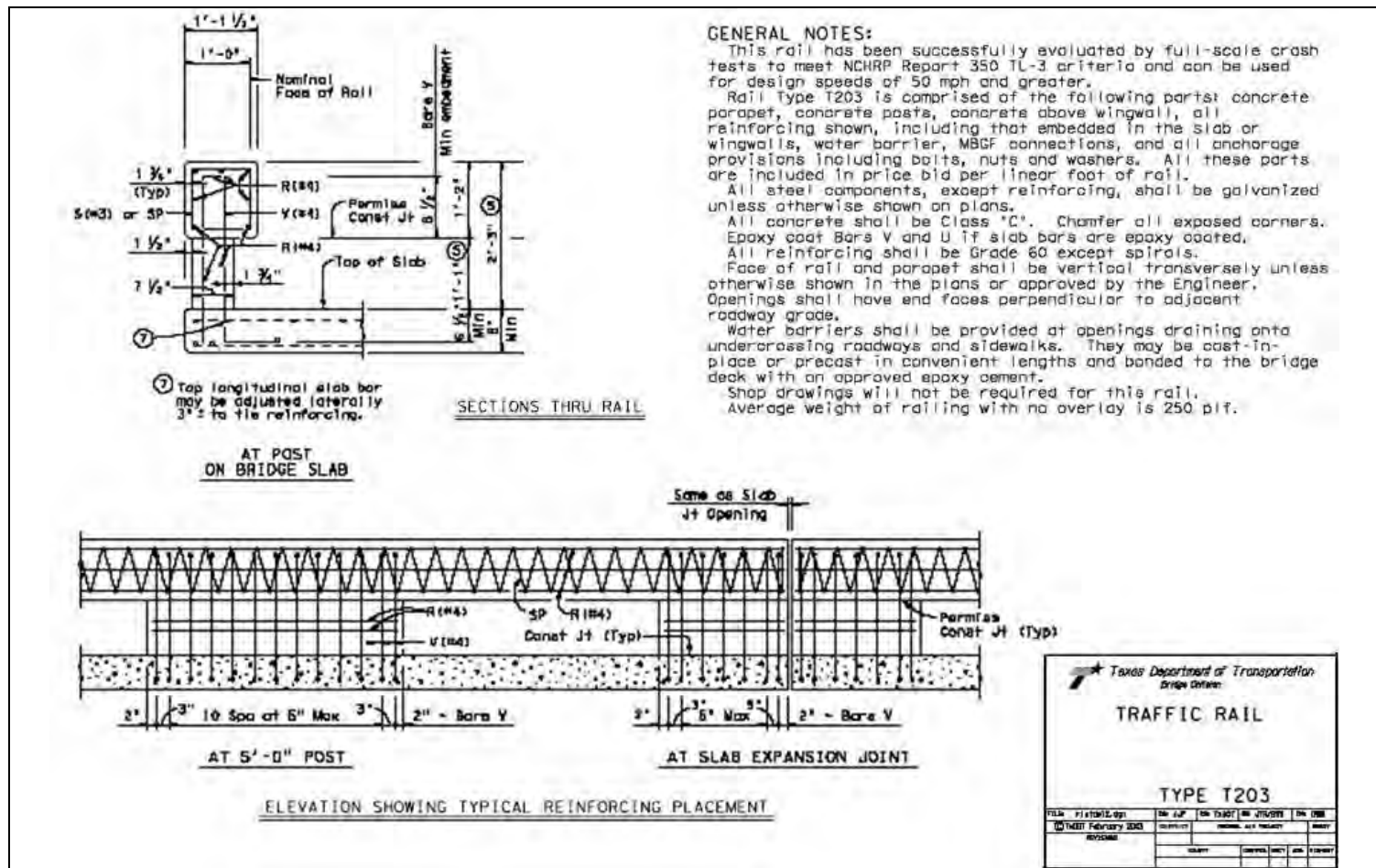


Figure 6.3: TxDOT Details of Type T203 Traffic Rail (TxDOT 2004)

6.2.3 Develop Each PART

The easiest way to create the correct geometry for a five-foot section of barrier is to create two rectangular prisms and then join them together. The process of meshing and joining the prisms is discussed in Section 6.2.4. The dimensions of each barrier portion are specified in Table 6.1. The upper portion of the barrier must be positioned globally so that its base is at the same elevation as the top of the lower portion. In addition, the top portion must extend 114 mm (4.5 in.) over the front and 38 mm (1.5 in.) over the back of the lower portion. The correct positioning of each piece is shown in Figure 6.4.

Table 6.1: Dimensions (mm) of cast-in-place T203 barrier

| <i>Barrier Portion</i> | <i>Length</i> | <i>Width</i> | <i>Height</i> |
|------------------------|---------------|--------------|---------------|
| Lower | 1524 | 190.5 | 330.2 |
| Upper | 1524 | 342.9 | 355.6 |

6.2.4 Create the Mesh

Once both barrier sections have been created, they must be meshed individually. Mesh sizes should be selected so that elements are the same size in each barrier section. In addition, element width should be no larger than 38.1 mm (1.5 in.) so that elements line up in the upper and lower barrier portions. The mesh selected for most of the barrier models consisted of cubic elements measuring 38.1 mm (1.5 in.) in each dimension (Figure 6.4). After meshing each barrier section, they are joined to form a single entity, using the *CHECK COINCIDENT* command under the *NODES* menu. The user is prompted to select a tolerance value, or distance between nodes, for checking for nodal coincidences. The default value of 0.01 mm (3.94×10^{-4} in.) is acceptable for this purpose, though other values can be selected to suit individual modeling needs. Once a tolerance value is selected, a region must be chosen where coincident nodes will be checked. The user should select the entire region over which the upper and lower barrier portions are in contact. LS-DYNA will give the user the option of merging the nodes located at the same positions. The *MERGE* option should be selected to create a unified barrier.

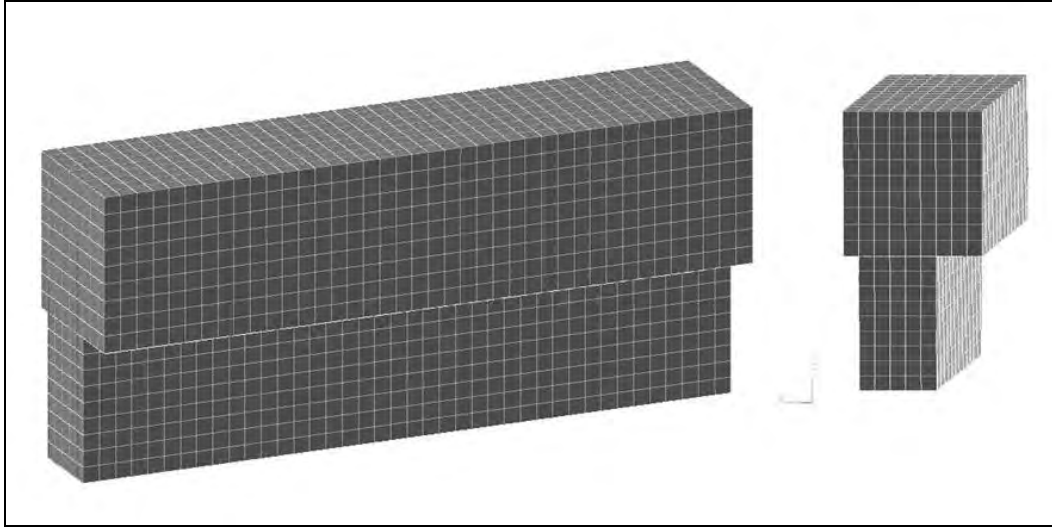


Figure 6.4: DYNA model of cast-in-place concrete barrier

6.2.5 Select the Concrete Material Model

Concrete is a relatively difficult material to model using finite element analyses due to its brittle behavior, the effects of confinement and reinforcement, and its descending-branch response characteristics. One way of dealing with the material characteristics of concrete is to use a simple material model, such as an elastic material, and include criteria for erosion of elements. To model the cast-in-place barrier, the *ISOTROPIC_ELASTIC_FAILURE* material was selected. The failure criteria were set so that elements would erode if the strain in an element reached 0.06. The *CARD* for this material, specifying each property that defines it, is shown in Table 6.2. Criteria for element failure and erosion, defined on the second *CARD*, are shown in Table 6.3.

Table 6.2: CARD 1 for concrete, modeled as Isotropic Elastic Failure Material

| <i>Variable</i> | <i>Description</i> | <i>Value</i> | <i>Units</i> |
|-----------------|---------------------------|--------------|---------------------|
| MID | Material ID | - | - |
| RO | Mass Density | 2.4028e-009 | ton/mm ³ |
| G | Shear Modulus | 1.0807e+004 | MPa |
| SIGY | Yield Stress | 2.7579e+001 | MPa |
| ETAN | Plastic Hardening Modulus | 0 | MPa |
| BULK | Bulk Modulus | 1.1836e+004 | MPa |

Table 6.3: CARD 2 for concrete, modeled as Isotropic Elastic Failure Material

| <i>Variable</i> | <i>Description</i> | <i>Value</i> | <i>Units</i> |
|-----------------|-------------------------------|--------------|--------------|
| EPF | Plastic Failure Strain | 6.0000e-002 | - |
| PRF | Failure Pressure | 0 | - |
| REM | Element Erosion Option | 0 | - |
| TREM | Time step for Element Erosion | 0 | - |

6.2.6 Treatment of Steel Reinforcement

For the cast-in-place barrier, due to the distribution of reinforcing bars, it is efficient to assume that the concrete and steel act compatibly. The assumption is valid if the bond between concrete and reinforcement is adequate. The end conditions, however, and specifically the connection between the barrier section and the deck slab, need to be modeled appropriately. It was assumed that these elements are primarily axial in behavior. Individual spring elements were created for each reinforcing bar, and they extend between the base of the barrier and deck slab. In total, 26 spring elements were created, each with the appropriate equivalent stiffness, calculated as EA/L for axial elements, where L is the length of the flexural reinforcement. The length, L , for the cast-in-place barrier is approximately the height of the barrier, 686 mm (27 in.) (Figure 6.5). Other material properties are Young's modulus for steel, and the cross-sectional area of a #4 bar. The appropriate material for this type of element is *ELASTIC SPRING*. The *CARD* for this material is shown in Table 6.4.

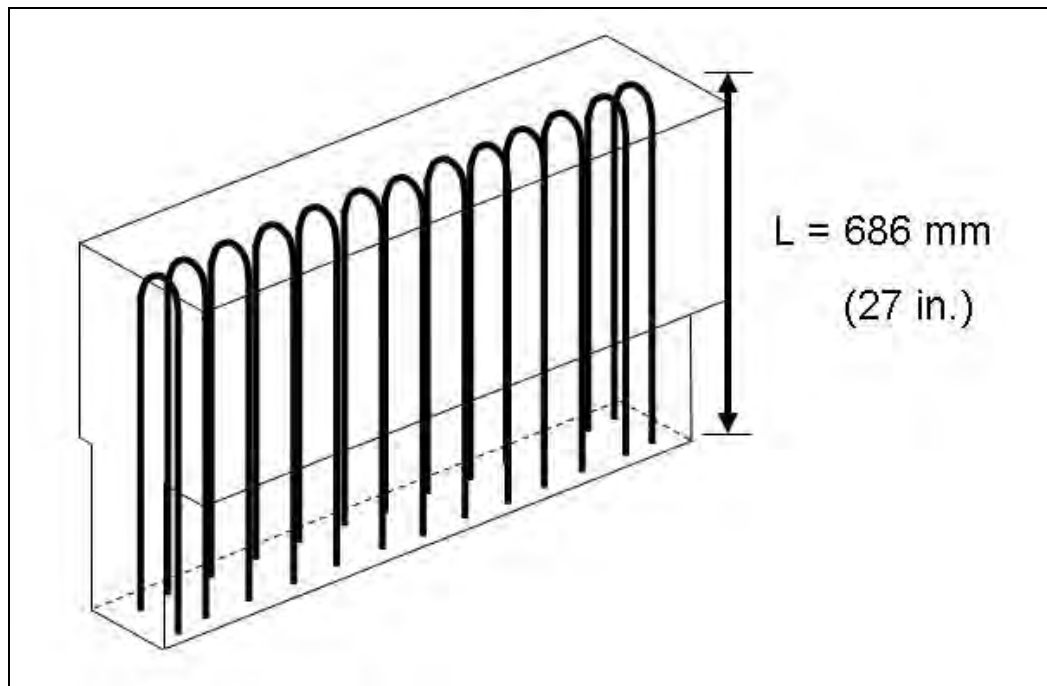


Figure 6.5: Placement of reinforcing bars in cast-in-place barrier

Table 6.4: CARD 1 for Reinforcing Bars, modeled as Elastic Spring Material

| <i>Variable</i> | <i>Description</i> | <i>Value</i> | <i>Units</i> |
|-----------------|--------------------|--------------|--------------|
| MID | Material ID | - | - |
| K | Spring Stiffness | 3.7620e+004 | N/mm |

6.3 Analytical Modeling of Retrofit Barrier

An analytical model of the proposed retrofit barrier design was needed for comparison with the cast-in-place model. The model for the retrofit barrier used the same dimensions, materials and mesh as the cast-in-place barrier model.

The retrofit barrier design, which is the subject of the experimental and analytical testing, is described in the following section. Based upon the current state of knowledge on anchorage to concrete using post-installed mechanical anchors (Mitchell 2005), the retrofit barrier design shown in Figure 6.6 was proposed. It will likely require further modification based on the results of future research in this study.

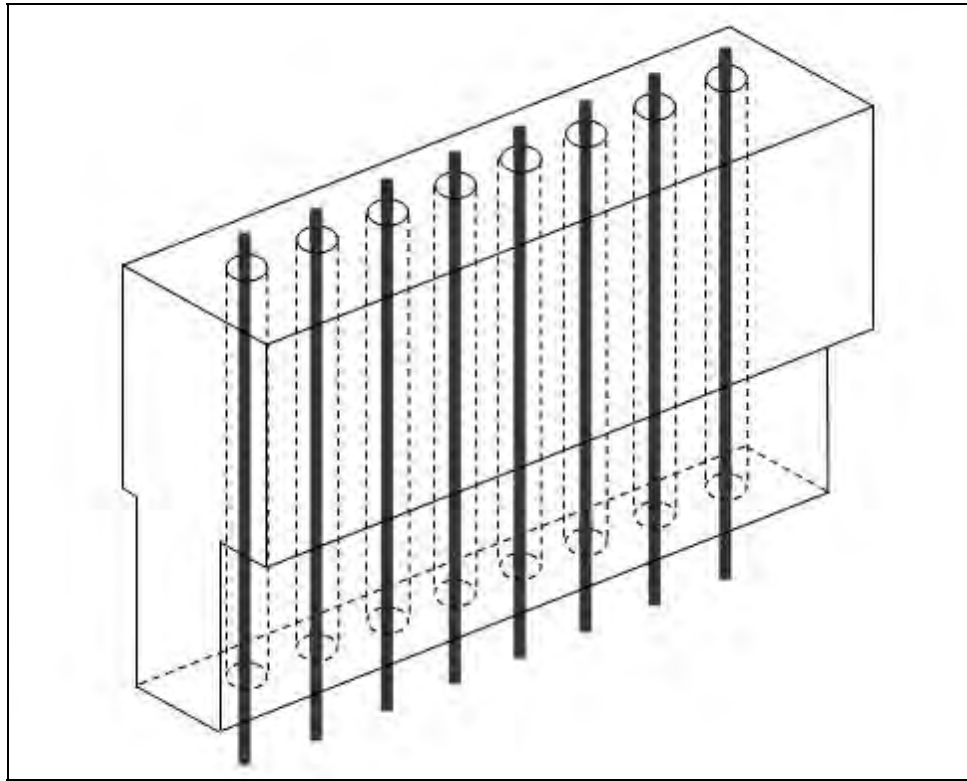


Figure 6.6: Schematic of proposed retrofit barrier design

This design could either be cast-in-place or precast. The retrofit barrier does not have the same steel reinforcement as the cast-in-place design. Its flexural reinforcement is post-installed, and the amount of steel will be varied depending on the desired barrier response under impact loads. For this purpose, the pre-cast barrier section contains hollow ducts, spaced at approximately 165 mm (6.75 in.) on center, with a diameter that can be varied depending on the

amount of steel to be installed. The current proposal for the post-installed steel is threaded rods held underneath the deck with external nuts.

6.3.2 Modify the Cast-in-Place Barrier

The LS-DYNA analytical model for the retrofit barrier begins with the completed cast-in-place model, excluding the reinforcing-bar elements. The models differ principally in the inclusion, in the retrofit design, of hollow ducts into which post-installed reinforcement or anchors can be placed. One must first determine, based on the dimensions of the finite elements, how many elements must be deleted to create the correct cross-sectional area of the void space representing the hollow ducts. For this preliminary retrofit design, a series of eight equally spaced ducts had to be created. Based upon the element cross-sectional area of 1451 mm^2 (2.25 in.^2), a void one element wide in each radial direction was needed. Once the void was created, elements at the top of each hollow void were re-created so that the reinforcing bar could be anchored to them. The process for accomplishing this task is described in the following sections.

6.3.3 Create Hollow Ducts for Retrofit Reinforcement or Anchors

To delete the necessary elements in an efficient manner, the user should use a two-dimensional view of the top of the barrier model. Using the *DELETE* command under the *ELEMENT* menu, elements can be deleted from the given region by clicking and dragging the mouse over them in that view. Vertically aligned elements in the dragged window are deleted, creating a vertically oriented, elongated void in the barrier. In other words, to create the vertically oriented three-dimensional void, the user must select elements defining the cross-sectional area of each duct in a horizontal plane. This procedure is shown in Figure 6.7.

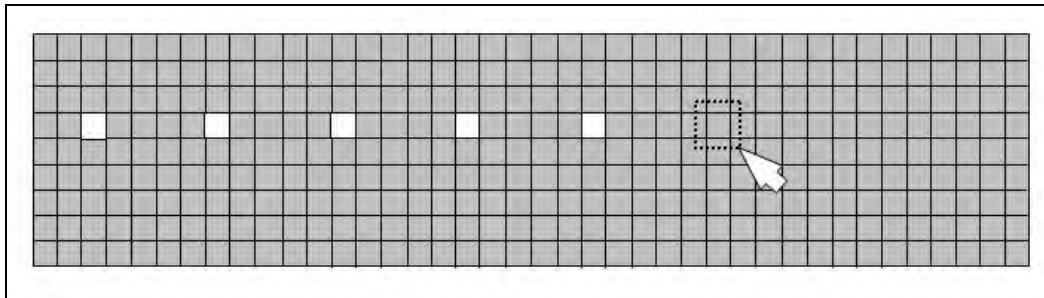


Figure 6.7: Selection of elements to be deleted to form ducts for reinforcement or anchors

6.3.4 Create Elements for Anchorage of Reinforcement

Even though the reinforcing steel in the actual retrofit design is anchored outside of the dimensions of the concrete, the reinforcing steel in the analytical model is anchored at the upper boundary of the barrier. This modeling approach should not affect the overall behavior significantly. The user must first create the anchorage points by re-creating a single element at the top of each hollow duct, preferably when the barrier is in the three-dimensional view and the *fill-color* view option is selected. Under the *ELEMENT* menu, the user selects *CREATE* followed by *SOLID*, and is then prompted to select eight nodes to define a single element. It is easiest to select the eight nodes of the surrounding elements to define a single cube at the top of each duct (Figure 6.8). Once the element has been created, it must be subdivided to allow the axial

reinforcing steel elements to be attached in the center of the hollow duct. Subdividing the element is accomplished using the *SPLIT* command under the *ELEMENT* menu. The correct option under the *SPLIT* menu is the *SOLID TO 8 SOLIDS* option. When the desired element is selected, LS-DYNA automatically subdivides the cubic element into eight identical smaller cubic elements (Figure 6.9).

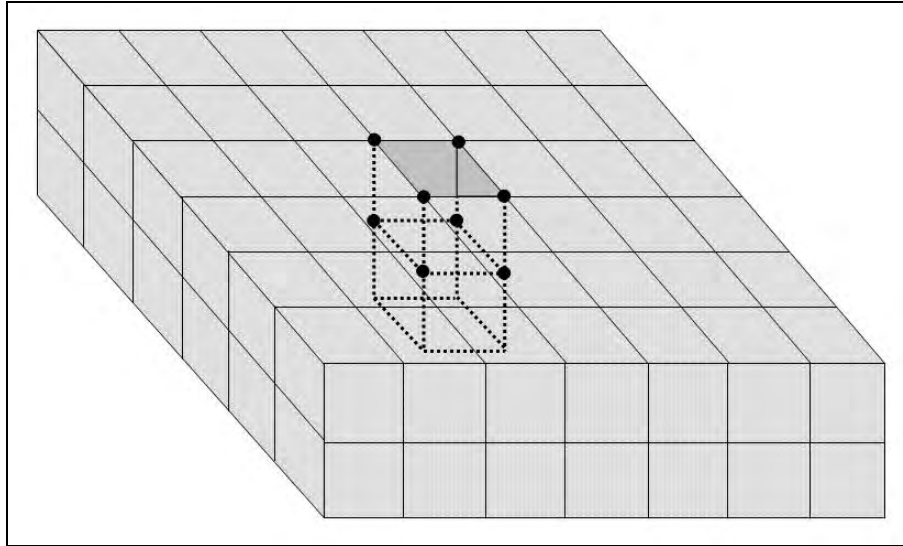


Figure 6.8: Re-creation of element at top of hollow duct

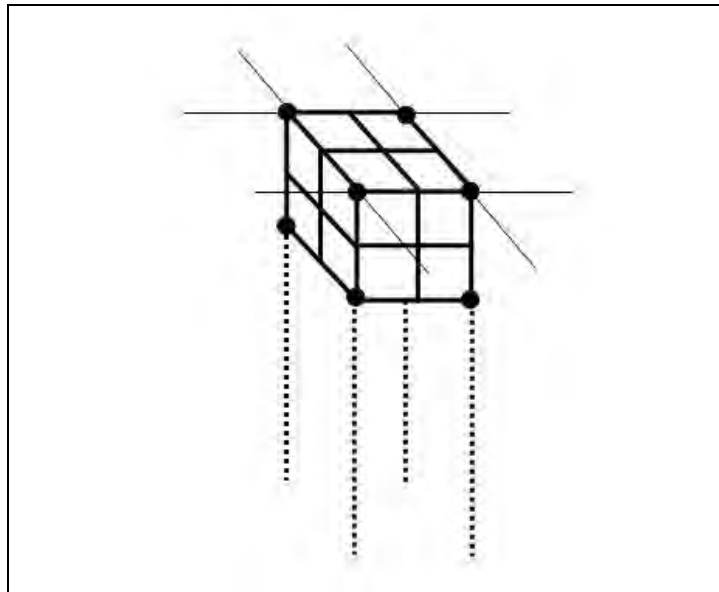


Figure 6.9: Division of LS-DYNA element for attachment of reinforcing bar

6.3.5 Treatment of Post-Installed Reinforcing Bars

Post-installed reinforcing bars were created using line elements, assuming primarily axial behavior and a standard threaded rod with an effective diameter of approximately 31.75 mm (1.25 in.). This assumption may be modified by future research.

First, lines defining each reinforcing bar must be created within a separate *PART*, connecting the node at the center of the elements at the top of the hollow duct with a corresponding node located directly below the first node in the rigid deck. The finished element should appear as shown in Figure 6.8.

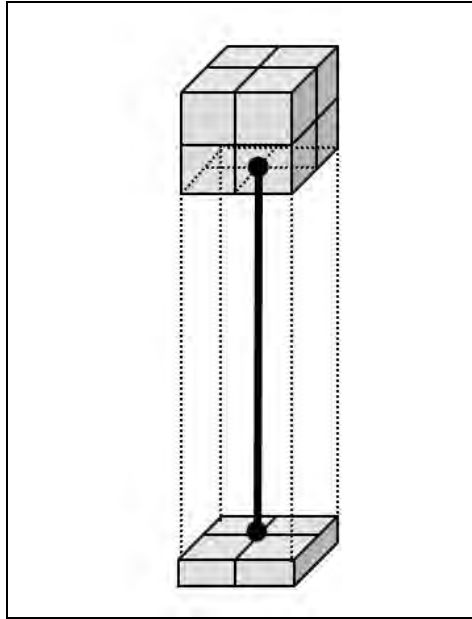


Figure 6.10: Analytical representation of post-installed reinforcement as a line element inside a hollow duct

Next, each line is subdivided into the desired number of elements (for this research project, ten elements). Under the *ELEMENT* menu, the user selects the *LINE MESH* command, followed by the *BEAM ELEMENT* option, and is then prompted to select the lines to be meshed and the number of elements into which each line should be subdivided.

Because LS-DYNA lists truss elements under the heading of “beam,” beam elements were used, with a cross-sectional area equal to the effective cross-sectional area of the threaded rod, and a moment of inertia equal to zero. Under the *SECTION* menu, the *BEAM* option was selected. When the input *CARDs* are displayed, the user must select an *element formulation* option in addition to inputting other information, all shown in Table 6.5. Most values were kept as the default values, with the exception of the cross-section type which was changed to Option 1, tubular. According to the *LS-DYNA Theory Manual*, an appropriate choice of element properties for a circular cross-section beam element is the Belytschko-Schwer beam element (Livermore Software Technology Corporation 1998). This type of element is given as Option 5 within the *ELFORM* field, also shown in Table 6.5. LS-DYNA then automatically displays the appropriate *CARDs* for the beam section depending on which option is selected. Once selected, LS-DYNA also displays *CARD 4* for user input, which includes information on beam dimensions. Values used for the preliminary design of the reinforcing steel are shown in Table

6.6. In Table 6.6, TS1 and TS2 refer to the outer diameter of the element at nodes 1 and 2, respectively. TT1 and TT2 refer to the inner diameter at the same nodes.

Table 6.5: CARD 1 for reinforcement, modeled as SECTION_BEAM

| <i>Variable</i> | <i>Description</i> | <i>Value</i> | <i>Units</i> |
|-----------------|---------------------------|--------------|--------------|
| SECID | Section ID | - | - |
| ELFORM | Element Formulation | 5 | - |
| SHRF | Shear Factor | 1.0000e+000 | - |
| QR/IRID | Quadrature Rule | 2 | - |
| CST | Cross Section Type | 1 | - |
| SCOOR | Location of Triad | 0 | - |
| NSM | Nonstructural Mass Per... | 0.0000e+000 | - |

Table 6.6: CARD 4 for preliminary reinforcement, modeled as SECTION_BEAM

| <i>Variable</i> | <i>Description</i> | <i>Value</i> | <i>Units</i> |
|-----------------|-------------------------|--------------|--------------|
| TS1 | Beam Thickness in s-dir | 3.2258e+001 | mm |
| TS2 | Beam Thickness in s-dir | 3.2258e+001 | mm |
| TT1 | Beam Thickness in t-dir | 0.0000e+000 | mm |
| TT2 | Beam Thickness in t-dir | 0.0000e+000 | mm |

Although many different material models can be used to model steel within LS-DYNA, the selection of beam elements for the reinforcing bar limits the material models that can subsequently be selected. A model in which the steel could yield and deform was desirable for assessing overall barrier behavior in the inelastic range. After reviewing several possibilities, the plastic-kinematic material model was selected, with the input variable values shown in Table 6.7.

Table 6.7: CARD 1 for preliminary modeling of reinforcement as a Plastic Kinematic Material

| <i>Variable</i> | <i>Description</i> | <i>Value</i> | <i>Units</i> |
|-----------------|---------------------------|--------------|---------------------|
| MID | Material ID | - | - |
| RO | Mass Density | 7.9291e-009 | ton/mm ³ |
| E | Young's Modulus | 1.9995e+005 | MPa |
| PR | Poisson's Ratio | 3.0000e-001 | - |
| SIGY | Yield Stress | 3.4474e+002 | MPa |
| ETAN | Plastic Hardening Modulus | 2.7579e+003 | MPa |
| BETA | Hardening Parameter | 0 | - |

In contrast with the cast-in-place barrier model for which the reinforcing bar and concrete were considered as a single solid entity, the retrofit barrier model used distinct concrete barrier and steel elements with an associated contact surface. The standard *AUTOMATIC_NODES_TO_SURFACE* contact for contact with two-dimensional elements was selected, using the concrete as the master surface and the reinforcing bar as the slave surface.

6.4 Overall Considerations in Modeling Barriers

Once all components of the barrier models are developed, several other aspects must still be considered to finish the creation of a useful, comprehensive model. The two most important of these issues are the treatment of finite versus infinitely long barriers, and the modeling of the bridge slab.

6.4.1 Modeling of Finite-Length versus Infinitely Long Barriers

The critical structural case for bridge rails is a barrier with a finite length of 1.5 m (5.0 ft), representing a reasonable lower limit for out-of-plane stiffness and strength. Therefore, the default analytical model of the barrier used that length. This section addresses the modifications required to address the opposite limiting case of an infinitely long barrier.

6.4.2 Modeling of Infinitely Long Barriers

An infinitely long barrier can be handled analytically as a 1.5-m (5.0 ft) barrier with out-of-plane springs at each end, with stiffness values calculated to match the case of an infinitely long barrier. Spring elements were created in the horizontal direction for each node at the face of the upper parapet sections at each end of the barrier, as shown in Figure 6.11, and represent only the out-of-plane translational stiffness due to adjacent barrier segments.

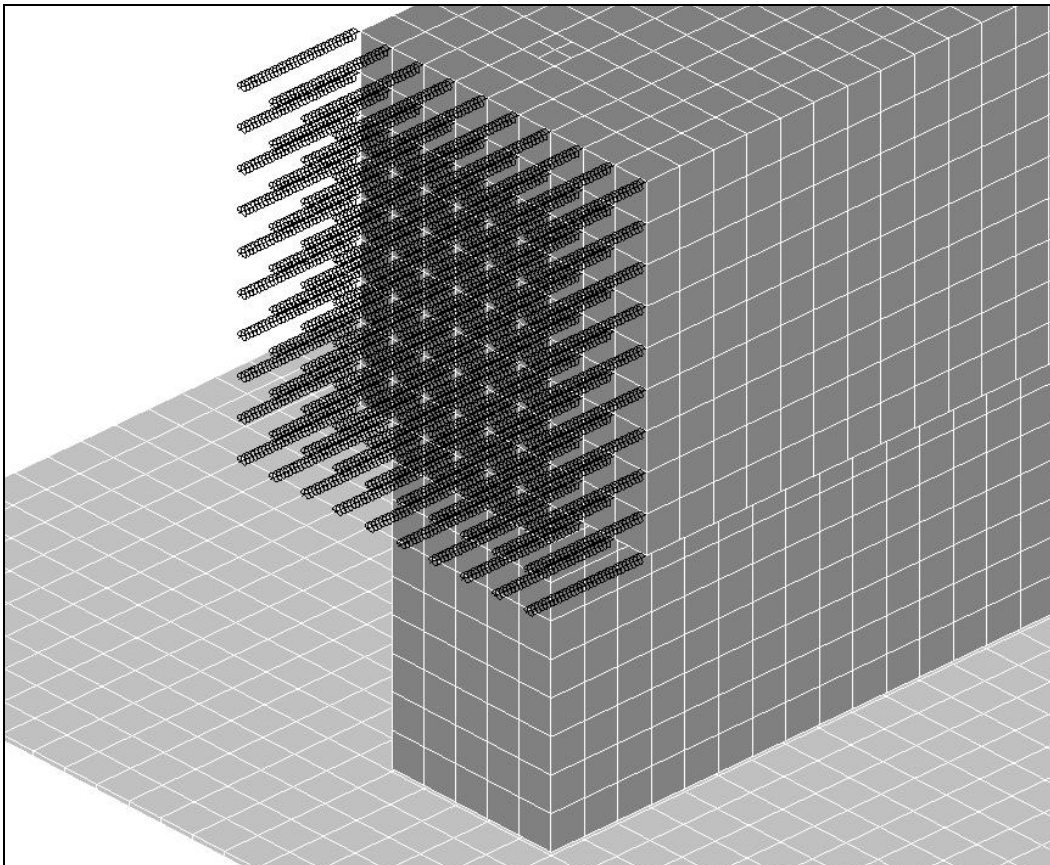


Figure 6.11: Spring elements added at ends of barrier segments to simulate the restraining effects of infinitely long barriers

At this point in the research project, it was not known what stiffness assumptions would be the most accurate. The spring stiffnesses used here merit further study on a future project. An upper bound on the stiffness was established by considering the sum of two translational stiffness components.

The first contribution to the translational stiffness is based on the assumption that two segments, adjacent to the barrier segment being modeled, are allowed to deflect while their far ends are fixed. The total out-of-plane stiffness that they provide, k_t , is equal to $24EI / \ell^3$. The stiffness contribution of one adjacent barrier segment is depicted in Figure 6.12.

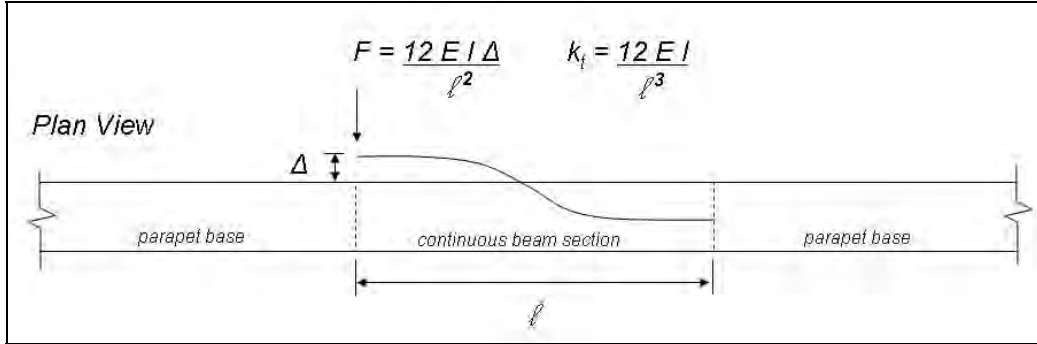


Figure 6.12: Assumptions used in developing stiffnesses of equivalent springs to represent an infinitely long barrier

The other translational stiffness considered was that of the segment alone, based on a preliminary crash simulation with the finite-length barrier section and a Geo Metro vehicle model. That stiffness, $k_{segment}$, is equal to the out-of-plane force at the interface divided by the out-of-plane barrier deflection (Figure 6.13). This stiffness value was much smaller than the beam stiffness value. The upper-bound stiffness for an infinitely long barrier was assumed as the sum of the two translational stiffness contributions, k_t and $k_{segment}$.

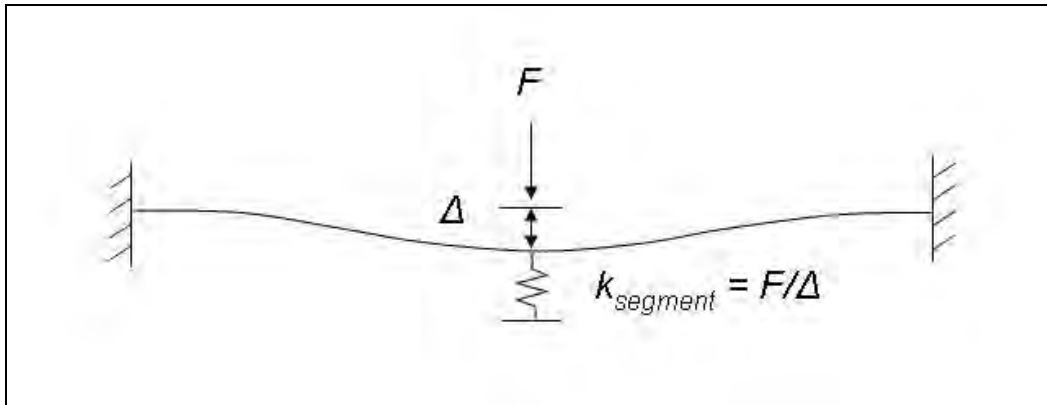


Figure 6.13: Assumptions used in developing equivalent beam stiffness for finite-length section

6.4.3 Analytical Model of Reinforced Concrete Bridge Deck

To develop the crush package and analyze the cast-in-place barriers and preliminary retrofit designs, the concrete deck was modeled as a rigid base. Fixed boundary conditions were applied to all degrees of freedom attached to it, and it was used as an anchorage point for cast-in-place and post-installed reinforcing bars. Though the behavior of the barrier is the focus of this study, that behavior is influenced by the behavior of the deck. Subsequent analytical models used in this study and described in Chapter 11 included a deformable bridge deck.

6.5 Development of Analytical Model for Impact Pendulum

The mass of the laboratory impact pendulum, shown in Figure 6.14, consists of a long center spine plate, two end plates, a top plate, and several smaller side plates added to achieve the desired weight. A finite element model of the pendulum mass was created using those components and steel material properties, as described in the following sections.

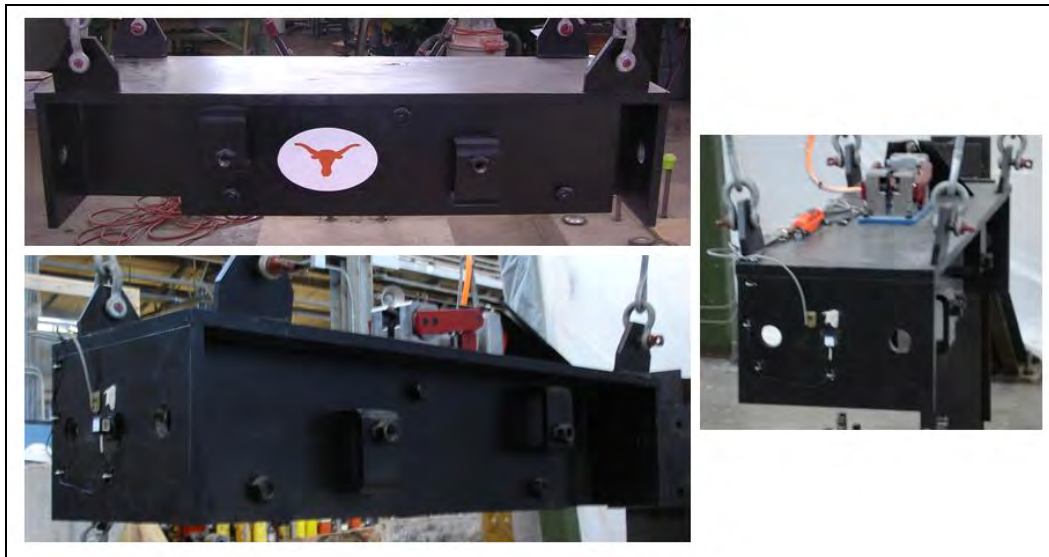


Figure 6.14: Laboratory pendulum mass

6.5.2 Geometry of Pendulum Mass

The steel plates of the laboratory pendulum mass are 25.4-mm (1-in.) thick. It measures 1447-mm (57-in.) long, 457-mm (18-in.) wide, and 304.8-mm (12-in.) high. The plates and dimensions were modeled as accurately as possibly, though the plates used for additional weight were modeled as a single part.

6.5.3 Creation of Finite Element Mesh for Laboratory Pendulum Mass

Due to the orientation, dimensions, and connectivity of the steel plates in the laboratory pendulum, a detailed mesh needed to be created. The mesh became more complex with smaller elements where the steel plates needed to be joined with geometric accuracy. For instance, as shown in **A** of Figure 6.15, the long, center vertical plate could only be joined at the center of the front plate. **B** of Figure 6.15 shows a similar connection between the center vertical plate and the

horizontal top plate. While a mesh of elements of approximately 16387 mm^3 (1 in.^3) would have been sufficient to capture pendulum behavior, a mesh of elements approximately 2048 mm^3 (0.125 in.^3) was necessary to allow for the joining of plates as described previously. An example of the resulting meshed pendulum is shown in **C** of Figure 6.15. Due to the large number of relatively small elements, however, computer run times using this pendulum model were unreasonably long. A simpler pendulum model was therefore developed to give shorter run times.

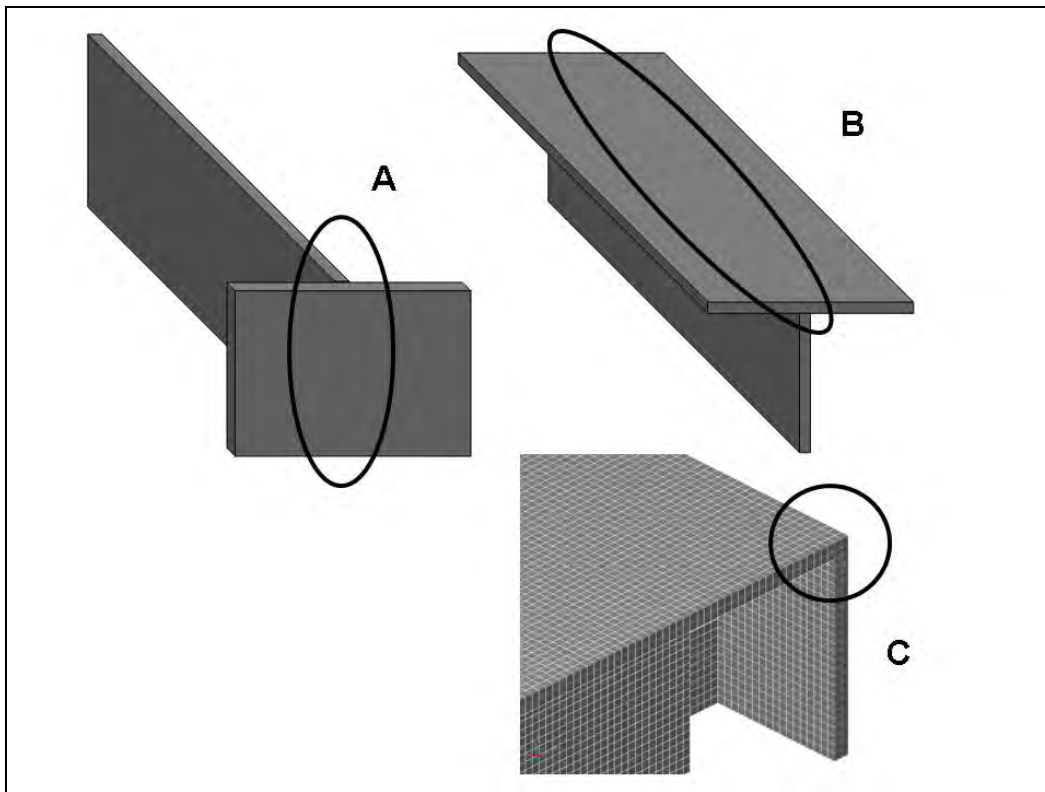


Figure 6.15: Creating initial mesh for DYNA model of laboratory pendulum

6.5.4 Mesh for Simplified DYNA Model of Pendulum Mass

Several factors were considered when creating the mesh for a simplified DYNA model of the pendulum mass. Most important, the mass of the pendulum had to be preserved in order to preserve the impact impulse. Also, the overall length of the pendulum mass was essentially maintained to preserve the time that an axial stress wave would take to travel the length of the pendulum during a crash simulation. The resulting simplified pendulum mass was 1397-mm (55-in.) long, 305-mm (12-in.) wide, and 229-mm (9-in.) high. Its frontal cross-sectional area was still sufficient to allow placement of the crush package. The simplified pendulum model is shown in Figure 6.16.

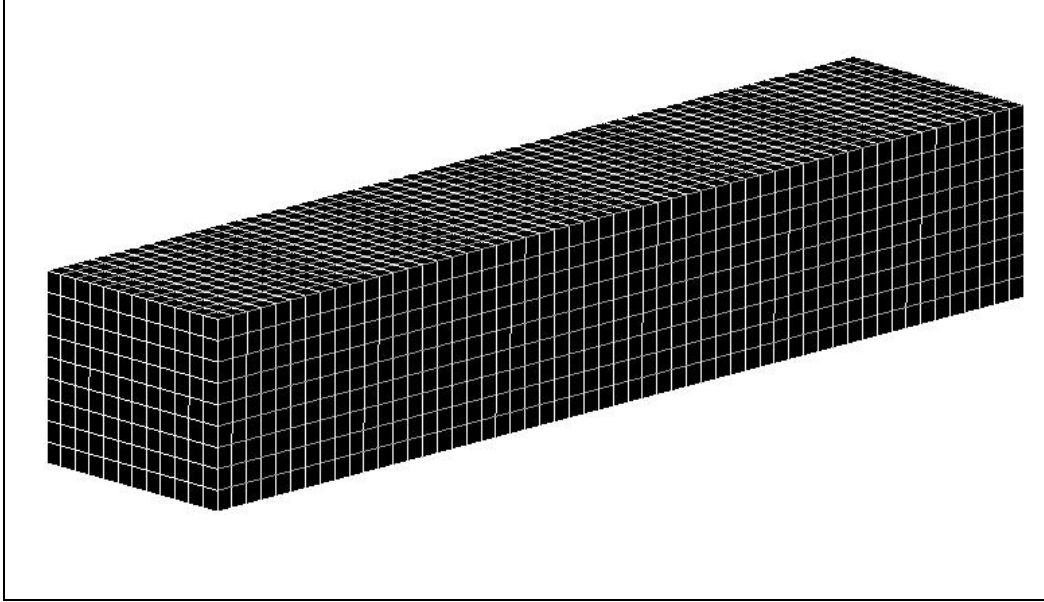


Figure 6.16: Simplified DYNA model of laboratory pendulum mass

6.5.5 Material Model for Laboratory Pendulum Mass

The material model for the laboratory pendulum mass was selected to address elastic and plastic behavior. The simplest material model including these features is the *ISOTROPIC_ELASTIC_PLASTIC* material model, which requires only basic material properties for its definition. The values for steel, shown in Table 6.8, were used as input to LS-DYNA.

Table 6.8: CARD 1 for pendulum mass, modeled as an Isotropic Elastic Plastic material

| <i>Variable</i> | <i>Description</i> | <i>Value</i> | <i>Units</i> |
|-----------------|---------------------------|--------------|---------------------|
| MID | Material ID | - | - |
| RO | Mass Density | 7.9278e-009 | Ton/mm ³ |
| G | Shear Modulus | 7.9903e+004 | MPa |
| SIGY | Yield Stress | 4.1369e+002 | MPa |
| ETAN | Plastic Hardening Modulus | 2.7579e+003 | MPa |
| BULK | Bulk Modulus | 1.6662e+005 | MPa |

6.6 Design of Crush Package

Development and calibration of the crush package design is discussed in detail in Chapter 5. The process by which a crush package is created and appropriately modeled is covered in this section, however.

6.6.1 Overview of Preliminary Design of Crush Package

The crush package is a structure attached to the front of the pendulum mass, intended to absorb impact energy and thereby replicate the crushing characteristics of a vehicle during an impact. The preliminary crush package was created using 25-mm (1-in.) hollow tubular steel arranged in layers with the cross-section perpendicular to the direction of impact, as shown in Figure 6.17. In that figure, the left end of the package impacts the barrier, and the right end is attached to the pendulum mass. The crush package is shown in its proper orientation with the pendulum during a crash test in Figure 6.18.

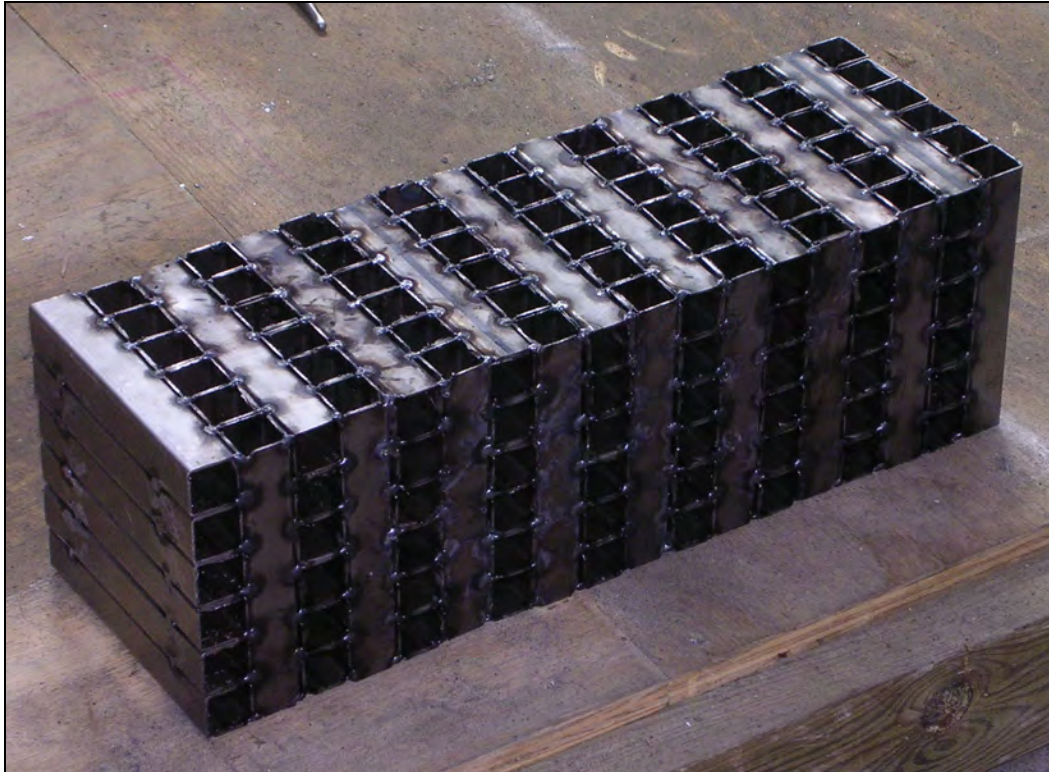


Figure 6.17: Preliminary design of tubular steel crush package



Figure 6.18: Crush package in position on pendulum during a crash test

6.6.2 Creation and Connection of Layers for Model of Preliminary Crush Package

Using the processes described in Chapter 4, each layer of the crush package must be created as a separate *PART*. Each layer of steel crushes individually, and creating separate *PARTs* for each layer allows the analytical model to behave in the same way.

Once each layer of steel tubes is created and meshed individually, the *FIND COINCIDENT* command under the *NODES* menu heading is used to merge the nodes at the interface of each layer and also at the interface between the pendulum and the crush package. In the preliminary design of the crush package, each layer had a cross section of 152 mm (6 in.) by 152 mm (6 in.) and a depth of 25 mm (1 in.). A total of 18 layers were joined to form the complete crush package (Figure 6.19).

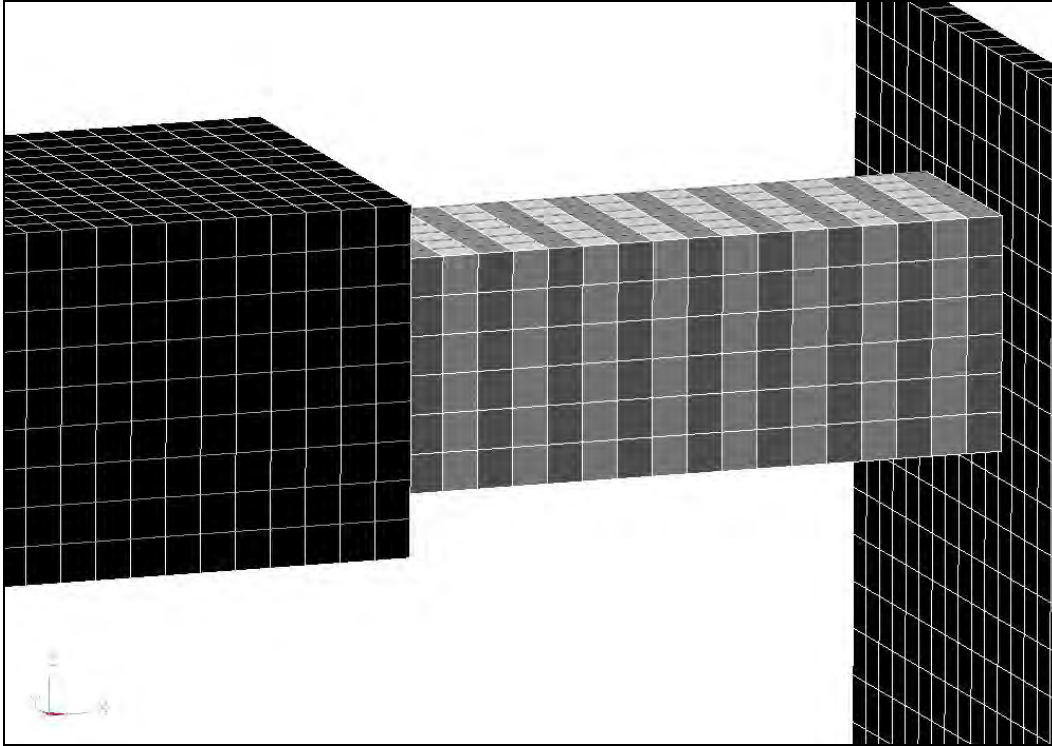


Figure 6.19: DYNA model of preliminary crush package

6.6.3 Material Model for Preliminary Crush Package

The crush package consists of distinct steel layers that crush individually. The LS-DYNA material model most suited for this type of behavior is the *HONEYCOMB* material model, intended for metal materials that crush with a defined load curve. The first *CARD* and the values for input for that model are shown in Table 6.9. Each value given is standard for steel, with the exception of the mass density, which represents the overall density of the crush package, including voids as well as steel.

Table 6.9: CARD 1 for Honeycomb Material

| <i>Variable</i> | <i>Description</i> | <i>Value</i> | <i>Units</i> |
|-----------------|--------------------------------|--------------|--------------|
| MID | Material ID | - | - |
| RO | Mass Density | 1.1654e-009 | ton/mm |
| E | Young's Modulus | 1.9995e+005 | MPa |
| PR | Poisson's Ratio | 3.0000e-001 | - |
| SIGY | Yield Stress | 4.1369e+002 | MPa |
| VF | Fully Compacted Rel. Vel. | 3.8000e-001 | - |
| MU | Material Viscosity Coefficient | 5.0000e-002 | - |
| BULK | Bulk Viscosity Flag | 0 | - |

The second *CARD* of input information used to define the honeycomb material (Table 6.10), supplies force-deformation information for the honeycomb material. A single load curve can be used for each of the LCA, LCB, LCC, and LCS variables. LCA, LCB, LCC, and LCS represent the load curve ID for the normal stress-volumetric strain curve for each of the primary coordinate axes. LCAB, LCBC, LCCA, and LCSR are the load curve IDs for the shear stress-volumetric strain for each of the primary axes. If the fields for the variables LCAB, LCBC, LCCA, and LCSR are left blank, those variables are assumed to have the same values as those of the direct stress-volumetric strain curves. The input of the load curve is described in Section 6.6.4. The final *CARD* used to define the honeycomb material is shown in Table 6.11. Values for elastic and shear moduli are listed for each axis.

Table 6.10: CARD 2 for Honeycomb Material

| <i>Variable</i> | <i>Description</i> | <i>Value</i> | <i>Units</i> |
|-----------------|-----------------------------|--------------|--------------|
| LCA | LCID: Sigma-AA vs. Vol. | # | - |
| LCB | LCID: Sigma-BB vs. Vol. | # | - |
| LCC | LCID: Sigma-CC vs. Vol. | # | - |
| LCS | LCID: Shear Stress vs. Vol. | # | - |
| LCAB | LCID: Sigma-AB vs. Vol. | - | - |
| LCBC | LCID: Sigma-BC vs. Vol. | - | - |
| LCCA | LCID: Sigma-CA vs. Vol. | - | - |
| LCSR | LCID: Strain Rate Effects | - | - |

Table 6.11: CARD 3 for Honeycomb Material

| <i>Variable</i> | <i>Description</i> | <i>Value</i> | <i>Units</i> |
|-----------------|-----------------------|--------------|--------------|
| EAAU | Elastic Modulus, EAAU | 6.2580e+001 | MPa |
| EBBU | Elastic Modulus, EBBU | 6.2580e+001 | MPa |
| ECCU | Elastic Modulus, ECCU | 6.2580e+001 | MPa |
| GABU | Shear Modulus, EABU | 2.2100e+001 | MPa |
| GBCU | Shear Modulus, EBCU | 4.6423e+001 | MPa |
| GCAU | Shear Modulus, ECAU | 2.2100e+001 | MPa |
| AOPT | Material Axes Option | - | - |

6.6.4 Input of Load Curve

The load curve specified in the *CARDS* for the honeycomb material model must be manually added by the user, and can be created using the *LOAD CURVE* command under the *DYNA MISC.* menu. Using this command, the user is prompted to enter information into a *CARD* similar to the material model *CARDS*. The values used to define the load curve are given in Table 6.12 and were obtained from a static crush test on the layers of hollow steel tube, converted to a

curve of stress versus volumetric strain, and entered into LS-DYNA. A further description of this static testing procedure is given in Section 5.1.1. The load-displacement data were converted to stress-volumetric strain data by dividing each load value by the cross-sectional area being loaded, and dividing each displacement value by the overall length of the specimen. In Table 6.12, the ordinate scale factor (SFO) has a value of 1.2, reflecting the probable higher strength of the material under dynamic loading conditions. Once the *DEFINE CURVE CARD* is completed, the user can enter the stress and strain values that define the load curve itself (Figure 6.20).

Table 6.12: Load curve definition CARD

| <i>Variable</i> | <i>Description</i> | <i>Value</i> | <i>Units</i> |
|-----------------|------------------------------|--------------|--------------|
| LCID | Load Curve ID | # | - |
| SIDR | Stress Initialization Opt. | 0 | - |
| SFA | Scale Factor: Abscissa Value | 1.0000e+000 | - |
| SFO | Scale Factor: Ordinate Value | 1.2000e+000 | - |
| OFFA | Offset Value: Abscissa | 0.0000e+000 | - |
| OFFO | Offset Value: Ordinate | 0.0000e+000 | - |
| DATTYP | Data Type | 0 | - |

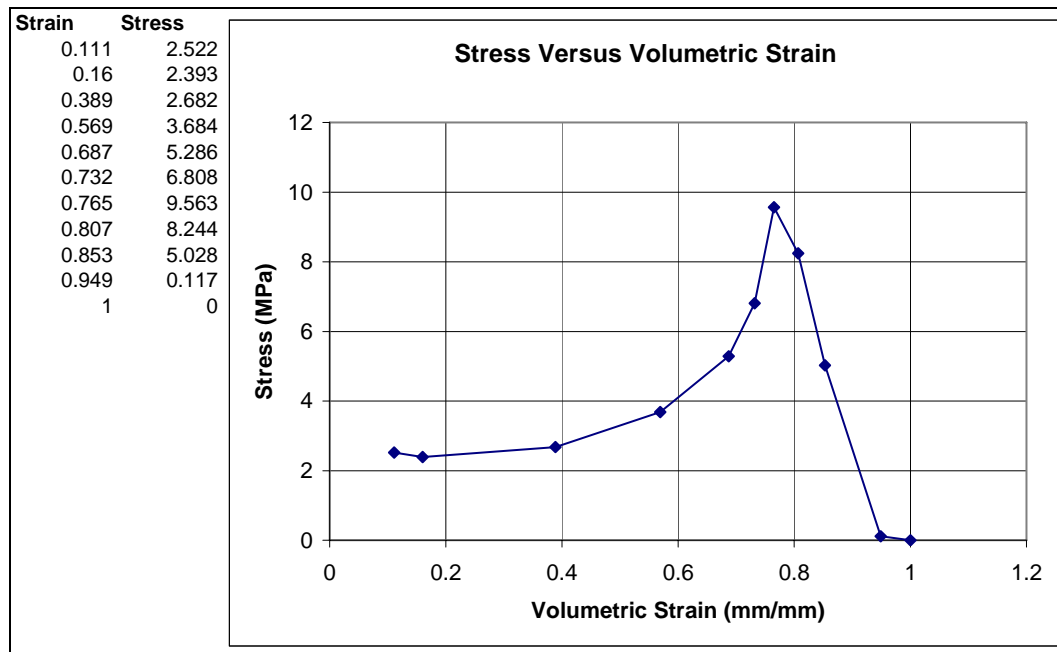


Figure 6.20: Stress-strain curve for honeycomb material

6.7 Incorporation of FHWA Vehicle Models into LS-DYNA Models

To use LS-DYNA to simulate real vehicular impacts, it is necessary to incorporate previously developed FHWA vehicle models, distinguished as previously discussed by a *.key* suffix. Once downloaded, the *.key* file of the vehicle model can be introduced into a pre-existing barrier model using the *IMPORT* command under the *FILE* menu. Manipulation of these models for use in various crash simulations is described in the following sections. To achieve TL- 3 under *NCHRP Report 350* guidelines, a vehicle within 820 ± 25 kg must be used (1993). The coarse Geo Metro model mass is within that tolerance and should be used.

6.7.1 Spatial Location and Orientation of Imported Vehicle Model

Each previously developed vehicle model has a pre-defined spatial location and orientation, which may or may not be correct for the desired crash simulation. The vehicle model can be translated and rotated as desired using the *TRANSLATE* and *ROTATE* commands under the *TRANSFORM* and *NODE* menus. Alternatively, the barrier itself can be translated and rotated. Whether the vehicle or the barrier is moved depends on the user's preference for the axis along which force output information is desired.

6.7.2 Initial Conditions for Pre-defined Vehicle Models

Just as the vehicle models have pre-defined locations and orientations, they also have initial translational and rotational velocities, which the user can adjust using the *MODIFY* command after selecting a particular condition under the *B.C.* menu heading.

6.7.3 Contact Surfaces for Pre-defined Vehicle Models

To complete the importation of a pre-defined vehicle model, a contact surface must be defined between the barrier and the vehicle. Most vehicle models have a defined *PART SET* that includes all *PARTs* of the vehicle. Using an *AUTOMATIC_SURFACE_TO_SURFACE* contact definition, the user can select the barrier as the slave *PART* and the vehicle as the master *PART SET*. Though the barrier is actually the least stiff of the barrier and vehicle, it was chosen at the *SLAVE* because its deformation was to be studied.

6.8 Output Considerations for LS-DYNA Impact Simulations

To compare analytical results from LS-DYNA simulations with data from experimental pendulum tests, *RCFORC* and *NODOUT* should be selected for output. The *RCFORC* command gives output for forces at the contact interface between the front of the crush package and the rigid barrier. The *NODOUT* command gives acceleration histories. As described in Section 3.14, this information is requested at specific *NODEs*. For the pendulum model, the selected *NODE* was located at the point where the accelerometer was mounted on the laboratory pendulum.

Chapter 7. Design of Crush Package, Validation of Test Methods, and Significance of Results

7.1 Preliminary Design of Crush Package for Impact Pendulum

The crush package attached to the nose of an impact pendulum serves several purposes: it absorbs energy during the impact, it limits the maximum impact force to the prescribed level, and it controls the duration of the impact. It can also simulate the force-time or acceleration-time history of a vehicular impact on the barrier. The acceleration-time history for a typical full-scale vehicular impact test is shown in Figure 7.1 (Mitchell 2005). Key characteristics of this history are a maximum acceleration of about 28 g, corresponding to a force of 246 kN (55.4 kips), and an impact duration of about 0.1 sec. The selected correspondence between vehicle crash tests and the simulated crashes for this research is the impact impulse (area under the force-time curve). The impulse of the simulated tests should match that of a Geo Metro during a crash test, which satisfies TL-3 of *NCHRP Report 350*. The impulse for a Geo Metro vehicular crash test is about 6900 N-sec, and the crush package should be designed to match that impulse.

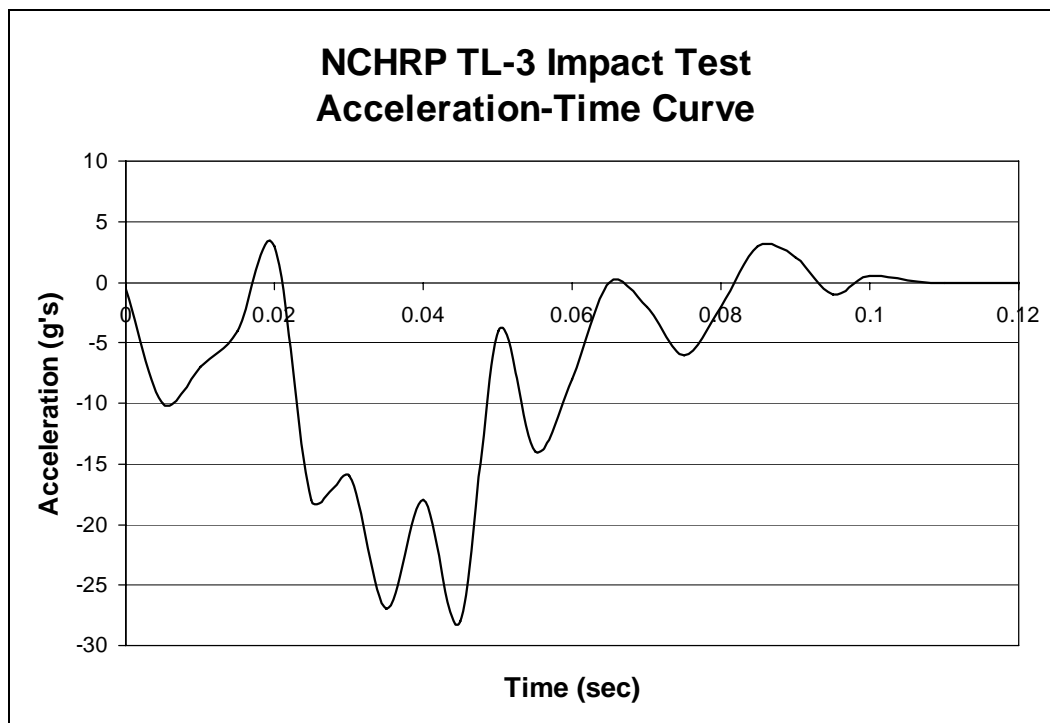


Figure 7.1: Acceleration-time history for full-scale vehicular crash test of Geo Metro under TL-3 of *NCHRP Report 350*

7.1.2 Select Material for Crush Package

Two principal options were considered in selecting the material for the crush package: autoclaved aerated concrete (AAC) and tubular steel.

Preliminary tests of an AAC crush package were completed using a block of unreinforced AAC measuring 610-mm (24-in.) long and 200-mm (8-in.) square in cross-section, attached to the front of the pendulum and impacting a rigid barrier. Results showed that the AAC did not have enough strength and stiffness to slow down the pendulum sufficiently during impact or absorb enough energy. After preliminary static testing indicated its general suitability, tubular steel was selected for trial as a potential material for the crush package. It proved to be appropriately strong, stiff and repeatable in behavior. The static test procedure used to verify these response characteristics is described.

An initial arrangement of steel tubes was created using 152.4-mm (6-in.) sections of 25.4-mm (1-in.) tubes, placed in six layers (Figure 7.2), alternating the orientation of adjacent layers by 90 degrees. This orthotropic arrangement was selected to reduce the chance of extreme side sway caused by simultaneous buckling of multiple adjacent layers in the same direction.

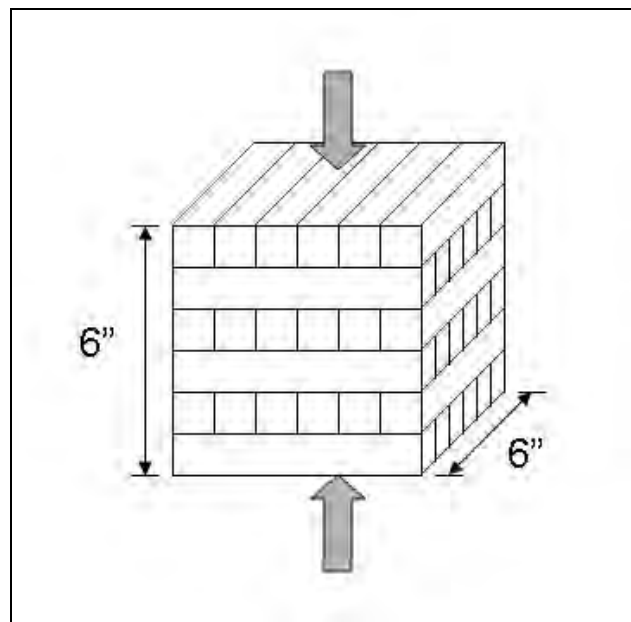


Figure 7.2: Arrangement of steel tubes for static crush test

The steel tube walls had a thickness of 1.25 mm (0.049 in.). The resulting cubical arrangement of steel tubes was tested statically to determine its load-deformation characteristics (Figure 7.3). As each layer of tubes crushes, it creates a peak in the curve of between 165 and 222 kN (37 and 50 kips), and crushes to about 40 percent of its initial length. The resulting curve was used to design an appropriate crush package as explained in Section 7.1.3.

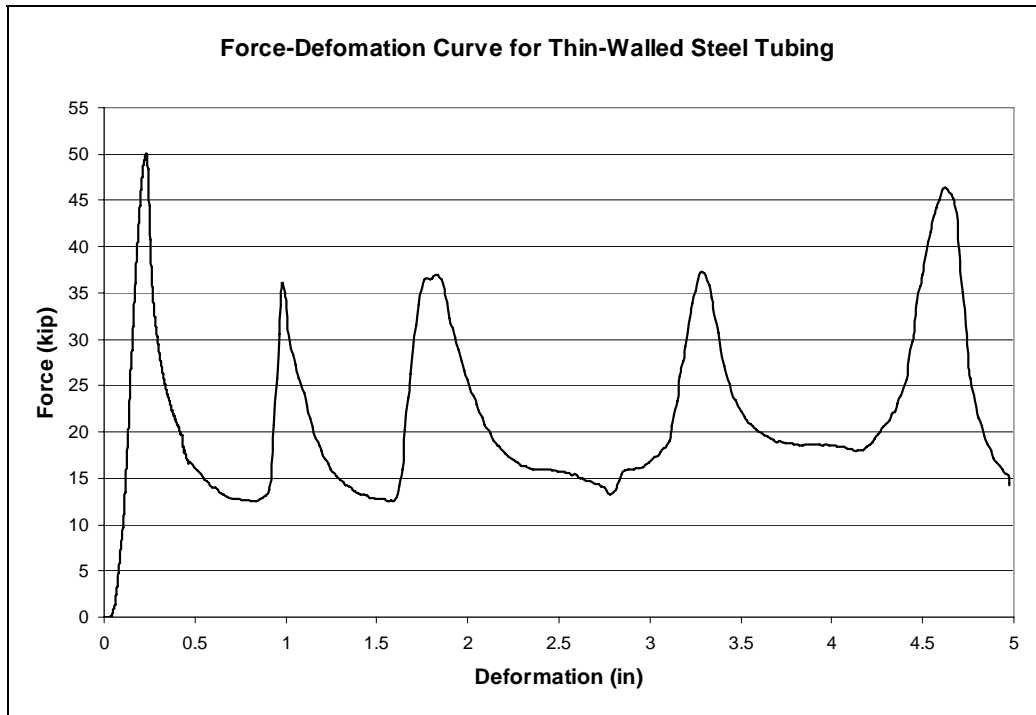


Figure 7.3: Force-deformation curve obtained from static test of first arrangement of steel tubing

7.1.3 Establish Geometry of Crush Package

The peak load produced during static testing of a crush package with a 152.4-mm (6-in.) square cross-sectional area (222 kN, or 50 kips) was quite similar to the required peak force in an *NCHRP Report 350* crash test to TL-3, indicating that this cross-sectional area of steel tubes would be a good starting point for design of the crush package. Based upon the area under the force-deformation curve from the static test, and its relationship to the desired amount of energy to be absorbed, an overall length of 457.2 mm (18 in.), representing 18 layers of tubes, was selected for the preliminary design of the crush package for the laboratory impact pendulum. Shown in Figure 7.4 are the resulting geometry for that crush package and the corresponding LS-DYNA model.

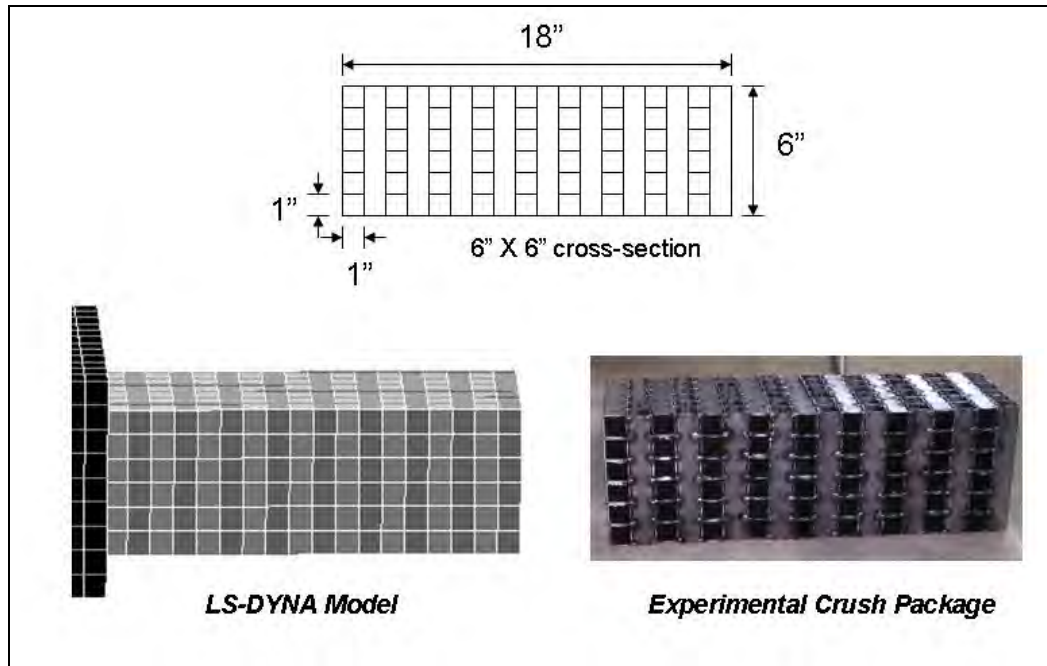


Figure 7.4: Geometry of preliminary design for crush package for laboratory pendulum and corresponding DYNA model

7.2 Testing and Simulation of Preliminary Design of Crush Package

The preliminary design of the crush package was tested experimentally by pendulum tests against a rigid barrier, and it was also simulated analytically using LS-DYNA. The rigid barrier was used to ensure that the resulting acceleration-time curves would be due to the deformations of the crush package only, independent of the barrier. Results of the experimental tests are given in Section 7.2.1, and results of the analytical simulations, in Section 7.2.2. As described in Section 7.2.3, the crush package design was subsequently modified based on both types of verification.

7.2.1 Results of Experimental Verification using Pendulum Testing

The acceleration-time curve for the preliminary design of the crush package, tested using the laboratory pendulum, is shown in Figure 7.5. The peak acceleration was about 25 g, which, multiplied by the mass of the laboratory pendulum (855 kg), gave a peak force of 210 kN (47 kips). The duration of the impact was about 0.09 sec, and the resulting impulse was about 6600 N-sec. These initial test conditions (vehicle mass and velocity) are within the ranges of variables permitted by *NCHRP Report 350*, and the impulse is also close to that of the Geo Metro, indicating that TL-3 was achieved by that pendulum test.

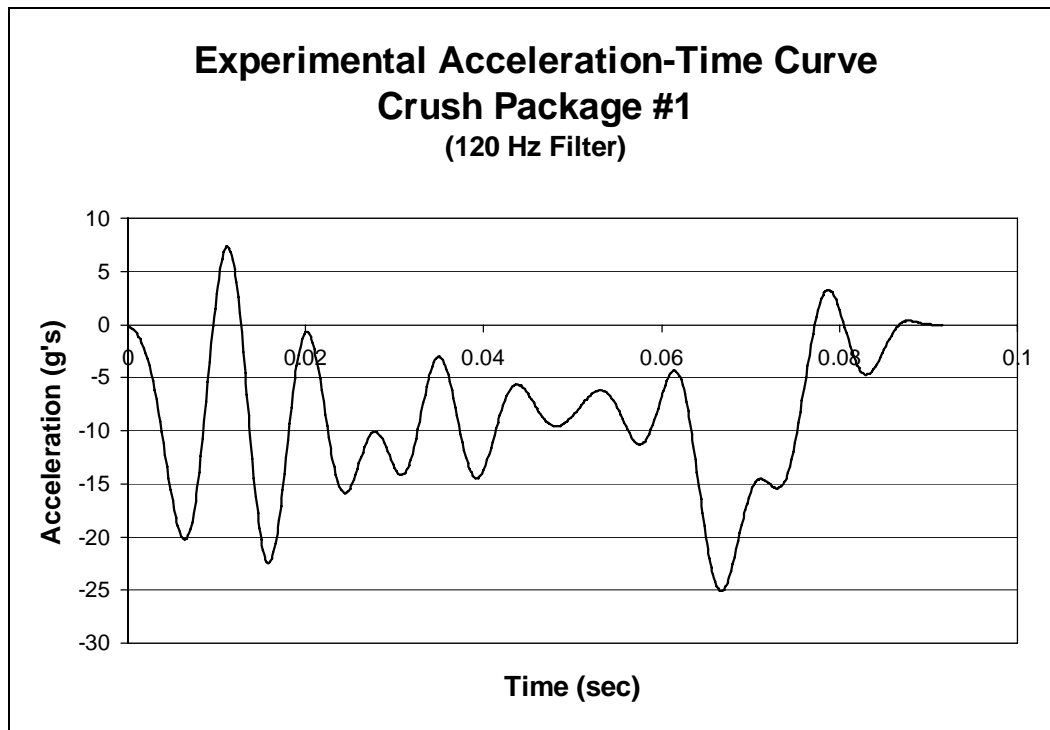


Figure 7.5: Acceleration-time curve for preliminary design of crush package (pendulum testing)

7.2.2 Results from LS-DYNA Simulation using Preliminary Design of Crush Package

The acceleration-time curve for the preliminary design of the crush package in a LS-DYNA impact simulation is shown in Figure 7.6. The finite-element simulations are used to qualify the pendulum tests to a particular level by *NCHRP Report 350* and also to verify the results of the experimental tests. Using the preliminary design for the crush package, the LS-DYNA simulation gives a peak force of 291 kN (65.5 kips) with a pendulum mass of 849 kg (836 kg simplified pendulum model and crush package) and an impact duration of about 0.05 sec. Although the duration is less than that of the experimental test, the impulse is quite similar, about 7700 N-sec. This comparison is consistent with assertions made by the authors and others (Chapter 2) that LS-DYNA can be used to corroborate the validity of results from experimental pendulum testing. In addition, the results of the simulations also show that they qualify by themselves at TL-3 of *NCHRP Report 350*.

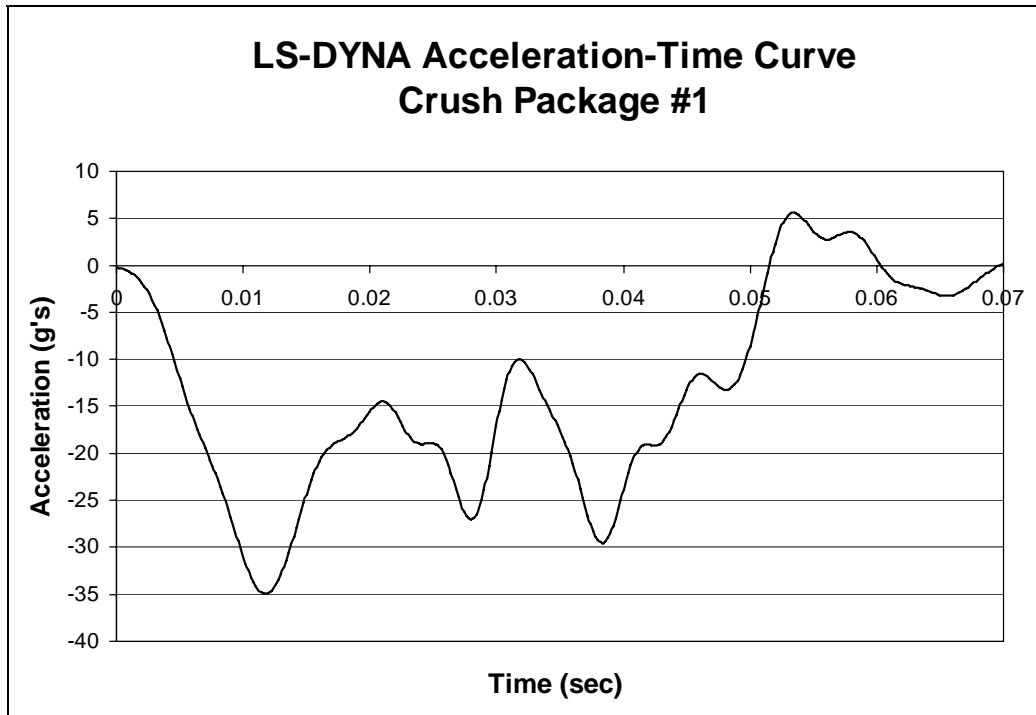


Figure 7.6: Acceleration-time curve for preliminary design of crush package (LS-DYNA simulation)

7.2.3 Modifications to Preliminary Design of Crush Package

In Figure 7.7, the acceleration-time curves obtained from pendulum testing with the preliminary design of the crush package, and the corresponding curve for the LS-DYNA simulation, are compared with the acceleration-time curve obtained in a real crash test involving angled impact on a real barrier by a Geo Metro. In Figure 7.8 are compared the impulses from each test to TL-3 of NCHRP 350, for the laboratory pendulum with the preliminary design for the crush package, for a Geo Metro impacting a barrier at an angle, and for the LS-DYNA simulation of the laboratory pendulum with the preliminary design for the crush package. Figure 7.9 shows the corresponding peak forces. The impulses from the surrogate vehicles were respectively 3% and 13% different than that of the Geo Metro, and the maximum forces were different by 15% and 18% respectively. These agreements were considered acceptable. Both the pendulum and its LS-DYNA simulation, however, reached their maximum acceleration quite quickly, in contrast to the gradual ramp of the Geo Metro test. The preliminary design of the crush package was therefore modified to achieve a more gradual increase of acceleration to the peak value.

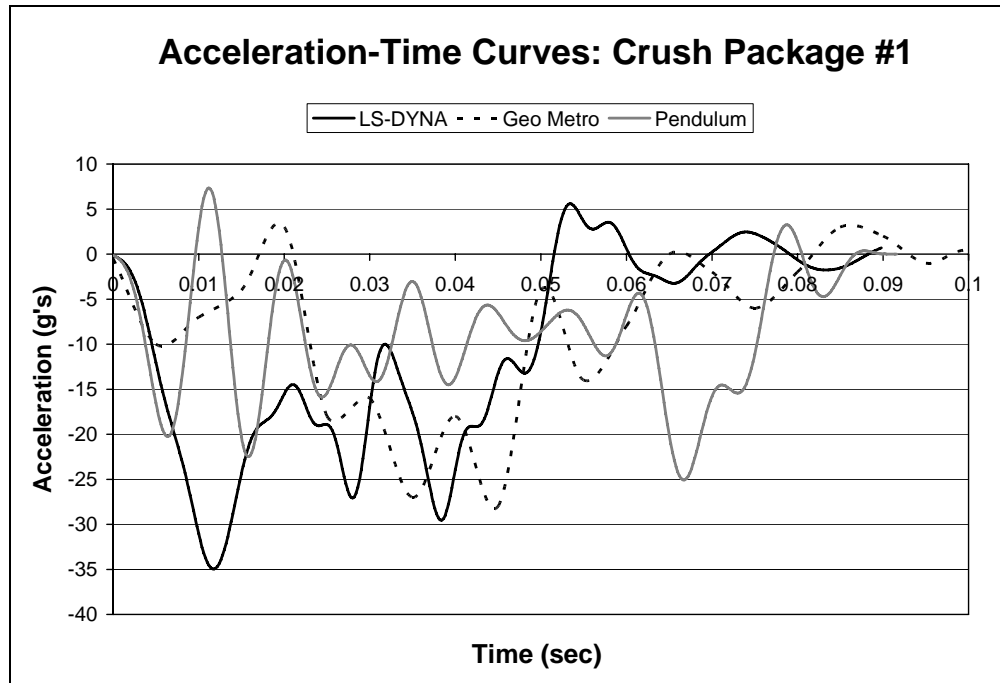


Figure 7.7: Comparison of acceleration-time curves for preliminary design of crush package (LS-DYNA simulation of laboratory pendulum; Geo Metro test; and laboratory pendulum)

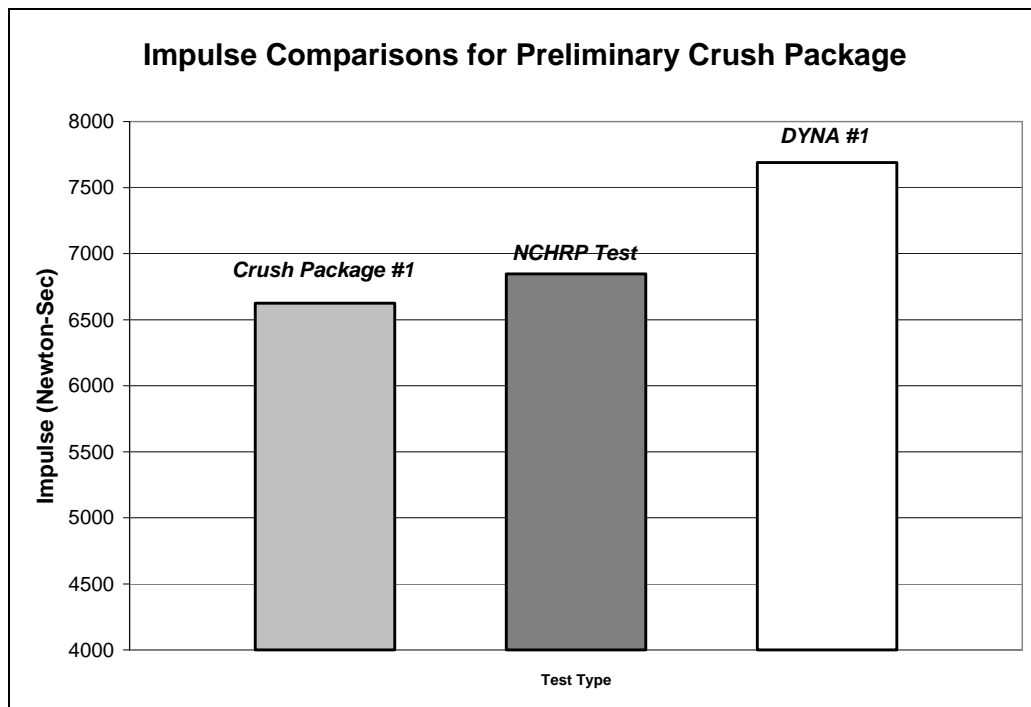


Figure 7.8: Comparison of impulses for real and surrogate tests to NCHRP TL-3 (pendulum tests with preliminary crush package; Geo Metro test; and LS-DYNA simulation of pendulum test with preliminary crush package)

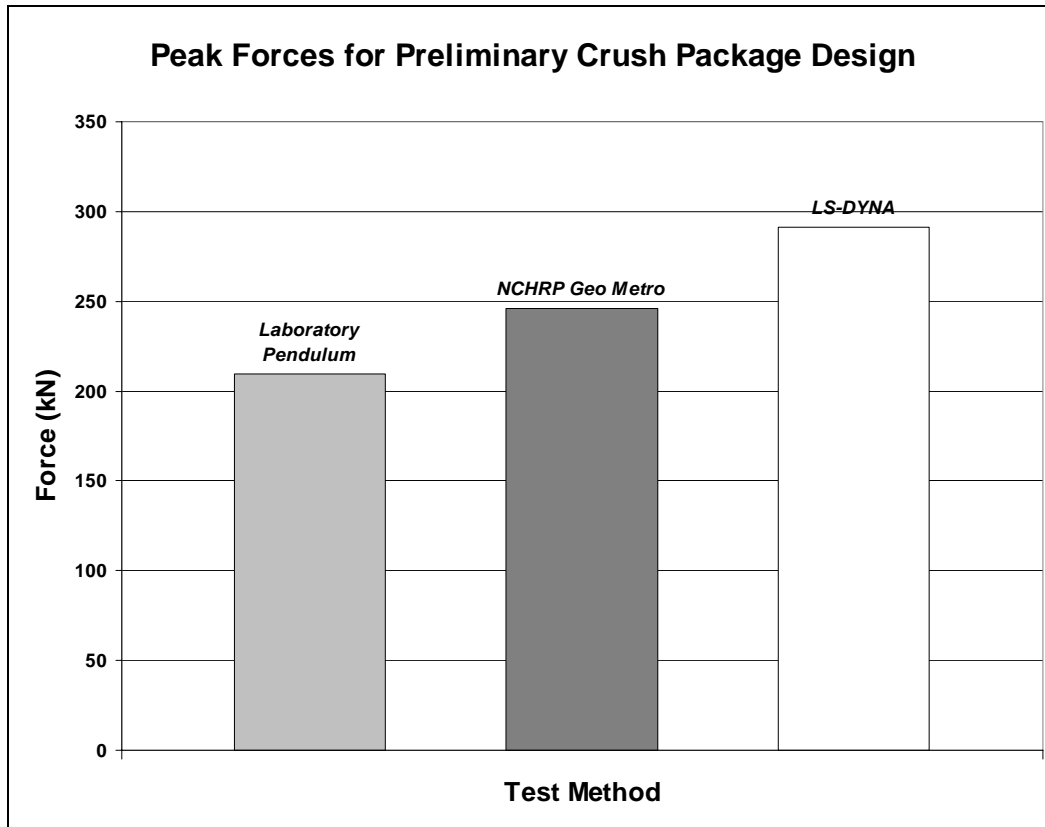


Figure 7.9: Comparison of peak forces for real and surrogate tests to NCHRP TL-3 (pendulum tests with preliminary crush package; Geo Metro test; and LS-DYNA simulation of pendulum test with preliminary crush package)

7.3 Modified Design of Crush Package for Laboratory Pendulum

Because the peak force at which the crush package begins to crush is directly proportional to the package's cross-sectional area, the design of the crush package was modified so that its cross-sectional area would increase in steps from the front of the package to the point of attachment to the pendulum mass. Each successive layer of increasing cross-sectional area was intended to crush at a higher force than the preceding layer, resulting in a force-time curve with a more gradual rise to the maximum force.

7.3.1 Geometry of Modified Crush Package

As shown in Figure 7.10, the overall length of the modified crush package was increased to 558.8 mm (22 in.). Because the smaller cross-sectional areas crush at lower forces and absorb less energy, it was anticipated that the increased length would maintain the proper duration of the impact time. The majority of the crush package length (twelve layers) was kept at the 152.4-mm (6-in.) square cross-section used previously for the preliminary design. Added were six layers that were 127 mm (5 in.) square in cross-section, and four layers that were 102 mm (4 in.) square in cross-section. To separate the different cross-sections and ensure that the impact surface would stay flat against the rigid barrier during the crushing process, 6.35-mm (0.25-in.) thick

steel plates were inserted between layers of different cross-sections. These steel spacing plates were modeled in LS-DYNA using the same steel material and *PART* properties as the pendulum model.

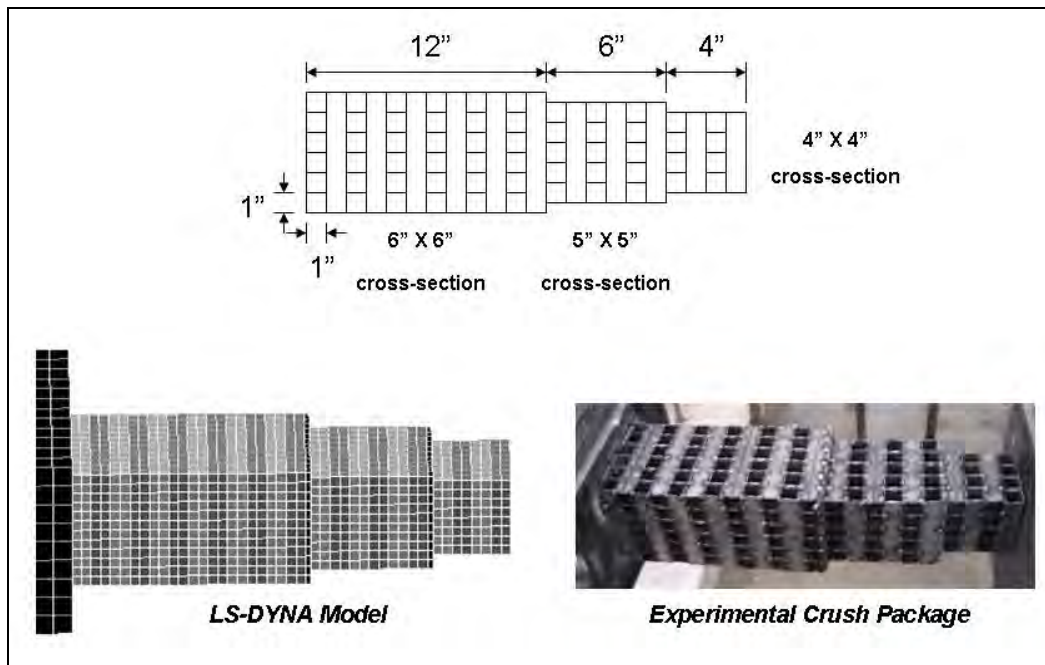


Figure 7.10: Geometry of modified design for crush package, and corresponding LS-DYNA model

7.3.2 Experimental Results from Pendulum Testing with Modified Design of Crush Package

Figure 7.11 shows the acceleration-time curve for a laboratory pendulum test against a rigid barrier, using the modified design for the crush package. The peak acceleration was approximately 25 g, corresponding to a peak force of about 210 kN (47 kips), the same as with the preliminary design of the crush package. The duration of the impact was again about 0.09 sec. The increase in acceleration to peak did take longer with the modified design than the preliminary design. The resulting impulse, however, was now about 5600 N-sec, lower than before but still similar to that of the real Geo Metro test. The vehicle mass and initial velocity were also within the tolerances specified by *NCHRP Report 350*. The initial conditions and similar impulse indicate that TL-3 was again achieved.

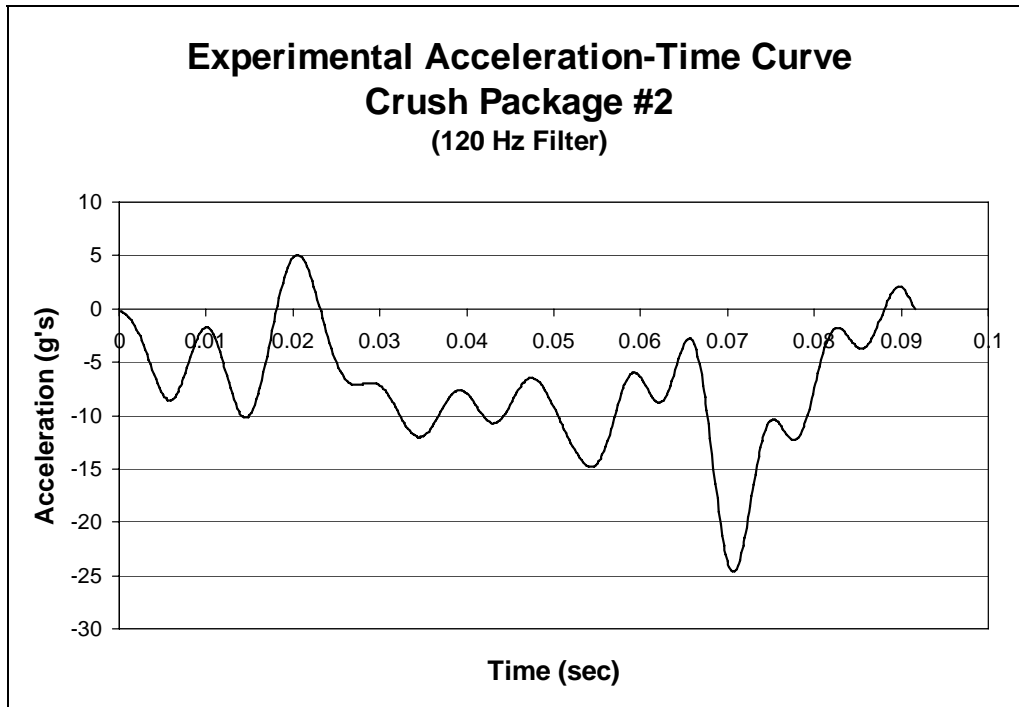


Figure 7.11: Acceleration-time curve from laboratory pendulum testing (modified design of crush package)

7.3.3 Results of LS-DYNA Simulation of Pendulum Testing using Modified Design for Crush Package

In Figure 7.12 is shown the acceleration-time curve for the LS-DYNA simulation of the laboratory pendulum test using the modified design of the crush package. The LS-DYNA curve shows a peak acceleration of 35 g, which corresponds to a peak force of 292 kN (65.7 kips) with a pendulum mass of 851 kg and a duration of about 0.05 sec. Unlike the initial simulations using the preliminary design of the crush package, the LS-DYNA simulations of laboratory pendulum testing with the modified crush package do exhibit a significant delay in reaching the peak acceleration value. Although the impact duration of the LS-DYNA simulations is somewhat less than that of the experimental pendulum tests, the impulse of 7200 N-sec and the experimental value of 5700 N-sec, are within tolerances of TL-3 of *NCHRP Report 350*.

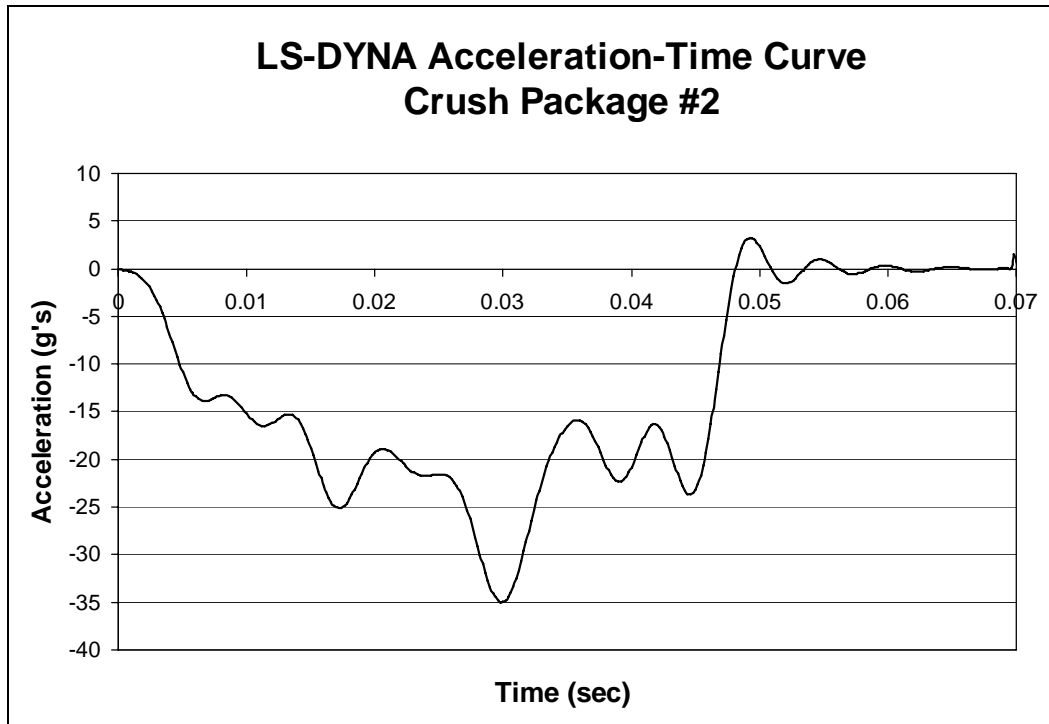


Figure 7.12: Acceleration-time curve from LS-DYNA simulation (laboratory test pendulum with modified design of crush package)

7.3.4 Recommendations for Refined Design of Pendulum Crush Package

In Figure 7.13, acceleration-time curves for laboratory pendulum testing with the modified crush package and for LS-DYNA simulation of that pendulum testing are compared with the curve for a real Geo Metro crash test. Although the impact durations differ slightly between the experimental pendulum test and its analytical simulation, the curves are again quite similar in shape to that of the real Geo Metro test. Also, as shown in Figure 7.14, the impulses for the pendulum test and its LS-DYNA simulation differ by only 18% and 6%, respectively, from the Geo Metro impulse, indicating that the modified design of the crush package meets the criteria for TL-3. Design of the crush package could be further refined, if desired, by changing the number of layers in each cross-section, and the cross-sectional areas of each layer to more closely match the vehicle crash curve. For stability under centrifugal accelerations, the length of the crush package should not exceed 610 mm (24 in.). To maintain the correct peak force, the cross-sectional dimensions should not exceed 152 mm (6 in.) on each side. Using several layers of gradually increasing cross-sectional area at the front of the crush package will extend the rise time of the force-time curve to its peak force; using more layers of the 152-mm (6-in.) square cross-section will maintain the desired impulse.

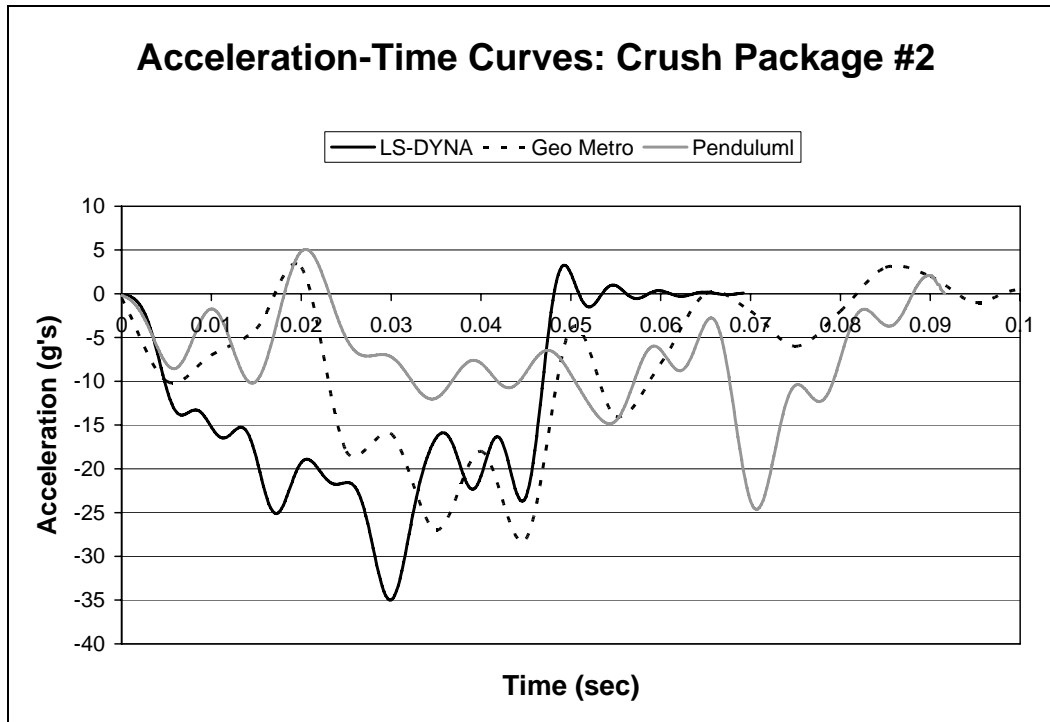


Figure 7.13: Comparison of acceleration-time curves (laboratory pendulum testing with modified design of crush package; LS-DYNA simulation of that testing; and Geo Metro test)

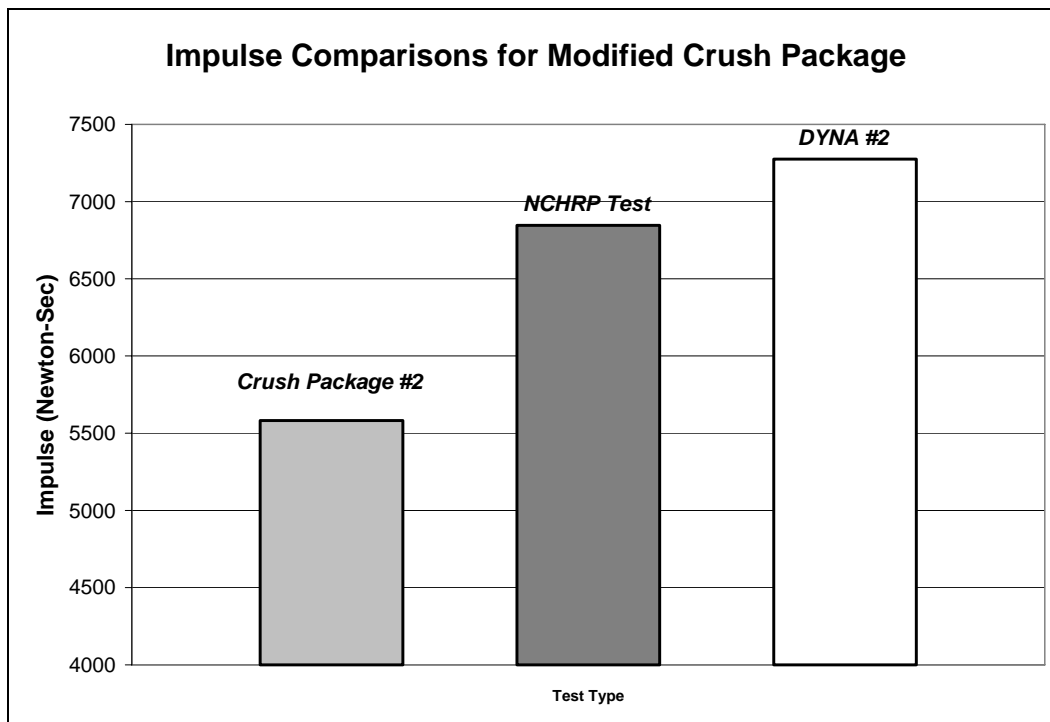


Figure 7.14: Comparison of impulses (laboratory pendulum testing with modified design of crush package; Geo Metro test; and LS-DYNA simulation of pendulum test)

7.4 Validity of Testing Methods and Significance of Results

As shown in the preceding sections of this chapter, laboratory pendulum testing can be qualified under TL-3 of *NCHRP Report 350* by appropriately modifying the mass and drop height of the pendulum to deliver the correct amount of energy to the barrier and by appropriately modifying the load-deformation properties of the crush package to match the impulse and acceleration-time history to those obtained from real impacts of vehicles against rigid barriers.

The impulse of the actual vehicle crash test is about 6800 N-sec, which is shown in the *NCHRP Test* column of Figure 7.15. Used with the laboratory pendulum, the preliminary design and the modified design for the crush package have impulses of about 6500 N-sec and 5500 N-sec respectively, as shown in the *Crush Package #1* and *Crush Package #2* columns of Figure 7.15. The impulses for the LS-DYNA simulations of pendulum tests with each crush package design are also shown in Figure 7.15, in the columns labeled *DYNA #1*, with a value of about 7600 N-sec, and *DYNA #2*, with a value of about 7200 N-sec. Finally, the theoretical impulse of about 8000 N-sec for a TL-3 crash test, calculated using impulse-momentum theory, is shown in the *Theoretical* column of Figure 7.15 for purposes of comparison. The theoretical impulse was calculated using Equation 7.1, where I is the impulse, m is the mass, and v_i and v_f are the initial and final velocities, respectively. The mass was assumed to be 850 kg and the final velocity was assumed to be zero.

$$I = F \cdot \Delta t = m \cdot v_i - m \cdot v_f \quad (7.1)$$

Although the impulses for each surrogate differ from that of the real test, each impulse qualifies the corresponding test as acceptable under *NCHRP Report 350*, because each impulse is similar to that of an actual vehicle crash test. Therefore, the testing plan developed for this research project, including the laboratory pendulum testing and LS-DYNA simulations of that testing, is acceptable for testing concrete barriers to TL-3 of *NCHRP Report 350*.

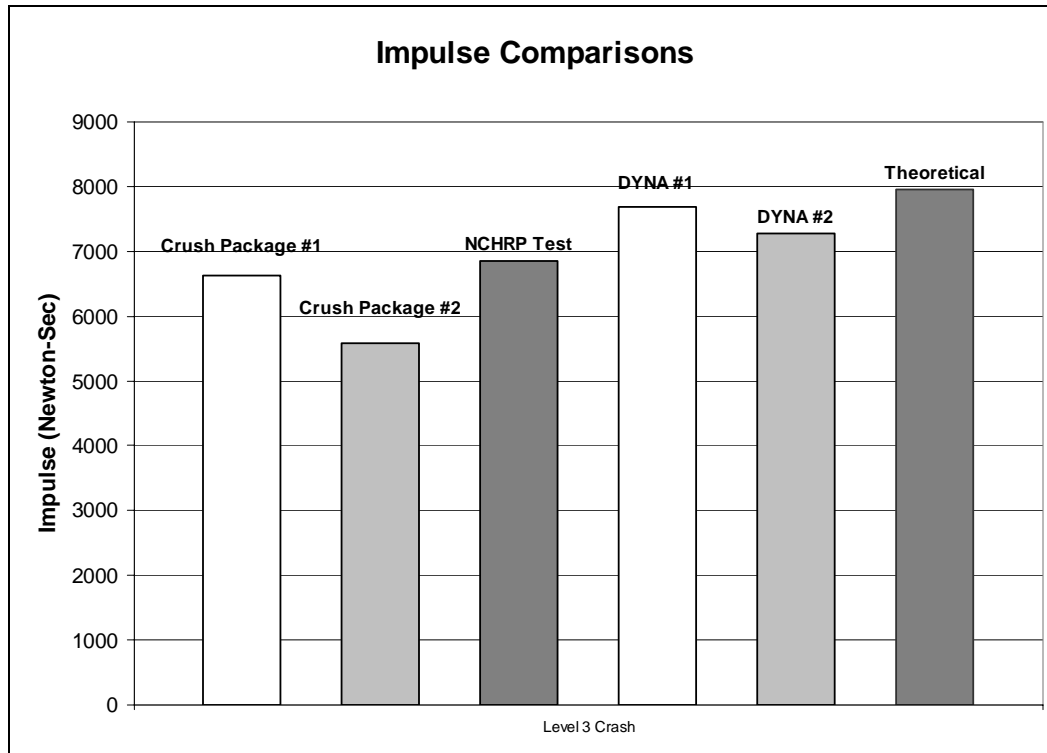


Figure 7.15: Comparison of impulses from different tests and simulations to TL- 3 of NCHRP 350

7.5 Later Refinements to Current LS-DYNA Models

At the end of this stage of the study, basic LS-DYNA models had been developed for the cast-in-place barrier, for current designs of the retrofit barrier, and also for the laboratory pendulum and crush package. Later in the study (Chapter 11), several aspects of the modeling were addressed or developed further. These aspects include evaluation of different material models, evaluation of the discrete and continuous barrier boundary conditions, and development of a model for the bridge deck.

7.5.1 Evaluation of Material Models

At the end of this stage of the study, the cast-in-place barrier model was based on the assumption that the concrete and reinforcing bar within the parapet itself behave compatibly. This assumption, in effect, resulted in a single material model with smeared properties. Once laboratory tests were completed using the cast-in-place specimens (Chapter 4), the analytical models were refined as discussed in Chapter 11.

7.5.2 Evaluate Boundary Conditions for Barrier Segments and Infinitely Long Barriers

Previous sections of this report have treated barriers as though they were segments of finite length, like the laboratory test specimens. In reality, their length could be anywhere from that finite length to the infinite length of an ideal continuous barrier. To address the expected difference in behavior between those limiting cases, it is useful to idealize the effect of adjacent

barrier segments on a particular barrier segment. To do so, the adjacent segments are idealized as translational springs attached to the ends of the barrier segment in question. This modeling is discussed further in Chapter Chapter 9.

7.5.3 Develop Analytical Models for the Bridge Deck

Though the retrofit design for the concrete barrier is based primarily upon the behavior of the cast-in-place barrier itself, the behavior of the bridge deck also affects overall barrier response. At the end of this stage of the research, the bridge deck overhang was modeled as rigid. Later in this report (Chapter 11), a more realistic model for the bridge deck is developed, incorporating a material model addressing deformation and also erosion of elements, to permit the LS-DYNA model to include flexural yielding of the deck and concrete breakout around the anchors attaching the barrier to the slab.

Chapter 8. Results from Experimental Testing of T203 Bridge Barriers

8.1 Introduction

This chapter presents the test results obtained from dynamic pendulum tests and the confirmatory quasi-static tests on laboratory specimens representing a T203 barrier and its associated bridge deck. Test results are presented in the following order:

- pendulum impact tests on cast-in-place T203 barrier specimens;
- pendulum impact tests on retrofit T203 barrier specimens; and
- quasi-static tests on a retrofit T203 barrier specimen.

8.2 Results of Pendulum Impact Tests on Cast-in-Place T203 Barriers

Impact pendulum tests (*NCHRP Report 350* TL-3) were conducted on two stand-alone cast-in-place T203 bridge barrier specimens at The University of Texas at Austin. In this section, the following results are discussed:

- still images from videos of the test;
- impact force versus time; and
- barrier displacement versus time.

A still image from one of these impact pendulum tests (Figure 8.1) shows the crushing of the tubes of the crush package and the displacement of the barrier with respect to the vertical during impact.



Figure 8.1: Still image from impact pendulum test on stand-alone, cast-in-place T203 bridge barrier and deck specimen

8.2.1 Impact Force versus Time from Pendulum Impact Tests of Cast-in-Place T203 Barrier

Figure 8.2 shows a graph of force versus time obtained from the pendulum impact test on cast-in-place T203 bridge barrier and deck specimens. The peak acceleration obtained from the accelerometer was about 27g. The peak acceleration multiplied by the weight of the pendulum (mass of the vehicle multiplied by acceleration due to gravity) gives the peak force of impact, about 49 kips. The peak dynamic capacity is at least equal to this value. As explained in Chapter 4 the dynamic capacity of the barrier can be estimated as the static capacity, multiplied by a dynamic increase of about 1.3 (Rodriguez *et al.* 2001). Therefore, dividing the observed dynamic capacity of at least 49 kips by 1.3 gives an estimated static capacity of at least 38 kips. The 50-msec dynamic peak force is about 25 kips; the duration of impact is about 0.1 seconds; and the impulse of impact is about 1.49 kip-sec (6600 N-sec).

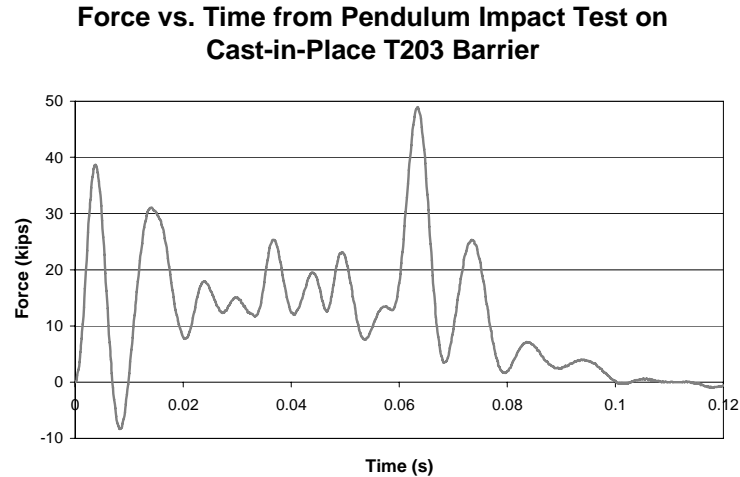


Figure 8.2: Force versus time from pendulum impact test on stand-alone cast-in-place T203 bridge barrier and deck specimen

8.2.2 Barrier Displacement versus Time from Pendulum Impact Tests of Cast-in-Place T203 Barrier

Figure 8.3 shows the displacement versus time in the cast-in-place T203 barrier, obtained at the location discussed in Section 4.6.1. The peak displacement is about 0.9 in (Figure 8.3).

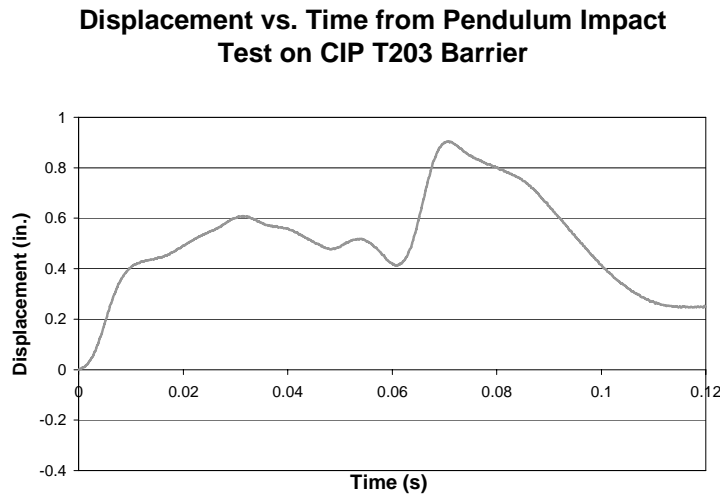


Figure 8.3: Barrier displacement-versus-time graph from pendulum impact test on standalone cast-in-place T203 bridge barrier and deck specimen

8.2.3 Strains from Pendulum Impact Tests on Cast-in-place T203 Barrier

The strains obtained in strain gages of Rows R2 and R4 (slab reinforcement perpendicular to the direction of impact) of Figure 4.18 are negligible compared to the strains

obtained from strain gages of Rows R1, R3 and R5 (slab reinforcement parallel to the direction of impact). These results indicate that the bridge deck behaves like a one-way slab in the direction of impact.

The strains in the barrier and the deck indicate that the reinforcement did not yield. Accordingly, the barrier and the slab remain essentially elastic in resisting the pendulum impact. These results for the cast-in-place barrier are presented in detail in Appendix A.

8.3 Test Results for Retrofit T203 Barriers with Through-Anchor Configuration

Impact pendulum tests (*NCHRP Report 350 TL-3*) were conducted on two stand-alone retrofit T203 bridge barrier specimens at The University of Texas at Austin. In this section, the following results are discussed:

- still images from videos of the test;
- impact force versus time; and
- barrier displacement versus time.

A still image from one of these impact pendulum tests (Figure 8.4) shows the crushing of the tubes of the crush package and the displacement of the barrier with respect to the vertical during impact.

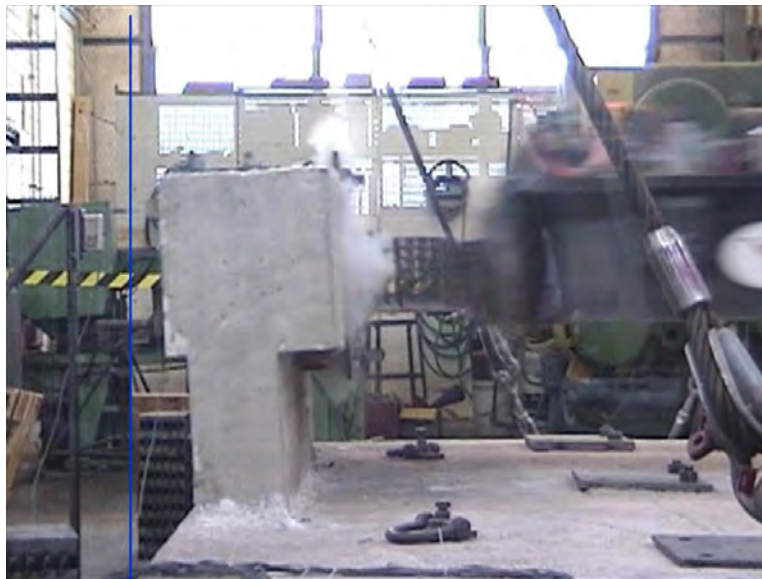


Figure 8.4: Still image from impact pendulum test on stand-alone retrofit T203 bridge barrier and deck specimen

8.3.2 Impact Force versus Time from Pendulum Impact Tests on Retrofit T203 Barrier

Figure 8.5 shows a graph of force versus time obtained from the pendulum impact test on a retrofit T203 bridge barrier and deck specimen. The peak acceleration obtained from the

accelerometer was about 20g. This acceleration gives a peak force of impact of about 38 kips. The 50-msec dynamic capacity is about 20 kips; the duration of impact is about 0.1 seconds; and the impulse of impact is about 1.44 kip-sec (6400 N-sec). The retrofit barrier has lower capacity than the cast-in-place barrier due to tensile concrete breakout of the retrofit anchors.

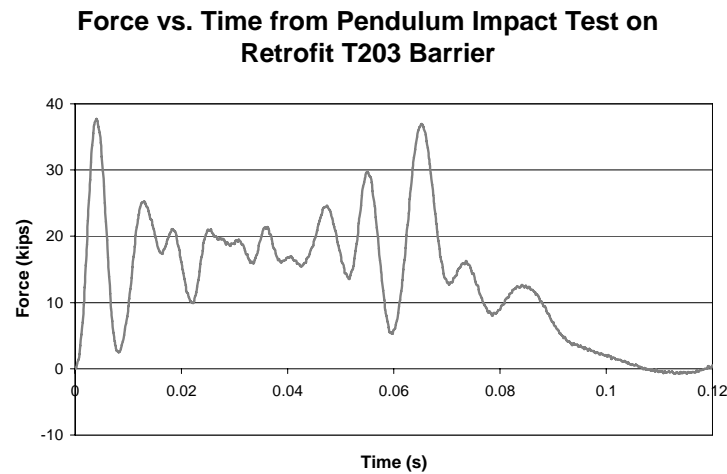


Figure 8.5: Force-versus-time graph from pendulum impact test on standalone retrofit T203 bridge barrier and deck specimen

8.3.3 Barrier Displacement versus Time from Pendulum Impact Tests on Retrofit T203 Barrier

Figure 8.6 shows the displacement versus time in the retrofit T203 barrier, obtained at the location discussed in Section 4.6.1. The peak displacement in the barrier is about 1 in. (Figure 8.3).

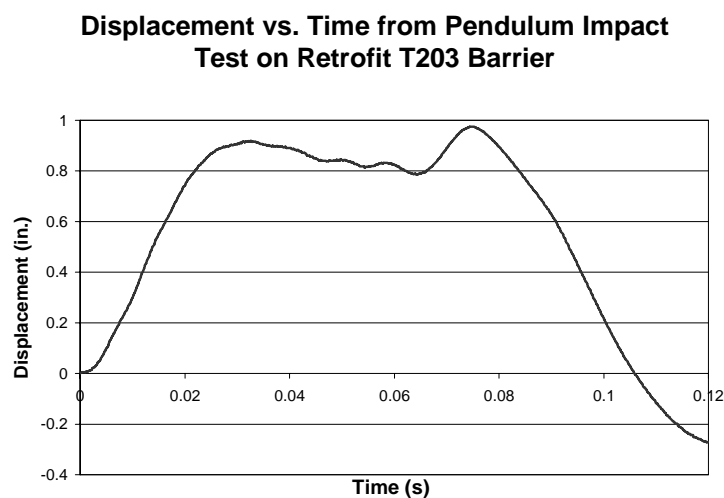


Figure 8.6: Barrier displacement-versus-time graph from pendulum impact test on standalone retrofit T203 bridge barrier and deck specimen

8.3.4 Strains from Pendulum Impact Tests on Retrofit T203 Barrier

Strains obtained in strain gages of Rows R2 and R4 (slab reinforcement perpendicular to the direction of impact) of Figure 4.18 are negligible as compared to the strains obtained from strain gages of Rows R1, R3 and R5 (slab reinforcement parallel to the direction of impact). These results indicate that the bridge deck behaves like a one-way slab in the direction of impact.

Strains in the bridge deck indicate that the reinforcement did not yield, and that the slab remains essentially elastic. The strains in the barrier reinforcement indicate that the barrier has yielded, however. Results for the retrofit barrier are presented in detail in Appendix A of this report.

8.4 Results from Quasi-Static Test on Retrofit T203 Barrier

The quasi-static test setup for the retrofit T203 bridge barrier and deck specimen is discussed in Section 4.3. Figure 8.7 shows the force versus displacement graph obtained from the quasi-static test on the retrofit T203 barrier and bridge deck specimen. It can be seen that the static capacity of this barrier is about 25 kips. The estimated static capacity of this barrier (as discussed in Section 4.5.2) was 24 kips, which is almost the same as the test value. As expected, failure is by concrete breakout.

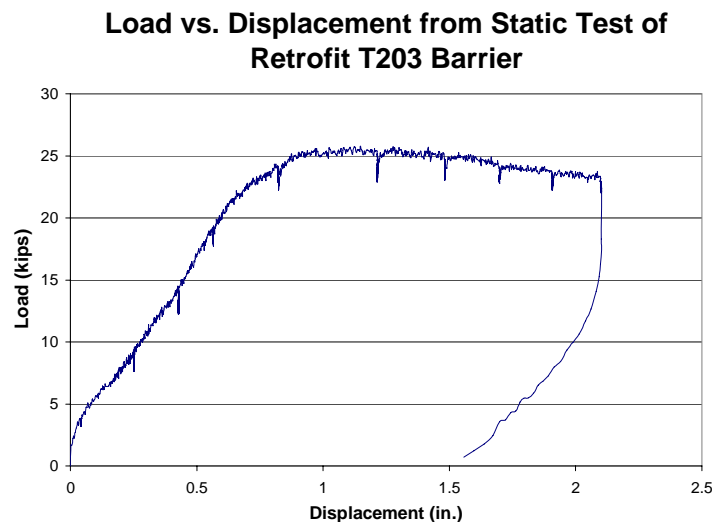


Figure 8.7: Force-versus-displacement graph from quasi-static test on stand-alone retrofit T203 bridge barrier and deck specimen

Chapter 9. Significance of Test Results for T203 Barriers

9.1 Introduction

In this chapter, the significance of the previously presented test results for T203 barriers is discussed, first in terms of *NCHRP Report 350* test criteria, and then in terms of the revised TxDOT performance criteria for retrofit barriers. Based on the significance of the test results, a final design of the retrofit T203 barrier is proposed.

9.2 Significance of Test Results in Terms of NCHRP Test Criteria

In this section, the *NCHRP Report 350* TL-3 criteria to compare the cast-in-place and retrofit T203 barrier, based on the results from pendulum impact tests, are discussed. Next, the cast-in-place and retrofit T203 barrier pendulum impact test results are compared using these criteria to understand the significance of those results in terms of the TxDOT criteria for retrofit barriers.

9.2.1 Barrier Criteria for NCHRP 350 TL-3

NCHRP performance criteria for highway barriers are outlined in Chapter 2. The standard T203 cast-in-place barrier has been designed and tested to *NCHRP Report 350* TL-3. If the retrofit T203 barrier behaves similarly to its cast-in-place counterpart under impact testing, it also can be considered to have met *NCHRP Report 350* TL-3.

The behavior of the cast-in-place T203 barrier was characterized using the impact pendulum test setup. Impact pendulum tests were conducted to understand the dynamic response of the retrofit T203 barrier. To evaluate the performance of the retrofit T203 barrier for NCHRP TL-3, the pendulum impact test behavior of the two barriers were compared based on the *NCHRP Report 350* requirements using the following criteria:

- the impact energy imparted to the retrofit T203 barrier by the impact pendulum test setup must be the same as that imparted to the cast-in-place T203 barrier and must meet the NCHRP TL-3 requirements;
- the impulse of impact for the retrofit T203 barrier must be similar to that for the cast-in-place T203 barrier; and
- the duration of impact for the retrofit T203 barrier must be similar to that for the cast-in-place T203 barrier.

In addition, the barrier displacements during impact were compared using the following criteria:

- the displacement of the retrofit T203 barrier obtained from the pendulum test should be similar that of the cast-in-place T203 barrier.

9.2.2 Comparison of Cast-in-place and Retrofit T203 Barriers

Figure 9.1 shows that the Force-versus-time graphs for both the cast-in-place and retrofit T203 barriers, obtained from an NCHRP TL-3 impact, are similar to each other. The duration of impact for both of these barriers is close to 0.1 sec.

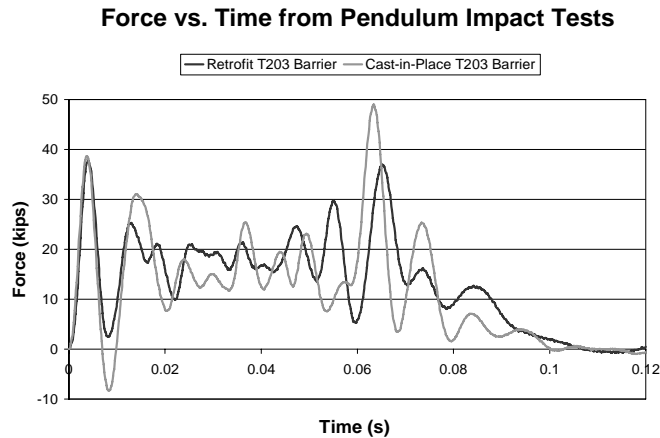


Figure 9.1: Force-versus-time graphs from pendulum impact test on standalone cast-in-place and retrofit T203 bridge barrier and deck specimens

Table 9.1 compares the impact energy, impulse of impact, duration of impact and peak displacement values for the cast-in-place and the through-anchor retrofit barriers. The energy imparted to both barriers by the impact pendulum test setup is the same and meets NCHRP TL-3 requirements. The impulse of impact of the retrofit barrier is about 1.44 kip-sec (6400 N-sec), 3% less than that obtained from pendulum tests on its cast-in-place counterpart (1.46 kip-sec (6600 N-sec)). The peak displacements are almost the same for both of these barriers.

Table 9.1: Comparison of cast-in-place and retrofit T203 barrier for NCHRP TL-3 criteria

| <i>Version of T203 Barrier</i> | <i>Comparison Criterion</i> | | | |
|--------------------------------|-----------------------------|------------------------------------|---------------------------------|-------------------------|
| | <i>Impact Energy (kJ)</i> | <i>Impulse of Impact (kip-sec)</i> | <i>Duration of Impact (sec)</i> | <i>Peak Disp. (in.)</i> |
| Cast-in-Place | 38.5 | 1.49 | 0.1 | 0.9 |
| Retrofit with through-anchors | 38.5 | 1.44 | 0.1 | 1.0 |

From Table 9.1's comparison, it can be concluded that the retrofit T203 barrier behaves similarly to its cast-in-place counterpart under an NCHRP TL-3 impact. This observation signifies that the retrofit T203 barrier with through-anchor configuration passes the NCHRP 350 TL-3 test.

9.3 Significance of Test Results in Terms of TxDOT Performance Criteria

In this section, TxDOT performance criteria for barriers are discussed in terms of dynamic capacity, dynamic capacity over a 50-msec window, and static capacity.

It is first necessary to discuss, in general terms, the relationship between TxDOT performance criteria and the test results previously presented. TxDOT performance criteria are in terms of capacities of a long section of barrier (referred to in this report as a “T203 barrier system”). A T203 barrier system is shown in Appendix E. The test results of this report are for a much shorter 5-ft section of barrier (referred to as “stand-alone T203 barrier”) tested in the laboratory. The procedure for relating the two kinds of information is given in Section 4.5.3.

After relating the test results to the TxDOT performance criteria, the significance of the T203 barrier system capacities is discussed in terms of the TxDOT performance criteria to evaluate the retrofit T203 barriers.

9.3.1 Discussion of TxDOT Performance Criteria for Barrier Systems

Dynamic capacity

Dynamic capacity is the peak force generated between the barrier and a vehicle (or surrogate vehicle such as a pendulum). It includes peaks whose durations are very short, and it is based on filtered data (Section 4.6.2). The dynamic capacity of the barrier system includes the dynamic capacity of the stand-alone barrier (the mechanical connection with the slab), plus the contribution of the longitudinal stiffness and inertia of the length of the barrier affected by vehicular impact. The contribution from the stand-alone depends on the stand-alone barrier’s dynamic capacity, which is generally about 1.3 times its static capacity (Rodriguez *et al.* 2001). The contribution from the rest of the barrier depends partly on the dynamic stiffness of the affected barrier length and partly on its inertia. The motion far away from the impact location is not large, and, under these conditions, the dynamic stiffness can be approximated from the static stiffness because inertial effects are not important. The inertial contribution, in contrast, is present only in the dynamic case, and is completely absent in the static case.

Dynamic Capacity over a 50-msec Window

Dynamic capacity over a 50-msec window is discussed in Section 4.5.4.

Static Capacity

Static capacity is the capacity under static or quasi-static loading. It depends on the static strength of the stand-alone retrofit barrier (the mechanical connection with the slab), plus the contribution from the static stiffness of the length of the barrier that is affected by vehicular impact. In a continuously connected barrier, this length is independent of the location of the point of impact. In a discontinuously connected barrier (such as the T203 barrier system), the affected length does depend on the location of the point of impact. It also depends in general on the location of the point of impact with respect to an end of the barrier.

9.3.2 Probable Capacities of T203 Barrier Systems

In this section, the various barrier system capacity measures are obtained for the T203 barrier systems with cast-in-place, retrofit with through-anchor and retrofit with undercut anchor

configurations from FSEL test results. This is done to evaluate the performance of the retrofit T203 barriers in terms of the TxDOT performance criteria.

Peak Dynamic Capacities

The peak dynamic capacity of a T203 cast-in-place barrier system obtained from TTI results is about 160 kips. About 70% of this value (110 kips) comes from continuity of the barrier, and the remaining 30% (50 kips) comes from the resistance of the stand-alone barrier (refer to Appendix D). The contribution due to barrier continuity is assumed to remain the same for the different scenarios addressed in the following sections. Failure is by a form of concrete breakout (straightening of the bent reinforcement connecting the barrier to the slab).

- The contribution of the barrier continuity (110 kips) added to the dynamic capacity of the standalone cast-in-place T203 barrier (49 kips), obtained from the FSEL pendulum impact test, gives the capacity of the cast-in-place T203 barrier system to be 159 kips. This result is similar to the value obtained from TTI tests.
- The contribution of the barrier continuity (110 kips) added to the dynamic capacity of the standalone retrofit T203 barrier (38 kips) with the through-anchor configuration, obtained from the FSEL pendulum impact test, gives the capacity of this retrofit T203 barrier system to be 148 kips. Failure is by concrete breakout.
- The contribution of the barrier continuity (110 kips) added to the dynamic capacity of the standalone retrofit T203 barrier (15 kips) with the undercut anchor configuration (estimated in Chapter 4) gives the capacity of this retrofit T203 barrier system to be 125 kips. Failure is by concrete breakout.

Dynamic Capacities over a 50-msec Window

The 50-msec dynamic capacity of a T203 cast-in-place barrier system obtained from TTI results is about 68 kips. About 60% of this value (40 kips) comes from continuity of the barrier, and the remaining 40% comes from the capacity of the stand-alone barrier (refer to Appendix D). The contribution due to barrier continuity is assumed to remain the same for the different scenarios that follow. Failure is by a form of concrete breakout (straightening of the bent reinforcement connecting the barrier to the slab).

- The contribution of the barrier continuity (40 kips) added to the 50-msec dynamic capacity of the standalone cast-in-place T203 barrier (25 kips), obtained from the FSEL pendulum impact test, indicates the capacity of the cast-in-place T203 barrier system to be 65 kips. This value is 4% less than the value obtained from the TTI tests.
- The contribution of the barrier continuity (40 kips) added to the 50-msec dynamic capacity of the standalone retrofit T203 barrier (21 kips) with the through-anchor configuration, obtained from the FSEL pendulum impact test, gives the capacity of this retrofit T203 barrier system to be 61 kips. Failure is by concrete breakout.
- The contribution of the barrier continuity (40 kips) added to the 50-msec dynamic capacity of the standalone retrofit T203 barrier (9 kips) with the undercut anchor configuration gives the capacity of this retrofit T203 barrier system to be 49 kips. Failure is by concrete breakout.

Static Capacities

The static capacity of a T203 cast-in-place barrier system obtained from TTI results is about 72 kips. About half of this value (35 kips) comes from continuity of the barrier, and the other half (37 kips) comes from the capacity of the stand-alone barrier (refer to Appendix D). The contribution due to barrier continuity is assumed to remain the same for the different scenarios that follow. Failure is by a form of concrete breakout (straightening of the bent reinforcement connecting the barrier to the slab).

- The contribution of the barrier continuity (35 kips) added to the static capacity of the standalone cast-in-place T203 barrier (38 kips) gives the capacity of the cast-in-place T203 barrier system to be 72 kips. This value is almost same as the value obtained from the TTI tests.
- The contribution of the barrier continuity (35 kips) added to the static capacity of the standalone retrofit T203 barrier (25 kips) with the through-anchor configuration (obtained from the quasi-static testing at FSEL) gives the capacity of this retrofit T203 barrier system to be 61 kips. Failure is by concrete breakout.
- The contribution of the barrier continuity (35 kips) added to the static capacity of the standalone retrofit T203 barrier (11 kips) with the undercut anchor configuration (estimated in Chapter 4.) gives the capacity of this retrofit T203 barrier system to be 46 kips. Failure is by concrete breakout.

9.3.3 Significance of Probable Capacities of T203 Barrier Systems

Table 9.2 gives a summary of the different capacities for various versions of the T203 barrier systems. Failure for all these versions is by a form of concrete breakout.

Table 9.2: Capacities of T203 barrier systems

| <i>Version of T203 Barrier</i> | <i>Capacity of T203 Barrier System, kips</i> | | |
|--------------------------------|--|--|------------------------|
| | <i>Peak Dynamic Capacity</i> | <i>Dynamic Capacity (50-msec window)</i> | <i>Static Capacity</i> |
| Cast-in-Place | 160 | 68 | 72 |
| Retrofit with through-anchor | 148 | 61 | 60 |
| Retrofit with undercut anchors | 125 | 49 | 46 |

In terms of the updated TxDOT performance criteria, the capacities summarized in Table 9.2 lead to the following conclusions:

- The retrofit barrier with the through-anchor configuration, like the cast-in-place barrier, meets current TxDOT requirements. Its dynamic capacity over a 50-msec window (60 kips) is not less than 60 kips, and its static capacity (60 kips) is not less than 54 kips.
- The retrofit barrier with undercut anchors, however, probably will not meet current TxDOT requirements. Its probable dynamic capacity over a 50-msec window (49

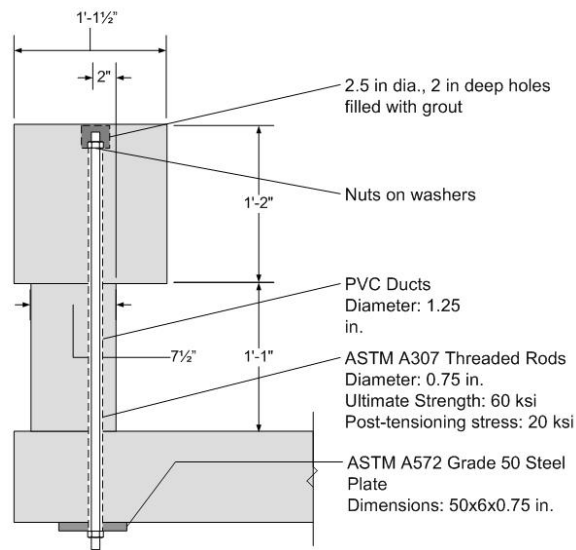
kips) is less than 60 kips, and its probable static capacity (46 kips) is less than 54 kips. Because both the dynamic (50-msec window) and the static capacities of this retrofit barrier with undercut anchors are reasonably close to the required levels, it is probably premature to discard this retrofit barrier immediately. It will be necessary to conduct static and dynamic tests of retrofit barriers with undercut anchors to refine the probable capacities described.

- At movement joints between barrier sections, the capacity of the proposed T203 retrofit barriers is reduced because longitudinal continuity of the rail exists on one side of the barrier only. Because the breakout capacity of the barrier base is not reduced by the movement joint, and because the reduction in longitudinal continuity is identical to that experienced by cast-in-place barriers, the proposed retrofit T203 design can be used at end locations as well as at interior locations.

9.4 Final Design of Retrofit T203 Barrier

Based on the conclusions and project time constraints, the possibility of testing and recommending T203 retrofit barriers with undercut anchors was eliminated. It was decided that the retrofit T203 barrier with the through-anchor configuration will be the best possible design to retrofit T203 barriers with mechanical anchors.

The recommended design is shown in Figure 9.2. One aesthetic change was made based on suggestions by TxDOT. The top plate used in the preliminary design is eliminated and replaced by nuts and washers placed in countersunk holes in the top of the retrofit barrier. The countersunk holes are to be subsequently grouted.

 $\rightarrow 2^n$

- 2.5 in dia., 2 in deep holes
filled with grout

n washers

- Nuts on washers

- PVC Ducts
Diameter: 1.25
in.

| | |
|--|--|
| | |
|--|--|

1'-1''

- ASTM A307 Threaded Rods
- Diameter: 0.75 in.
- Ultimate Strength: 60 ksi
- Post-tensioning stress: 20 ksi

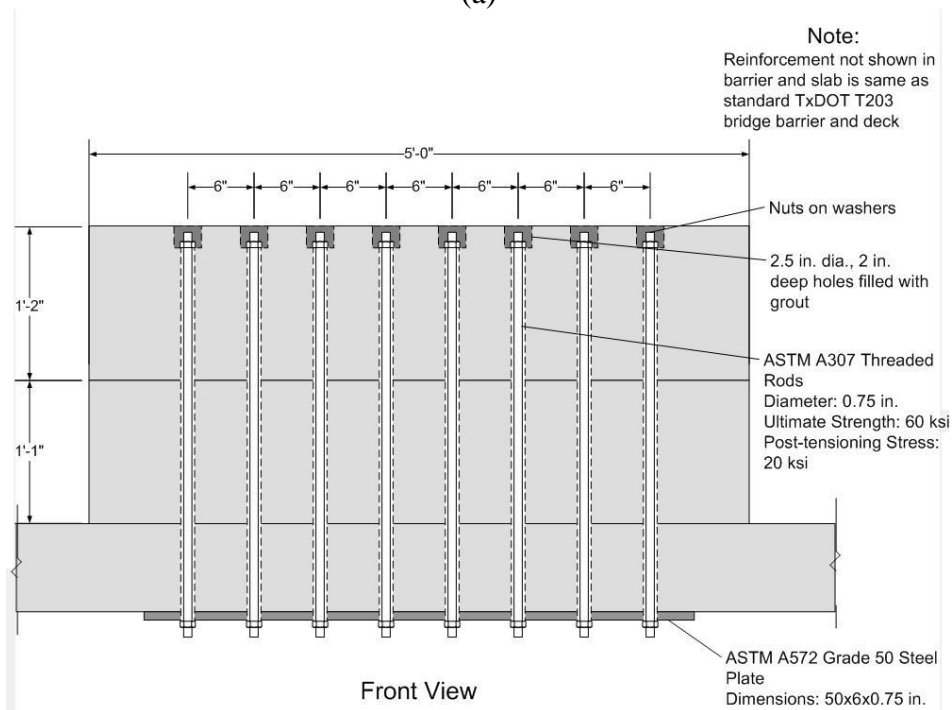
ASTM A572 Grade 50 Steel
Plate
Dimensions: 50x6x0.75 in.

Note:

Reinforcement not shown in barrier and slab is same as standard TxDOT T203 bridge barrier and deck

Side View

(a)



6"

6"

6"

6"

100

1'-2'

1'-1"

Note:

Reinforcement not shown in barrier and slab is same as standard TxDOT T203 bridge barrier and deck

— Nuts on washers

2.5 in. dia., 2 in.
deep holes filled with
grout

ASTM A307 Threaded
Rods
Diameter: 0.75 in.
Ultimate Strength: 60 ksi
Post-tensioning Stress:
20 ksi

ASTM A572 Grade 50 Steel
Plate
Dimensions: 50x6x0.75 in.

Front View

(b)

Figure 9.2: Recommended design of retrofit T203 barrier (a) side view and (b) front view

- probable capacities of T501 barrier systems obtained from FSEL retrofit T501 barrier specimen capacities to determine if the preliminary retrofit T501 barrier design meets the revised TxDOT performance criteria for retrofit barriers;
- experimental testing plan to test the retrofit T501 barrier and bridge deck specimens; and
- recommendations to use future test results to check if the preliminary retrofit T501 barrier design meets the TxDOT barrier performance criteria.

10.2 T501 Bridge Barrier and Deck Test Specimens

First, the development the basic design of the T501 barrier and bridge deck specimen at FSEL to represent the standard TxDOT bridge deck and T501 barrier is discussed. Next, a preliminary design of retrofit T501 barrier test specimens to be used at FSEL is presented. Finally, static and dynamic capacities of this test specimen are estimated.

10.2.1 Basic T501 Barrier and Bridge Deck Test Specimens

The T501 specimens must have the following characteristics:

- the specimens must be capable of representing retrofit as well as cast-in-place barriers;
- the specimens must include relevant details of the T501 barrier and the standard TxDOT 3-ft (0.9-m) bridge deck overhang;
- the specimens must fit into the impact test pendulum setup; and
- the specimens must incorporate details permitting the retrofit barrier to be attached to the bridge deck.

Test specimens of retrofit T501 barriers were designed within these constraints. Due to time constraints, it was decided not to develop cast-in-place T501 barrier specimens for testing.

The bridge deck test specimen to be used for testing T501 barriers is the same as that used for tests on T203 barriers and is discussed in Chapter 4. . The test specimen representing the T501 bridge barrier has the same cross-sectional shape as shown in Figure 10.1(b). The length of the barrier test specimen is 5 ft. so that it can easily fit into the impact pendulum test setup.

10.2.2 Design of Retrofit T501 Barrier and Probable Capacities of Test Specimens

The retrofit T501 design uses Drillco flush-mount undercut anchors as mechanical anchors. These anchors are used to attach the barrier to the bridge deck. As discussed previously regarding the development of the retrofit T203 specimens, the anchor diameter was selected so that the tensile capacity as governed by anchor steel would be slightly greater than the expected capacity as governed by group tensile breakout. The diameter of the anchors is $\frac{3}{4}$ in. They are to be installed in the bridge deck at an angle of 35° to the vertical at a spacing of 8 in., selected to maximize the breakout capacity of the anchor group as well as preserve the reinforcing details of the original barrier. The embedment length of the anchors is 8 in.

Figure 10.2 shows the schematic of the retrofit T501 barrier using flush-mount anchors. ASTM A307 threaded rods, $\frac{3}{4}$ -in. in diameter, are attached to the flush-mount in the undercut

anchors. The rods pass through PVC ducts in the barrier and are bolted in the countersunk holes on the back side of the barrier. These threaded rods act as the primary reinforcement of the retrofit T501 barrier. Each threaded rod is post-tensioned to 20 ksi for serviceability purposes. The countersunk area is then filled with grout to give a finished surface at the back.

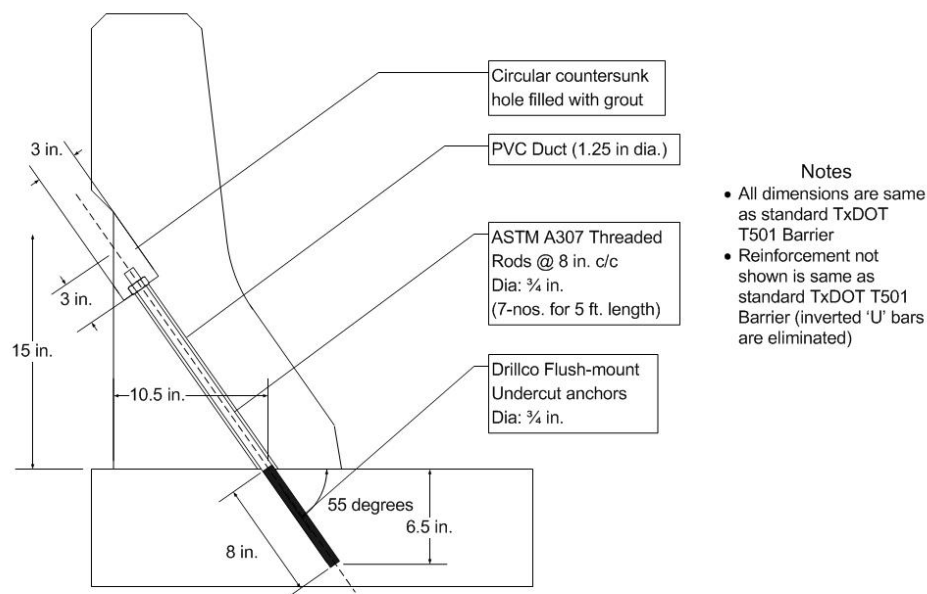


Figure 10.2: Schematic of cross-section of retrofit T501 barrier using Drillco flush-mount undercut anchors

The retrofit barriers have the same dimensions and reinforcement configuration as that of the original cast-in-place T501 barrier, except that the U-bars which attach the cast-in-place barrier to the slab (Figure 10.1(b)) are eliminated.

The retrofit T501 barrier test specimen is 5 ft. long. Seven flush-mount undercut anchors are to be installed in this 5 ft. length of the retrofit T501 barrier test specimen.

The static capacity of the retrofit T501 barrier test specimen using undercut anchors is governed by tensile breakout of concrete. Provisions of ACI 318-05 Appendix D were used to estimate the nominal static capacity (lower 5% fractile) of the test specimen of the retrofit T501 barrier as 21 kips. The mean capacity, representing the expected test value, can be estimated by multiplying the lower 5% fractile capacity by 1.4, obtaining 30 kips (refer to Appendix B of this report for calculations).

Impact pendulum tests for NCHRP TL-3 were used to evaluate the dynamic capacity of a T203 barrier test specimen. Finite element simulation in LS-DYNA of an impact pendulum test on a retrofit T203 bridge barrier and deck specimen (Chapter 11.) gave a peak impact force of about 44 kips, reasonably close to the experimental value of 38 kips. Using similar finite element simulation of the pendulum impact test on a retrofit T501 barrier test specimen (Chapter 11.), a dynamic capacity of 53 kips was obtained.

The 50-msec window dynamic capacity is calculated from the force-time curve obtained from the finite element simulation of the pendulum impact test on the retrofit T501 test specimen

(Chapter 11) and is estimated as 33 kips. These capacities were subsequently verified by conducting laboratory tests on retrofit T501 barrier specimens.

10.3 Probable Capacities of Retrofit T501 Barrier System

TxDOT performance criteria are in terms of capacities of a long section of the T501 barrier. A T501 barrier system is shown in Appendix E. The T501 test specimens and their estimated capacities are for a much shorter 5-ft. section of barrier. It is necessary to relate the capacity estimates of the 5-ft. section of the T501 barrier to TxDOT barrier performance criteria.

Dynamic capacity, 50-msec window dynamic capacity and static capacity were estimated for the retrofit T501 barrier system using the capacity estimates of the 5-ft. long test specimen coupled with information obtained from TTI test results, linear and nonlinear finite element analyses, and on reasonable predictions of the capacities of mechanical anchors. The three steps used to find the retrofit T501 barrier system capacities from T501 barrier post capacities are shown in Figure 10.3.

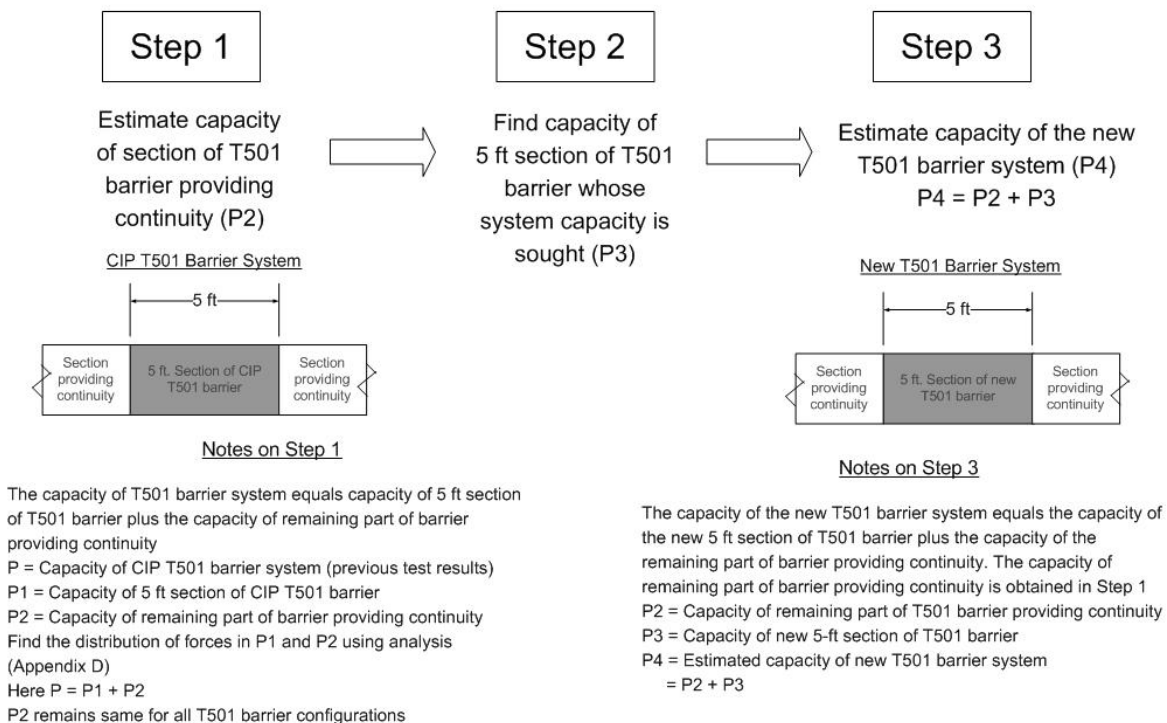


Figure 10.3: Steps to find capacity of T501 barrier system from capacity of 5 ft. section of T501 barrier

These steps to find capacity of the retrofit T501 barrier system from capacity of 5-ft. section of the T501 barrier are as follows:

- 1) Estimate the absolute increase in barrier capacity due to longitudinal continuity. The capacity of the section of the T501 barrier system providing continuity to the 5-ft. section of the T501 barrier is obtained using TTI test results of cast-in-place T501 barrier systems and analyses.

- 2) Estimate the capacity of the 5-ft. section of the retrofit T501 barrier as described in Section 10.2.2.
- 3) Add the estimated capacity of the 5-ft. section of the retrofit T501 barrier to the estimated increase in capacity due to longitudinal continuity to give an estimate of the capacity of the retrofit T501 barrier system.

These steps were used to obtain the dynamic capacity, 50-msec dynamic capacity and static capacity of the retrofit T501 barrier system with undercut anchors. The significance of the retrofit T501 barrier system capacity measures is then discussed in terms of the TxDOT performance criteria for retrofit barriers.

10.3.2 Dynamic Capacity

The peak dynamic capacity of a T501 cast-in-place barrier system obtained from TTI results is about 155 kips. The dynamic capacity of a 5-ft. section of cast-in-place T501 barrier obtained from an LS-DYNA simulation of an impact pendulum test (refer to Chapter 11.) is about 60 kips. Hence about 60% of the system capacity (95 kips) comes from continuity of the barrier system and 40% of the capacity (60 kips) comes from the 5-ft. barrier section (this is Step 1). The contribution due to barrier continuity is assumed to remain the same for the following different scenarios. Failure is by a form of concrete breakout (straightening of the bent reinforcement connecting the barrier to the slab).

The dynamic capacity of the 5-ft. section of the retrofit T501 was estimated to be 53 kips (Section 10.2.2). This calculation represents Step 2.

The contribution of the barrier continuity (95 kips) added to the dynamic capacity of a 5-ft. section of the retrofit T501 barrier (53 kips) gives the dynamic capacity of the retrofit T501 barrier system to be 147 kips. Failure is by concrete breakout. This represents Step 3.

The steps are given in Table 10.1.

Table 10.1: Steps to obtain dynamic capacity of retrofit T501 barrier system

| <i>Version of Retrofit T501 Barrier</i> | <i>Values from:</i> | | |
|--|---|--|---|
| | <i>Step1 (kips)—Capacity from Barrier Continuity</i> | <i>Step2 (kips) – Capacity of 5ft. section of barrier</i> | <i>Step3 (kips)- System Capacity (= Step1 + Step2)</i> |
| Retrofit with undercut anchors | 95 | 53 | 147 |

10.3.3 Dynamic Capacity over a 50-msec Window

The peak dynamic capacity over a 50 msec window of a T501 cast-in-place barrier system obtained from TTI results is about 68 kips. The 50-msec dynamic capacity of a 5-ft. section of cast-in-place T501 barrier obtained from the LS-DYNA simulation of an impact pendulum test (refer to Chapter 11.) is about 37 kips. Hence about 46% of the system capacity (31 kips) comes from continuity of the barrier system, and 54% of the capacity (37 kips) comes from the 5-ft. barrier section (this is Step 1). The contribution due to barrier continuity is

assumed to remain the same for the different scenarios that follow. Failure is by a form of concrete breakout (straightening of the bent reinforcement connecting the barrier to the slab).

As explained in Section 10.2.2, the 50-msec dynamic capacity of the 5 ft. section of the retrofit T501 was estimated to be 33 kips. This calculation represents Step 2.

The contribution of the barrier continuity (31 kips) added to the 50-msec dynamic capacity of a 5-ft. section of the retrofit T501 barrier (33 kips) gives the 50-msec dynamic capacity of the retrofit T501 barrier system to be 64 kips. Failure is by concrete breakout. This represents Step 3. The steps are given in Table 10.2.

Table 10.2: Steps to obtain 50-msec dynamic capacity of retrofit T501 barrier system

| <i>Retrofit T501 Barrier</i> | <i>Values from:</i> | | |
|--------------------------------|---|---|--|
| | <i>Step1 (kips)— Capacity from Barrier Continuity</i> | <i>Step2 (kips) – Capacity of 5ft. section of barrier</i> | <i>Step3 (kips)- System Capacity (= Step1 + Step2)</i> |
| Retrofit with undercut anchors | 31 | 33 | 64 |

10.3.4 Static Capacity

The static capacity of a T501 cast-in-place barrier system obtained from TTI results is about 70 kips. About 43% of the system capacity (30 kips) comes from continuity of the barrier system and 57% of the capacity (40 kips) comes from the 5-ft. barrier section (refer to Appendix D). This value is needed for Step 1. The contribution due to barrier continuity is assumed to remain the same for the different scenarios that follow. Failure is by a form of concrete breakout (straightening of the bent reinforcement connecting the barrier to the slab).

The static capacity of the 5-ft. section of the retrofit T501 was estimated to be 30 kips (Section 10.2.2). This represents Step 2.

The contribution of the barrier continuity (30 kips) added to the static capacity of a 5-ft. section of the retrofit T501 barrier (30 kips) gives the static capacity of the retrofit T501 barrier system to be 60 kips. Failure is by concrete breakout. This represents Step 3. These steps are given in Table 10.3.

Table 10.3: Steps to obtain static capacity of retrofit T501 barrier system

| <i>Retrofit T501 Barrier</i> | <i>Values from:</i> | | |
|--------------------------------|---|---|--|
| | <i>Step1 (kips)— Capacity from Barrier Continuity</i> | <i>Step2 (kips) – Capacity of 5ft. section of barrier</i> | <i>Step3 (kips)- System Capacity (= Step1 + Step2)</i> |
| Retrofit with undercut anchors | 30 | 30 | 60 |

10.3.5 Significance of Probable Retrofit T501 Barrier System Capacities

The summary of the capacities of T501 barrier systems is given in Table 10.4. The estimated capacities of the retrofit T501 barrier system with undercut anchors show that, like the cast-in-place barrier, the retrofit barrier meets current TxDOT requirements (Section 4.5.4). Its dynamic capacity over a 50-msec window (64 kips) is not less than 60 kips, and its static capacity (60 kips) is not less than 54 kips.

Table 10.4: Summary of estimated probable of T501 barrier systems

| <i>Version of T501 Barrier</i> | <i>Capacity of T501 Barrier System, kips</i> | | |
|---|--|---|----------------------------|
| | <i>Peak Dynamic Capacity</i> | <i>Dynamic Capacity (50- msec window)</i> | <i>Static Capacity</i> |
| Cast-in-Place (TTI Results) | 155 | 68 | 70 |
| Estimated Retrofit with undercut anchors (estimate) | 147 | 64 | 60 |

As discussed in Chapter 12, these estimated capacities of retrofit T501 barrier systems were then verified using results obtained from experimental tests.

Chapter 11. Analytical Simulations of Bridge Barrier Performance Using LS-DYNA

11.1 Introduction

In this chapter, the following are discussed:

- a review of the development and validation of an LS-DYNA model of the pendulum mass and crush package by Tolnai (2005);
- basic LS-DYNA model of T203 barrier and bridge deck;
- simulation of the pendulum impact test on the cast-in-place T203 barrier and bridge deck using effective elastic properties and the reasons for not continuing with this model;
- development of the LS-DYNA models of cast-in-place and retrofit T203 barrier and bridge deck using *MAT_SOIL_AND_FOAM* for concrete and separate elements to model the reinforcing and retrofit details (referred to as “reinforced concrete” models in this report);
- validation of the reinforced concrete LS-DYNA models of the T203 barrier and bridge deck using analytical simulations of pendulum impact tests;
- NCHRP TL-3 and TL-4 vehicular crash simulations on the validated reinforced concrete LS-DYNA models of T203 barrier and bridge deck;
- evaluation of the retrofit T203 barrier for NCHRP TL-3 and TL-4 using the developed crash simulations;
- development of reinforced concrete LS-DYNA models of cast-in-place and retrofit T501 barrier and bridge deck;
- pendulum impact test simulations on the developed T501 barrier and bridge deck models; and
- evaluation of the retrofit T501 barrier for NCHRP TL-3 and TL-4 using the same crash simulations that were developed for the T203 barrier and bridge deck.

11.2 Simulation of Pendulum Mass and Crush Package

The LS-DYNA model of the pendulum mass and crush package was developed by Tolnai (2005). A brief description and validation of this LS-DYNA model is discussed in this section.

11.2.1 LS-DYNA Model of the Pendulum Mass and Crush Package

The pendulum mass was modeled using solid elements and is 55 in. (1397 mm) long, 12 in. (305 mm) wide, and 9 in. (229 mm) high to represent the laboratory pendulum mass. It was assigned the *ISOTROPIC_ELASTIC_PLASTIC* material property, the input parameters of which are given in Tolnai (2005). The mass of the LS-DYNA model of the pendulum was the same as

the laboratory pendulum mass. Its length was the same as the laboratory mass to preserve the time required for an axial stress wave to travel the length of the pendulum during a crash simulation (Tolnai). Figure 11.1 shows the LS-DYNA model of the pendulum mass.

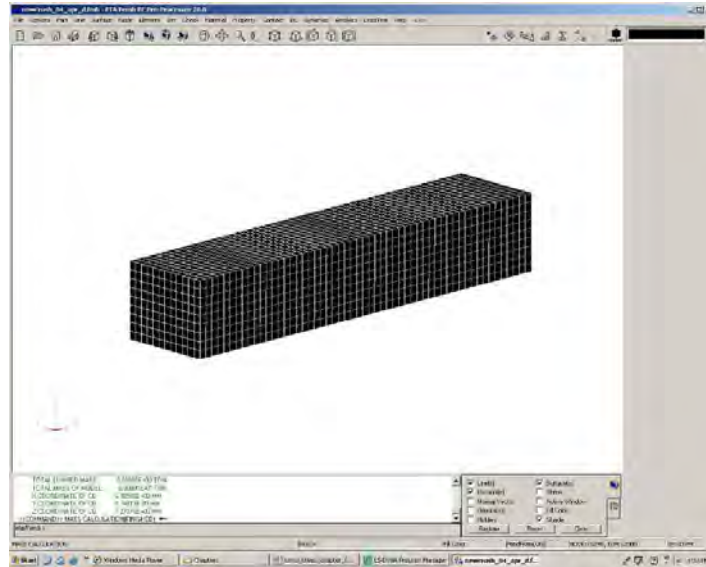


Figure 11.1: LS-DYNA Model of the laboratory pendulum mass (Tolnai 2005)

The crush package was made of 18 layers of 1-in. (25.4-mm) square steel tubes, oriented with the axis of each tube perpendicular to the direction of impact (Section 4.2.2). In the LS-DYNA model of the crush package, each layer of the steel tube was modeled as a separate *PART*. Each layer measured 6 in. (152 mm) \times 6 in. (152 mm) in cross-section and 1 in. (25.4 mm) in thickness and was modeled using *SOLID* elements (Tolnai 2005). The 18 layers were merged together using the *FIND COINCIDENT* command under the *NODES* menu to form a complete crush package. The *HONEYCOMB* material model was assigned to each part of the crush package. This material model is intended for metals that crush with a defined load curve, just like the steel tubes (Tolnai 2005). A stress-volumetric strain curve for the crush package was obtained by physically testing a layer of steel tubes in the laboratory and was input in LS-DYNA using the *LOAD CURVE* command under the *LS-DYNA MISC.* menu. The input parameters for the *HONEYCOMB* material and the *LOAD CURVE* are discussed in detail by Tolnai (2005).

The entire crush package was attached to the pendulum mass using the *FIND COINCIDENT* command under the *NODES* menu. Figure 11.2 shows the LS-DYNA model of the crush package attached to the pendulum mass. The validation of this model is discussed in the next sub-section.

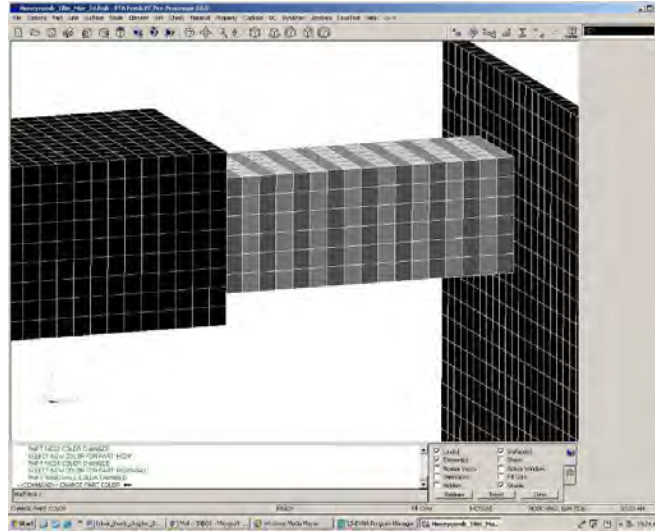


Figure 11.2: LS-DYNA simulation of pendulum mass and crush package impacting a rigid barrier (Tolnai)

11.2.2 Validation of LS-DYNA Model of Crush Package and Pendulum Mass

A laboratory test on a steel barrier was simulated in LS-DYNA by Tolnai (2005) using the crush package and pendulum mass model described in the previous sub-section. The simulation (Figure 11.2) used a rigid wall made of solid elements to represent the steel frame of the actual test (Tolnai 2005). Using the *VELOCITY* option within the *INITIAL CONDITION* menu, the LS-DYNA model of the crush package and pendulum mass was given an initial velocity of 9500 mm/sec (34.2 km/hr), the same as the velocity of the laboratory pendulum mass at the time of impact.

Based on the *NCHRP Report 350* requirements, the simulation was validated using the following criteria (Tolnai 2005):

- it should impart the same impact energy as the laboratory impact pendulum setup, which is validated for NCHRP 350 TL-3; and
- it should produce an impulse of impact similar to that obtained from the laboratory test.

In addition to the impulse of impact, the graph of acceleration versus time obtained from an impact contains the following information: 1) peak force of impact and 2) duration of impact. Hence, in addition to that criteria, the simulation was also validated using the following two criteria (Tolnai 2005):

- it should produce a peak force of impact similar to that obtained from the laboratory test; and
- it should produce a duration of impact similar to that obtained from the laboratory test.

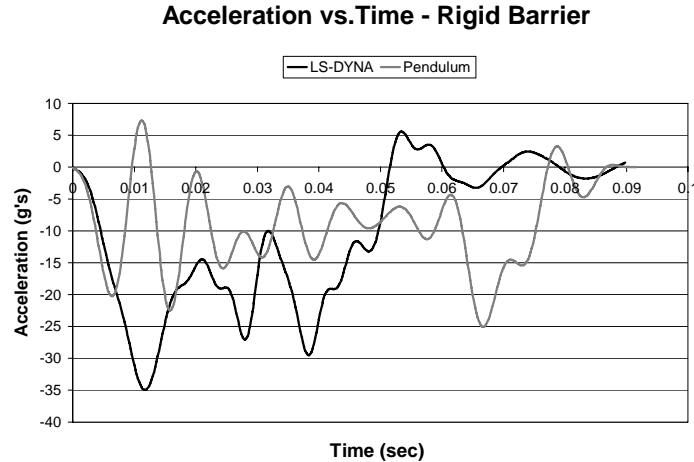


Figure 11.3: Comparison of acceleration versus time graphs from laboratory test of impact pendulum on steel barrier in laboratory and simulation of the same test using LS-DYNA (Tolnai)

Figure 11.3 shows the acceleration-time history of the impact pendulum test on a steel barrier at FSEL as well as the LS-DYNA simulation. Table 11.1 shows a comparison of the simulation with the laboratory experiments based on the criteria discussed.

Table 11.1: Comparison between impact pendulum test on a steel barrier and its LS-DYNA simulation

| <i>Comparison Between:</i> | <i>Comparison Criterion</i> | | | |
|--|-----------------------------|------------------------------------|--------------------------|---------------------------------|
| | <i>Impact Energy (kJ)</i> | <i>Impulse of Impact (kip-sec)</i> | <i>Peak Force (kips)</i> | <i>Duration of impact (sec)</i> |
| Pendulum Impact Test on Steel Barrier | 38.5 | 1.49 | 47.5 | 0.1 |
| LS-DYNA Simulation of Pendulum Impact on Steel Barrier | 38.5 | 1.73 | 65 | 0.07 |

The impact energy imparted to the barrier in the simulation was the same as in a laboratory pendulum test. The impulse of impact obtained from the FSEL test was about 1.49 kip-sec (6600 N-sec). The impulse of impact obtained from its simulation was 16% greater at about 1.73 kip-sec (7700 N-sec). The peak force of impact from the simulation was about 65 kips (291 kN) compared to the peak force from the laboratory test of about 47.5 kips (210 kN). The duration of impact from the simulation was about 0.07 sec, compared to the 0.1 sec from the laboratory test.

The agreement between the test data and computer-based simulation was considered acceptable by Tolnai (2005) and the supervisors of TxDOT Project 0-4823. This validated pendulum mass and crush package model was used to simulate the pendulum impact testing of the T203 and T501 bridge barrier and deck specimens in this research.

11.3 Basic LS-DYNA Model of T203 Barrier and Bridge Deck

The bridge deck test specimen developed at FSEL is 127 in. long (parallel to the direction of pendulum swing), 120 in. wide (perpendicular to the direction of pendulum swing), and 8 in. thick. The deck is modeled as a separate *PART* in LS-DYNA using *SOLID* elements. The bridge deck rests on two concrete blocks and has an overhang of 3 ft. on the side of the barrier along its length. It is appropriate to model the boundary conditions provided by the concrete blocks using a combination of pinned and roller supports. These boundary conditions are specified in LS-DYNA using the *SPC* command under the *BOUNDARY* menu.

The basic geometry of the T203 barrier is given in Chapters 2Chapter 2. and 4. The development of the basic LS-DYNA model of a T203 barrier using *SOLID* elements is discussed by Tolnai (2005). Figure 11.4 shows the LS-DYNA model of the T203 barrier and bridge deck with support conditions.

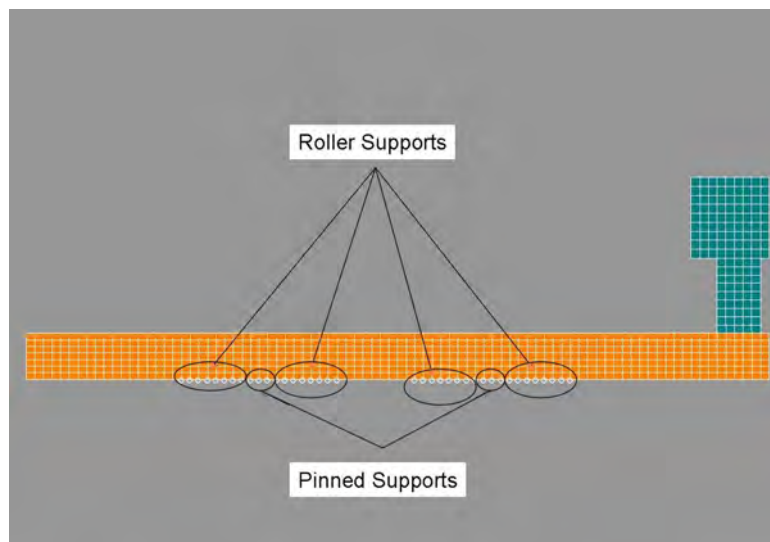


Figure 11.4: Basic LS-DYNA model of the T203 barrier and bridge deck with support conditions

The T203 barrier model is positioned with respect to the deck model so that it represents the T203 barrier and bridge deck laboratory test setup. This is done using the *TRANSLATE* command within the *TRANSFORM* menu (within the *NODE* menu). The size of the *SOLID* elements of the barrier and the slab is selected so that the *SOLID* elements of the barrier lie exactly on top of the *SOLID* elements of the slab. The slab and the barrier are merged together using the *FIND COINCIDENT* command under the *NODE* menu.

It is necessary to specify certain assignments, such as material properties, and to modify this basic model of the T203 barrier and bridge deck specimen to simulate impacts on it in LS-DYNA. These assignments and modifications are discussed in Sections 11.4 and 11.5.

11.4 Simulation of Pendulum Impact Test on Cast-in-Place T203 Barrier and Deck Using Effective Elastic Properties

Impact pendulum tests were carried out at FSEL on cast-in-place T203 barrier and bridge deck specimens for NCHRP TL-3 (Test Designation 3-10) to characterize their behavior. Simulation of this impact pendulum test in LS-DYNA requires:

- a T203 barrier and bridge deck model with the representative material properties and required addition of reinforcement elements, if necessary;
- the validated pendulum and crush package model with the required initial velocity of 9500 mm/sec;
- specification of contact between the crush package and barrier; and
- validation of the model by comparison with physical test results.

This section discusses the following:

- development of an effective elastic material model to be assigned to the T203 barrier and bridge deck to represent reinforced concrete;
- simulation of pendulum impact test using the effective elastic T203 barrier and bridge deck model;
- criteria for validation of the elastic T203 barrier and bridge deck model;
- validation of the elastic T203 barrier and bridge deck; and
- limitations of simulation of T203 barrier and bridge deck models using elastic material properties.

11.4.1 Development of Effective Elastic Material Model

This section discusses the representation of the T203 concrete barrier and deck, discussed in Section 11.3, using an effective elastic material model. An elastic material model can be justified to represent reinforced concrete because, as discussed in Chapter 8, laboratory results from the impact pendulum tests show that the cast-in-place T203 bridge barrier and deck remain essentially elastic for NCHRP TL-3 (Test Designation 3-10) impact.

The effective material properties for both the barrier and the deck were obtained from their moment-curvature relationships. These relationships of the concrete bridge deck and the cast-in-place T203 barrier with concrete strength of 4000 psi are shown in Figure 11.5. The moment-curvature relationships are obtained using a layered sectional analysis program called RECONASANCE (Alaoui 2004). The slope of a moment-curvature diagram at any point gives the flexural stiffness EI , where E is the effective elastic modulus and I is the moment of inertia of the section at that point. In this idealization, an effective E was used, rather than an effective I , so that the gross cross-sectional dimensions of the cross-section could be maintained. Only the slope of the initial part of the curve is considered because the focus is on developing an equivalent elastic material model. The effective elastic moduli of the barrier and slab were obtained by dividing their EI values by their respective elastic moments of inertia. The effective elastic moduli of the barrier and the slab were 750 ksi (5180 MPa) and 700 ksi (4840 MPa), respectively.

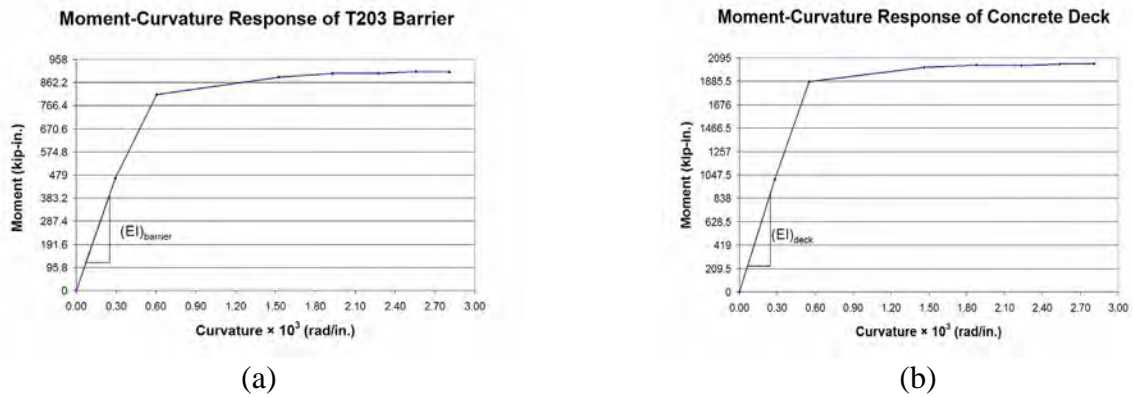


Figure 11.5: Moment-curvature relationship of (a) T203 barrier and (b) bridge deck from RECONASANCE

The *ELASTIC* material model in LS-DYNA was selected to model the T203 bridge barrier and deck. The input parameters for this material model for the barrier and slab are specified in Tables 11.2 and 11.3, respectively.

Table 11.2: CARD 1 for T203 barrier modeled as elastic material

| <i>Variable</i> | <i>Description</i> | <i>Value</i> | <i>Units</i> |
|-----------------|--------------------------------|--------------|----------------------|
| MID | Material ID | - | - |
| RO | Mass Density | 2.32e-009 | ton/ mm ³ |
| E | Young's Modulus | 5.180e+003 | MPa |
| PR | Poisson's Ratio | 0.3 | - |
| DA | Axial Damping Factor | 0.0 | - |
| DB | Bending Damping Factor | 0.0 | - |
| K | Bulk Modulus (only for fluids) | 0.0 | MPa |

Table 11.3: CARD 1 for bridge deck, modeled as elastic material

| <i>Variable</i> | <i>Description</i> | <i>Value</i> | <i>Units</i> |
|-----------------|--------------------------------|--------------|----------------------|
| MID | Material ID | - | - |
| RO | Mass Density | 2.32e-009 | ton/ mm ³ |
| E | Young's Modulus | 4.840e+003 | MPa |
| PR | Poisson's Ratio | 0.3 | - |
| DA | Axial Damping Factor | 0.0 | - |
| DB | Bending Damping Factor | 0.0 | - |
| K | Bulk Modulus (only for fluids) | 0.0 | MPa |

11.4.2 Elastic Model of Pendulum Impact Test Simulation

A *.dyn* file of the LS-DYNA model of the pendulum mass and crush package was imported to the *.fmb* file of the T203 bridge barrier and deck using the *IMPORT* command under the *FILE* menu. The imported model was spatially located as required using the *TRANSFORM* command under the *NODE* menu. Using the *INITIAL CONDITION* menu (within *B.C.*), an initial *VELOCITY* of 9500 mm/sec (34.2 km/hr) was assigned to the pendulum and crush package to represent NCHRP TL-3 (Test Designation 3-10) conditions. Figure 11.6 shows the LS-DYNA model of the impact test pendulum simulation.

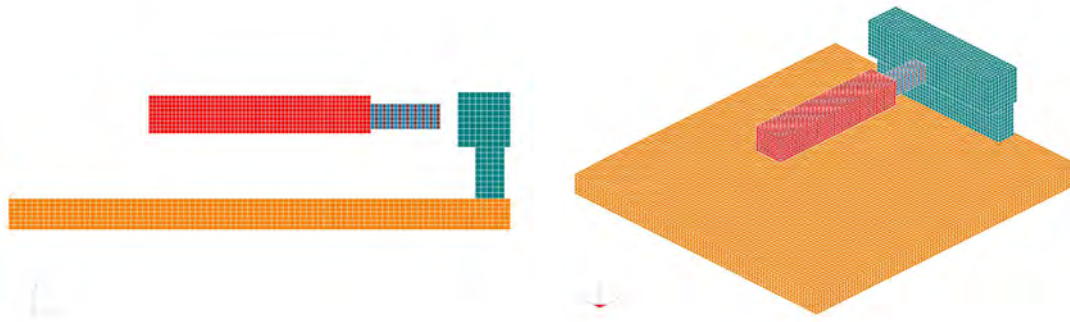


Figure 11.6: LS-DYNA model of pendulum impact test simulation on T203 barrier and deck

11.4.3 Criteria for Validation of Elastic Model of Pendulum Impact Test Simulation

The following criteria were used to validate the pendulum impact test simulation using an elastic T203 barrier and bridge deck:

- the simulation should impart the same impact energy to the T203 barrier and bridge deck model as the laboratory impact pendulum setup which is validated for NCHRP 350 TL-3;
- it should produce an impulse of impact similar to that obtained from the laboratory test;
- it should produce a peak force of impact similar to that obtained from the laboratory test; and
- it should produce a duration of impact similar to that obtained from the laboratory test.

The reasons for selecting these criteria are given in Section 11.2.2. In addition, to compare the barrier behavior, the following criterion was used:

- the simulation should produce barrier displacements similar to those obtained from the laboratory tests.

11.4.4 Validation of Elastic Model of Pendulum Impact Test Simulation

Figure 11.7 shows the acceleration-time histories of impact obtained from the laboratory test and its simulation.

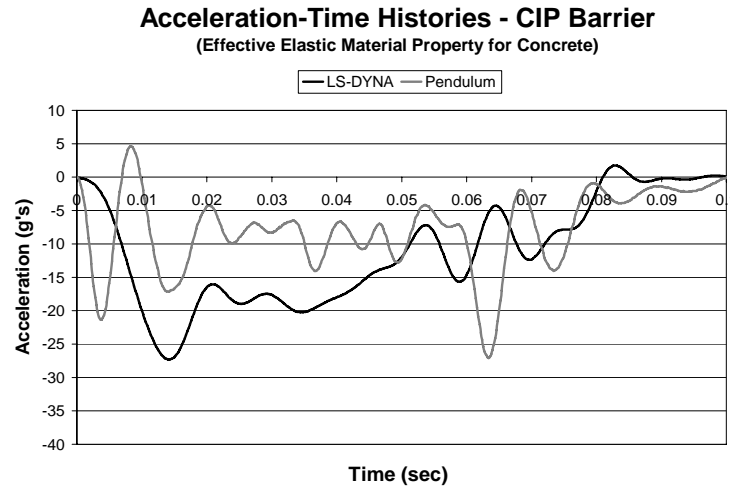


Figure 11.7: Acceleration-time histories from pendulum impact test on cast-in-place T203 barrier and deck, and its effective elastic simulation in LS-DYNA

Table 11.4 shows the comparison of the results of the pendulum impact test on a cast-in-place T203 barrier and bridge deck and its elastic simulation in LS-DYNA.

Table 11.4: Comparison of results of pendulum impact test on cast-in-place T203 barrier and bridge deck and its elastic simulation in LS-DYNA.

| <i>Comparison Between:</i> | <i>Comparison Criterion</i> | | | | |
|--|-----------------------------|------------------------------------|--------------------------|---------------------------------|---------------------------|
| | <i>Impact Energy (kJ)</i> | <i>Impulse of Impact (kip-sec)</i> | <i>Peak Force (kips)</i> | <i>Duration of impact (sec)</i> | <i>Barrier Disp. (in)</i> |
| Pendulum Impact Test on CIP T203 barrier and bridge deck | 38.5 | 1.49 | 49 | 0.1 | 0.9 |
| LS-DYNA Simulation of Pendulum Impact Test on CIP T203 barrier and bridge deck (elastic model) | 38.5 | 2.05 | 49.5 | 0.08 | 0.6 |

The impact energy imparted to the barrier by the simulation is the same as the impact energy imparted to the barrier by the laboratory pendulum and conforms to the NCHRP TL-3 criterion. The impulse of impact obtained from LS-DYNA was approximately 2.05 kip-sec (9120 N-sec), about 40% more than the test value of about 1.49 kip-sec (6600 N-sec). The peak force obtained from the test was approximately 49 kips (216 kN) compared to about 49.5 kips (220 kN) obtained from the LS-DYNA simulation. The duration of impact obtained from the

simulation is about 0.08 sec as compared to the test value of 0.1 sec. The peak barrier displacement obtained from the simulation was about 0.6 in. (15 mm), which is 35% less than the test value of about 0.9 in. (23 mm).

Based on the impact of impulse and barrier displacement values obtained from the simulation, it was concluded that the elastic model of the T203 barrier and bridge deck did not capture the barrier behavior with sufficient accuracy.

11.4.5 Limitations of Simulation using Effective Elastic Material Properties for Concrete

Results from the LS-DYNA simulation illustrated in Figure 11.7 do not represent the test results well. Reinforced concrete is a non-linear, non-homogenous material. To represent it with a homogenous effective elastic material is virtually impossible.

Use of a homogenous material makes it very difficult to distinguish between a model of a retrofit barrier with post-tensioned unbonded reinforcement and a cast-in-place barrier with bonded reinforcement, particularly if the geometry and cross-sectional area of reinforcement is the same for both barriers. An effective elastic material can be used only as long as the section being analyzed remains elastic. It cannot be used to model an impact test in which the barrier or slab reinforcement yield, making it a material with very limited use in the case of simulating impact tests.

As a result of these limitations, it was decided to use separate elements and material properties for the concrete and the reinforcement. The development of parameters to define the material properties for concrete and reinforcement is discussed in the next section.

11.5 Reinforced Concrete Model of T203 Barrier and Bridge Deck

A 'Reinforced Concrete' LS-DYNA model refers to a model which uses separate elements and nonlinear material properties for concrete and reinforcement. Using the same terminology, an LS-DYNA model of a T203 barrier and bridge deck with different properties for concrete and reinforcement is called 'Reinforced Concrete Model of T203 Barrier and Bridge Deck'.

This section discusses the following:

- development of input parameters of *MAT_SOIL_AND_FOAM* to represent concrete;
- modeling of bonded reinforcement;
- modeling retrofit T203 barrier and bridge deck;
- reinforced concrete model of cast-in-place T203 barrier and bridge deck; and
- reinforced concrete model of retrofit T203 barrier and bridge deck.

11.5.1 Concrete Material Model

The selection of *MAT_SOIL_AND_FOAM* material model to represent concrete is discussed in Chapter 2. According to Schwer (2001), the following parameters are required to characterize the *MAT_SOIL_AND_FOAM*:

- state of hydrostatic compression (HSC), that is, pressure versus volumetric strain response;
- shear failure surface parameters obtained from a triaxial compression test (TXC);
- elastic shear modulus (G);
- unloading bulk modulus; and
- tensile pressure cut-off (PC).

These material parameters are obtained for a concrete strength of 4000 psi (27.6 MPa), which is the design strength used for the T203 bridge barrier and deck. Chen (1982) gives a curve of pressure (p) versus volumetric strain for a typical concrete. After considerable investigation, it was decided to use that curve for the nonlinear material modeling of concrete. The input parameters for HSC in LS-DYNA are in the format of pressure (p) in MPa versus logarithmic relative volume. By multiplying the dimensionless curve from Chen (1982) by the concrete strength (27.6 MPa), it was converted to the LS-DYNA format for the design concrete strength and is given in Figure 11.8.

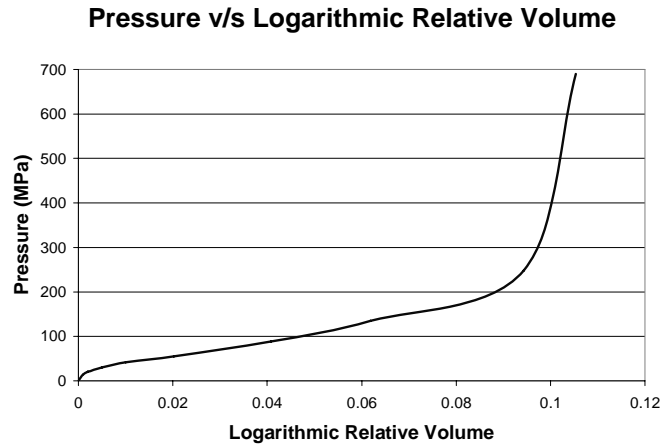


Figure 11.8: Graph of pressure (p) versus logarithmic relative volume curve for 27.6-MPa concrete

The shear failure surface for *MAT_SOIL_AND_FOAM* has the functional form of Equation 11.1, where J_2 is the second invariant of the stress tensor and p is the pressure.

$$J_2 = a_0 + a_1 p + a_2 p^2 \quad (11.1)$$

Figure 11.9 shows the curve of J_2 versus p for a 4000-psi (27.6-MPa) concrete, obtained from the dimensionless curve of Chen (1982). The constants a_0 , a_1 , and a_2 are obtained by fitting a quadratic equation through points on the curve.

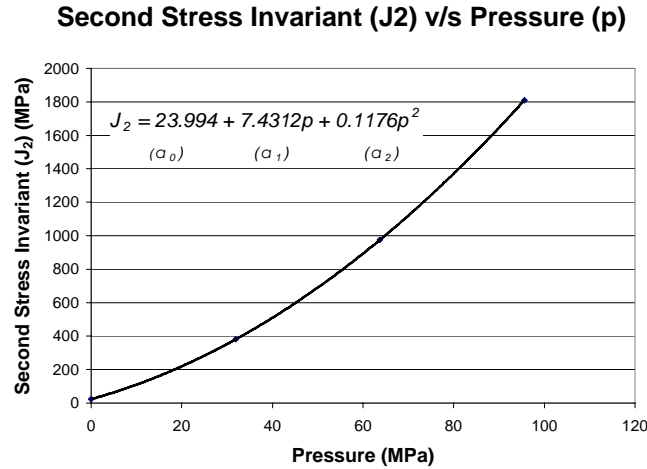


Figure 11.9: Graph of second stress invariant (J_2) versus pressure (p) for 27.6-MPa concrete

According to Schwer (2001), the unloading bulk modulus should be greater than the loading bulk modulus. The unloading bulk modulus used for the material model in LS-DYNA units is 39990 MPa. Even though this value is much higher than the elastic loading bulk modulus of 13000 MPa (in LS-DYNA units), if any lower value is specified, LS-DYNA automatically converts it to 39990 MPa.

Based on recommendations from Schwer (2001), the pressure cut-off (PC) value for this concrete can be taken as the tensile strength (f_t) of concrete using this formula:

$$f_t = 4\sqrt{f_c} \text{ psi} \quad (11.2)$$

Converting the tensile strength to LS-DYNA compatible units gives a value of 1.75 MPa (253 psi). The data entry lines used to characterize a 4000-psi (27.6-MPa) concrete with *MAT_SOIL_AND_FOAM* are given in Tables 11.5–11.10.

Table 11.5: CARD 1 for T203 bridge barrier and deck modeled with *MAT_SOIL_AND_FOAM*

| <i>Variable</i> | <i>Description</i> | <i>Value</i> | <i>Units</i> |
|-----------------|--------------------------------------|--------------|----------------------|
| MID | Material Identification | - | - |
| RO | Mass Density | 2.32e-9 | ton/ mm ³ |
| G | Shear Modulus | 10600 | MPa |
| BULK | Bulk Modulus for Unloading | 39990 | MPa |
| A0 | Yield Function Constant 1 | 23.0040 | MPa |
| A1 | Yield Function Constant 2 | 7.4312 | - |
| A2 | Yield Function Constant 3 | 0.1170 | 1/MPa |
| PC | Pressure Cutoff for tensile fracture | -1.75 | MPa |

Table 11.6: CARD 2 for T203 bridge barrier and deck modeled with MAT_SOIL_AND_FOAM

| <i>Variable</i> | <i>Description</i> | <i>Value</i> | <i>Units</i> |
|-----------------|---|--------------|--------------|
| VCR | Volumetric Crushing Option | 0.0 | - |
| REF | Reference Geometry to initialize Pressure | 0.0 | - |

Table 11.7: CARD 3 for T203 bridge barrier and deck modeled with MAT_SOIL_AND_FOAM

| <i>Variable</i> | <i>Description</i> | <i>Value</i> | <i>Units</i> |
|-----------------|---------------------------|--------------|--------------|
| EPS1 | Volumetric Strain Value 1 | 0 | - |
| EPS2 | Volumetric Strain Value 2 | -0.001001 | - |
| EPS3 | Volumetric Strain Value 3 | -0.002002 | - |
| EPS4 | Volumetric Strain Value 4 | -0.005013 | - |
| EPS5 | Volumetric Strain Value 5 | -0.010050 | - |
| EPS6 | Volumetric Strain Value 6 | -0.020203 | - |
| EPS7 | Volumetric Strain Value 7 | -0.040822 | - |
| EPS8 | Volumetric Strain Value 8 | -0.061875 | - |

Table 11.8: CARD 4 for T203 bridge barrier and deck modeled with MAT_SOIL_AND_FOAM

| <i>Variable</i> | <i>Description</i> | <i>Value</i> | <i>Units</i> |
|-----------------|----------------------------|--------------|--------------|
| EPS9 | Volumetric Strain Value 9 | -0.094311 | - |
| EPS10 | Volumetric Strain Value 10 | -0.105361 | - |

Table 11.9: CARD 5 for T203 bridge barrier and deck modeled with MAT_SOIL_AND_FOAM

| <i>Variable</i> | <i>Description</i> | <i>Value</i> | <i>Units</i> |
|-----------------|--------------------|--------------|--------------|
| P1 | Pressure Value 1 | 0 | MPa |
| P2 | Pressure Value 2 | 13.8 | MPa |
| P3 | Pressure Value 3 | 20.7 | MPa |
| P4 | Pressure Value 4 | 30.36 | MPa |
| P5 | Pressure Value 5 | 41.4 | MPa |
| P6 | Pressure Value 6 | 55.2 | MPa |
| P7 | Pressure Value 7 | 88.32 | MPa |
| P8 | Pressure Value 8 | 135.24 | MPa |

Table 11.10: CARD 6 for T203 bridge barrier and deck modeled with MAT_SOIL_AND_FOAM

| <i>Variable</i> | <i>Description</i> | <i>Value</i> | <i>Units</i> |
|-----------------|--------------------|--------------|--------------|
| P9 | Pressure Value 9 | 248.4 | MPa |
| P10 | Pressure Value 10 | 690 | MPa |

11.5.2 Modeling of Bonded Reinforcement in LS-DYNA

In the LS-DYNA modeling for this report, it is assumed that the deformed reinforcement in the barrier and bridge deck is perfectly bonded to the surrounding concrete. This assumption is justified because the reinforcement in the test specimens has requisite development length to prevent bond slip. The bonded reinforcement is modeled using the following steps:

- 1) Using the *CREATE* command under the *LINE* menu, a line is created between two nodes in the LS-DYNA model of the T203 bridge barrier and deck, oriented along the longitudinal axis of the bar to be modeled and along the edge of *SOLID* elements.
- 2) The line is then assigned the *TRUSS* element property within the *PROPERTY* menu. When defining *TRUSS* elements, their cross-sectional area needs to be specified depending on the size of the reinforcing bar being used. Each segment comprising the line is now a *TRUSS* element. Hence, the number of *TRUSS* elements is equal to the number of *SOLID* elements along the length of the bar, and the nodes of each *TRUSS* element coincide with two nodes of each *SOLID* element.
- 3) The coinciding nodes are merged together using the *FIND COINCIDENT* command within the *NODES* menu. Because the displacement functions of the *SOLID* elements and the *TRUSS* elements are the same (linear), this modeling approach ensures compatibility of strains between the reinforcing bar and the surrounding concrete in the LS-DYNA model, signifying bonded reinforcement.
- 4) The reinforcing bars of the T203 barrier and bridge deck have a yield strength of 415 MPa (60 ksi) and an elastic modulus of 200000 MPa (29000 ksi). It is appropriate to model them using an elasto-plastic material (Nilson 1982). *MAT_PLASTIC_KINEMATIC* is the elasto-plastic material model in LS-DYNA. Reinforcing bars are assigned the *MAT_PLASTIC_KINEMATIC* material model, using the parameters given in Table 11.11.

Table 11.11: CARD 1 for modeling rebars with MAT_PLASTIC_KINEMATIC

| <i>Variable</i> | <i>Description</i> | <i>Value</i> | <i>Units</i> |
|-----------------|-------------------------|--------------|----------------------|
| MID | Material Identification | - | - |
| RO | Mass Density | 7.85e-9 | ton/ mm ³ |
| E | Elastic Modulus | 2.00e+5 | MPa |
| PR | Poisson's Ratio | 0.3 | - |
| SIGY | Yield Stress | 415 | MPa |
| ETAN | Tangent Modulus | 1000 | MPa |
| BETA | Hardening Parameter | 0 | - |

11.5.3 Modeling Retrofit T203 Bridge Barrier

The details of the retrofit T203 barrier specimens are given in Section 4.5.2. Each PVC duct in the barrier and drilled hole in the slab is modeled by deleting a column of elements of the barrier and slab using the *DELETE* command under the *ELEMENT* menu. The resulting vertical void created by this deletion in the LS-DYNA model of the barrier and the slab at the required location represents a PVC duct and drilled hole to accommodate a threaded rod. Each vertical void is one element wide. The detailed procedure of element deletion is discussed in Tolnai (2005).

The steel plates shown are modeled in LS-DYNA using *SOLID* elements. The size and the position of the plates in the LS-DYNA model are the same as those in the actual specimen. *MAT_PLASTIC_KINEMATIC*, with the same parameters given in Table 11.11, is assigned to the steel plates. *AUTOMATIC_SURFACE_TO_SURFACE* contact is assigned between the steel plates and the barrier as well as the barrier and the slab.

To model each threaded rod, a *LINE* is created from the top of the top plate to the bottom of the bottom plate, coinciding with the position of the threaded rod in the test specimen as well as the centerline of the applicable vertical void. The line is divided into elements which are assigned *TRUSS* element properties. *MAT_PLASTIC_KINEMATIC*, with the same parameters given in Table 11.11, is assigned to the threaded rod elements.

The threaded rods are attached to the plates using the *FIND COINCIDENT* command under the *NODE* menu. There is no bond between the threaded rods and the surrounding concrete of the barrier and the slab. *AUTOMATIC_SURFACE_TO_SURFACE* contact is assigned between the threaded rods and the barrier and the slab to keep the threaded rods confined within the vertical void (representing the PVC pipes) during simulation.

The post-tensioning in the rods is modeled by assigning a temperature difference to the nodes of the truss elements of the threaded rods. A temperature difference of approximately -55°C can represent the 20-ksi post-tension given to each rod. The temperature difference is given in LS-DYNA using the *TEMPERATURE* command under the *LOAD* menu. The *LOAD* menu is under the *BOUNDARY* menu. The bonded reinforcement in the retrofit T203 barrier test specimen is modeled using the procedure discussed in Section 11.5.2.

11.5.4 Reinforced Concrete LS-DYNA model of Cast-in-Place T203 Barrier and Bridge Deck

The cast-in-place TxDOT T203 bridge barrier and deck uses only bonded reinforcement. Each reinforcing bar in the laboratory test specimen was modeled in LS-DYNA following the guidelines of Section 11.5.2. *MAT_SOIL_AND_FOAM* with the parameters given in Section 11.5.1 was assigned to the solid elements of the model. The side view and back view of this reinforced concrete LS-DYNA model is shown in Figure 11.10.

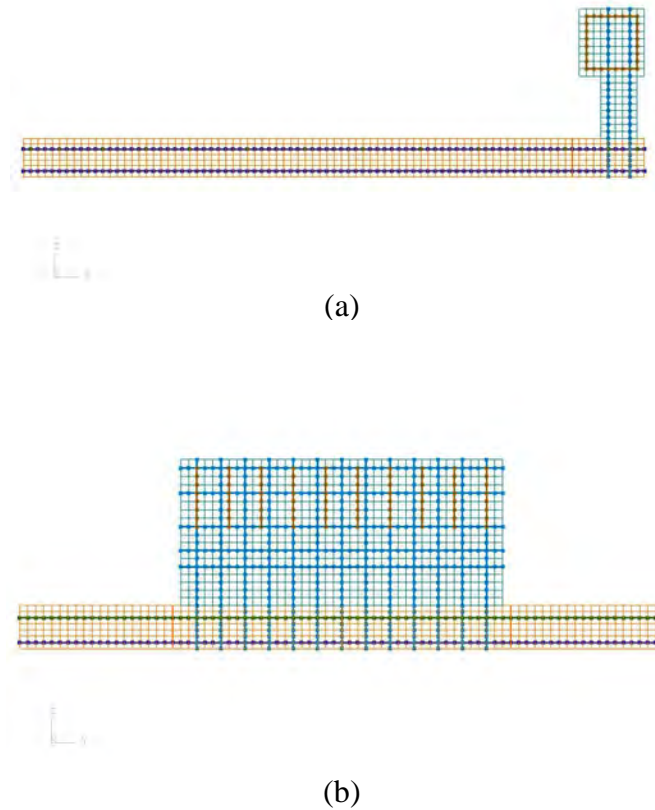
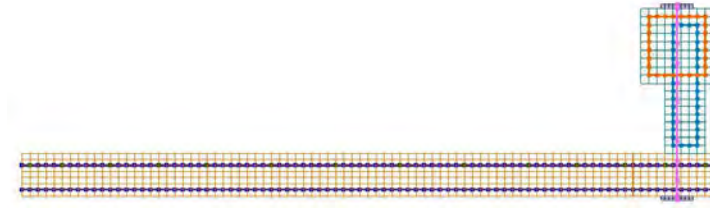


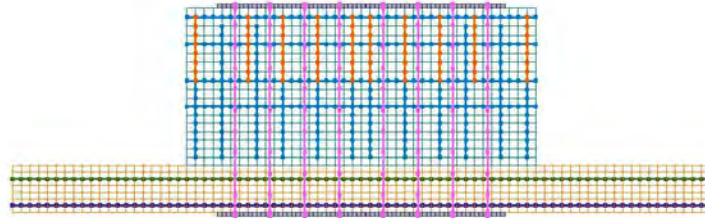
Figure 11.10: (a) Side view and (b) back view of the reinforced concrete LS-DYNA model of cast-in-place T203 barrier and bridge deck

11.5.5 Reinforced Concrete LS-DYNA Model of Retrofit T203 Barrier and Bridge Deck

The retrofit T203 barrier and bridge deck has the same configuration of reinforcement as its cast-in-place counterpart, except for the inclusion of threaded rods in the retrofit barrier. The reinforcing bars were modeled as discussed in Section 11.5.2, and the retrofit details were modeled as outlined in Section 11.5.3. Figure 11.11 shows the reinforced concrete LS-DYNA model of the retrofit T203 barrier and bridge deck.



(a)



(b)

Figure 11.11: (a) Side view and (b) back view of the reinforced concrete LS-DYNA model of retrofit T203 barrier and bridge deck

11.6 Validation of Reinforced Concrete Models of T203 Barrier and Bridge Deck

This section discusses the validation of the reinforced concrete LS-DYNA models of the cast-in-place and retrofit T203 barrier and bridge deck. Simulations of the laboratory impact pendulum tests on cast-in-place and retrofit T203 barrier and bridge deck specimens were created as discussed in Section 11.4.2. The models were validated by comparing the simulation results with the laboratory results, using the same criteria that had been used to validate the elastic model of the T203 barrier and bridge deck (Section 11.4.3).

11.6.1 Validation of Reinforced Concrete LS-DYNA Model of Cast-in-place T203 Barrier and Bridge Deck

The acceleration versus time graphs and the displacement-versus-time graphs from the pendulum impact test on a cast-in-place T203 barrier and bridge deck specimen and its reinforced concrete LS-DYNA simulation are given in Figure 11.12. The acceleration versus

time graph obtained from the simulation is much smoother than the laboratory graph. The peaks and the valleys in the laboratory graph of acceleration versus time represent the crushing of the hollow steel tubes used to fabricate the crush package. These peaks and valleys are absent in the acceleration versus time graph obtained from the simulation.

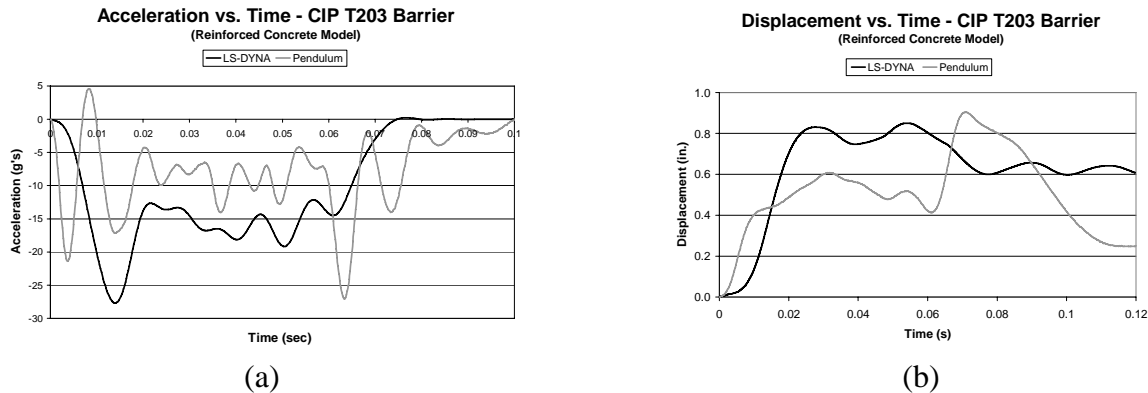


Figure 11.12: (a) Acceleration-versus-time graphs and (b) displacement-versus-time graphs from pendulum impact test on cast-in-place T203 barrier and bridge deck and its reinforced concrete LS-DYNA simulation

Table 11.12 shows the comparison between the pendulum impact test results and the results obtained from its simulation.

Table 11.12: Comparison of results of pendulum impact test on cast-in-place T203 barrier and bridge deck and its reinforced concrete simulation in LS-DYNA

| <i>Comparison Between:</i> | <i>Comparison Criterion</i> | | | | |
|--|-----------------------------|------------------------------------|--------------------------|---------------------------------|---------------------------|
| | <i>Impact Energy (kJ)</i> | <i>Impulse of Impact (kip-sec)</i> | <i>Peak Force (kips)</i> | <i>Duration of impact (sec)</i> | <i>Barrier Disp. (in)</i> |
| Pendulum Impact Test on CIP T203 barrier and bridge deck | 38.5 | 1.49 | 49 | 0.1 | 0.9 |
| LS-DYNA Simulation of Pendulum Impact Test on CIP T203 barrier and bridge deck (reinforced concrete model) | 38.5 | 1.89 | 49.5 | 0.08 | 0.9 |

The impact energy imparted to the barrier by the simulation is the same as the impact energy imparted to the barrier by the laboratory pendulum and conforms to the NCHRP TL-3 criterion. The impulse of impact obtained from LS-DYNA was about 1.89 kip-sec (8400 N-sec), 27% more than the test value of about 1.49 kip-sec (6600 N-sec). The peak force obtained from the test was about 49 kips (216 kN), which compares quite well to the value of approximately 49.5 kips (219 kN) obtained from the LS-DYNA simulation. The peak barrier displacement obtained from the simulation was about 0.9 in. (22 mm), which closely matches the laboratory test value of about 0.9 in. (23 mm).

Except for the impulse of impact value, all the other comparison values obtained from the simulation are similar to those of the laboratory test. In the laboratory, hollow steel tubes are used to fabricate the crush package. *SOLID* elements are used to model this crush package in LS-DYNA. These elements do not accurately capture the buckling behavior of the steel tubes during the pendulum impact. The use of *SOLID* elements smoothes the acceleration-versus-time graph. This effect gives an increased impulse value over that obtained from the pendulum test. Due to the differences in the modeling of the crush package and its actual behavior observed in the lab, the 27% difference in the impulse value was considered acceptable.

It can thus be concluded that the reinforced concrete LS-DYNA model of the cast-in-place T203 barrier and bridge deck is an acceptable representation of the actual specimens, and it is appropriate to use this LS-DYNA model for crash simulations to understand the cast-in-place T203 barrier behavior during vehicular collisions.

11.6.2 Validation of Reinforced Concrete LS-DYNA Model of Retrofit T203 Barrier and Bridge Deck

The Acceleration-versus-time graphs and the displacement-versus-time graphs from the pendulum impact test on a retrofit T203 barrier and bridge deck and its reinforced concrete LS-DYNA simulation are given in Figure 11.13. As before, the Acceleration-versus-time graph obtained from the simulation is much smoother as compared to the laboratory graph.

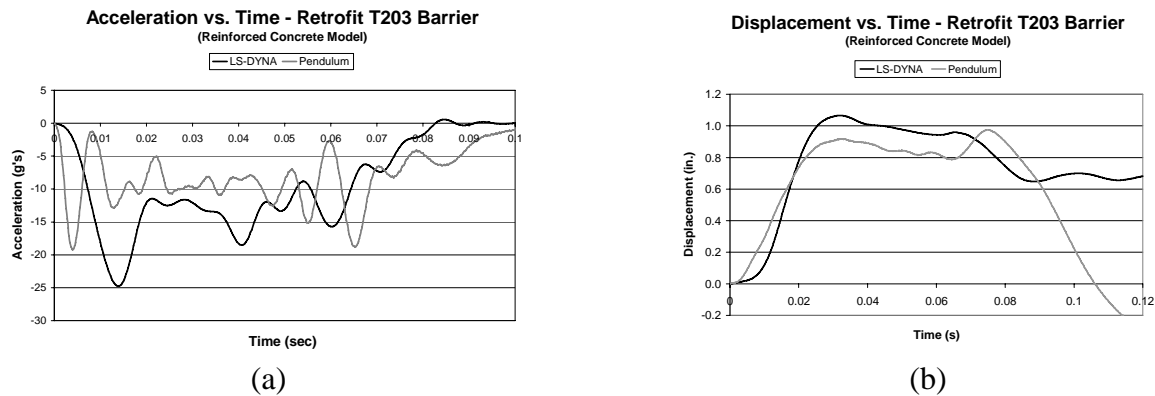


Figure 11.13: (a) Acceleration-versus-time graphs and (b) displacement-versus-time graphs from pendulum impact test on retrofit T203 barrier and bridge deck and its reinforced concrete LS-DYNA simulation

Table 11.13 shows the comparison between the pendulum impact test results and the results obtained from its simulation using the criteria discussed.

Table 11.13: Comparison of results of pendulum impact test on retrofit T203 barrier and bridge deck and its reinforced concrete simulation in LS-DYNA

| <i>Comparison Between:</i> | <i>Comparison Criterion</i> | | | | |
|---|-----------------------------|------------------------------------|--------------------------|---------------------------------|---------------------------|
| | <i>Impact Energy (kJ)</i> | <i>Impulse of Impact (kip-sec)</i> | <i>Peak Force (kips)</i> | <i>Duration of impact (sec)</i> | <i>Barrier Disp. (in)</i> |
| Pendulum Impact Test on retrofit T203 barrier and bridge deck | 38.5 | 1.44 | 38 | 0.1 | 1 |
| LS-DYNA Simulation of Pendulum Impact Test on retrofit T203 barrier and bridge deck (reinforced concrete model) | 38.5 | 1.89 | 45 | 0.09 | 1.1 |

The impact energy imparted to the barrier by the simulation is the same as the impact energy imparted to the barrier by the laboratory pendulum and conforms to the NCHRP TL-3 criterion. The impulse of impact obtained from LS-DYNA was approximately 1.89 kip-sec (7750 N-sec), which is 21% greater than the test value of 1.44 kip-sec (6400 N-sec). The peak force obtained from the test was about 38 kips (169 kN), 17% lower than the 45 kips (200 kN) obtained from the LS-DYNA simulation. The peak barrier displacement obtained from the simulation was about 1.1 in. (27 mm), which is similar to the laboratory test value of about 1 in. (25 mm).

Except for the impulse of impact value and peak force value, all the other comparison values obtained from the simulation are similar to the laboratory test. Again, in this case, the higher impulse value of impact obtained from the simulation is due to the use of *SOLID* elements to model the crush package, and the 21% difference in the impulse value was considered acceptable. Because every comparison quantity except the peak force was considered acceptable, and because the impulse of impact and the peak displacement values are considered to be the most important criteria, it was concluded that this model is acceptable.

This reinforced concrete LS-DYNA model of the retrofit T203 barrier and bridge deck can appropriately be used for crash simulations to understand the retrofit T203 barrier behavior during vehicular collisions.

11.7 Vehicular Crash Simulations on Reinforced Concrete LS-DYNA Models of T203 Barrier and Bridge Deck

The validated reinforced concrete LS-DYNA models of the cast-in-place and retrofit T203 bridge barrier and deck specimens are appropriate for use in extrapolation studies such as crash simulations.

This section discusses the following:

- various initial conditions used for vehicular crash simulations on reinforced concrete models of T203 barrier and bridge deck sections;
- use of vehicle models in LS-DYNA used for the vehicular crash simulations; and

- criteria for performance evaluation of the retrofit T203 barrier.

11.7.1 Initial Conditions for Crash Simulations

NCHRP Report 350 gives six test levels that can be selected to design and evaluate the performance of longitudinal highway barriers. NCHRP TL-3 and TL-4 crash criteria are outlined in Chapter 2 (Table 2.1). Most of the longitudinal barriers in the United States, including the T203 barrier, are qualified for *NCHRP Report 350* TL-3.

It was decided to evaluate the behavior of the retrofit T203 barrier under crash simulations conforming to the NCHRP TL-3 (the design test level for the T203 barrier) in the following way:

- 1) Develop TL-3 (Test Designation 3-10) and TL-3 (Test Designation 3-11) simulations on the reinforced concrete models of the cast-in-place and retrofit T203 barrier and bridge deck.
- 2) Compare the TL-3 crash simulation results of the retrofit T203 barrier to that of the cast-in-place T203 (evaluated for TL-3) barrier using the *NCHRP Report 350* requirements. The comparison criteria are discussed in Section 11.7.3.

In addition, it was decided to simulate NCHRP TL-4 vehicular crashes to characterize the barrier behavior under a test level higher than the design test level. These TL-4 simulations would help indicate the robustness of the T203 retrofit barrier design. The retrofit barrier was evaluated for the TL-4 in the following way:

- 1) Develop TL-4 (Test Designation 4-12) simulations on the reinforced concrete models of the cast-in-place and retrofit T203 barrier and bridge deck sections.
- 2) Compare the TL-4 crash simulation results of the retrofit T203 barrier to that of the cast-in-place T203 barrier using the *NCHRP Report 350* requirements. The comparison criteria are discussed in Section 11.7.3.

11.7.2 LS-DYNA Vehicle Models for Vehicular Crash Simulations

To use LS-DYNA to simulate vehicular impacts, it is necessary to incorporate previously developed FHWA vehicle models distinguished by a *.key* file. The FHWA vehicle models can be downloaded from the National Crash Analysis Center website (FHWA 2006). Once downloaded, the *.key* file of the vehicle model can be introduced in the *.fmb* file of a reinforced concrete T203 barrier and bridge deck model using the *IMPORT* command under the *FILE* menu. The imported vehicle model then has to be spatially oriented using the *TRANSFORM* command under the *ELEMENT* menu (Tolnai 2005). *AUTOMATIC_SURFACE_TO_SURFACE* contact is assigned to the vehicle and the barrier. The vehicle is specified as the master surface and the barrier is designated as the slave surface. The vehicle is then given initial translation and rotational velocities using the *INITIAL* command under the *BOUNDARY* menu as discussed by Tolnai.

To simulate NCHRP TL-3, Test Designation 3-10 (or TL-4, Test Designation 4-10), a coarse model of the 1997 Geo Metro was used. A coarse model of the Chevrolet C2500 Truck was used to simulate TL-3 (Test Designation 3-11). To simulate NCHRP TL-4 (Test Designation 4-12) a reduced model of the Ford Single Unit Truck was used. Figure 11.14 shows the various vehicular models used to simulate these test cases.

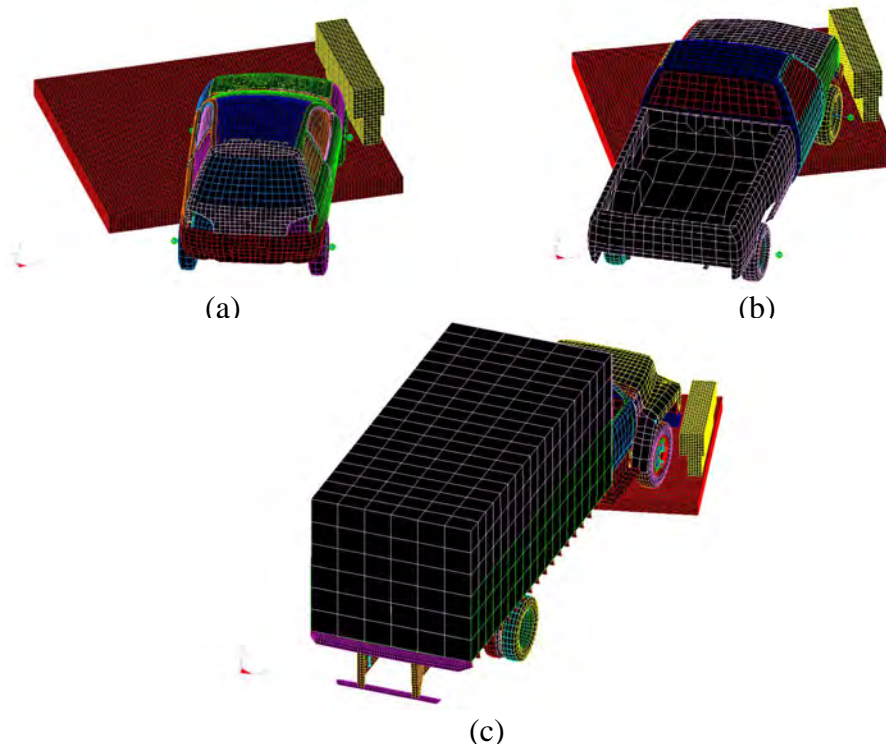


Figure 11.14: LS-DYNA models of T203 barrier crash simulations with (a) 1997 Geo Metro (b) Chevrolet C2500 Truck and (c) Ford Single Unit Truck

Each vehicle model qualifies for the weight requirements (Table 2.1) for the test case it is used to represent within the NCHRP requirements. Each model is then manipulated so that it has the same impact conditions (Table 2.1) as those required by the test case it simulates. The positions of the vehicle models in the simulations are also shown in Figure 11.14.

11.7.3 Criteria for Evaluation of Retrofit T203 Barrier

The performance of the retrofit T203 barrier was evaluated for NCHRP TL-3 and TL-4 based on *NCHRP Report 350* requirements using the following criteria:

- the crash simulation for a particular test level should impart the same impact energy to the retrofit T203 barrier and bridge deck model as the crash simulation imparts to the cast-in-place T203 barrier and bridge deck;
- the crash simulation should produce a similar impulse of impact for the retrofit T203 barrier as it does with cast-in-place T203 barrier for a particular test level; and
- the displacements of the retrofit T203 barrier should be similar to the cast-in-place T203 barrier for a particular test level simulation.

11.8 Evaluation of Retrofit T203 Barrier and Bridge Deck Using LS-DYNA Simulations

This section evaluates the performance of the retrofit T203 barrier for NCHRP TL-3 and TL-4 using the simulations discussed in Section 11.7.

11.8.1 Evaluation of Retrofit T203 Barrier for NCHRP TL-3 (Test Designation 3-10)

Figure 11.15 shows the force versus time and the displacement-versus-time graphs obtained from NCHRP TL-3 (Test Designation 3-10) crash simulation on reinforced concrete models of cast-in-place and retrofit T203 barrier and bridge deck LS-DYNA models. The force-versus-time and displacement-versus-time graphs for the retrofit T203 barrier are similar to those of its cast-in-place counterpart. As shown in Figure 11.14 (a), the 1997 Geo Metro LS-DYNA model is used for this test case simulation.

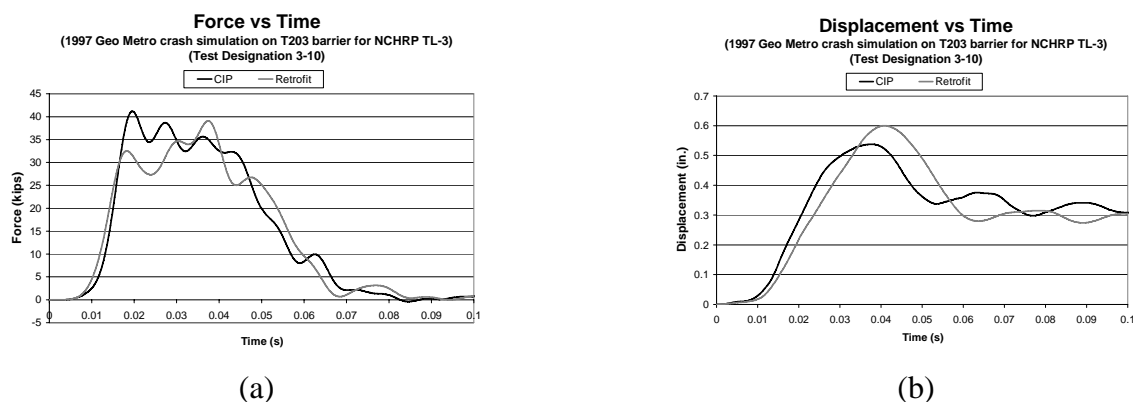


Figure 11.15: (a) Force-time histories and (b) displacement-time histories for NCHRP TL-3 (Test Designation 3-10) crash simulation using 1997 Geo Metro

Table 11.14 shows the comparison between the cast-in-place and retrofit T203 barrier for this test level using the criteria discussed.

Table 11.14: Comparison between cast-in-place and retrofit T203 barriers for NCHRP TL-3 (Test Designation 3-10)

| <i>Comparison Between:</i> | <i>Comparison Criterion</i> | | |
|--------------------------------|-------------------------------|--|-------------------------------|
| | <i>Impact Energy (kJ)</i> | <i>Impulse of Impact (kip-sec)</i> | <i>Barrier Disp. (in)</i> |
| CIP T203 Barrier | 37 | 1.45 | 0.55 |
| Retrofit T203 Barrier | 37 | 1.42 | 0.6 |

The same impact energy (required by TL-3, Test Designation 3-10) is imparted to both the cast-in-place and retrofit T203 barriers. The impulse of impact for the cast-in-place T203 barrier is about 1.45 kip-sec (6450 N-sec). The impulse of impact for the retrofit T203 barrier is 1.42 kip-sec (6300 N-sec), very similar to that of its cast-in-place counterpart. The peak

displacement of the retrofit T203 barrier is about 0.6 in. (15 mm), 7% greater than that of the cast-in-place T203 barrier, which has a displacement of about 0.55 in. (14 mm).

It can be concluded from this comparison that the behavior of the retrofit barrier is similar to its cast-in-place counterpart for TL-3 (Test Designation 3-10) based on the *NCHRP Report 350* requirements.

11.8.2 Evaluation of Retrofit T203 Barrier for NCHRP TL-3 (Test Designation 3-11) using LS-DYNA Simulations

Figure 11.16 shows the force versus time and the displacement-versus-time graphs obtained from NCHRP TL-3 (Test Designation 3-11) crash simulation on reinforced concrete models of cast-in-place and retrofit T203 barrier and bridge deck LS-DYNA models. The force versus time and the displacement-versus-time graphs for the retrofit T203 barrier are similar to its cast-in-place counterpart. As shown in Figure 11.14(b), the Chevrolet C2500 truck LS-DYNA model is used for this test case simulation.

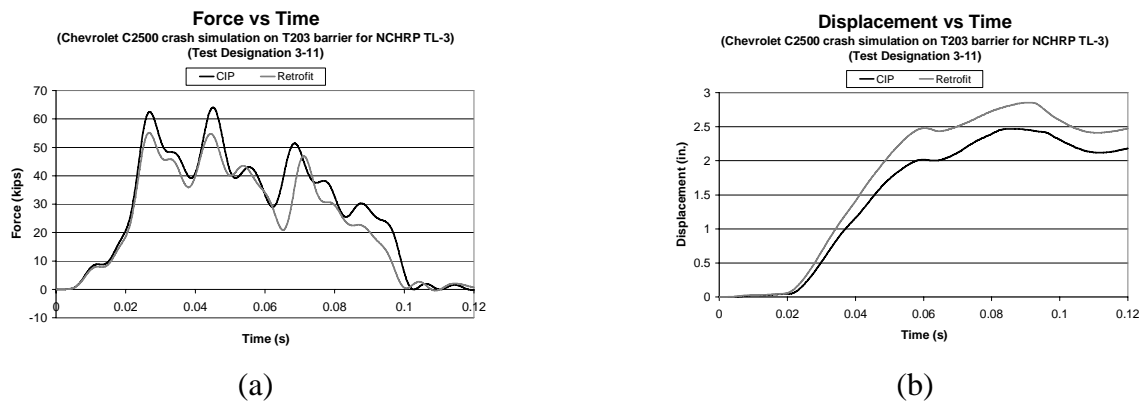


Figure 11.16: (a) Force-time histories and (b) displacement-time histories for NCHRP TL-3 (Test Designation 3-11) crash simulation using Chevrolet C2500 truck

Table 11.15 shows the comparison between the cast-in-place and retrofit T203 barrier for this test level using the criteria discussed.

Table 11.15: Comparison between cast-in-place and retrofit T203 barriers for NCHRP TL-3 (Test Designation 3-11) using LS-DYNA simulations

| <i>Comparison Between:</i> | <i>Comparison Criterion</i> | | |
|----------------------------|-----------------------------|------------------------------------|---------------------------|
| | <i>Impact Energy (kJ)</i> | <i>Impulse of Impact (kip-sec)</i> | <i>Barrier Disp. (in)</i> |
| CIP T203 Barrier | 90.25 | 3.31 | 2.5 |
| Retrofit T203 Barrier | 90.25 | 2.88 | 2.8 |

The same impact energy (required by TL-3, Test Designation 3-11) is imparted to both the cast-in-place and retrofit T203 barriers. The impulse of impact for the cast-in-place T203 barrier is about 3.31 kip-sec (14700 N-sec). The impulse of impact for the retrofit T203 barrier is 2.88 kip-sec (12800 N-sec), about 12% less than that of its cast-in-place counterpart. The peak

displacement of the retrofit T203 barrier is about 2.8 in. (71 mm), 10% greater than that of the cast-in-place T203 barrier (2.5 in. (64 mm)).

It can be concluded from this comparison that the behavior of the retrofit barrier is similar to that of its cast-in-place counterpart for TL-3 (Test Designation 3-11) based on the *NCHRP Report 350* requirements.

11.8.3 Evaluation of Retrofit T203 Barrier for NCHRP TL-4 (Test Designation 4-12) using LS-DYNA Simulations

Figure 11.17 shows the force versus time and the displacement-versus-time graphs obtained from *NCHRP Report 350* TL-4 (Test Designation 4-12) crash simulation on reinforced concrete models of cast-in-place and retrofit T203 barrier and bridge deck LS-DYNA models. The force versus time and the displacement-versus-time graphs for the retrofit T203 barrier are similar to its cast-in-place counterpart. As shown in Figure 11.14(c), the Ford Single Unit Truck LS-DYNA model is used for this test case simulation.

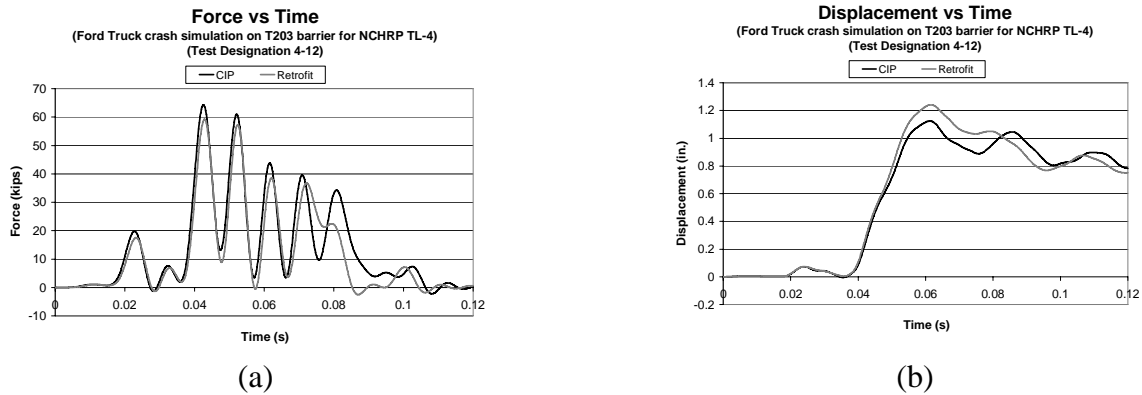


Figure 11.17: (a) Force-time histories and (b) displacement-time histories for NCHRP TL-4 (Test Designation 4-12) crash simulation using Ford Single Unit Truck

Table 11.16 shows the comparison between the cast-in-place and retrofit T203 barrier for this test level using the criteria discussed.

Table 11.16: Comparison between cast-in-place and retrofit T203 barriers for NCHRP TL-4 (Test Designation 4-12) using LS-DYNA simulations

| <i>Comparison Between:</i> | <i>Comparison Criterion</i> | | |
|----------------------------|-----------------------------|------------------------------------|---------------------------|
| | <i>Impact Energy (kJ)</i> | <i>Impulse of Impact (kip-sec)</i> | <i>Barrier Disp. (mm)</i> |
| CIP T203 Barrier | 231 | 1.64 | 1.15 |
| Retrofit T203 Barrier | 231 | 1.46 | 1.25 |

The same impact energy (required by *NCHRP Report 350* TL-4, Test Designation 4-12) is imparted to both the cast-in-place and retrofit T203 barriers. The impulse of impact for the cast-in-place T203 barrier is about 1.64 kip-sec (7300 N-sec). The impulse of impact for the retrofit T203 barrier is 1.46 kip-sec (6500 N-sec), about 11% less than that of its cast-in-place counterpart. The peak displacement of the retrofit T203 barrier is about 1.25 in. (31.5 mm), 7% greater than that of the cast-in-place T203 barrier at about 1.15 in. (29.5 mm).

It can be concluded from this comparison that the behavior of the retrofit barrier is similar to that of its cast-in-place counterpart for TL-4 (Test Designation 4-12) based on the *NCHRP Report 350* requirements.

11.8.4 Concluding Remarks on the Predicted Performance of Retrofit T203 Barrier Using LS-DYNA Simulations

The analytical simulations just described show that the performance of the retrofit T203 barrier is predicted to be similar to that of the cast-in-place T203 barrier for *NCHRP Report 350* TL-3 and TL-4. Hence, it can be concluded that, like the cast-in-place T203 barrier, the retrofit T203 barrier passes the *NCHRP Report 350* TL-3 and TL-4 requirements and can be considered a robust barrier.

11.9 Development of Reinforced Concrete LS-DYNA Models of T501 Barrier and Bridge Deck

Previously in this chapter, the development and validation of a reinforced concrete model of the T203 barrier and bridge deck specimen was discussed. From a finite-element modeling perspective, a T501 barrier is different from the T203 barrier only in terms of its shape and reinforcing details. Hence, a similar reinforced concrete model (with the same properties) can be developed for the T501 barrier and bridge deck specimen to predict its behavior.

This section discusses the following:

- basic geometry of the LS-DYNA model of the T501 barrier;
- meshing the LS-DYNA model of the T501 barrier;
- basic LS-DYNA model of the T501 barrier and bridge deck;
- reinforced concrete LS-DYNA model of the cast-in-place T501 barrier and bridge deck; and
- reinforced concrete LS-DYNA model of the retrofit T501 barrier and bridge deck.

11.9.1 Basic Geometry of LS-DYNA Model of T501 Barrier

The cross-section of a TXDOT T501 bridge barrier is given in Chapter 10. The reinforcement details of the cast-in-place and retrofit T501 barrier are also given in Chapter 10. The LS-DYNA model of the T501 barrier should closely represent the geometry of the barrier as well as have element positions to accommodate the reinforcement details of both the cast-in-place and the newly designed retrofit T501 barrier.

The cross-sectional geometry for the T501 barrier was selected keeping these constraints into perspective. Figure 11.18 shows the cross-sectional geometry of the LS-DYNA model of the T501 barrier. The basic geometry of the cross-section is created in LS-DYNA using *NODEs* and *LINEs*. The method of creating any shape in LS-DYNA using nodes and lines is discussed in detail by Tolnai (2005).

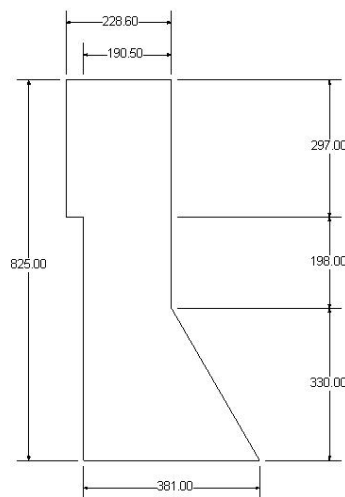


Figure 11.18: Cross-sectional geometry of LS-DYNA model of T501 barrier in LS-DYNA compatible units (mm)

11.9.2 Meshing LS-DYNA Model of T501 Barrier

Various sections were created in the overall cross-section of the LS-DYNA model of the T501 barrier using *LINES*. These sections are shown in Figure 11.19(a).

Plate elements were created in each of these sections of the cross-section of the T501 barrier model using the 3-line plate/solid meshing tool under the *ELEMENT* menu. Meshing is discussed in detail by Tolnai (2005). The plate mesh can be seen in Figure 11.19(b). For the sections with triangular elements, the *OPTION* (under the *ELEMENT* menu) was changed to 'triangular element' from the default 'rectangular element' option before meshing.

The purpose of meshing is to create appropriate *SOLID* elements to represent the T501 barrier and its reinforcement details. The plate elements created have to be converted to *SOLID* elements, which is done using the *EXTRUDE* command under the *ELEMENT* menu. The result is a 1524-mm (5-ft.) long basic LS-DYNA model of a T501 barrier (created with solid elements) to represent the 5-ft. section constructed at FSEL (Figure 11.19(c)).

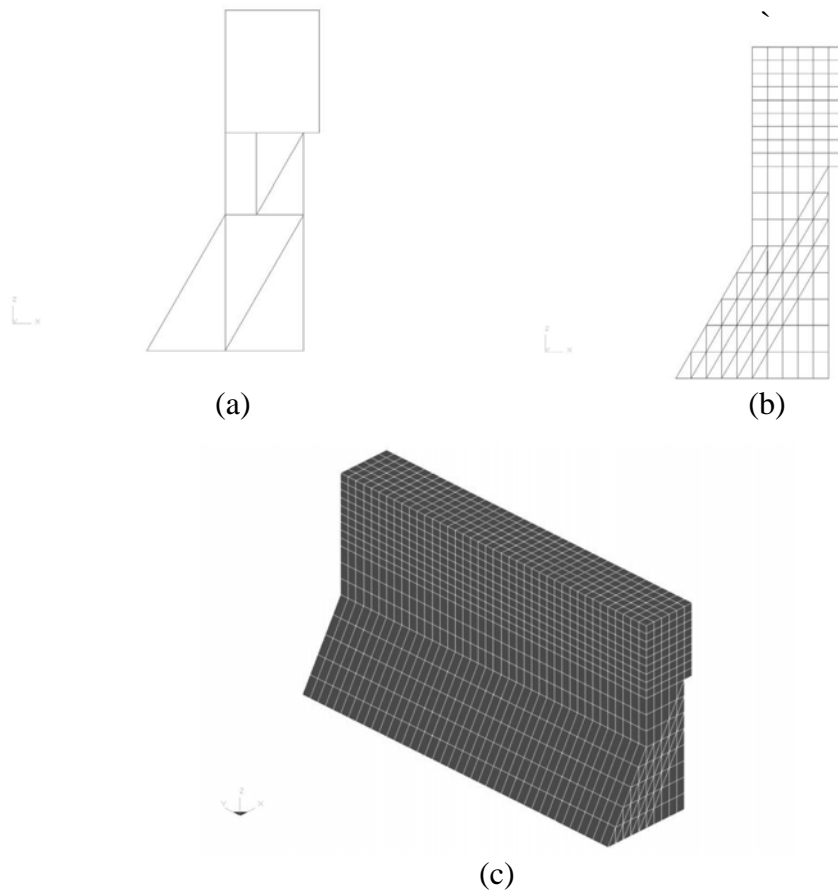


Figure 11.19: Steps for creating basic LS-DYNA model of T501 barrier using SOLID elements

11.9.3 Basic LS-DYNA Model of T501 Barrier and Bridge Deck

As discussed in Chapter 10, the same test slab used for testing T203 barriers was used to test T501 barriers. Hence, the LS-DYNA model of the test slab for the T501 barriers is the same as for the T203 barriers.

The creation of a basic bridge barrier and deck model for the T203 barrier was discussed in detail in Section 11.3. The procedure is the same for the T501 barrier except that the barrier is different. The LS-DYNA model of the T501 barrier, discussed in the previous section, was attached the slab model at the appropriate location using the *FIND COINCIDENT* command to form a basic T501 barrier and bridge deck model. The created model is shown in Figure 11.20. This basic model was used to create reinforced concrete LS-DYNA models of the cast-in-place and retrofit T501 barriers.

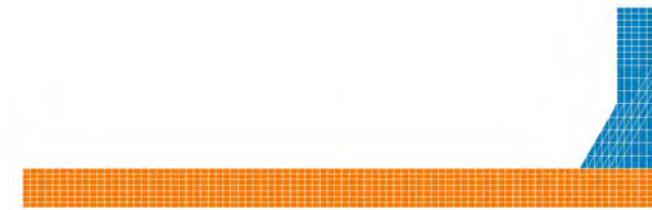


Figure 11.20: Basic LS-DYNA model of T501 barrier and bridge deck

11.9.4 Reinforced Concrete LS-DYNA Model of Cast-in-Place T501 Barrier and Bridge Deck

To develop a reinforced concrete T501 barrier and bridge deck model, reinforcing details and a material model have to be assigned to the basic model of the T501 barrier and bridge deck discussed in the previous section.

Reinforcing details of the deck are the same as that for the T203 bridge deck. Reinforcing details of the cast-in-place T501 barrier are given in Chapter 10. These reinforcement details were assigned using the guidelines given in Section 11.5.2.

The *MAT_SOIL_AND_FOAM* material model was assigned to the solid elements forming the barrier and bridge deck. The input parameters were the same as discussed in Section 11.5.1. This constitutes the reinforced concrete LS-DYNA model of the cast-in-place T501 barrier and bridge deck. Figure 11.21 shows this LS-DYNA model.

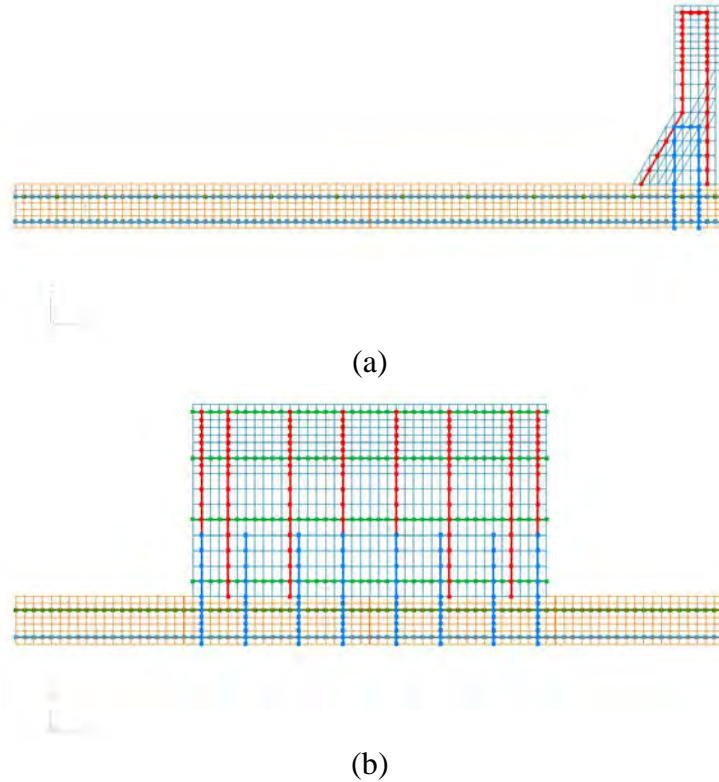


Figure 11.21: (a) Side view and (b) back view of reinforced concrete LS-DYNA model of cast-in-place T501 barrier and bridge deck

11.9.5 Reinforced Concrete LS-DYNA Model of Retrofit T501 Barrier and Bridge Deck

The laboratory test specimen of the retrofit T501 barrier and bridge deck is discussed in Chapter 10. Reinforcing details were assigned to the basic LS-DYNA model (Section 11.9.3) according to the guidelines provided in Section 11.5.2. Also, the *MAT_SOIL_AND_FOAM* material model was assigned to the solid elements forming the barrier and bridge deck.

The modeling of the retrofit details of the T501 barrier is similar to the modeling of retrofit T203 barrier (discussed in Section 11.5.3). The only major difference in the retrofit T501 barrier is the modeling of undercut anchors instead of the bottom plate to which threaded rods are attached. A minor difference is that the threaded rods and PVC pipes in the T203 barrier are oriented vertically, whereas in the T501 barrier they are inclined.

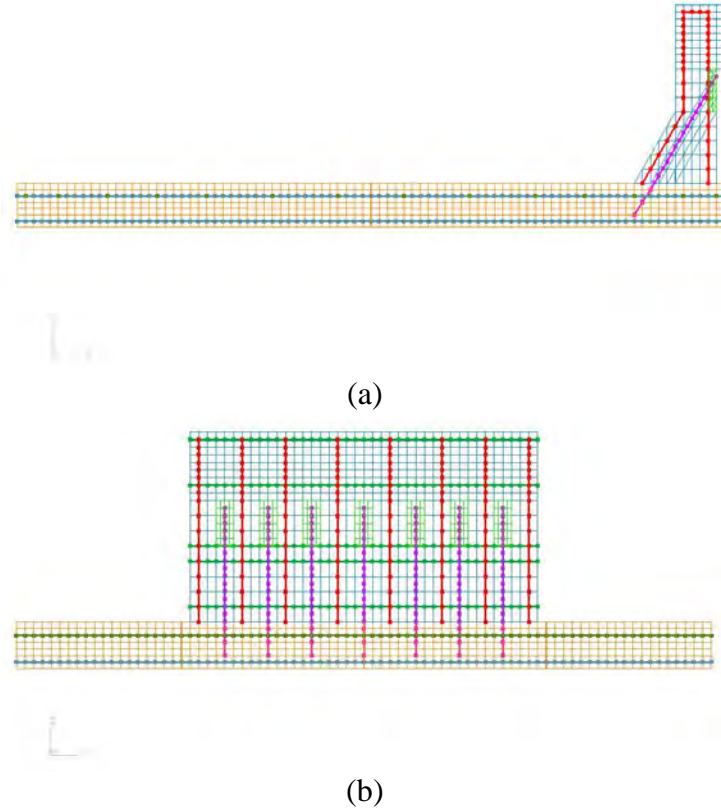


Figure 11.22: (a) Side view and (b) back view of reinforced concrete LS-DYNA model of retrofit T501 bridge barrier and deck

Figure 11.22 shows the reinforced concrete LS-DYNA model of the retrofit T501 barrier and bridge deck. The PVC pipes and the barrier end attachment of the threaded rods to a steel plate were modeled as per the guidelines given in Section 11.5.3. As with the retrofit T203 barrier, *TRUSS* elements and *MAT_PLASTIC_KINEMATIC* were used to model the threaded rods of the T501 barrier. *AUTOMATIC_SURFACE_TO_SURFACE* contact was assigned between the threaded rods and the surrounding concrete in the model, just like the retrofit T203 barrier.

LS-DYNA models of a concrete slab and undercut anchors with different embedment lengths were created. The slab was modeled using *SOLID* elements and was assigned the *MAT_SOIL_AND_FOAM* concrete material. The undercut anchors were modeled using *TRUSS* elements, the nodes of which were attached to the *SOLID* element nodes of the slab using the *FIND COINCIDENT* command under the *NODE* menu. The breakout capacities of the undercut anchors were obtained for various embedment lengths from the simulation as well as using the ACI 318-05 Appendix D calculations. On average, the breakout capacities obtained from the simulations were about 1.35 times the breakout capacities computed using ACI 318-05 Appendix D calculations. As discussed before, the mean anchor breakout capacities are about 1.4 times the lower 5% fractile capacities obtained from the ACI 318-05 Appendix D calculations. Hence, the breakout capacities obtained from the simulations are similar to the mean anchor breakout capacities. It can be concluded that LS-DYNA simulations provide a reasonably accurate method to model undercut anchors.

Undercut anchors in the retrofit T501 barrier were modeled in LS-DYNA using the guidelines discussed. The *TRUSS* elements representing the threaded rods are extended into the slab as shown in Figure 11.22. The depth and angle of this extension was the same as the depth and angle of the undercut anchors in the laboratory test slab. The nodes of the *TRUSS* elements of the threaded rods and the *SOLID* elements of the deck were merged together using the *FIND COINCIDENT* command under the *NODE* menu.

11.10 Pendulum Impact Test Simulations on T501 Barrier and Bridge Deck Using LS-DYNA

The impact pendulum test on a T501 barrier and bridge deck model can be simulated in the same way as that on a T203 barrier and bridge deck model (discussed in Section 11.4.2). The pendulum impact test simulation on the T501 barrier is shown in Figure 11.22.

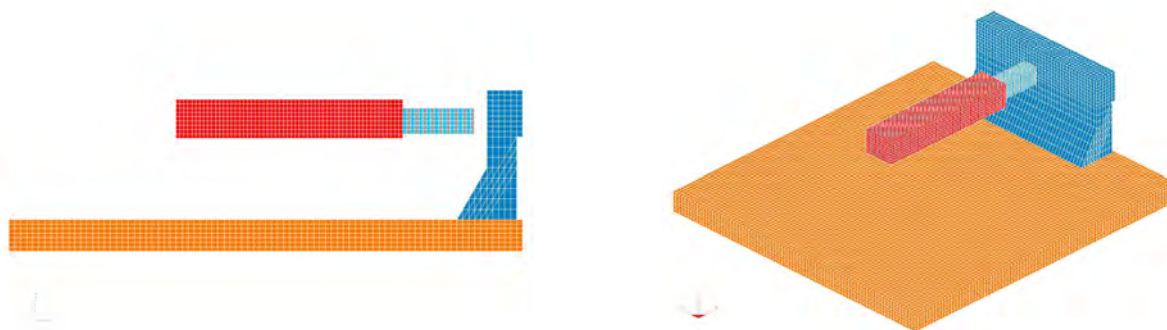


Figure 11.23: Pendulum impact test simulation on T501 barrier and bridge deck using LS-DYNA model

In this section, the results obtained from the pendulum impact test simulations on the cast-in-place and retrofit T501 barrier and bridge deck models developed in the previous section are discussed. One purpose of these simulations is to predict the behavior of the retrofit T501 barrier and bridge deck sections under an impact pendulum test, as discussed later in this report. The other purpose is to use the results obtained from the simulations to predict if the retrofit T501 barrier meets the TxDOT performance criteria for retrofit barriers, which is discussed in detail in Chapter 10.

11.10.2 Results from Impact Pendulum Test Simulation on Cast-in-Place T501 Barrier and Bridge Deck using LS-DYNA

Figure 11.24 shows the force-time histories and the displacement-time histories obtained from pendulum impact test simulations on the cast-in-place T501 barrier and bridge deck LS-DYNA model.

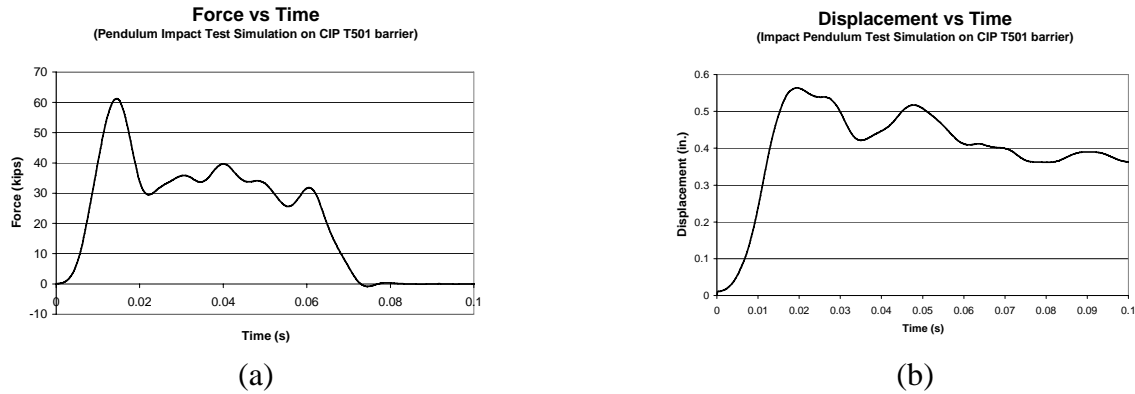


Figure 11.24: (a) Force-versus-time and (b) displacement-versus-time graphs from pendulum impact test simulation on cast-in-place T501 barrier and bridge deck

The peak force of impact is about 60 kips (267 kN). The 50-msec dynamic capacity is about 37 kips (164 kN); the duration of impact is about 0.08 seconds; and the impulse of impact is about 2.16 kip-sec (9600 N-sec). The peak displacement is about 0.6 in. (16 mm).

11.10.3 Results from Pendulum Impact Test Simulation on Retrofit T501 Barrier and Bridge Deck using LS-DYNA

Figure 11.25 shows the force-time histories and the displacement-time histories obtained from pendulum impact test simulations on the retrofit T501 barrier and bridge deck LS-DYNA model.

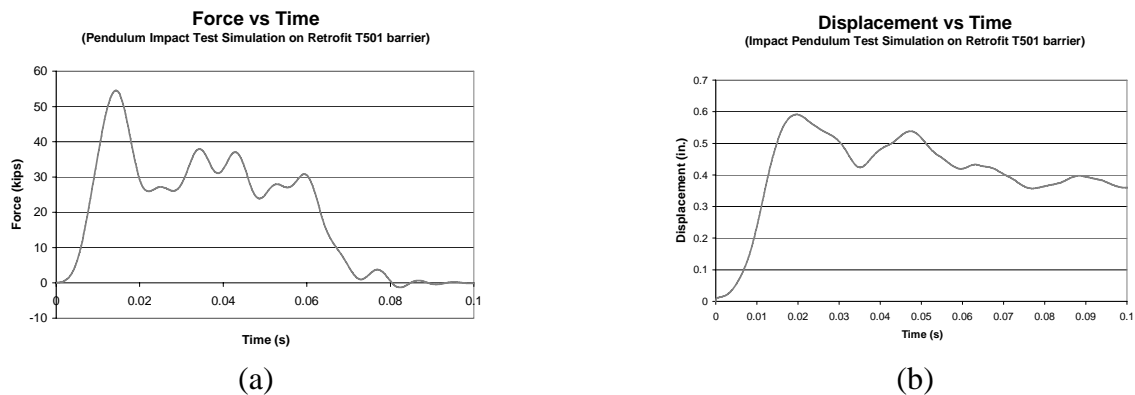


Figure 11.25: (a) Force-versus-time and (b) displacement-versus-time graphs from pendulum impact test simulation on retrofit T501 barrier and bridge deck

The peak force of impact is about 52 kips (231 kN). The 50-msec dynamic capacity is about 33 kips (147 kN); the duration of impact is about 0.08 seconds; and the impulse of impact is about 1.95 kip-sec (8650 N-sec). The peak displacement is about 0.6 in. (17 mm).

11.11 Evaluation of Retrofit T501 Barrier and Bridge Deck Using Vehicular Crash Simulations with LS-DYNA

This section evaluates the performance of the retrofit T501 barrier for NCHRP TL-3 and TL-4 using the simulations discussed in Section 11.7. The same methodology and performance criteria used to evaluate the retrofit T203 barrier are used for the retrofit T501 barrier.

11.11.1 Evaluation of Retrofit T501 Barrier for NCHRP TL-3 (Test Designation 3-10) using LS-DYNA Simulations

Figure 11.26 shows the force-versus-time and the displacement-versus-time graphs obtained from *NCHRP Report 350* TL-3 (Test Designation 3-10) crash simulation on reinforced concrete LS-DYNA models of cast-in-place and retrofit T501 bridge barrier and deck sections. The force-versus-time and the displacement-versus-time graphs for the retrofit T501 barrier are similar to those of its cast-in-place counterpart. The 1997 Geo Metro LS-DYNA model is used for this test case simulation.

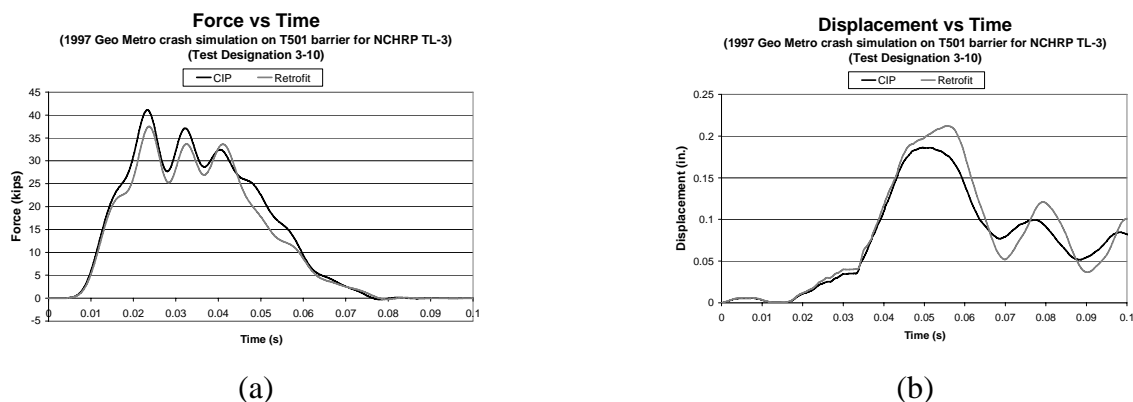


Figure 11.26: (a) Force-time histories and (b) displacement-time histories for NCHRP TL-3 (Test Designation 3-10) crash simulation using 1997 Geo Metro

Table 11.17 shows the comparison between the cast-in-place and retrofit T501 barrier for this test level using the criteria discussed.

Table 11.17: Comparison between cast-in-place and retrofit T501 barriers for NCHRP TL-3 (Test Designation 3-10)

| <i>Comparison Between:</i> | <i>Comparison Criterion</i> | | |
|----------------------------|-----------------------------|------------------------------------|---------------------------|
| | <i>Impact Energy (kJ)</i> | <i>Impulse of Impact (kip-sec)</i> | <i>Barrier Disp. (in)</i> |
| CIP T501 Barrier | 37 | 1.37 | 0.55 |
| Retrofit T501 Barrier | 37 | 1.25 | 0.6 |

The same impact energy (required by TL-3, Test Designation 3-10) is imparted to both the cast-in-place and retrofit T501 barriers. The impulse of impact for the cast-in-place T501

barrier is about 1.37 kip-sec (6100 N-sec). The impulse of impact for the retrofit T501 barrier is about 1.25 kip-sec (5550 N-sec), about 8% less than that of its cast-in-place counterpart. The peak displacement of the retrofit T501 barrier is about 0.6 in. (15 mm), 7% greater than that of the cast-in-place T501 barrier (0.55 in. (14 mm)).

It can be concluded from this comparison that the behavior of the retrofit barrier is predicted to be similar to that of its cast-in-place counterpart for TL-3 (Test Designation 3-10) based on the *NCHRP Report 350* requirements.

11.11.2 Evaluation of Retrofit T501 Barrier for NCHRP TL-3 (Test Designation 3-11) using LS-DYNA Simulations

Figure 11.27 shows the force-versus-time and the displacement-versus-time graphs obtained from *NCHRP Report 350* TL-3 (Test Designation 3-11) crash simulation on reinforced concrete models of cast-in-place and retrofit T501 barrier and bridge deck LS-DYNA models. The LS-DYNA model of the Chevrolet C2500 truck is used for this test case simulation.

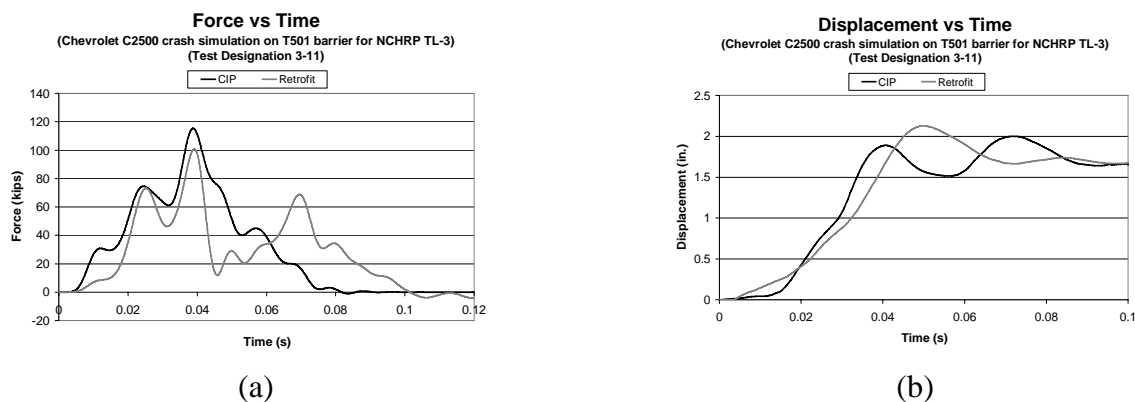


Figure 11.27: (a) Force-time histories and (b) displacement-time histories for NCHRP TL-3 (Test Designation 3-11) crash simulation using Chevrolet C2500 truck

Table 11.18 shows the comparison between the cast-in-place and retrofit T501 barrier for this test level using the criteria discussed.

Table 11.18: Comparison between cast-in-place and retrofit T501 barriers for NCHRP TL-3 (Test Designation 3-11)

| <i>Comparison Between:</i> | <i>Comparison Criterion</i> | | |
|----------------------------|-----------------------------|------------------------------------|---------------------------|
| | <i>Impact Energy (kJ)</i> | <i>Impulse of Impact (kip-sec)</i> | <i>Barrier Disp. (in)</i> |
| CIP T501 Barrier | 90.25 | 3.45 | 1.9 |
| Retrofit T501 Barrier | 90.25 | 3.29 | 2.2 |

The same impact energy (required by TL-3, Test Designation 3-11) is imparted to both the cast-in-place and retrofit T501 barriers. The impulse of impact for the cast-in-place T501 barrier is about 3.45 kip-sec (15350 N-sec). The impulse of impact for the retrofit T501 barrier is

3.29 kip-sec (14600 N-sec), about 5% less than that of its cast-in-place counterpart. The peak displacement of the retrofit T501 barrier is about 2.2 in. (56 mm), 13% greater than that of the cast-in-place T501 barrier (1.9 in. (48.5 mm)).

It can be concluded from this comparison that the behavior of the retrofit barrier is predicted to be similar to that of its cast-in-place counterpart for TL-3 (Test Designation 3-11) based on the *NCHRP Report 350* requirements.

11.11.3 Evaluation of Retrofit T203 Barrier for *NCHRP Report 350* TL-4 (Test Designation 4-12)

Figure 11.28 shows the force-versus-time and the displacement-versus-time graphs obtained from *NCHRP Report 350* TL-4 (Test Designation 4-12) crash simulation on reinforced concrete models of cast-in-place and retrofit T501 barrier and bridge deck LS-DYNA models. The force-versus-time and the displacement-versus-time graphs for the retrofit T501 barrier are similar to its cast-in-place counterpart. The Ford Single Unit Truck LS-DYNA model is used for this test case simulation.

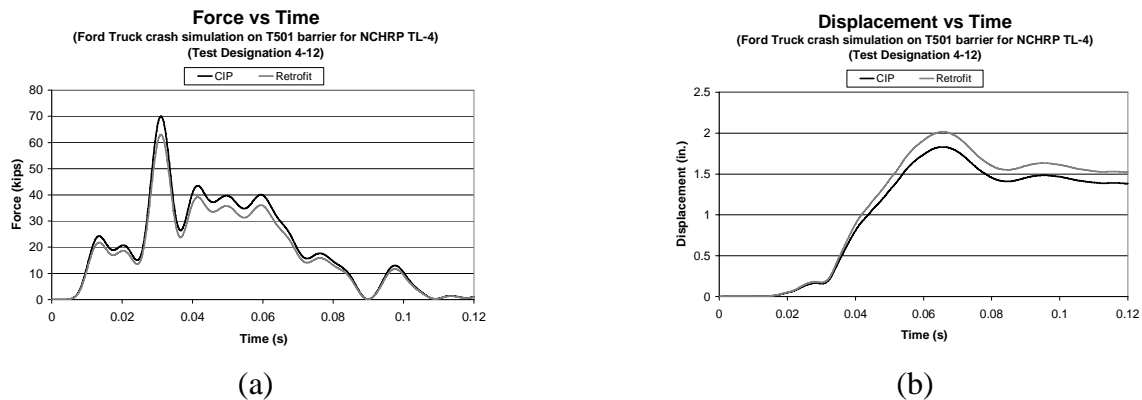


Figure 11.28: (a) Force-time histories and (b) displacement-time histories for NCHRP TL-4 (Test Designation 4-12) crash simulation using Ford Single Unit Truck

Table 11.19 shows the comparison between the cast-in-place and retrofit T501 barrier for this test level using the criteria discussed.

Table 11.19: Comparison between cast-in-place and retrofit T501 barriers for NCHRP TL-4 (Test Designation 4-12)

| <i>Comparison Between:</i> | <i>Comparison Criterion</i> | | |
|----------------------------|-----------------------------|------------------------------------|---------------------------|
| | <i>Impact Energy (kJ)</i> | <i>Impulse of Impact (kip-sec)</i> | <i>Barrier Disp. (in)</i> |
| CIP T501 Barrier | 231 | 2.39 | 1.8 |
| Retrofit T501 Barrier | 231 | 2.14 | 2 |

The same impact energy (required by *NCHRP Report 350* TL-4, Test Designation 4-12) is imparted to both the cast-in-place and retrofit T501 barriers. The impulse of impact for the

cast-in-place T501 barrier is about 2.39 kip-sec (10600 N-sec). The impulse of impact for the retrofit T501 barrier is 2.14 kip-sec (9500 N-sec), about 11% less than that of its cast-in-place counterpart. The peak displacement of the retrofit T501 barrier is about 2 in. (51 mm), 7% greater than that of the cast-in-place T501 barrier (1.8 in. (46 mm)).

It can be concluded from this comparison that the behavior of the retrofit barrier is predicted to be similar to that of its cast-in-place counterpart for TL-4 (Test Designation 4-12) based on the *NCHRP Report 350* requirements.

11.11.4 Concluding Remarks on the Predicted Performance of Retrofit T203 Barriers using LS-DYNA Simulations

These evaluations show that the performance of the retrofit T501 barrier is predicted to be similar to that of the cast-in-place T501 barrier for *NCHRP Report 350* TL-3 and TL-4. Hence, it is conjectured that, like the cast-in-place T501 barrier, the retrofit T501 barrier would pass the NCHRP TL-3 and TL-4 requirements and can be considered a robust barrier. This hypothesis is tested as described in the next chapter.

Chapter 12. Results from Experimental Testing of T501 Bridge Barriers

12.1 Introduction

Pendulum tests and quasi-static tests were carried out on two prototype retrofit T501 barriers, one with 7 mild steel anchors and the other with 4 high-strength steel anchors. This chapter presents the test results obtained from the dynamic pendulum tests and the confirmatory quasi-static test on laboratory specimens representing a T501 barrier and its associated bridge deck. Test results for a retrofit T501 barrier with seven anchors, a retrofit T501 barrier with four anchors using a pendulum drop height of 16 feet, and a retrofit T501 barrier with four anchors using a pendulum drop height of 19.5 feet are presented.

12.2 Test Results for Retrofit T501 Barriers with Seven Anchors

Impact pendulum testing to *NCHRP Report 350* TL-3 was conducted on the stand-alone retrofit T501 bridge barrier specimen, attached to the specimen's bridge slab using seven ASTM A307 threaded rods running through PVC ducts installed in the retrofit barrier. In this section, the following results are discussed:

- a still image from videos of the test;
- impact force versus time;
- barrier displacement versus time;
- strain of steel rods; and
- force versus barrier displacement.

A still image from this impact pendulum test (Figure 12.1) shows how the tubes of the crush package crush and the barrier deflects during impact. The barrier survived this TL-3 impact loading and remained standing after the test.



Figure 12.1: Still image from impact pendulum test on stand-alone retrofit T501 bridge barrier with seven anchors and deck specimen

12.2.2 Impact Force versus Time from Pendulum Impact Tests on Retrofit T501 Barrier

Figure 12.2 shows a graph of force versus time obtained from the pendulum impact test on the retrofit T501 bridge barrier specimen with seven anchors. The peak acceleration of the pendulum at impact was about 32.3 g, corresponding to a peak impact force of about 60.9 kips. The 50-msec dynamic capacity is about 29.6 kips; the duration of impact is about 0.1 seconds; and the impulse of impact is about 1.95 kip-sec (8666.7 N-sec).

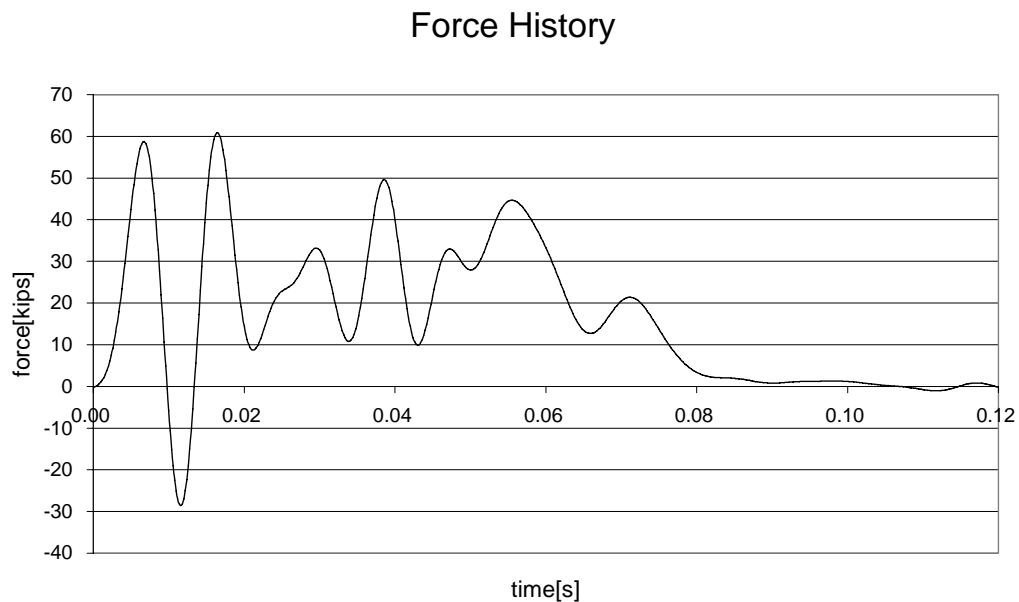


Figure 12.2: Force-versus-time graph from pendulum impact test on standalone retrofit T501 bridge barrier with seven anchors and deck specimen

12.2.3 Barrier Displacement versus Time from Pendulum Impact Tests on Retrofit T501 Barrier with Seven Anchors

Figure 12.3 shows the displacement versus time for the retrofit T501 barrier with seven anchors. The displacement was obtained at the top of the barrier. The peak displacement was about 1.1 in.

12.2.4 Strain of Steel Rods from Pendulum Impact Test on Retrofit T501 Barrier with Seven Anchors

Figure 12.4 shows the measured strains in the steel rods as a function of time. Strain gages on 5 of the 7 rods gave valid results, which are plotted in Figure 12.4. Because each steel rod was pretensioned to 20 ksi, their corresponding initial strain was 0.00067. Four of the five steel rods yielded during impact (corresponding to a strain value of 0.00172), and the other rod almost yielded. Strains were not recorded for the other two steel rods, and it is likely that these gages were damaged during installation.

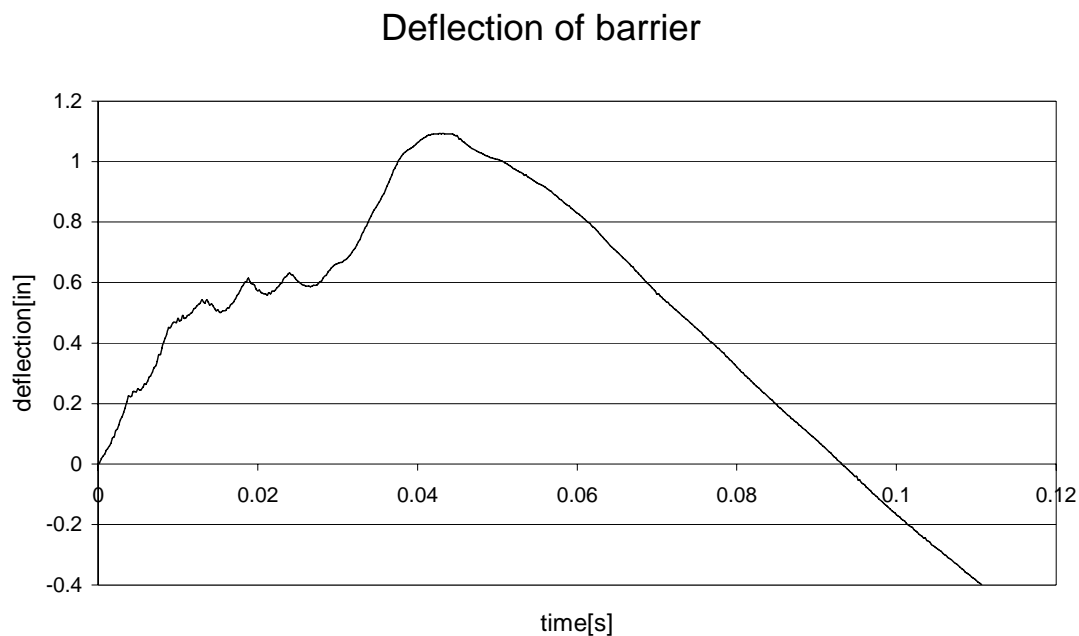


Figure 12.3: Barrier displacement-versus-time graph from pendulum impact test on standalone retrofit T501 bridge barrier with seven anchors and deck specimen

Strain of Steel Rods

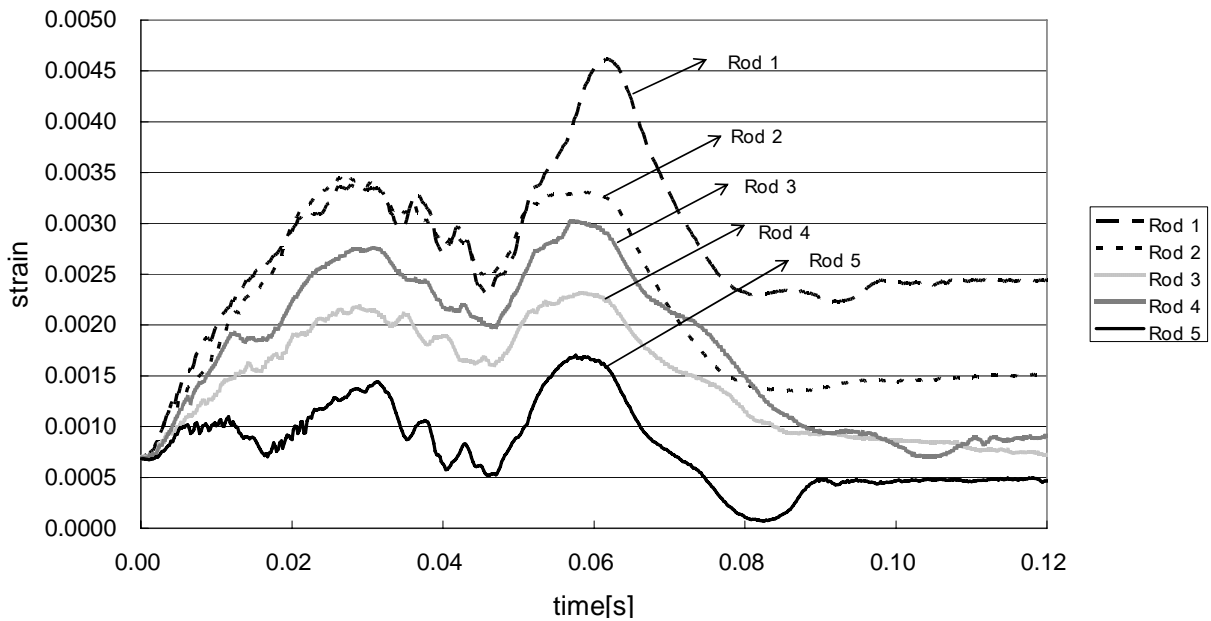


Figure 12.4: Strain values of steel rods from pendulum impact test on standalone retrofit T501 bridge barrier with seven anchors and deck specimen

12.2.5 Results from Quasi-Static Test on Retrofit T501 Barrier with Seven Anchors

Figure 12.5 shows the Force-versus-displacement graph obtained from the quasi-static test on the retrofit T501 barrier with seven anchors and bridge deck specimen. The tested static capacity of this barrier, about 39 kips, exceeded the estimate of 27.9 kips. Static capacity was underestimated by the concrete breakout equations of ACI 318-05 Appendix D because those formulas were not intended to address inclined anchors, and can only be approximately applied to them. As expected, failure is governed by concrete breakout.

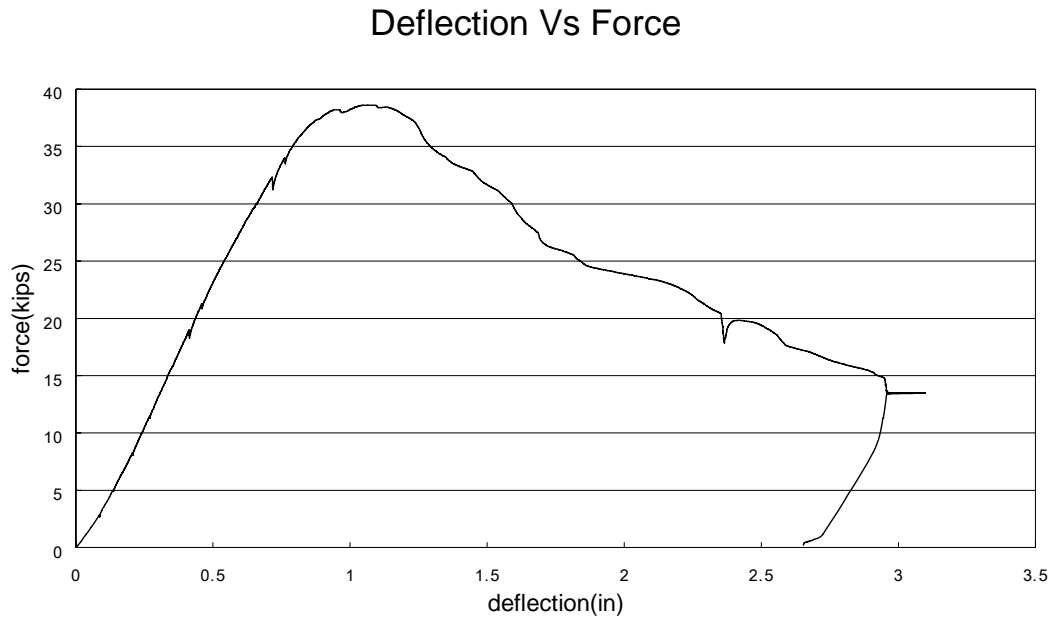


Figure 12.5: Force-versus-displacement graph from quasi-static test on stand-alone retrofit T501 bridge barrier with seven anchors and deck specimen

12.3 Results of the First Test for Retrofit T501 Barrier with Four Anchors

To improve the constructability of the retrofit T501 barrier, a variant with fewer anchors than the first specimen was considered. The retrofit barrier was identical to that discussed previously, with the exception that it had four ASTM A-193 Grade B7 threaded rods running through PVC ducts rather than seven A307 rods. The yield stress of those high-strength rods is 100 (ksi).

Two impact pendulum tests (*NCHRP Report 350 TL-3*) were conducted on this four-anchor, stand-alone retrofit T501 specimen. In the first test of a retrofit T501 barrier with four anchors, a drop height of 16 ft. was used (the elevation above the laboratory floor to which the pendulum was raised prior to testing).

In this section, the following results are discussed:

- a still image from videos of the test;
- impact force versus time;
- barrier displacement versus time; and
- strain of steel rods.

A still image from the impact test (Figure 12.6) shows the barrier deflection during impact.



Figure 12.6: Still image from impact pendulum test on stand-alone retrofit T501 bridge barrier with four anchors and deck specimen for a drop height of 16 feet

12.3.2 Impact Force versus Time from the First Pendulum Impact Test on Retrofit T501 Barrier with Four Anchors

Figure 12.7 shows a graph of force versus time from the impact test on the retrofit T501 bridge barrier specimen with four anchors. The peak acceleration of the pendulum at impact was about 33.6 g, corresponding to a peak impact force of about 63.29 kips. The 50-msec dynamic capacity is about 25.43 kips; the duration of impact is about 0.1 seconds; and the impulse of impact is approximately 1.69 kip-sec (7511.14N-sec).

12.3.3 Barrier Displacement versus Time from the First Pendulum Impact Test on Retrofit T501 Barrier with Four Anchors

Figure 12.8 shows the displacement versus time for the retrofit T501 barrier with four anchors. The peak displacement of the barrier is about 1.1 in.

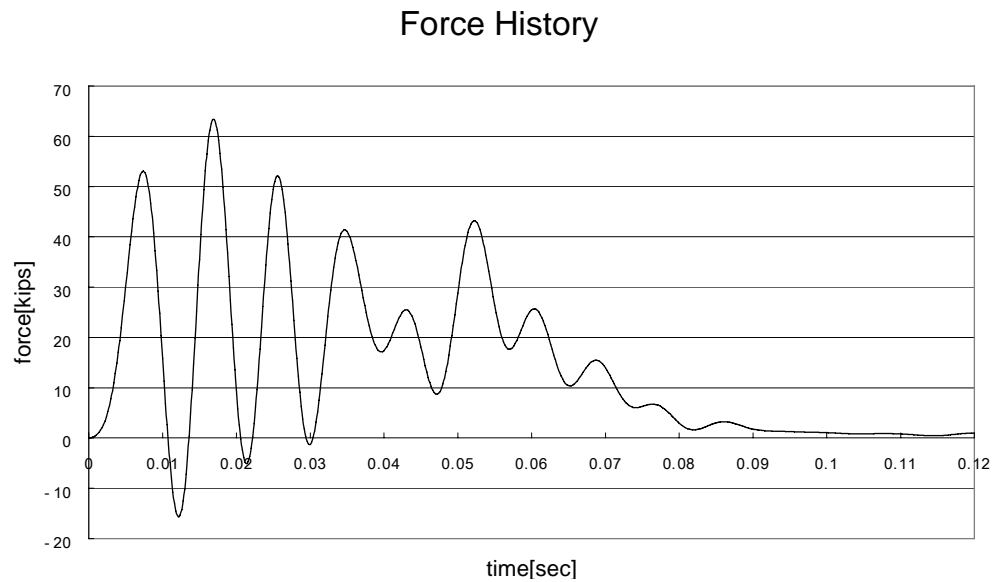


Figure 12.7: Force-versus-time graph from pendulum impact test on standalone retrofit T501 bridge barrier with four anchors and deck specimen for a drop height of 16 feet

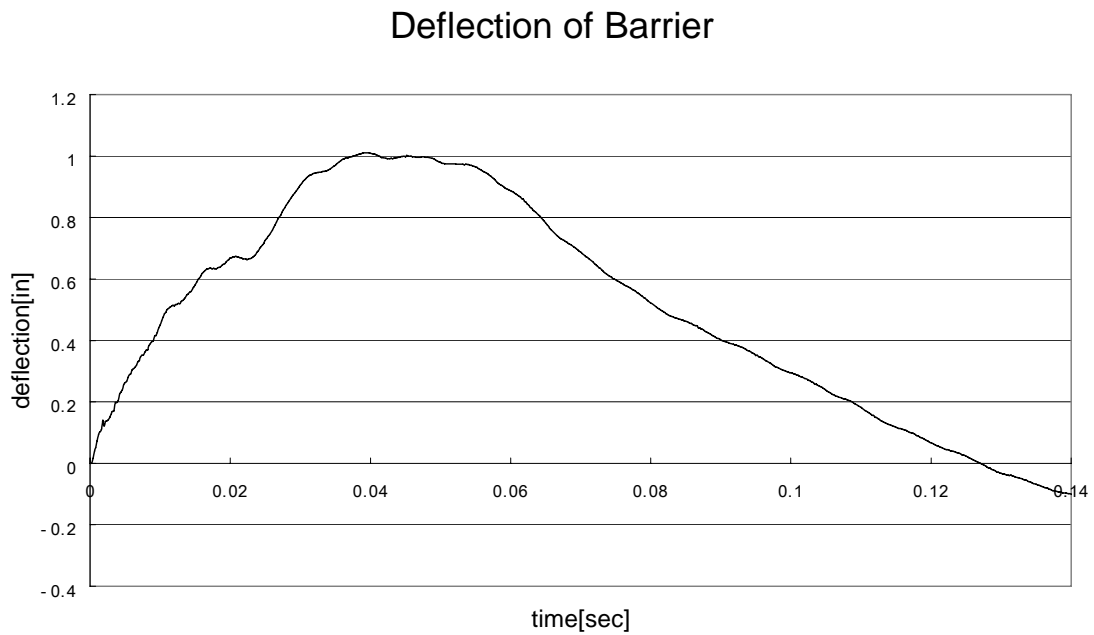


Figure 12.8: Barrier displacement versus time from pendulum test on standalone retrofit T501 bridge barrier specimen with four anchors, drop height of 16 ft

12.3.4 Strain of Steel Rods from the First Pendulum Impact Test on Retrofit T501 Barrier with Four Anchors

Figure 12.9 shows the strain of the steel rods in the barrier as a function of time. Strain gages on three of the four rods gave valid data, with the fourth rod not providing acceptable results most likely due to damage to the strain gages during installation. Because each steel rod was pretensioned to 35 ksi, their corresponding initial strains were 0.0012. All rods remained below their yield strain (0.003448) during impact (i.e., all rods remained elastic).

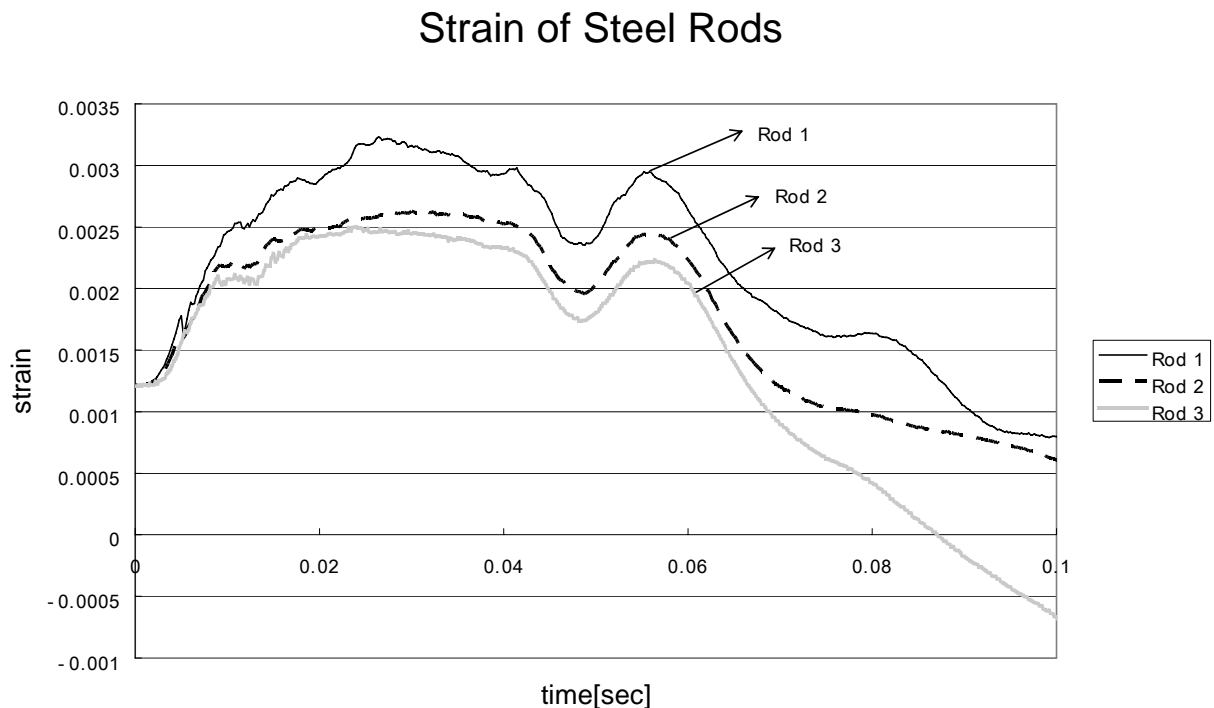


Figure 12.9: Strain values of steel rods from pendulum impact test on standalone retrofit T501 bridge barrier with four anchors and deck specimen for a drop height of 16 feet

12.4 Results of the Second Test on Retrofit T501 Barrier with Four Anchors

The only difference between the first test and the second test of the Retrofit T501 Barrier with four anchors is the pendulum drop height. The drop height for the second test of the Retrofit T501 Barrier with four anchors was 19.5 (ft.), which is 3.5 ft. higher than that of the first test. Four ASTM A-193 Grade B7 threaded rods running through the four PVC ducts were installed in the retrofit T501 barrier. The yield stress of ASTM A-193 Grade B7 threaded rods is 100 ksi. In this section, the following results are discussed:

- a still image from videos of the test;
- impact force versus time;
- barrier displacement versus time; and
- strain of steel rods.

A still image from this impact test is shown in Figure 12.10. Horizontal displacement and barrier overturning is evident as the crush package deforms against the barrier.



Figure 12.10: Still image from impact pendulum test on stand-alone retrofit T501 bridge barrier with four anchors and deck specimen for a drop height of 19.5 feet

12.4.2 Impact Force versus Time from the Second Pendulum Impact Test on Retrofit T501 Barrier with Four Anchors

Figure 12.11 shows a graph of force versus time obtained from the second pendulum impact test on the retrofit T501 bridge barrier specimen with four anchors. The peak acceleration of the pendulum at impact was about 48.75 g, corresponding to a peak impact force of about 91.88 kips. The 50-msec dynamic capacity is about 27.22 kips; the duration of impact is about 0.06 seconds; and the impulse of impact is about 1.48 kip-sec (6577.8 (N-sec)).

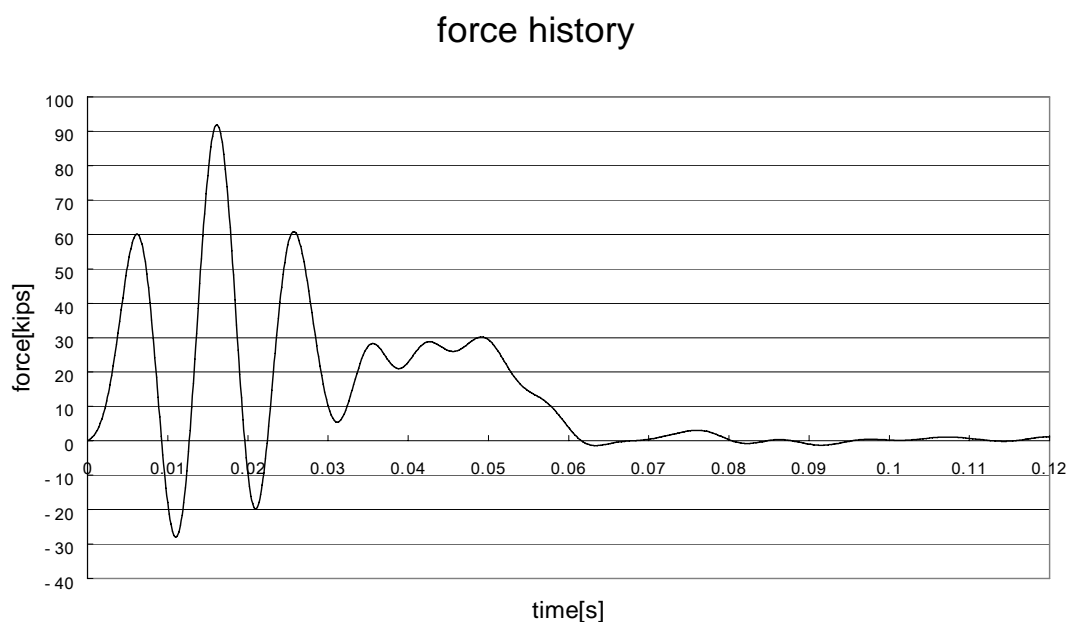


Figure 12.11: Force-versus-time graph from pendulum impact test on standalone retrofit T501 bridge barrier with four anchors and deck specimen for a drop height of 19.5 feet

12.4.3 Barrier Displacement versus Time from the Second Pendulum Impact Test on the Retrofit T501 Barrier Specimen

Figure 12.12 shows the displacement versus time for the second test on the retrofit T501 barrier specimen with 4 anchors. The pendulum impact led to concrete breakout failure, overturning of the barrier, and large displacements.

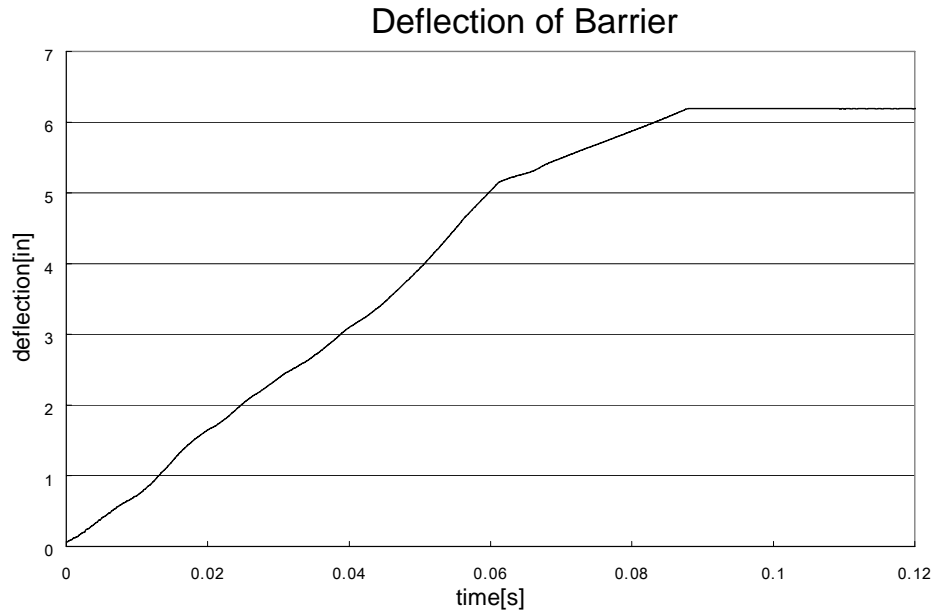


Figure 12.12: Barrier displacement versus time from pendulum test on standalone retrofit T501 bridge barrier specimen with four anchors (drop height of 19.5 ft)

12.4.4 Strain of Steel Rods from the Second Pendulum Test on Retrofit T501 Barrier with Four Anchors

Figure 12.13 shows strains in the steel rods versus time. Strain gages on 3 of the 4 rods gave valid data, plotted in Figure 12.13. Because each steel rod was pretensioned to 35 ksi, their corresponding initial strain values are 0.0012. Because the yield strain of ASTM A-193 Grade B7 is 0.003448, and because all strain values remain less than the yield strain, all the steel rods remained elastic during the impact test.

Strain of Steel Rods

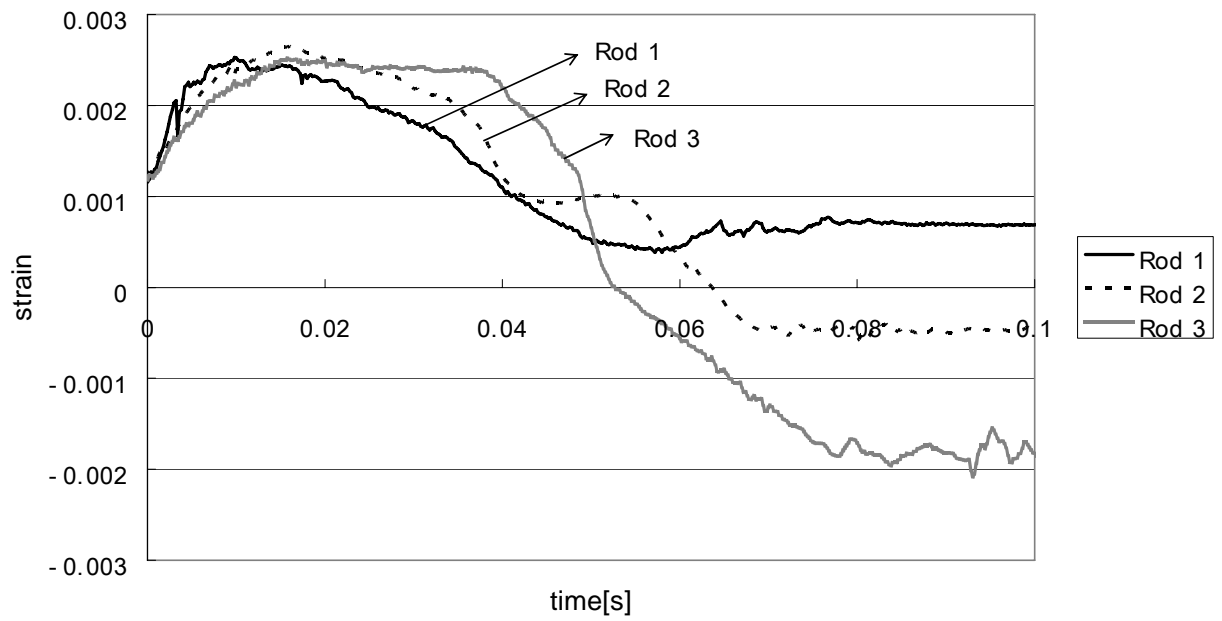


Figure 12.13: Strain values of steel rods from pendulum impact test on standalone retrofit T501 bridge barrier with four anchors and deck specimen for a drop height of 19.5 feet

Chapter 13. Significance of Test Results for T501 Barriers

13.1 Introduction

Pendulum tests and quasi-static tests were carried out on two prototype retrofit T501 barriers, one with 7 low-strength steel anchors and the other with 4 high-strength steel anchors. To discuss the significance of the previously presented test results for T501 barriers in terms of the revised TxDOT performance criteria for retrofit barriers, the following information (common to all tests) is considered for each test.

General Information: Barrier Designation and Test Date

Load-related information

- 1) drop height
- 2) recorded maximum acceleration
- 3) recorded peak force
- 4) 50-msec dynamic force
- 5) impact impulse

Dynamic resistance-related information

- 6) probable dynamic concrete breakout capacity
- 7) probable dynamic fracture capacity of steel rods
- 8) maximum recorded force in rods during impact
- 9) probable dynamic capacity of stand-alone barrier section as governed by concrete breakout
- 10) probable dynamic capacity of stand-alone barrier section as governed by steel rods
- 11) probable dynamic capacity of barrier system
- 12) probable dynamic capacity of barrier system based on static test results

Static resistance-related information

- 13) probable static capacity of stand-alone barrier section
- 14) observed static capacity of retrofit T501 barrier section
- 15) probable static capacity of barrier system using calculated breakout capacities

16) probable static capacity of barrier system using observed static capacity

In the following sections, each listed item is discussed. Final information is presented in Table 13.1 near the end of this chapter.

13.2 Load-Related Information

13.2.1 Drop Height

The term “drop height” refers to the elevation above the laboratory floor to which the pendulum was raised prior to testing. The term “drop distance” refers to the change in elevation of the pendulum during the test. The drop distance is the drop height minus the final elevation of the pendulum (3.5 ft above the laboratory floor).

- Specimen 1 (the first T501 retrofit barrier) used a drop height of 19 ft., corresponding to a drop distance of 15.5 ft.
- Specimen 2a (the second T501 retrofit barrier, first test) used a drop height of 16 ft., corresponding to a drop distance of 12.5 ft.
- Specimen 2b (the second T501 retrofit barrier, second test) used a drop height of 19.5 ft., corresponding to a drop distance of 16 ft.

The theoretical drop distance required to match the required velocity of NCHRP 350 TL-3 (100 km/hr at an angle of 20 degrees, or 9.5 m/sec) can be determined by using the law of energy conservation. That calculation is given here:

$v = 9.5[\text{m/s}] = \text{impact velocity of the pendulum mass}$

from the energy equation, $h = \frac{v^2}{2g}$

drop distance = $h = 4.6 \text{ m} = 15.09 \text{ ft}$ (1 ft = 0.3048 m)

13.2.2 Recorded Maximum Acceleration

Values of maximum acceleration are based on the experimentally determined acceleration record, with low-pass filtering as described here and in Mitchell (2005). Maximum accelerations for Retrofit T501 Specimen 1, Retrofit T501 Specimen 2a, and Retrofit T501 Specimen 2b are provided in Chapter Chapter 12.

13.2.3 Recorded Peak Force

The recorded peak force is determined by multiplying the recorded maximum acceleration by the pendulum mass (855 kg).

13.2.4 50-msec Dynamic Force

Values of 50-msec dynamic force are obtained by multiplying the corresponding value for 50-msec dynamic acceleration by the pendulum mass. The 50-msec dynamic acceleration is obtained by averaging the experimentally determined, filtered acceleration history over a 50-

msec window. For Retrofit T501 Specimen 1, Retrofit T501 Specimen 2a, and Retrofit T501 Specimen 2b, the force is provided in Chapter 12.

13.2.5 Impact Impulse

Values of impact impulse are obtained by integrating the filtered acceleration history over the length of the impulse and multiplying that integral by the pendulum mass. Impact impulses for Retrofit T501 Specimen 1, Retrofit T501 Specimen 2a, and Retrofit T501 Specimen 2b are provided in Chapter Chapter 12.

13.3 Dynamic Resistance-Related Information

13.3.1 Probable Dynamic Concrete Breakout Capacity

The probable mean dynamic concrete breakout capacity of the 7-anchor group is calculated in Appendix D as 90.89 kips. Because the projected areas of the 4-anchor group overlap, their total projected area is the same as for the 7-anchor group, and so is their predicted mean dynamic concrete breakout capacity.

13.3.2 Probable Dynamic Fracture Capacity of Steel Rods

For each specimen, the dynamic fracture capacity of the steel rods is obtained by multiplying the specified ultimate tensile strength of the anchor steel by the effective tensile stress area of the anchor rod and then by 1.2 to represent the increase in fracture capacity at dynamic strain rates.

Probable Dynamic Fracture Capacity of Seven A307 Steel Rods for Retrofit T501 Specimen 1

The rods used were ASTM A307 Grade C, with a specified ultimate tensile strength of 58 to 80 ksi (probable value 60 ksi), and a nominal diameter of 3/4 in. If the effective tensile stress area is approximated as 70% of the nominal area, the corresponding static fracture capacity of a single rod is 18.54 kips. If the dynamic capacity is taken as 1.2 times the static fracture capacity, the probable dynamic capacity of the seven A307 rods is 155.7 kips.

Dynamic Fracture Capacity of Four A193-B7 Steel Rods for Retrofit T501 Specimen 2

The rods used were ASTM A193 Grade B7, with a specified ultimate tensile strength of 125 ksi, and a nominal diameter of 3/4 in. If the effective tensile stress area is approximated as 70% of the nominal area, the corresponding static fracture capacity of a single rod is 38.63 kips. If the dynamic capacity is taken as 1.2 times the static fracture capacity, the probable dynamic capacity of the four A307 rods is 185.4 kips.

13.3.3 Maximum Recorded Force in Rods during Impact

During testing, strain gages on the threaded rods were used to measure the force history in the rods. That force history included the initial prestress placed in the rods prior to testing. Forces were obtained by multiplying the total strain in the rod by the initial modulus of the steel (29,000 ksi), and by the effective tensile stress area of the steel, approximated as 70% of the nominal area.

13.3.4 Probable Dynamic Capacity of Stand-alone Barrier Section as Governed by Concrete Breakout

Previous sections describe the calculation of the probable dynamic breakout capacity of the 7-rod and 4-rod configurations and the probable dynamic fracture capacity of the rods. To understand the significance of those numbers in the context of the dynamic testing, they must be converted to the corresponding probable dynamic capacity of the stand-alone barrier with a load applied at 21 in. above the deck, that is, the value expressed in terms of the corresponding load applied to the barrier at a height of 21 in. above the deck. Additionally, the effects of inertia forces acting on the barrier must be included.

Provided that the time of impulse is long compared to the period of response of the barrier to impulse load, inertial forces can be neglected. In this case, the stiffness of the barrier section as obtained from static testing is 49.3 kip/in. The barrier can be idealized as a generalized single-degree-of-freedom system, whose displacement is completely described in terms of rigid-body rotation about its compression toe. In terms of that model, the system's generalized stiffness, converted from that experimental value, is 21,700 kip-in./rad. Its generalized mass is calculated as 0.0874 kip-sec²-in. The corresponding period of vibration is 0.0126 sec. This period is increased considerably by the flexibility of the slab. During impact testing, the duration of the impact is 0.01 seconds, much shorter than the rise time (one-quarter period) of the barrier when slab flexibility and longitudinal flexibility are included. Therefore, the response of the barrier can be idealized as static, and the influence of inertial forces is not significant.

Calculation of Probable Dynamic Capacity for Retrofit T501 Specimen 1 as Governed by Concrete Breakout

In evaluating the rotational equilibrium of the barrier about its compressive edge, the perpendicular distance from the line of action of the steel rods is assumed to coincide with the line of action of breakout resistance. That perpendicular distance is 7.74 in. The perpendicular distance from the line of action of the applied load is 21 in. Therefore, neglecting inertial forces, the relationship between a load P applied at 21 in. above the slab, and a concrete breakout capacity $N_{breakout}$, is

$$P = \frac{7.74}{21} N_{breakout}$$

The probable dynamic capacity of the tested section of Retrofit T501 Specimen 1 (7 anchors) as governed by concrete breakout is therefore 33.50 kips.

Calculation of Probable Dynamic Capacity for Retrofit T501 Specimen 2 as Governed by Concrete Breakout

Because the dimensions of this specimen and the positioning of the steel rods are identical to Specimen 1, the same relationship given above also applies to Specimen 2. Thus, neglecting inertial forces, the relationship between a load P applied at 21 in. above the slab, and a concrete breakout capacity $N_{breakout}$, is

$$P = \frac{7.74}{21} N_{breakout}$$

The probable dynamic capacity of the tested section of Retrofit T501 Specimen 2 (4 anchors) as governed by concrete breakout is therefore 33.5 kips, the same as for the 7-anchor specimen.

13.3.5 Probable Dynamic Capacity of Stand-alone Barrier Section as Governed by Steel Rods

Previous sections of this chapter describe the calculation of the probable static breakout capacity of the 7-rod and 4-rod configurations and the probable static fracture capacity of the rods. To understand the significance of those numbers, they must be converted to the corresponding probable static capacity of stand-alone barrier with a load applied at 21 in. above the deck, that is, the value expressed in terms of the corresponding load applied to the barrier at a height of 21 in. above the deck. As discussed earlier in this report, that height was selected for the T203 barrier. It was maintained for the T501 barrier to permit direct comparison and to avoid having to change the dimensions of the test pendulum.

Calculation of Static Capacity for Retrofit T501 Specimen 1 as Governed by Steel Rods

In evaluating the rotational equilibrium of the barrier about its compressive edge, the perpendicular distance from the line of action of the steel rods is 7.74 in. The perpendicular distance from the line of action of the applied load is 21 in. Therefore, neglecting inertial forces, the relationship between a load P applied at 21 in. above the slab, and a steel rod capacity $N_{fracture}$, is

$$P = \frac{7.74}{21} N_{fracture}$$

The probable dynamic capacity of the tested section of Retrofit T501 Specimen 1 (7 anchors) as governed by fracture of the steel rods is therefore 57.4 kips. This value is clearly greater than the capacity as governed by concrete breakout, and breakout will probably govern.

Calculation of Static Capacity for Retrofit T501 Specimen 2 as Governed by Steel Rods

In evaluating the rotational equilibrium of the barrier about its compressive edge, the perpendicular distance from the line of action of the steel rods is 7.74 in. The perpendicular distance from the line of action of the applied load is 21 in. Therefore, neglecting inertial forces, the relationship between a load P applied at 21 in. above the slab, and a steel rod capacity $N_{fracture}$, is

$$P = \frac{7.74}{21} N_{fracture}$$

The probable dynamic capacity of the tested section of Retrofit T501 Specimen 1 (4 anchors) as governed by fracture of the steel rods is therefore 68.3 kips. This value is clearly greater than the capacity as governed by concrete breakout, and breakout probably governs.

13.3.6 Probable Dynamic Capacity of Barrier System

Using the procedure discussed in Section **Error! Reference source not found.** of this report, the corresponding probable dynamic capacities of the barrier system over a 50-msec window are calculated as the probable dynamic capacity of the barrier section, plus 31 kips. That 31-kip augmentation represents the combination of the static stiffness and additional inertia due to longitudinal continuity.

Using the previously calculated probable dynamic capacities, the probable dynamic capacity of both T501 retrofit barrier systems is governed by concrete breakout and is given by the dynamic capacity for the section (33.5 kips), plus 31 kips, or 64.5 kips.

13.3.7 Probable Dynamic Capacity of Barrier System Based on Static Test Results

Using the static test results from Retrofit T501 Specimen 1, it is possible to refine the above calculation. The static capacity of that specimen, 39 kips, is a more reliable estimate of the static capacity of the barrier as governed by concrete breakout than the calculated value from ACI 318-05 Appendix D because that calculated value is based on design models that are not completely accurate. The experimentally observed static capacity of 39 kips corresponds to a dynamic capacity 1.2 times greater, or 46.8 kips.

If the above calculation is repeated using 46.8 kips instead of the calculated 33.5 kips, the probable dynamic capacity of both T501 retrofit barrier systems is governed by concrete breakout, and it is given by the dynamic capacity for the section based on static testing (46.8 kips), plus 31 kips, or 77.8 kips.

13.4 Static Resistance-Related Information

13.4.1 Probable Static Capacity of Stand-alone Barrier Section

Previous sections of this chapter describe the calculation of the probable dynamic capacity of a stand-alone barrier section. Concrete breakout governed, and the value was the same for both Retrofit T501 specimens because their projected concrete breakout areas were identical. The governing static value is the corresponding governing dynamic value of 33.5 kips, divided by 1.2, or 27.9 kips.

13.4.2 Observed Static Capacity of Retrofit T501 Barrier Section

Static Capacity of Retrofit T501 Specimen 1

Based on the testing discussed in Chapter 12, the static capacity of the Retrofit T501 Specimen 1 section is 39 kips (Yang 2006). Because the Retrofit T501 Specimen 2 section failed during its second pendulum test, no value is available. Because the breakout geometry is the same for each specimen, however, its probable static capacity is the same 39 kips.

13.4.3 Probable Static Capacity of Barrier System Using Calculated Breakout Capacities

Using the procedure discussed in Section 10.3 of this report, the probable static capacity of the barrier system is calculated as the probable static capacity of the barrier section, plus 30 kips. That 30-kip augmentation represents the additional static stiffness due to longitudinal continuity of the rail system.

Using the previously calculated probable static capacities, the probable static capacity of both T501 retrofit barrier systems is governed by concrete breakout, and it is given by the calculated probable static capacity for the section (27.9 kips), plus 30 kips, or 57.9 kips.

13.4.4 Probable Static Capacity of Barrier System Using Observed Static Capacity

Using the procedure discussed in Section 10.3 of this report, the corresponding probable static capacities of the barrier system are calculated as the probable static capacity of the barrier section, plus 30 kips. That 30-kip augmentation represents the additional static stiffness due to longitudinal continuity.

Using the experimentally determined static capacity from Retrofit T501 Specimen 1, the probable static capacity of both T501 retrofit barrier systems is governed by concrete breakout, and it is computed from the observed static capacity for the section (39 kips), plus 30 kips, or 69 kips.

13.5 Significance of Results

13.5.1 Test Results and TxDOT Criteria

From the information presented in Chapter 12 the following observations can be made:

- The probable dynamic capacity of both the 7-anchor and the 4-anchor retrofit T501 barrier systems exceeds TxDOT's minimum criterion of 60 kips over a 50-msec window. The capacity of each system is governed by concrete breakout. If probable dynamic breakout capacity is calculated using the provisions of ACI 318-05 Appendix D, the 50-msec breakout capacity of the system is 64.5 kips; if probable dynamic breakout capacity is calculated using static test results for Retrofit T501 Specimen 1, the 50-msec breakout capacity of the system is 77.8 kips.
- The observed dynamic capacity of both the 7-anchor and the 4-anchor retrofit T501 barrier systems exceed or is very close to TxDOT's minimum criterion of 60 kips over a 50-msec window. For Specimen 1 (7 anchors), the observed capacity of 29.6 kips, plus 31 kips for continuity, gives 62 kips; for Specimen 2 (4 anchors), the observed capacity of 25.4 kips, plus 31 kips, gives 56 kips. Nevertheless, peak forces were higher for Specimen 2 than for Specimen 1, making the first Specimen 2 test very severe.
- The probable static capacity of both the 7-anchor and the 4-anchor retrofit T501 barrier systems exceeds TxDOT's minimum criterion of 54 kips. The capacity of each system is governed by concrete breakout. If probable static breakout capacity is calculated using the provisions of ACI 318-05 Appendix D, the static capacity of the system is 57.9 kips; if probable static breakout capacity is calculated using static test results for Retrofit T501 Specimen 1, the static capacity of the system is 69 kips.
- At movement joints between barrier sections, the capacity of the proposed T501 retrofit barriers is reduced because longitudinal continuity exists on one side of the barrier only. Because the breakout capacity of the barrier base is not reduced by the movement joint, and because the reduction in longitudinal continuity is identical to that experienced by cast-in-place barriers, the proposed retrofit T501 design can be used at end locations as well as at interior locations.

Table 13.1: Summary of pendulum-test data for T501 retrofit barrier specimens

| Type of Information | Barrier Designation | Retrofit T501 Specimen 1 | Retrofit T501 Specimen 2a | Retrofit T501 Specimen 2b |
|---------------------|---|--------------------------|---------------------------|---------------------------|
| | Testing Date | 7/28/2006 | 8/4/2006 | 8/8/2006 |
| Load | Drop Height (ft) | 19 | 16 | 19.5 |
| | Recorded Maximum Acceleration (g) | 32.3 | 33.6 | 48.75 |
| | Recorded Peak Force (kips) | 60.9 | 63.29 | 91.88 |
| | 50-msec Dynamic Force (kips) | 29.6 | 25.43 | 27.22 |
| | Impact Impulse (kip-sec) | 1.95 | 1.69 | 1.48 |
| Dynamic Resistance | Probable dynamic breakout capacity from ACI 318-05 Appendix (kips) | 90.89 | 90.89 | 90.89 |
| | Probable dynamic fracture capacity of steel rods (kips) | 155.74 | 185.4 | 185.4 |
| | Measured maximum force in rods during impact (kips) | 108.15 | 91.99 | 92 |
| | probable dynamic capacity of stand-alone barrier section as governed by concrete breakout | 33.5 | 33.5 | 33.5 |
| | probable dynamic capacity of stand-alone barrier section as governed by steel rods | 57.4 | 68.3 | 68.3 |
| | probable dynamic capacity of barrier system | 64.5 | 64.5 | 64.5 |
| | probable dynamic capacity of barrier system based on static test results | 77.8 | 77.8 | 77.8 |
| Static Resistance | probable static capacity of stand-alone barrier section as governed by concrete breakout | 27.9 | 27.9 | 27.9 |
| | observed static capacity of barrier section | 39 | / | / |
| | probable static capacity of barrier system using calculated breakout capacities | 57.9 | 57.9 | 57.9 |
| | probable static capacity of barrier system using observed static capacity | 69 | 69 | 69 |

13.5.2 Observations on Dynamic Behavior of Retrofit T501 Specimen 2

As shown in Table 13.1, the dynamic loading associated with the pendulum test on Retrofit T501 Specimen 2, in spite of its lower drop height, created a larger peak acceleration value than the corresponding test on Specimen 1. This result was probably due to slight differences in the behavior of the crush packages used for each test.

Table 13.1 indicates that Retrofit T501 Specimen 2 withstood an initial impact about 87% as large, and then failed under a second impact about 76% as large, as that withstood by Retrofit T501 Specimen 1. Because the cones of the breakout body of Specimen 2 in the second test were separated, it is believed that the first test produced an incipient breakout failure, reducing the subsequent resistance.

Chapter 14. Summary, Conclusions, and Recommendations

14.1 Summary

The purpose of TxDOT Research Project 0-4823 is to develop retrofit bridge barrier designs using mechanical anchors to replace original cast-in-place barriers that have been damaged by vehicular collisions, or older barriers that are obsolete. The retrofit barriers are required to conform to TxDOT performance criteria for retrofit barriers, and also satisfy *NCHRP Report 350* requirements.

To test barriers, an impact test pendulum setup was developed and validated at The University of Texas at Austin by researchers working on this project (Mitchell 2005, Tolnai 2005) using the *NCHRP Report 350* guidelines. TxDOT T203 barrier and bridge deck test specimens were developed for cast-in-place and retrofit designs. The retrofit T203 barriers used through-bolt retrofit mechanical anchors. The validated impact test pendulum setup was used to test the developed cast-in-place and retrofit T203 barrier and bridge deck test specimens. In addition to the dynamic tests, a quasi-static test was performed on a retrofit T203 barrier specimen.

Using the test results, the retrofit T203 barrier was evaluated using the *NCHRP Report 350* requirements for TL-3 as well as the TxDOT barrier performance criteria. Based on the evaluation, a final design of the retrofit T203 barrier using a through-anchor configuration was proposed.

LS-DYNA, a widely used dynamic non-linear finite-element package, was used to simulate pendulum and vehicular crashes on TxDOT barriers. Finite-element models of the cast-in-place and retrofit T203 barrier and bridge deck test specimens were validated by simulating pendulum impact tests on them and comparing the simulation results with the test data obtained from the pendulum impact testing in the laboratory.

NCHRP TL-3 and TL-4 vehicular crash tests were simulated on the validated T203 barrier and bridge deck models using LS-DYNA representations of vehicles developed by the National Crash Analysis Center. The retrofit T203 barrier was evaluated for NCHRP TL-3 and TL-4 using the conditions specified in *NCHRP Report 350*.

Finite-element models of the cast-in-place and retrofit T501 barrier and bridge deck were developed in LS-DYNA. Pendulum impact tests were simulated on these T501 barrier and bridge deck models. The results obtained from the pendulum impact simulations, along with other analyses, were used to predict that the retrofit T501 barrier would meet the TxDOT barrier performance criteria. This prediction was then evaluated through pendulum testing at FSEL.

In addition, NCHRP TL-3 and TL-4 vehicular crash tests were simulated on the T501 barrier and bridge deck LS-DYNA models using finite element representations of vehicles developed by the National Crash Analysis Center. The retrofit T501 barrier was evaluated for NCHRP TL-3 and TL-4 using the crash simulations based on the *NCHRP Report 350* requirements.

Finally, retrofit T501 barriers using undercut mechanical anchors were developed, designed, and constructed. The retrofit T501 barrier specimens were tested statically and using the impact pendulum. Results from these tests were able to confirm the earlier hypothesis, based on results from LS-DYNA simulations, that retrofit T501 barriers would meet all necessary performance criteria.

14.2 Conclusions

- 1) The proposed retrofit design for TxDOT T203 barriers using a through-anchor configuration meets the *NCHRP Report 350* performance criteria for TL-3. The proposed T203 retrofit design also meets the TxDOT performance criteria for retrofit barriers.
- 2) The LS-DYNA models of the T203 barrier and bridge deck were validated by comparing the results of pendulum impact simulation with laboratory test data. These validated models of the T203 barrier and bridge deck can be effectively used to predict T203 barrier behavior for different initial conditions and can be a cost-effective supplement to NCHRP crash tests.
- 3) NCHRP TL-3 and TL-4 vehicular crash simulations on the validated T203 barrier and bridge deck LS-DYNA models show that the proposed retrofit T203 barrier design passes the NCHRP TL-3 and TL-4 test criteria. The retrofit T203 barrier design is robust enough to replace the cast-in-place T203 barrier not only for the design level (TL-3), but also for a higher NCHRP TL-4.
- 4) Calculations and results from pendulum impact test simulations on LS-DYNA models of T501 barriers and bridge decks indicate that the retrofit T501 barrier design with undercut mechanical anchors will meet the TxDOT performance criteria for retrofit barriers.
- 5) NCHRP TL-3 and TL-4 vehicular crash simulations using the T501 barrier and bridge deck LS-DYNA models indicate that the retrofit T501 barrier design passes the NCHRP TL-3 and TL-4 test criteria.
- 6) Static and pendulum testing of the retrofit T501 barrier shows that two variants (one with 7 mild-steel anchors and another with 4 high-strength steel anchors) meet TxDOT performance criteria for retrofit barriers.

14.3 Recommendations

- 1) The retrofit design of the TxDOT T203 barrier proposed here using mechanical anchors with through-bolt configuration can be used to replace original T203 barriers damaged by vehicular impact. The same design could probably be modified to use undercut anchors rather than through-bolts and still perform according to TxDOT criteria.
- 2) The retrofit design of the TxDOT T501 barrier proposed here using mechanical undercut anchors (in either a 7-bolt or a 4-bolt configuration) can be used to replace original T501 barriers damaged by vehicular impact.
- 3) A combination of pendulum testing and numerical simulation, similar to that described in this report, should be used in the initial design and refinement of any TxDOT barrier configuration, cast-in-place or retrofit. It is a very cost-effective supplement to actual crash testing. Based on the results obtained from pendulum tests and crash simulations in LS-DYNA, the number of NCHRP crash tests can be greatly reduced and should be used for final validation only.

Pendulum testing and analytical simulation are very effective tools for studying how barriers can be expected to perform under a variety of crash scenarios.

References

- ABAQUS 2006: ABAQUS Analysis User's Manual (<http://www.abaqus.com>).
- AC Engineering, Inc. 1996: *A Special Topic Seminar: ABAQUS Contact Problems Made Easy*. West Lafayette, Indiana.
- ACI 318-05 2005: ACI Committee 318, *Building Code Requirements for Structural Concrete (ACI 318-05)*, American Concrete Institute, Farmington Hills, MI.
- Alaoui 2004: Alaoui, S.S., "RECONASANCE: Reinforced Concrete Analysis Spreadsheet Enhanced," M.S. Departmental Report, Department of Civil, Architectural and Environmental Engineering, The University of Texas at Austin, December 2004.
- Bank, *et al.* 1998: Bank, Lawrence C.; Jiansheng Yin; and T. Russell Gentry, "Pendulum Impact Tests on Steel W-Beam Guardrails." *Journal of Transportation Engineering*, Vol. 124, July/August 1998.
- Chen 1982: Chen, W.F., *Plasticity in Reinforced Concrete*, McGraw-Hill Book Company, New York, New York.
- Drillco 2006: http://www.drillcogroup.com/maxi_bolts/general/flush.html.
- Efunda 2006: Efunda Engineering Fundamentals, http://www.efunda.com/designstandards/screws/fasteners_intro.cfm.
- Eskandarian, *et al.* 1998: Eskandarian, Azim; Dhafer Marzougui; and Nabih E. Bedewi, "Finite element model and validation of a surrogate crash test vehicle for impacts with roadside objects." *International Journal of Crashworthiness*.
- FHWA 2005: FHWA/NHTSA National Crash Analysis Center, <http://www.ncac.gwu.edu/>.
- FHWA 2006: FHWA/NHTSA National Crash Analysis Center, <http://www.ncac.gwu.edu/>.
- Gokani 2006: Gokani, Vatsal, "Design and Evaluation of Retrofit T203 and T501 Barriers with Mechanical Anchors using Experimental Testing and Finite-Element Simulation," M.S. Thesis, Department of Civil, Architectural and Environmental Engineering, The University of Texas at Austin, August 2006.
- LabVIEW 2006: <http://www.ni.com/>.
- Livermore Software Technology Corporation 2003: *LS-DYNA Keyword User's Manual: April 2003, Version 970*.
- Livermore Software Technology Corporation 2005: <http://www.lstc.com>.
- Livermore Software Technology Corporation 2006: <http://www.lstc.com>.

- Logan 1993: Logan, Daryl L., *A First Course in the Finite Element Method, second edition*. Rose-Hulman Institute of Technology. PWS Publishing Company, Boston.
- Marzougui *et al.* 1996: Marzougui, Dhafer; Cing-Dao Kan; and Nabih E. Bedewi “Development and Validation of an NCAP Simulation using LS-DYNA3D.” *4th International LS-DYNA3D Conference*.
- MathWorks 2002: <http://www.mathworks.com>.
- Mitchell 2005: “Pendulum Simulation of Vehicular Impact on Retrofit Bridge Barriers,” M.S. Thesis, Department of Civil, Architectural and Environmental Engineering, The University of Texas at Austin, May 2005.
- NCHRP Report 350 1993: *NCHRP Report 350: Recommended Procedures for the Safety Performance Evaluation of Highway Features*, National Cooperative Highway Research Program, Transportation Research Board, National Research Council, National Academy Press, Washington, D.C.
- Nilson 1982: Nilson, A.H., *Finite Element Analysis of Reinforced Concrete*, Task Committee on Finite Element Analysis of Reinforced Concrete Structures, Structural Division Committee on Concrete and Masonry Structures, American Society of Civil Engineers, New York, New York.
- Reid *et al.* 1996: Reid, John D.; Dean L. Sicking; and Gene W. Paulsen, “Design and Analysis of Approach Terminal Sections Using Simulation.” *Journal of Transportation Engineering*, Vol. 122, September/October 1996.
- Rodriguez *et al.* 2001: Rodriguez, M., Lotze, D., Gross, J.H., Zhang, Y.G., Klingner, R.E. and Graves III, H.L., “Dynamic Behavior of Tensile Anchors to Concrete,” *ACI Structural Journal*, v 98, n 4, July/August 2001.
- Schwer 2003: Schwer, L., “Laboratory Tests for Characterizing Geomaterials-Draft”, December 2003.
- Sicking 1998: Sicking, Dean, “Alternative Techniques for Evaluating Roadside Safety Systems.” *Transportation Research Circular*, Number E-C002, Issue No. 0097-8515, July 1998.
- Tolnai 2005: Tolnai, Megan, “Analytical Simulation of Vehicular Impact on Retrofit Bridge Barriers,” M.S. Thesis, Department of Civil, Architectural and Environmental Engineering, The University of Texas at Austin, May 2005.
- TTI 2002: Bullard, D. L., Jr., Williams, W. F., Menges, W. L. and Haug, R. R., “Design and Evaluation of the TxDOT F411 and T77 Aesthetic Bridge Rails”, *Report No. 4288-1*, Texas Transportation Institute (TTI), Texas A&M University, College Station, Texas.
- TxDOT 2003: *Traffic Rail: Type T203 and Type 501*, Texas Department of Transportation, <http://www.dot.state.tx.us/insdtdot/orgchart/cmd/cserve/standard/bridge-e.htm> (accessed May 10, 2006).

Uddin *et al.* 2005: Uddin, N., Farhat, N.S. Vaidya, U. and Serrano-Perez, J.C., “Vulnerability Reduction of Bridge Piers”, University Transportation Center for Alabama (UTCA) *Report 03229*, The University of Alabama, The University of Alabama at Birmingham, The University of Alabama in Huntsville, August 2005

Appendix A: Standard TxDOT Bridge Barrier and Deck Details

A1. Standard TxDOT T203 Barrier and Bridge Deck Details

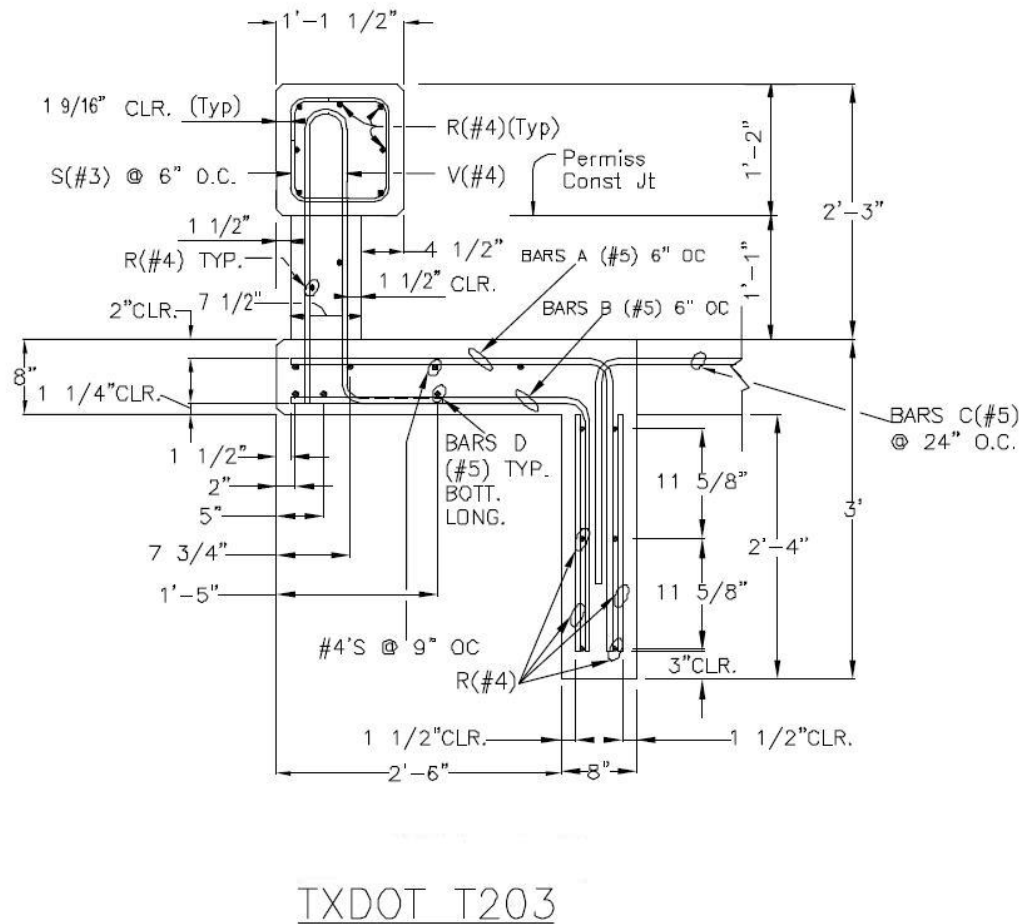


Figure A.1. Side sectional view of TxDOT T203 barrier and bridge deck tested by TTI (TxDOT 2003 and private communication, Texas Transportation Institute)

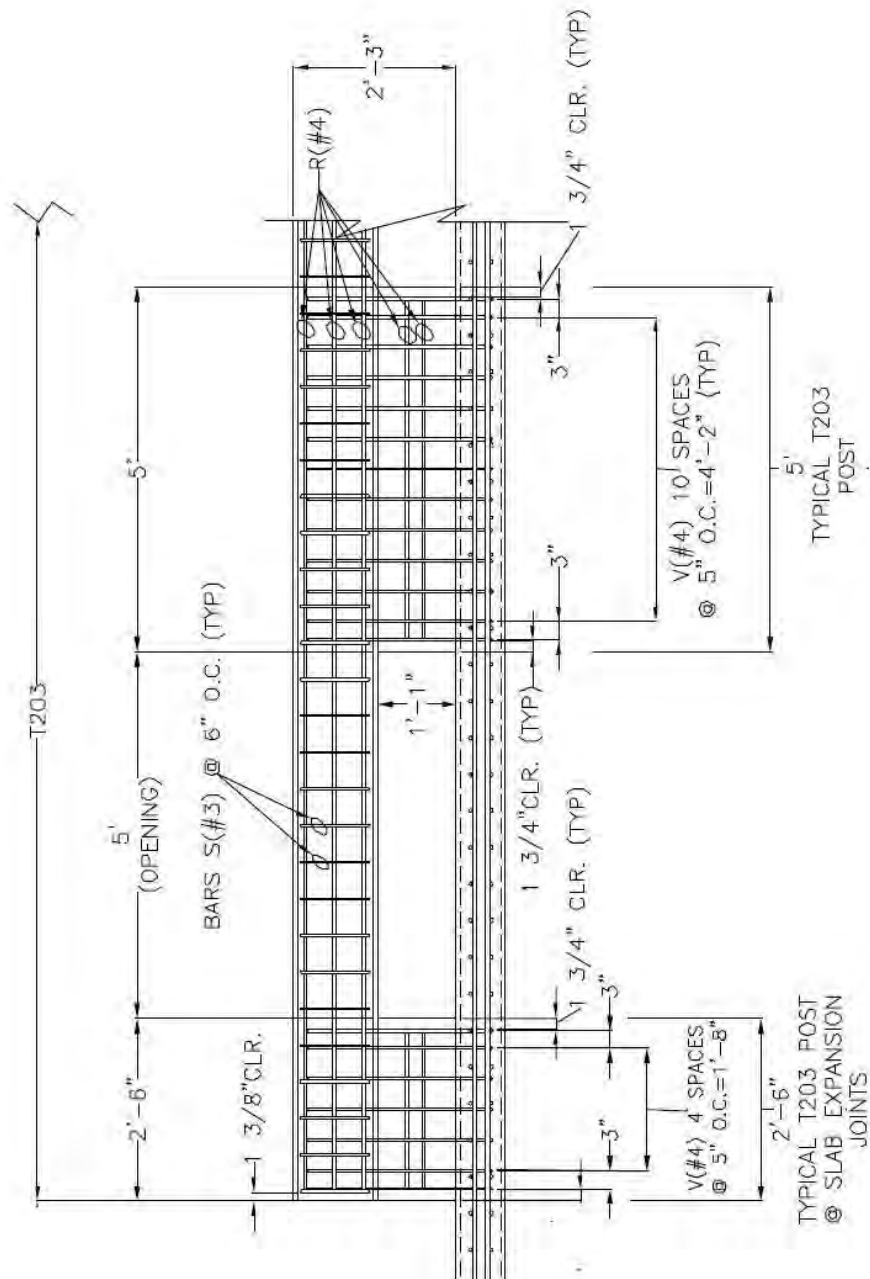


Figure A.2. Front sectional view of standard TxDOT T203 barrier and bridge deck (TTI 2003)

A.2. Standard TxDOT T501 Barrier and Bridge Deck Details

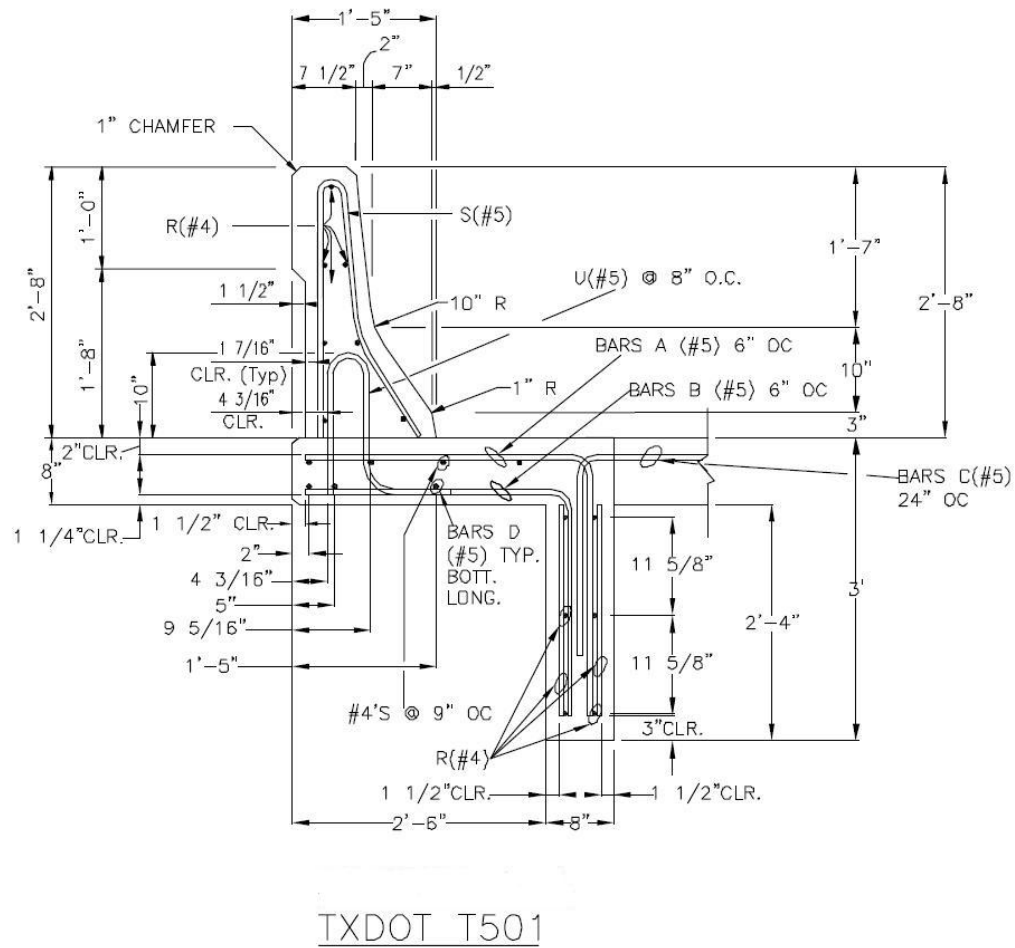


Figure A.3. Side sectional view of TxDOT T501 barrier and bridge deck tested by TTI (TxDOT 2003 and private communication, Texas Transportation Institute)

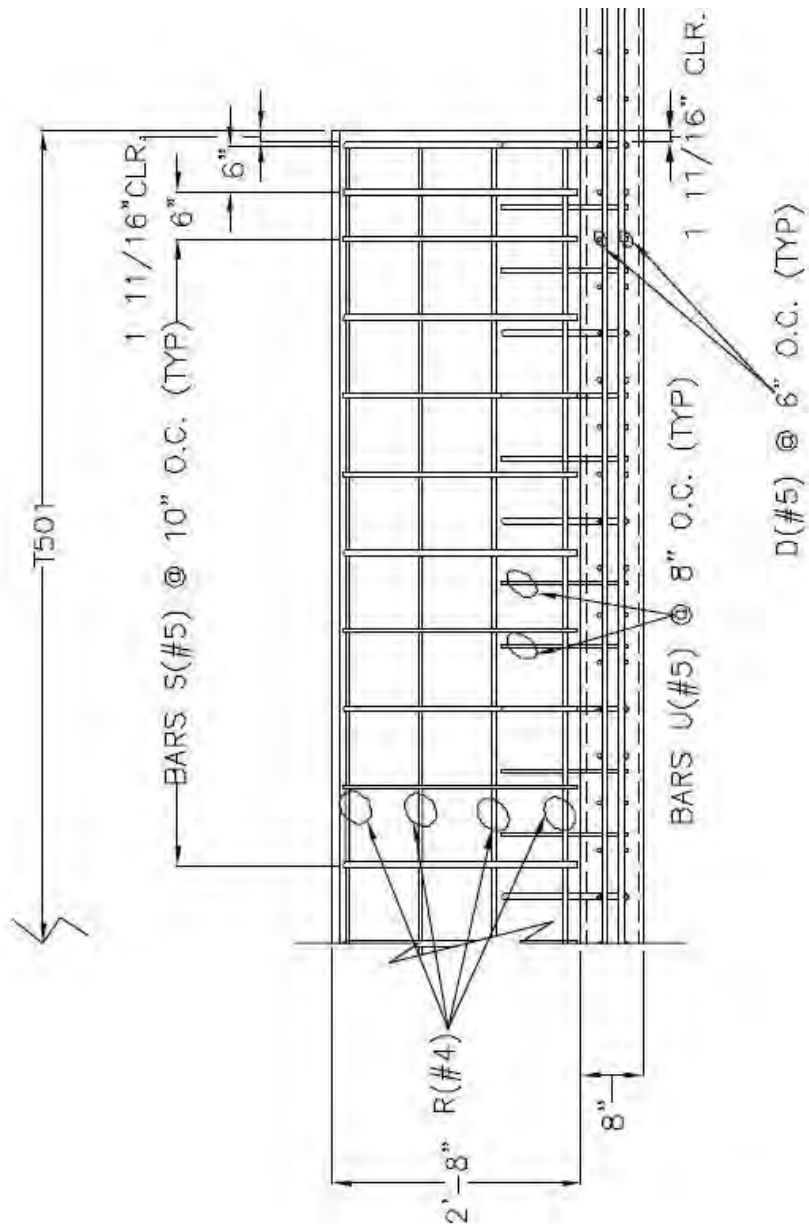


Figure A.4. Front sectional view of standard TxDOT T501 barrier and bridge deck (TTI 2003)

Appendix B: Comparison of Results from Tests and Simulations on T203 Barrier Specimens

B.1. Results from Pendulum Impact Test on Cast-in-Place T203 Barrier and Bridge Deck Specimen

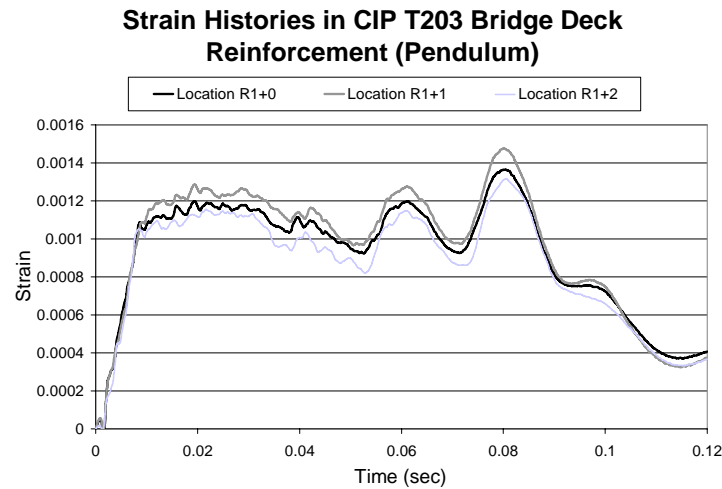


Figure B.1. Strain histories in row R1 of cast-in-place T203 bridge deck

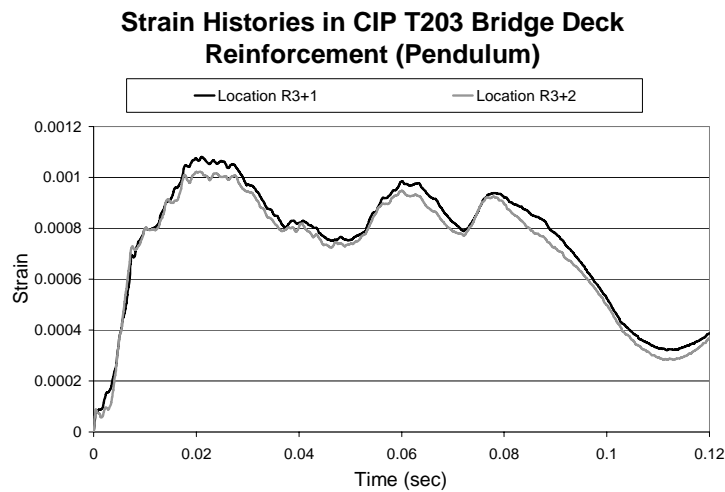


Figure B.2. Strain histories in row R3 of cast-in-place T203 bridge deck

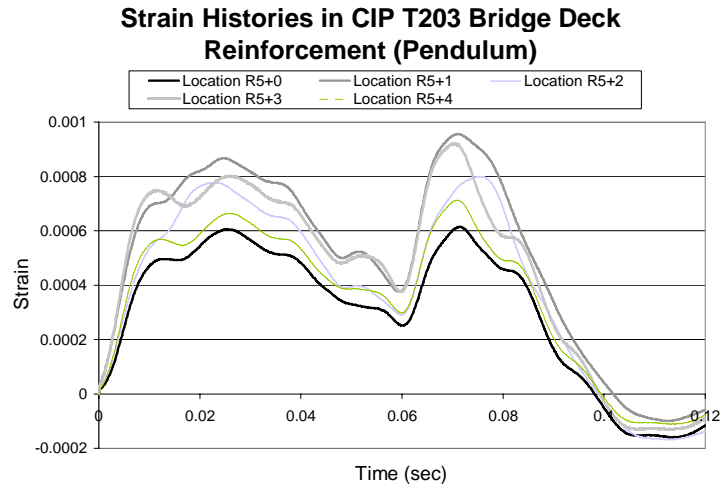


Figure B.3. Strain histories in row R5 of cast-in-place T203 bridge deck

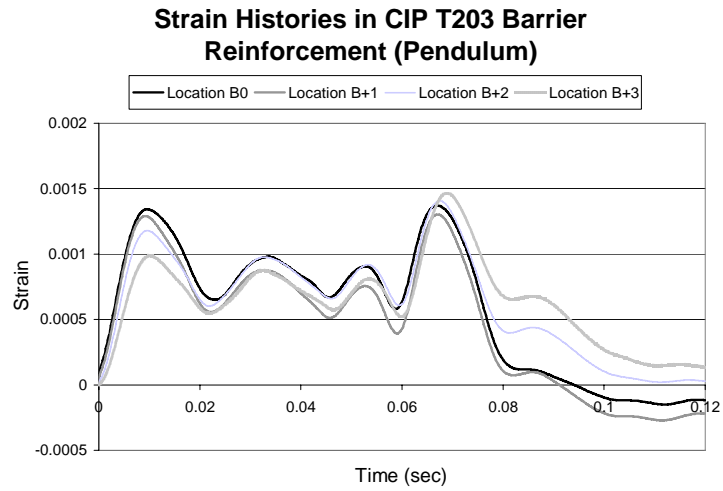


Figure B.4. Strain histories in row B of cast-in-place T203 bridge barrier

B.2. Results from Simulation of Pendulum Impact Test Cast-in-Place T203 Barrier and Bridge Deck Specimen using LS-DYNA

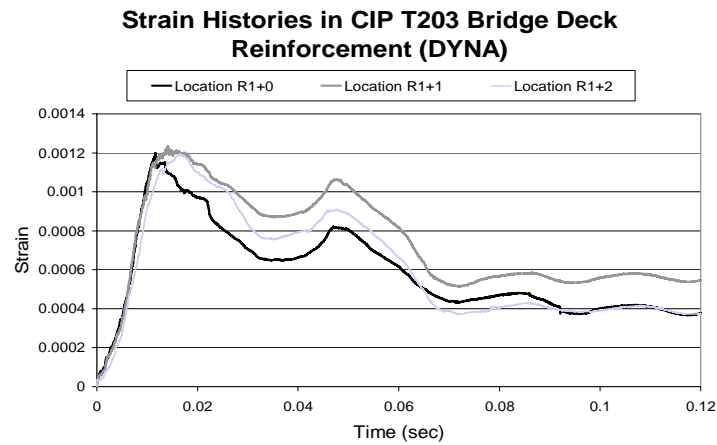


Figure B.5. Strain histories in row R1 of cast-in-place T203 bridge deck DYNA model

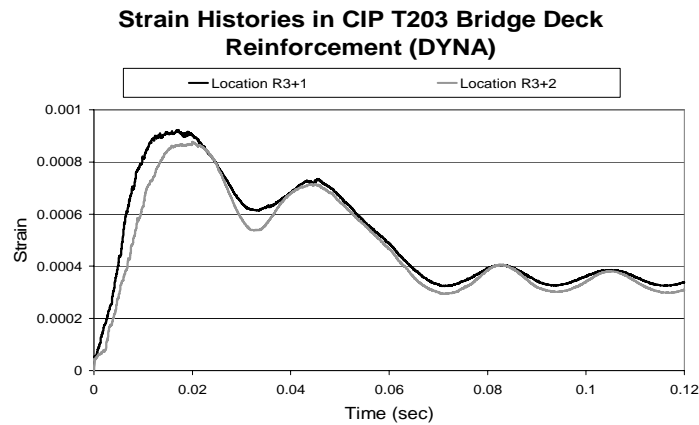


Figure B.6. Strain histories in row R3 of cast-in-place T203 bridge deck DYNA model

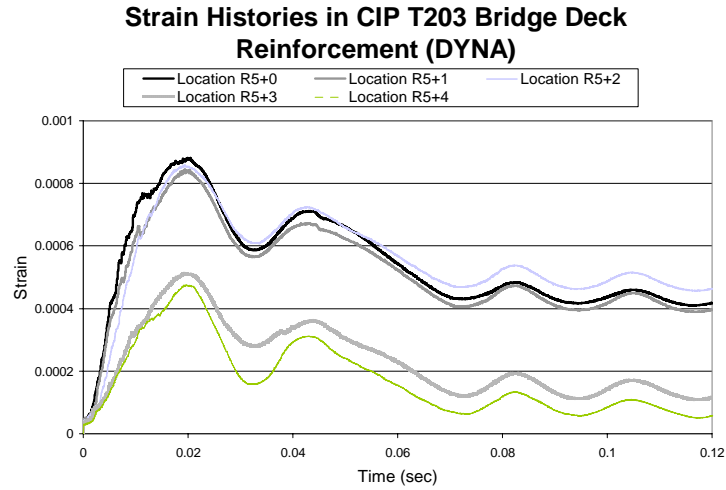


Figure B.7. Strain histories in row R5 of cast-in-place T203 bridge deck DYNA model

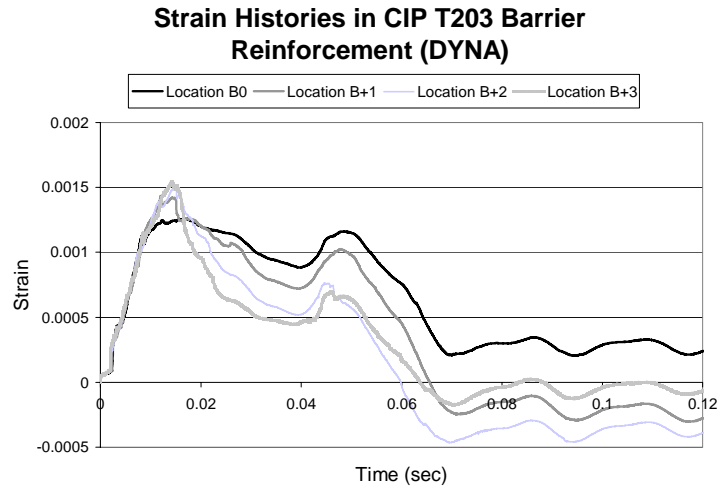


Figure B.8. Strain histories in row B of cast-in-place T203 bridge barrier DYNA model

B.3. Results from Pendulum Impact Test on Retrofit T203 Barrier and Bridge Deck Specimen

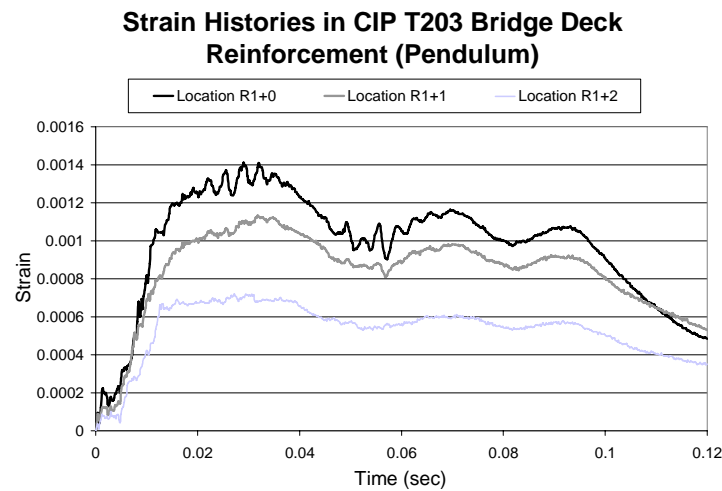


Figure B.9. Strain histories in row R1 of retrofit T203 bridge deck

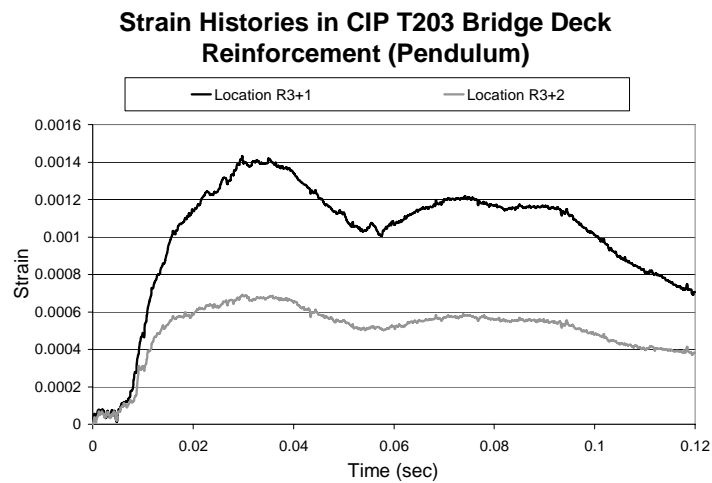


Figure B.10. Strain histories in row R3 of retrofit T203 bridge deck

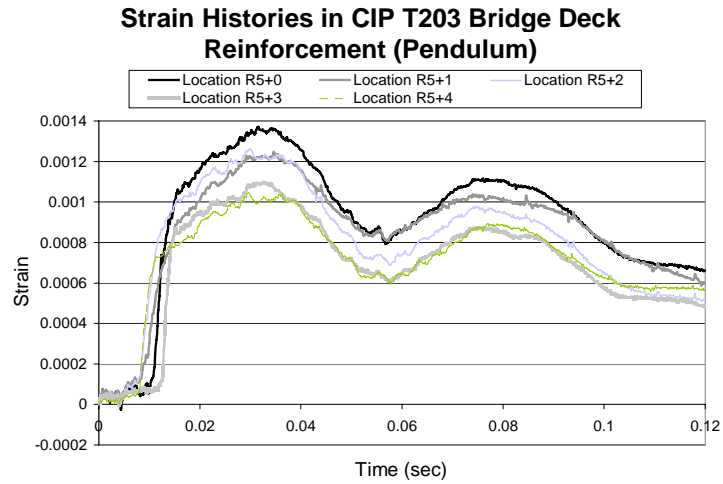


Figure B.11. Strain histories in row R5 of retrofit T203 bridge deck

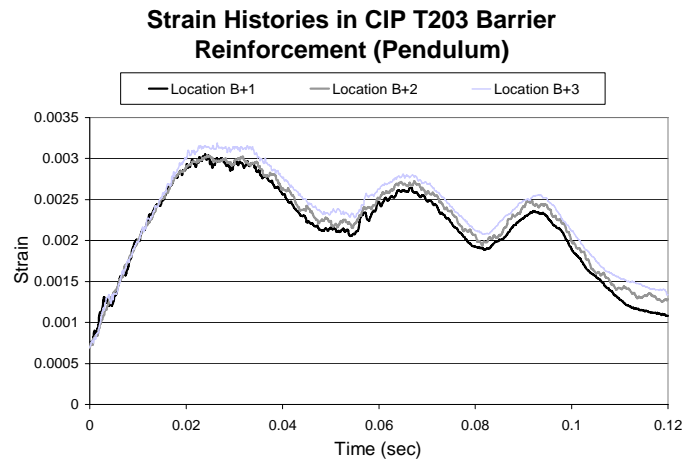


Figure B.12. Strain histories in row B of retrofit T203 bridge barrier

B.4. Results from Pendulum Impact Test on Retrofit T203 Barrier and Bridge Deck Specimen

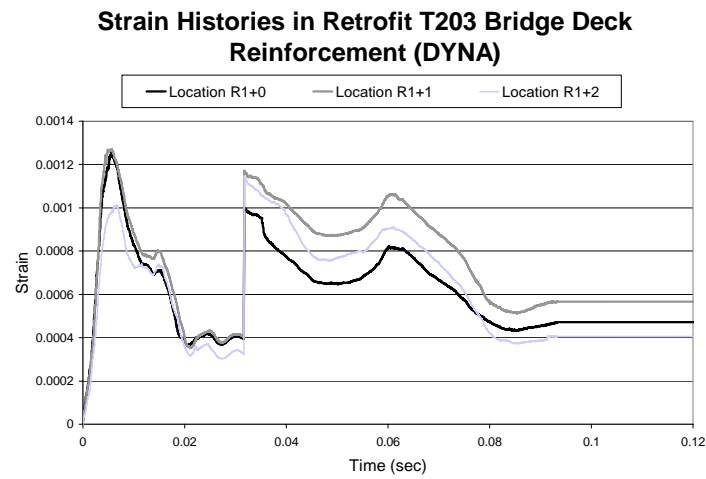


Figure B.13. Strain histories in row R1 of retrofit T203 bridge deck DYNA model

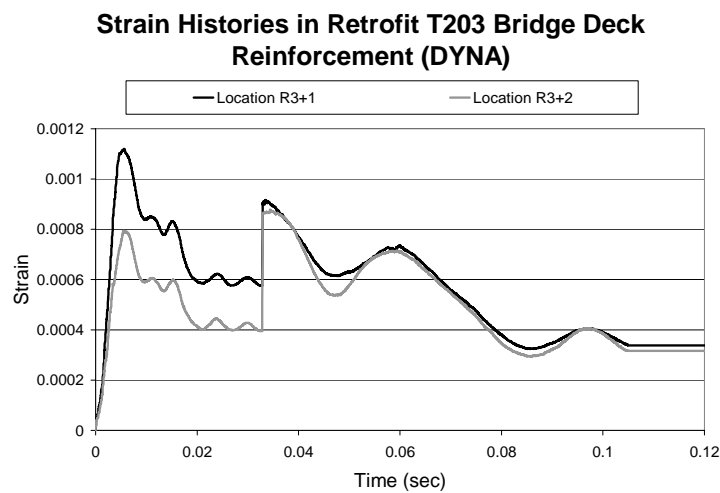


Figure B.14. Strain histories in row R3 of retrofit T203 bridge deck DYNA model

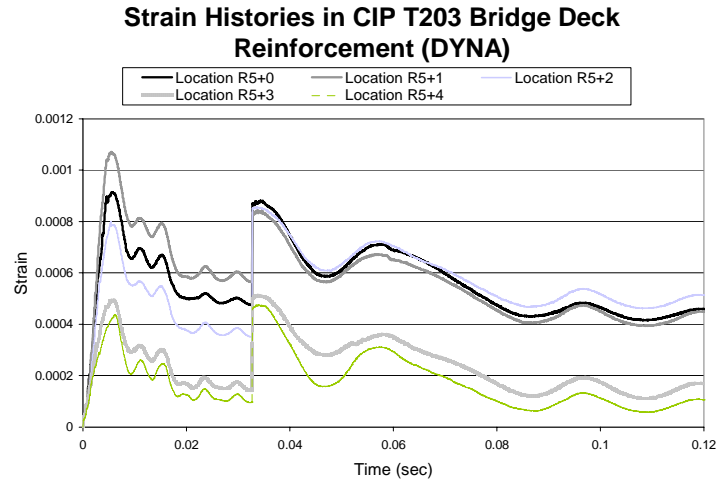


Figure B.15. Strain histories in row R5 of retrofit T203 bridge deck DYNA model

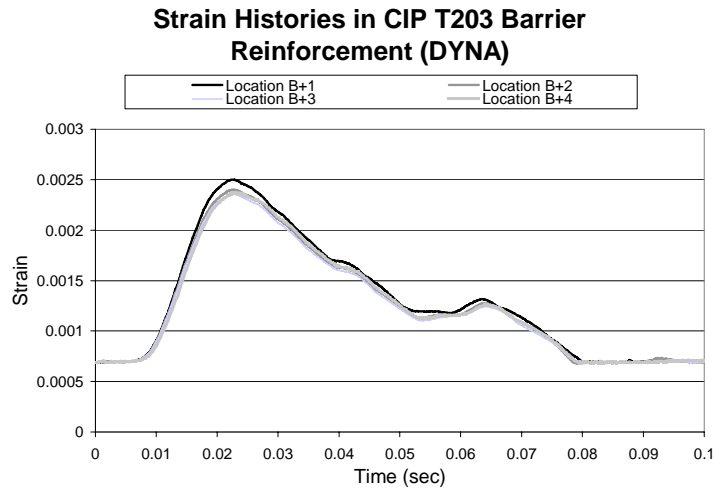


Figure B.16. Strain histories in row B of retrofit T203 bridge barrier DYNA model

Appendix C: Estimated Capacities of Retrofit Barriers

C.1. Capacity Estimation of Standalone Retrofit T203 Barrier with Undercut Anchors

Anchor breakout from bridge deck governs retrofit T203 barrier capacity with undercut anchors. Hence ACI 318-05 Appendix D calculations were used to estimate the capacity of the stand-alone T203 barrier with undercut anchors.

Breakout capacity (P kips) is calculated in terms of the horizontal force applied at a height of 21 in. from the base of the barrier.

Number of anchors = 8

Spacing of anchors = 6 in.

t = thickness of slab = 8 in.

s = distance between first and last anchor = 42 in.

$h_{ef} = 6.5$ in.

$f_c' = 4000$ psi

Concrete Breakout Strength of Anchors in Tension

$$N_b = k_c \sqrt{f_c'} h_{ef}^{1.5} \quad (C-1)$$

$k_c = 17$ (for post-installed anchors)

$$N_b = 17800 \text{ lbs} = 17.8 \text{ kips}$$

$$N_{cbg} = (A_{NC} \div A_{NCO}) \psi_{ec,N} \psi_{ed,N} \psi_{c,N} \psi_{cp,N} N_b \quad (C-2)$$

$$A_{NCO} = 9 h_{ef}^2 \quad (C-3)$$

$$= 380.25 \text{ in.}^2$$

$$A_{NC} = [c_{a1} + 1.5(h_{ef})][3((h_{ef}) + s)] \quad (C-4)$$

$$c_{a1} = 7 \text{ in.}$$

$$A_{NC} = 1030.125 \text{ in.}^2$$

$$\psi_{ec,N} = \psi_{c,N} = \psi_{cp,N} = 1$$

$$\psi_{ed,N} = 0.7 + (0.3 c_{a1} \div (1.5 h_{ef})) = 0.9 \quad (C-5)$$

Using equation C-2,

$$N_{cbg} = 43400 \text{ lbs} = 43.4 \text{ kips}$$

Hence, $N_n = 43.4$ kips

Concrete Breakout Strength of Anchors in Shear

$$V_b = 8(l_e \div d_o)^{0.2} \sqrt{d_o} \sqrt{f_c'} c_{al}^{1.5} \quad (C-6)$$

$$l_e = \text{least of } (h_{ef} \text{ and } 8 d_o) \quad (C-7)$$

$$l_e = 6 \text{ in.}$$

$$V_b = 12300 \text{ lbs} = 12.3 \text{ kips}$$

$$V_{cbg} = (A_{VC} \div A_{VCO}) \psi_{ec,V} \psi_{ed,V} \psi_{c,V} V_b \quad (C-8)$$

$$\psi_{ec,V} = \psi_{ed,V} = 1$$

$$\psi_{c,V} = 1.2$$

$$A_{VC} = 4.5 c_{al}^2 \quad (C-9)$$

$$= 220.5 \text{ in.}^2$$

$$A_{VCO} = [s + 1.5(h_{ef})][t] \quad (C-10)$$

$$= 414 \text{ in.}^2$$

Using equation (C-8)

$$V_{cbg} = 27700 \text{ lbs} = 27.7 \text{ kips}$$

$$\text{Hence, } V_n = 27.7 \text{ kips}$$

Relation between Applied Forces

V = Applied shear force to anchors

$$= P$$

M = Moment at base of barrier due to applied force = $21P$ kip-in.

$$\approx 0.9(N)d$$

N = Applied tensile force to anchors

d = effective depth of retrofit T203 barrier = 5.5 in.

Hence,

$$N = 4.25P$$

Barrier Capacity using Shear and Tensile Force Interaction

$$(N \div N_n) + (V \div V_n) \leq 1.2 \quad (C-12)$$

To find maximum force the barrier can withstand

$$(N \div N_n) + (V \div V_n) = 1.2$$

$$(4.25P \div 43.4) + (P \div 27.7) = 1.2$$

Solving we get

$$P \approx 8 \text{ kips}$$

This is the 5% fractile strength

P_{cap} = Mean breakout strength

$$= 1.4 P$$

Hence,

$$\underline{P_{cap} = 11 \text{ kips}}$$

C.2. Capacity Estimate of Standalone Retrofit T203 Barrier with Through Anchors (Bottom Plate)

Anchor breakout from bridge deck governs retrofit T203 barrier capacity with through-anchor configuration. Hence ACI 318-05 Appendix D calculations were used to estimate the capacity of the stand-alone T203 barrier with through-anchor configuration.

Breakout capacity (P kips) is calculated in terms of the horizontal force applied at a height of 21 in. from the base of the barrier.

Size of bottom plate = 50 in. \times 6 in. \times 0.75 in.

Hence here $s = 50$ in. and

$b = 6$ in.

$h_{ef} = 8$ in.

$f_c' = 4000$ psi

Concrete Breakout Strength of Anchors in Tension

$$N_b = k_c \sqrt{f_c'} h_{ef}^{1.5}$$

$k_c = 17$ (for post-installed anchors)

$$N_b = 24300 \text{ lbs} = 24.3 \text{ kips}$$

$$N_{cbg} = (A_{NC} \div A_{NCO}) \psi_{ec,N} \psi_{ed,N} \psi_{c,N} \psi_{cp,N} N_b$$

$$A_{NCO} = 9 h_{ef}^2$$

$$= 576 \text{ in.}^2$$

$$A_{NC} = [c_{al} + 0.5b + 1.5(h_{ef})][3((h_{ef}) + s)] \text{ (C-11)}$$

$$c_{al} = 7 \text{ in.}$$

$$A_{NC} = 2516 \text{ in.}^2$$

$$\psi_{ec,N} = \psi_{c,N} = \psi_{cp,N} = 1 \text{ (give reason)}$$

$$\psi_{ed,N} = 0.7 + (0.3 c_{al} \div (1.5 h_{ef})) = 0.875$$

Using equation B-2,

$$N_{cbg} = 92900 \text{ lbs} = 92.9 \text{ kips}$$

Hence, $N_n = 92.9$ kips

Concrete Breakout Strength of Anchors in Shear

$$V_b = 8(l_e \div d_o)^{0.2} \sqrt{d_o} \sqrt{f_c'} c_{al}^{1.5}$$

$l_e = \text{least of } (h_{ef} \text{ and } 8 d_o)$

$$l_e = 6 \text{ in.}$$

$$V_b = 12300 \text{ lbs} = 12.3 \text{ kips}$$

$$V_{cbg} = (A_{VC} \div A_{VCO}) \psi_{ec,V} \psi_{ed,V} \psi_{c,V} V_b$$

$$\psi_{ec,V} = \psi_{ed,V} = 1 \text{ (give reason)}$$

$$\psi_{c,V} = 1.2 \text{ (give reason)}$$

$$A_{VC} = 4.5 c_{al}^2$$

$$= 220.5 \text{ in.}^2$$

$$A_{VCO} = [s + 1.5(h_{ef})][t]$$

$$= 592 \text{ in.}^2$$

Using equation (B-8)

$$V_{cbg} = 39600 \text{ lbs} = 39.6 \text{ kips}$$

Hence, $V_n = 39.6$ kips

Relation between Applied Forces

V = Applied shear force to anchors

= P

M = Moment at base of barrier due to applied force = $21P$ kip-in.

$\approx 0.9(N)d$

N = Applied tensile force to anchors

d = effective depth of retrofit T203 barrier = 5.5 in.

Hence,

$N = 4.25P$

Barrier Capacity using Shear and Tensile Force Interaction

$(N \div N_n) + (V \div V_n) \leq 1.2$

To find maximum force the barrier can withstand

$(N \div N_n) + (V \div V_n) = 1.2$

$(4.25P \div 92.9) + (P \div 39.6) = 1.2$

Solving we get

$P \approx 17$ kips

This is the 5% fractile strength

P_{cap} = Mean breakout strength

= $1.4 P$

Hence,

$P_{cap} = 24$ kips

C.3. Capacity Estimate of 5-ft. Section of Retrofit T501 Barrier with Undercut Anchors

Anchor breakout from bridge deck governs retrofit T501 barrier capacity with undercut configuration. Hence ACI 318-05 Appendix D calculations were used to estimate the capacity of the 5-ft. section T501 barrier with undercut anchors.

Breakout capacity (P kips) is calculated in terms of the horizontal force applied at a height of 21 in. from the base of the barrier.

Number of anchors = 7

Spacing of anchors = 8 in.

s = distance between first and last anchor = 49 in.

$f'_c = 4000$ psi

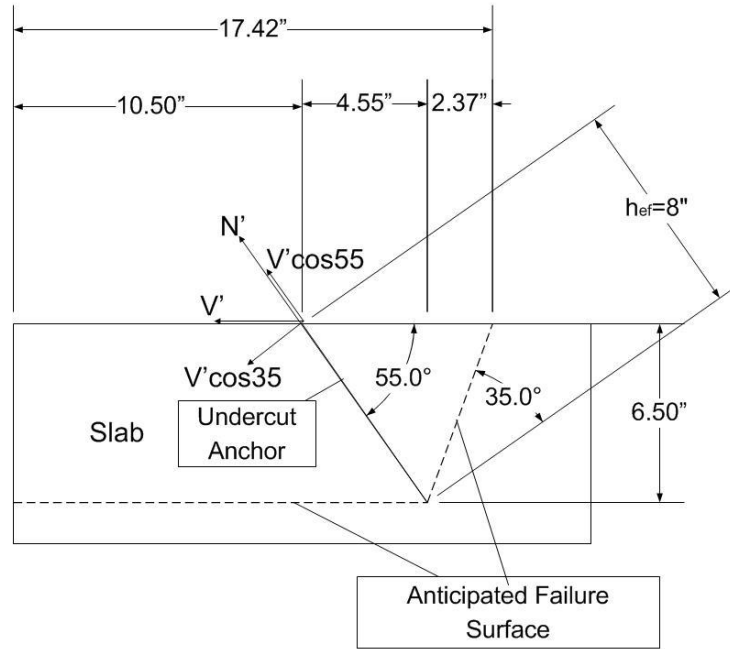


Figure C1. Forces in undercut anchors of retrofit T501 barrier and bridge deck and their anticipated failure surface

As seen in Figure C.1,

$$h_{ef} = 8 \text{ in.}$$

$$b' = 17.43 \text{ in.}$$

Concrete Breakout Strength of Anchors in Tension

$$N_b = k_c \sqrt{f_c'} h_{ef}^{1.5}$$

$$k_c = 17 \text{ (for post-installed anchors)}$$

$$N_b = 25 \text{ kips}$$

$$N_{cbg} = (A_{NC} \div A_{NCO}) \psi_{ec,N} \psi_{ed,N} \psi_{c,N} \psi_{cp,N} N_b$$

$$A_{NCO} = 9 h_{ef}^2$$

$$= 576 \text{ in.}^2$$

$$A_{NC} = [b'] [3(h_{ef} + s)] \text{ (B-12)}$$

$$A_{NC} = 1434.25 \text{ in.}^2$$

$$\psi_{ec,N} = \psi_{ed,N} = \psi_{cp,N} = 1$$

$$\psi_{c,N} = 1.3$$

Using equation B-2,

$$N_{cbg} = 81.5 \text{ kips}$$

$$\text{Hence, } N_n = 81.5 \text{ kips}$$

Relation between Applied Forces

V = Applied shear force to anchors

N = Applied tensile force to anchors

$$V' = P$$

M = Moment at base of barrier due to applied force = 26P kip-in.

$$\approx 0.9(N')d$$

d = effective depth of retrofit T203 barrier = 10.5 in.

Hence,

$$N' = 3.36P$$

$$V = V'(\cos 35) = 0.82P$$

$$N = N' + V'(\cos 55) = 3.94P$$

Barrier Capacity

$$(V \div N) = 0.208 \approx 0.2$$

Hence shear breakout does not govern.

$$N = N_n$$

$$3.94P = 81.25$$

$$P \approx 21 \text{ kips}$$

This is the 5% fractile strength

$$P_{cap} = \text{Mean breakout strength}$$

$$= 1.4 P$$

Hence,

$$\underline{P_{cap} = 30 \text{ kips}}$$

Appendix D: Concrete Breakout Capacity of Retrofit T501 Barrier (Yang)

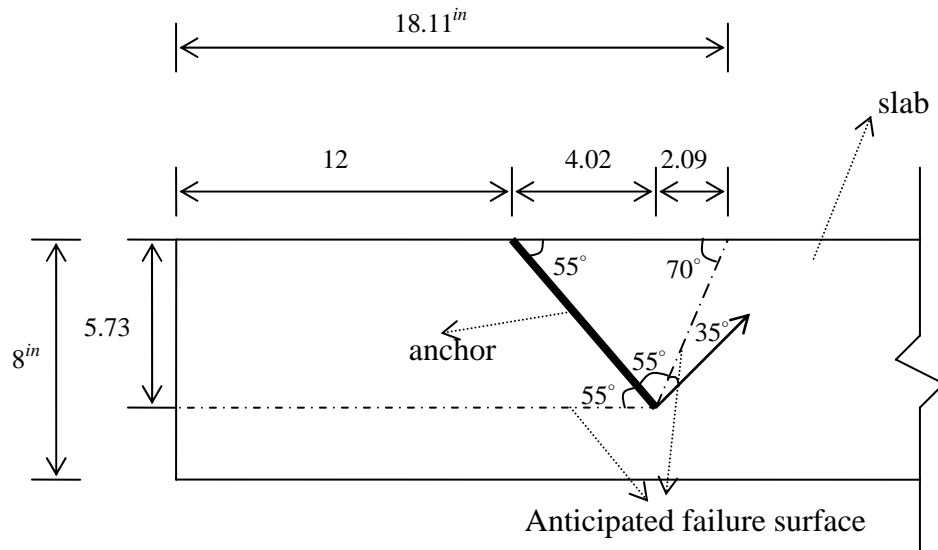


Figure D.1. Geometric configuration of inclined anchors used in T501 retrofit specimens

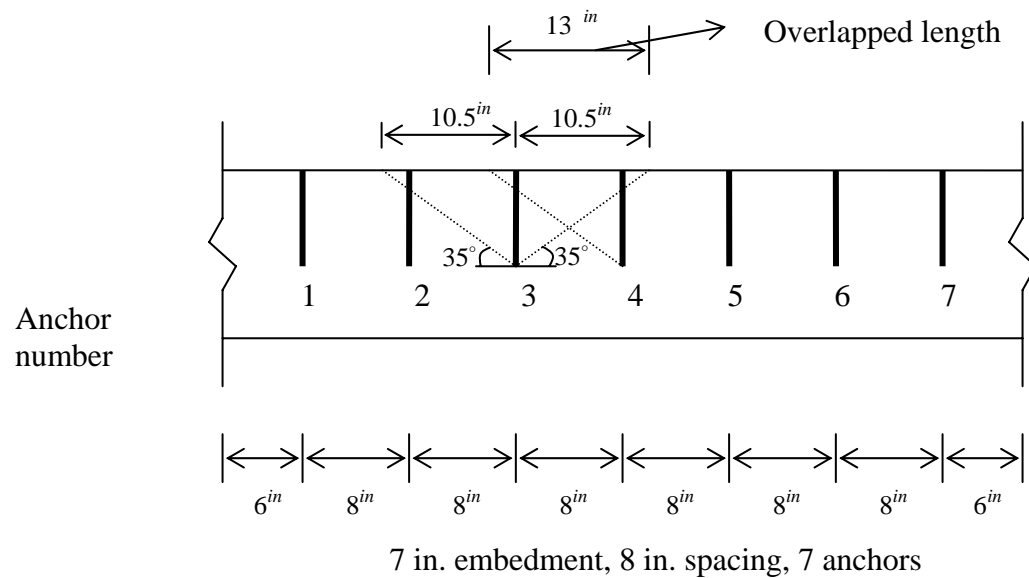


Figure D.2. Geometry of projected breakout areas by ACI 318-05 Appendix D for Retrofit T501 Specimen 1 (7 anchors)

The geometric configuration of the inclined anchors of the retrofit T501 specimens is presented in 0. In 0 is shown the geometry of projected breakout areas used to calculate the

combined breakout capacity of the 7 anchors used in Retrofit T501 Specimen 1, according to the provisions of ACI 318-05 Appendix D. Static breakout capacity is calculated assuming uncracked concrete; the resulting nominal capacity (a 5% fractile value) is multiplied by 1.4 to obtain the probable mean static capacity; and that value is multiplied by 1.2 to obtain the probable mean dynamic capacity.

For calculations for concrete breakout capacity by ACI 318-05 Appendix D for Retrofit T501 Specimens, the following parameters are defined symbolically.

Anchor spacing: S_a

Distance from first to last anchor: L_a

Concrete compressive strength: f_c'

Effective embedment depth of anchor: h_{ef}

Width of the pyramid base: b

Coefficient for basic concrete breakout strength in tension: k_c

Basic concrete breakout strength in tension of a single anchor in cracked concrete: N_b

Projected concrete failure area of a single anchor: A_{NCO}

Projected concrete failure area of group of anchors: A_{NC}

Factor used to modify tensile strength of anchors based on eccentricity of applied loads: $\Psi_{ec,N}$

Factor used to modify tensile strength of anchors based on proximity to edges of concrete member: $\Psi_{ed,N}$

Factor used to modify tensile strength of anchors based on presence or absence of cracks in concrete: $\Psi_{c,N}$

Factor used to modify tensile strength of post-installed anchors intended for use in uncracked concrete without supplementary reinforcement: $\Psi_{cp,N}$

Nominal concrete breakout strength in tension of a group of anchors: N_{cbg}

Calculations of the concrete breakout capacity by ACI 318-05 Appendix D for Retrofit T501 Specimen 1 (7 anchors) are carried out in the following way.

$$S_a = 8 \text{ (in)}$$

$$L_a = 48 \text{ (in)}$$

$$f_c' = 4000 \text{ (psi)}$$

$$h_{ef} = 7 \text{ (in)}$$

$$b = 18.01 \text{ (in)}$$

$$k_c = 17$$

$$N_b = 19.91 \text{ (kips)}$$

$$A_{NCO} = 441 \text{ (in}^2\text{)}$$

$$A_{NC} = 1249.04 \text{ (in}^2\text{)}$$

$$\Psi_{ec,N} = 1$$

$$\Psi_{ed,N} = 1$$

$$\Psi_{c,N} = 1.4$$

$$\Psi_{cp,N} = 0.686$$

$$N_{cbg} = 54.1 \text{ (kips)}$$

Dynamic mean breakout strength = $1.4 * 1.2 * 54.1 \text{ (kips)} = 90.89 \text{ (kips)}$

The predicted mean breakout capacity of the 7-anchor group is 90.89 kips.

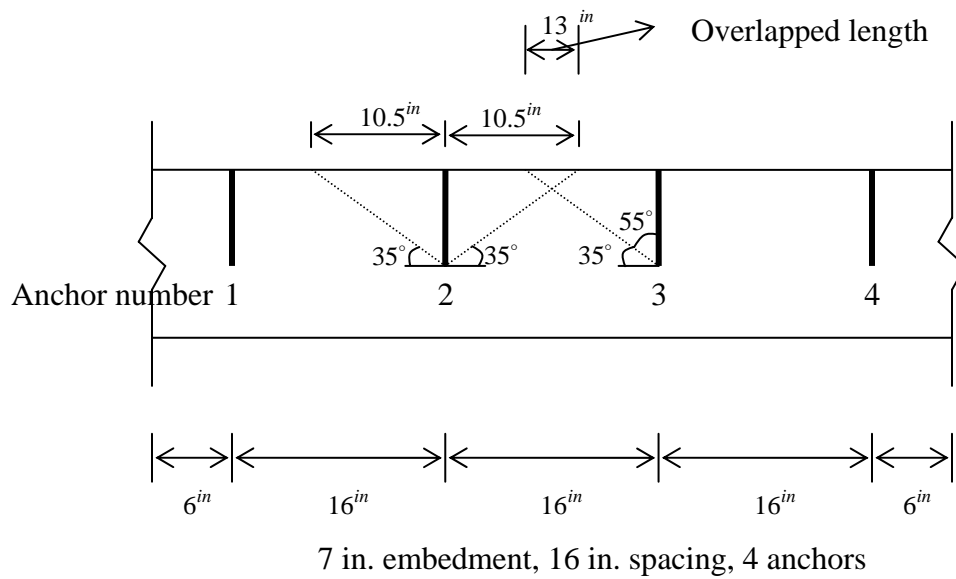


Figure D.3. Geometry of projected breakout areas by ACI 318-05 Appendix D for Retrofit T501 Specimen 2 (4 anchors)

In 0 is shown the geometry of projected breakout areas used to calculate the combined breakout capacity of the 7 anchors used in Retrofit T501 Specimen 2, according to the provisions of ACI 318-05 Appendix D. Static breakout capacity is calculated assuming uncracked concrete; the resulting nominal capacity (a 5% fractile value) is multiplied by 1.4 to obtain the probable mean static capacity; and that value is multiplied by 1.2 to obtain the probable mean dynamic capacity.

Calculations of the concrete breakout capacity by ACI 318-05 Appendix D for Retrofit T501 Specimen 1 (4 anchors) are carried out in the following way.

$$\begin{aligned}
S_a &= 8 \text{ (in)} \\
L_a &= 48 \text{ (in)} \\
f_c' &= 4000 \text{ (psi)} \\
h_{ef} &= 7 \text{ (in)} \\
b &= 18.01 \text{ (in)} \\
k_c &= 17 \\
N_b &= 19.91 \text{ (kips)} \\
A_{NCO} &= 441 \text{ (in}^2\text{)} \\
A_{NC} &= 1249.04 \text{ (in}^2\text{)} \\
\Psi_{ec,N} &= 1 \\
\Psi_{ed,N} &= 1 \\
\Psi_{c,N} &= 1.4 \\
\Psi_{cp,N} &= 0.686 \\
N_{cbg} &= 54.1 \text{ (kips)}
\end{aligned}$$

$$\text{Dynamic mean breakout strength} = 1.4 * 1.2 * 54.1 \text{ (kips)} = 90.89 \text{ (kips)}$$

Because the projected areas of the 4-anchor group overlap, their total projected area is the same as for the 7-anchor group, and the predicted mean breakout capacity of the 4-anchor group is also the same, 90.89 kips.

Appendix E: Conversions from Standalone to Continuous Barrier Models

E.1. SAP Analysis—TTI Static Test on Cast-in-place T203 Barrier System

The SAP model given in Figure E.1 was used to find the static force distribution between stand-alone T203 barrier and beams providing continuity. Elastic static analysis was used.

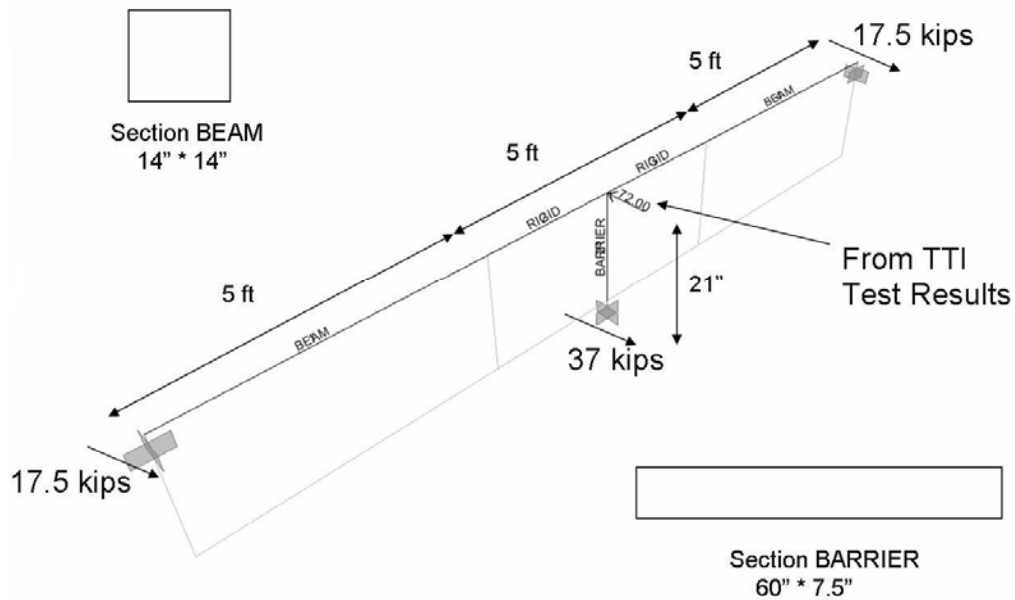


Figure E.1. Details of SAP analysis on cast-in-place T203 barrier system using TTI static test results

Results of Force Distribution:

$$P = 72 \text{ kips}$$

$$P_{\text{standalone}} = 37 \text{ kips}$$

$$P_{\text{continuity}} = 72 - 37 = 35 \text{ kips}$$

E.2. SAP Analysis—TTI Dynamic Test on Cast-in-Place T203 Barrier System

The SAP model given in Figure E.2. was used to find the dynamic force distribution between stand-alone T203 barrier and beams providing continuity. Elastic time-history analysis was used.

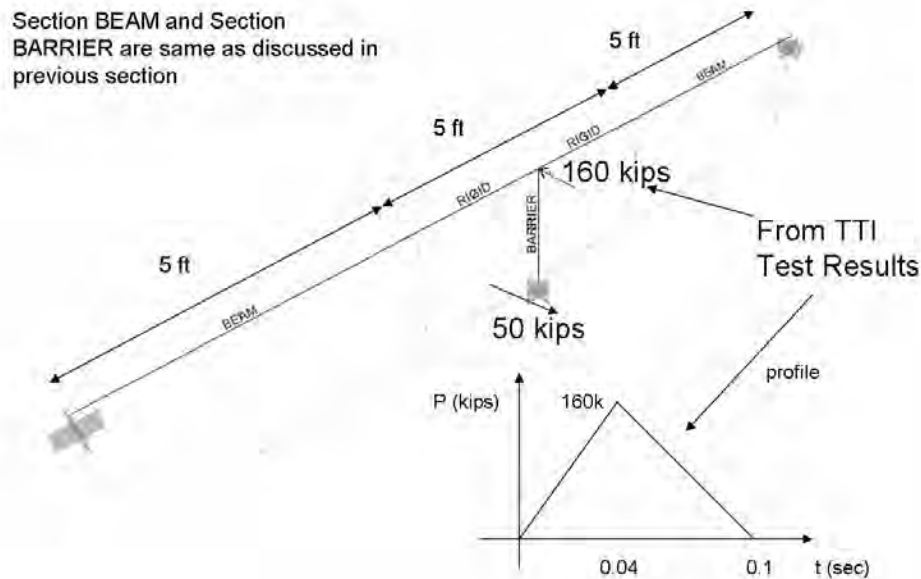


Figure E.2. Details of SAP analysis on cast-in-place T203 barrier system using TTI dynamic test results

The impulse, peak force and duration of impact of the profile shown in Figure E.2 are the same as the force-time profile obtained from the cast-in-place T203 barrier system dynamic tests conducted at TTI.

Results of Force Distribution:

$$P = 160 \text{ kips}$$

$$P_{\text{standalone}} = 50 \text{ kips}$$

$$P_{\text{continuity}} = 160 - 50 = 110 \text{ kips}$$

The SAP model given in Figure E.3. was used to find the 50-msec dynamic force distribution between stand-alone T203 barrier and beams providing continuity. Elastic time-history analysis was used.

The impulse, peak force and duration of impact of the profile shown in Figure E.3. are the same as the 50-msec force-time profile obtained from the cast-in-place T203 barrier system dynamic tests conducted at TTI.

E.3. SAP Analysis—TTI Static Test on Cast-in-Place T501 Barrier System

The SAP model given in Figure E.4 was used to find the dynamic force distribution between 5 ft. section of the T501 barrier and the remaining barrier providing continuity. Elastic static analysis was used.

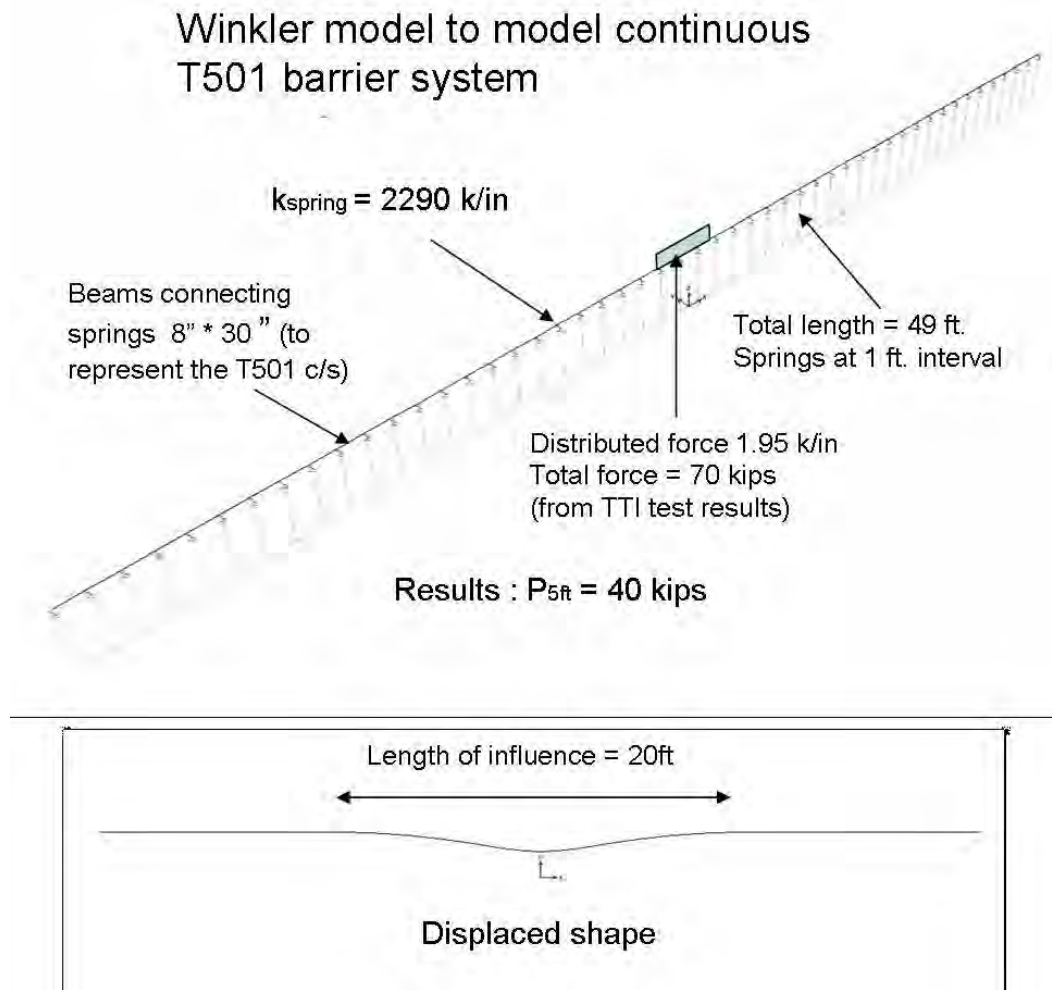


Figure E.4. Details of SAP analysis on cast-in-place T501 barrier system using TTI static test results

Appendix F: Continuous Barrier System Tested by TTI

F.1. TTI Continuous Barrier Systems

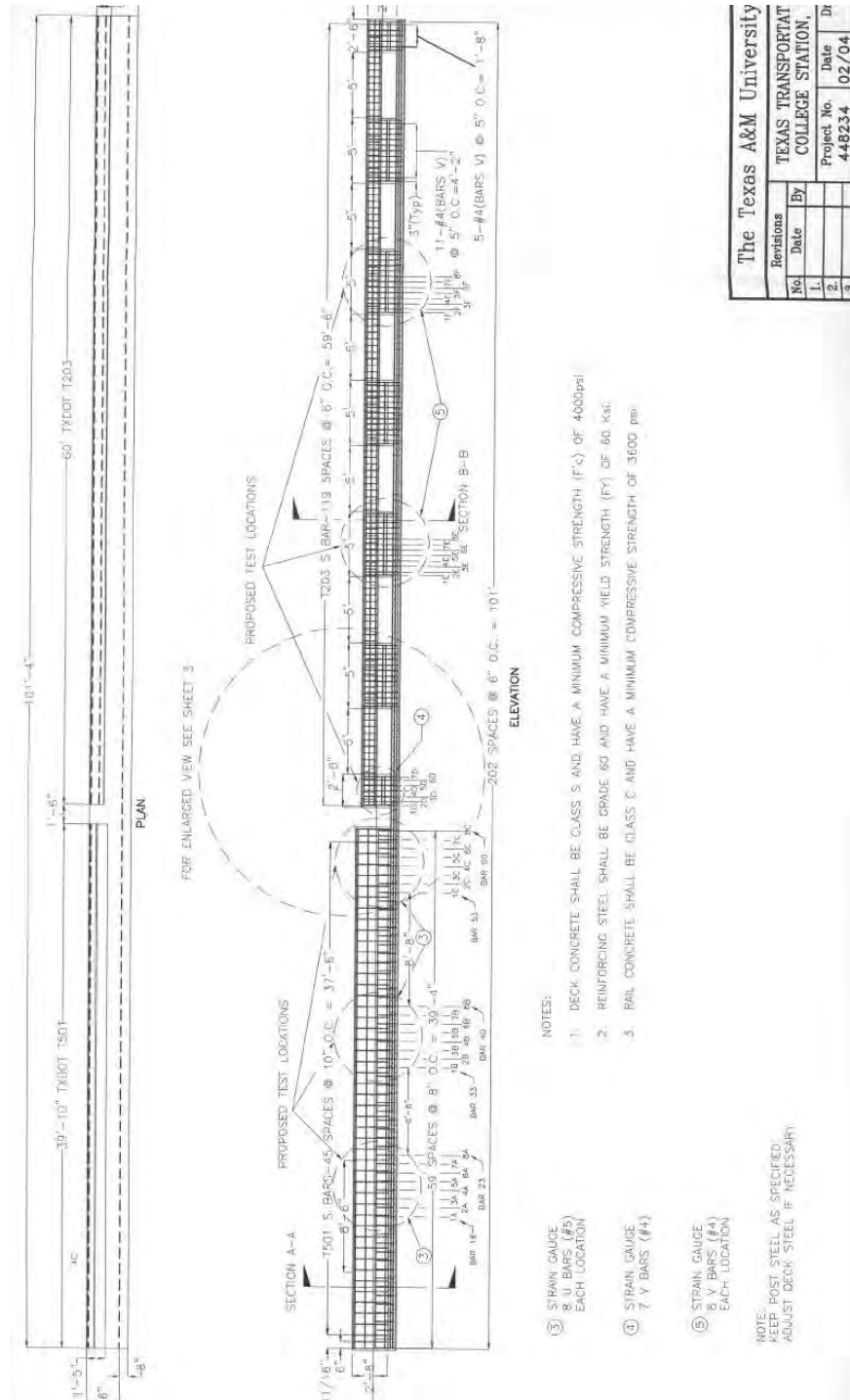


Figure F.1. TTI T501 and T203 barrier and bridge deck systems

Appendix G: Initial Studies on Modeling Barrier with ABAQUS

Modeling a barrier using ABAQUS is shown by this series of figures, originally prepared as a PowerPoint presentation by Picón.

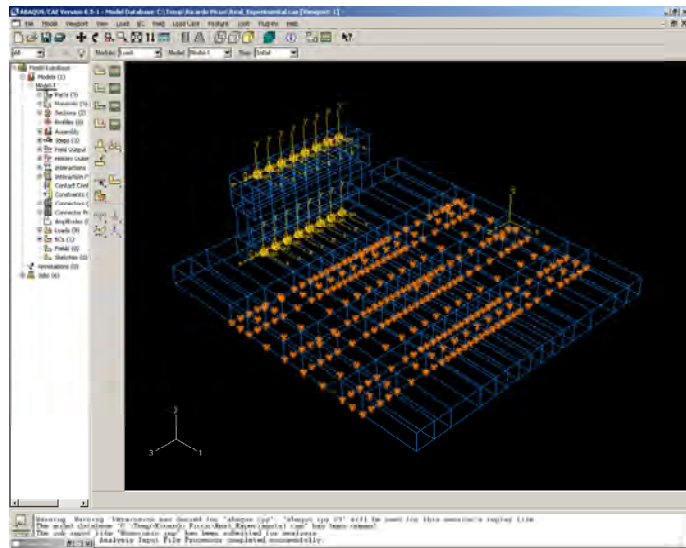
NUMERICAL SIMULATION OF DYNAMIC TEST ON TXDOT T203 BARRIER USING ABAQUS SOFTWARE

Boundary Conditions:

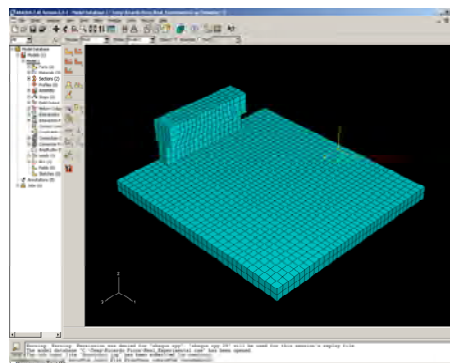
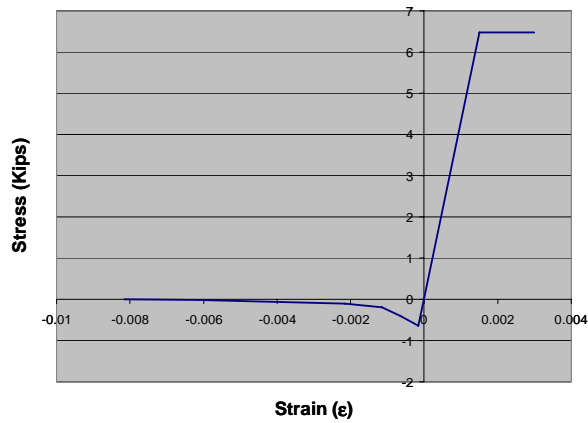
- Simple support on bottom of slab
- 12 connection points for tie-downs at top of slab

Connectors between the steel bars and the concrete elements:

- Zero-length hinges connecting ends of steel bars with the concrete (slab, barrier)



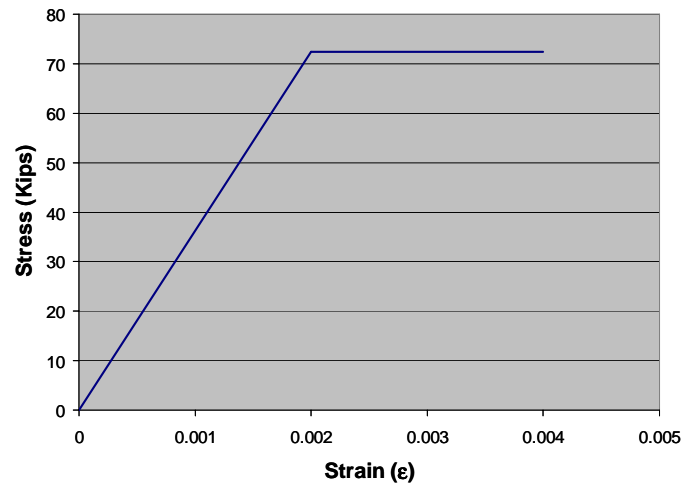
Inelastic Behavior of Concrete



```

**
** MATERIALS
**
*Material, name="Concreto sin Tension"
*Density
2.19e-04,
*Elastic
4.32e+06, 0.3
*Concrete Damaged Plasticity
0.5, 0.1, 1.16, 0.666, 0.1
*Concrete Compression Hardening
6480., 0.00
6480., 0.0015
*Concrete Tension Stiffening
648., 0.
400., 0.0005
200., 0.001
100., 0.002
20., 0.006
0., 0.008
**
**
    
```


Inelastic Behavior of Steel



**

*Material, name=Steel

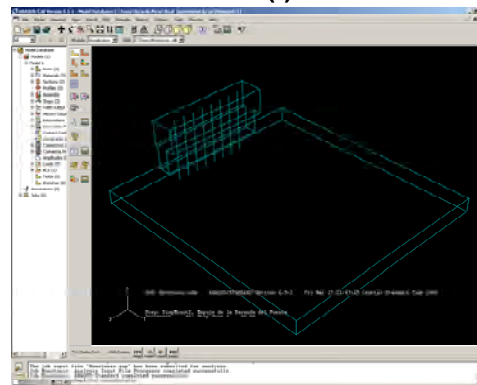
*Density
6.87e-04,

*Elastic
3.62e+07, 0.3

*Plastic
72400., 0.
72400., 0.02

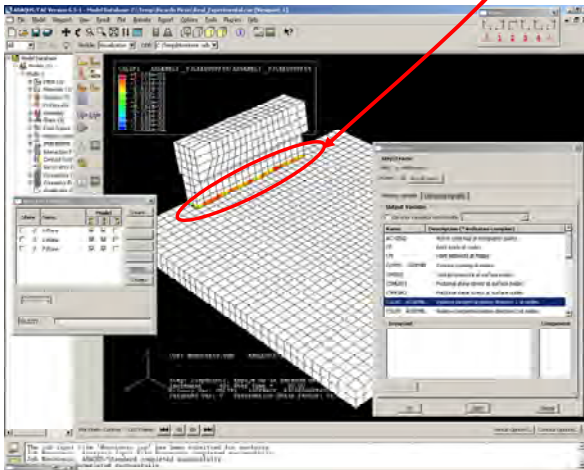
**

**



Contact Surface Behavior

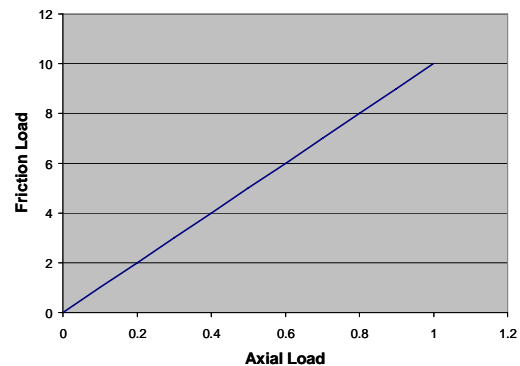
The friction coefficient was taken as 10 to reduce the sensitivity of the model to axial load, while permitting tensile separation at the interface between the barrier and the slab. This was established with a static check, and verified with dynamic checks.



```

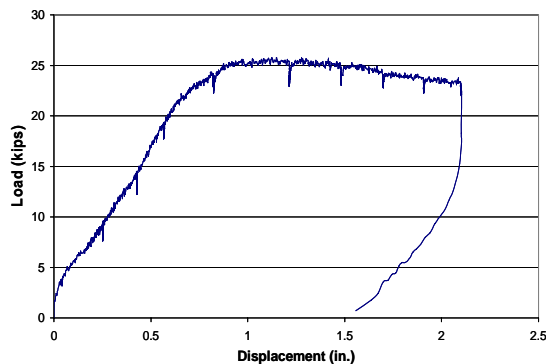
**
*Connector Behavior, name=ConnectRigid
*Connector Elasticity, rigid
1, 2, 3
**
** INTERACTION PROPERTIES
**
*Surface Interaction, name=Frictions
1.,
*Friction, slip tolerance=0.005
10.,
*Surface Behavior, pressure-overclosure=HARD
**

```

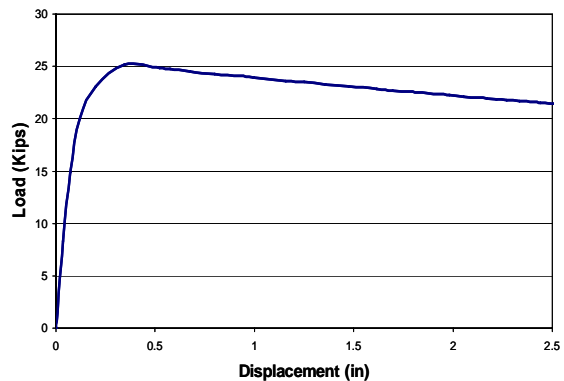


Validation of material parameters

Load vs. Displacement from Static Test of Retrofit T203 Barrier

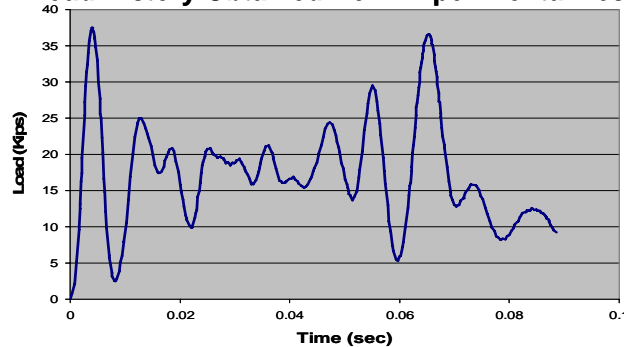


Monotonic Curve of ABAQUS Simulation

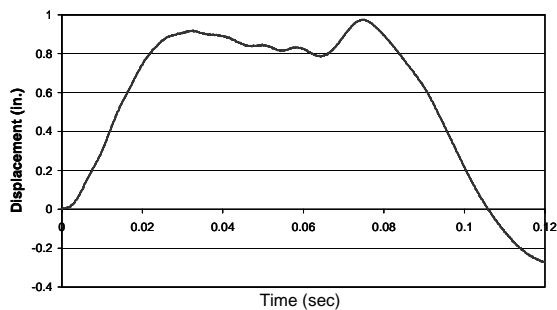


Numerical Simulation of Experimental Test using Impact Pendulum

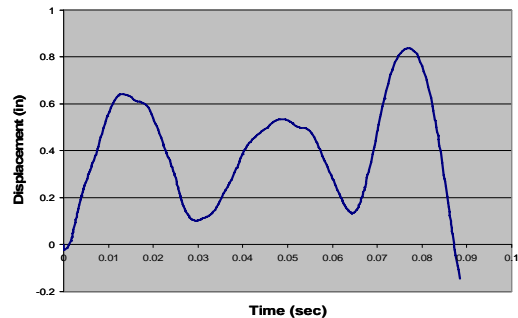
Load History Obtained from Experimental Test



Displacement vs. Time from Pendulum Impact Test on Retrofit T203 Barrier



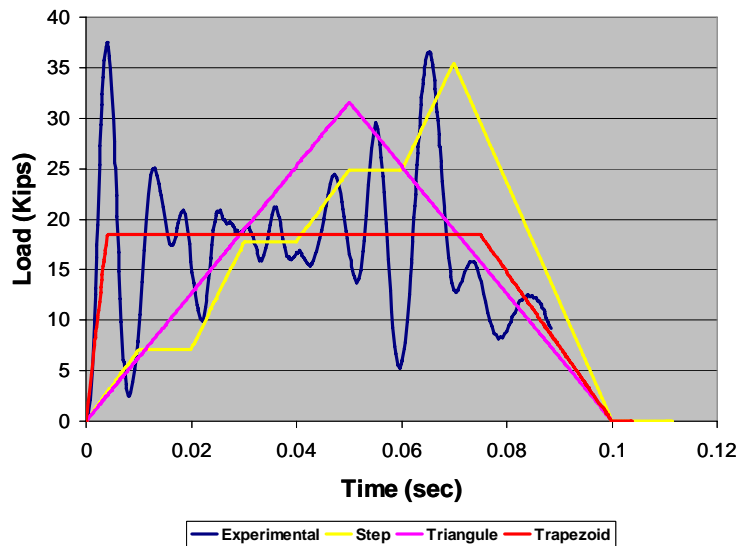
Displacement vs. Time from Numerical Simulation with ABAQUS



Input Data for ABAQUS

- A specialized program, DYNA, can be used to model the impact of a vehicle against a barrier directly. ABAQUS, in contrast, models the dynamic response of the barrier alone, and requires a history of load versus time.
- The input load history for ABAQUS can be either an experimentally determined history, or a history estimated using a known duration of impulse, known pendulum mass, and known pendulum velocity at impact.
- The following slides show the validation of an estimated loading history using an experimentally determined loading history, and demonstrate the general validity of an equivalent trapezoidal impulse with appropriate duration and area.

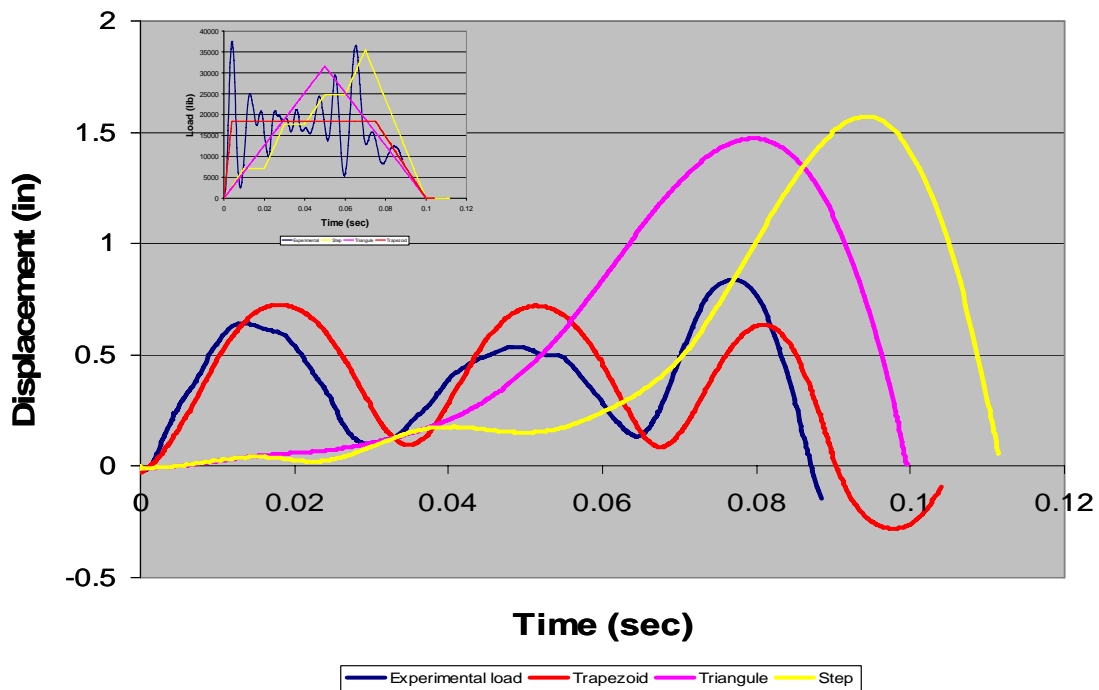
Comparison of experimentally determined load history with equivalent impulses of appropriate duration and different assumed shapes. This figure is repeated at the upper left-hand corner of the following slide.



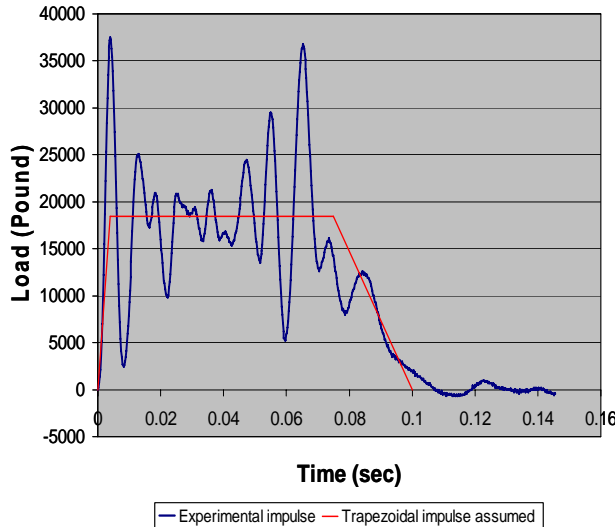
(Impulse) $I = \sum (\text{Force} \times \Delta \text{time})$

$$I_{\text{Exper}} = I_{\text{Trapez}} = I_{\text{triang}} = I_{\text{Step}}$$

The best equivalent impulse is a trapezoidal impulse, because the resulting displacement response (red curve) is closest to the displacement response from the experimentally determined history (blue curve)

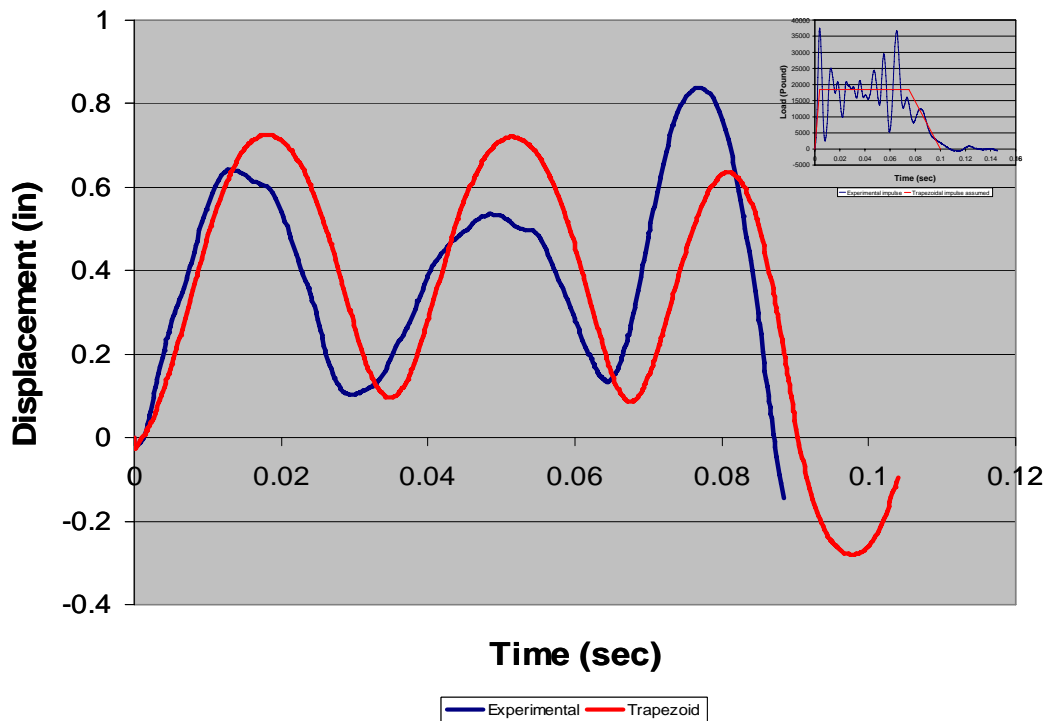


Rules for obtaining the equivalent trapezoidal impulse from an experimentally determined experimental impulse (repeated in the upper right-hand corner of the next slide)

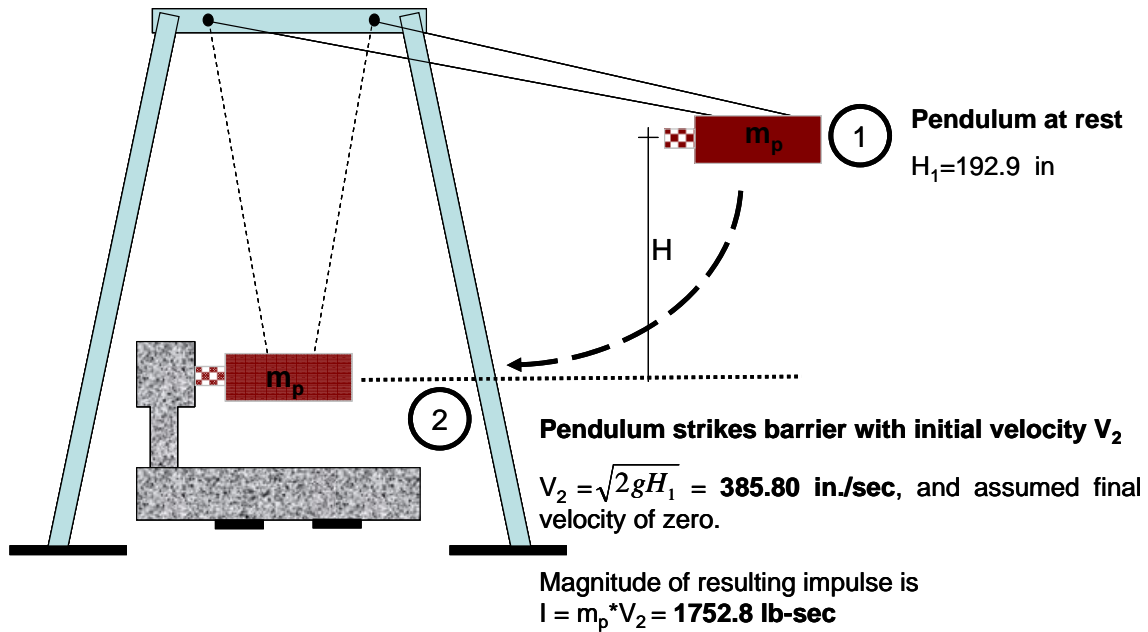


- Based on test results, the equivalent trapezoidal impulse is assigned a duration of 0.1 sec.
- The slope of the ascending portion is given by the initial stiffness of the system, and has a duration of 5% of the total duration of the impulse.
- The descending portion has a duration of 20% of the total duration, based on experimental results. This matches the experimental impulse well.
- Using this trapezoidal shape, the load level of the equivalent trapezoidal impulse is calculated. It is about half the maximum recorded experimental force, and quite close to the average value of that force.

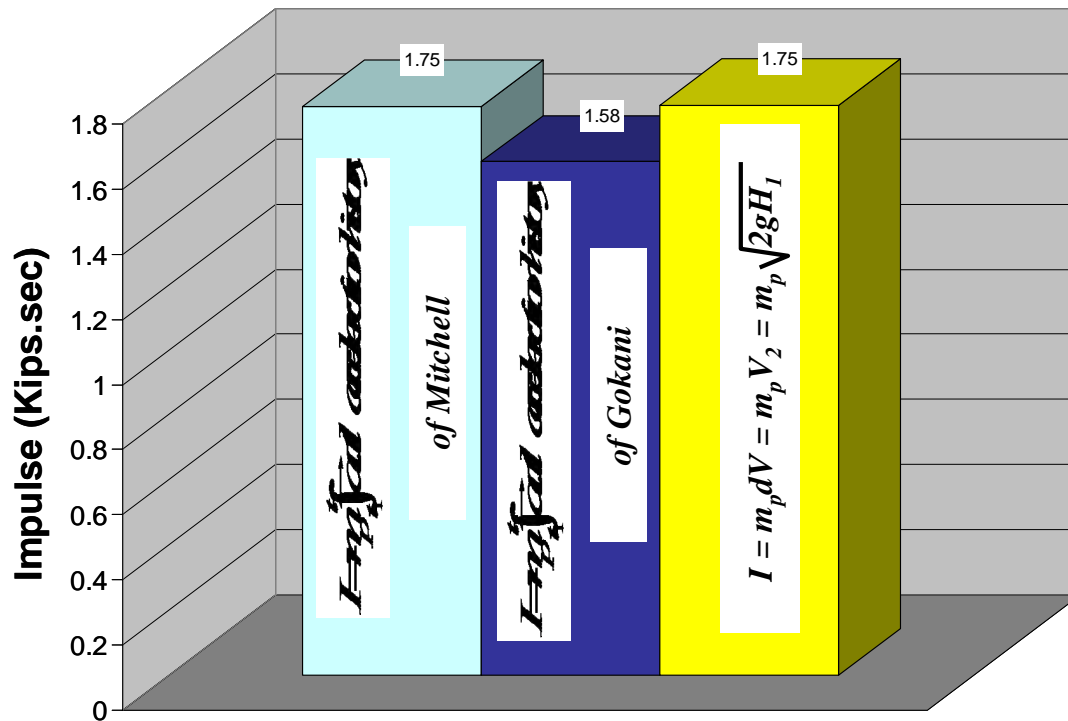
Similar displacement response from experimental and equivalent trapezoidal impulses



Calculate the equivalent impulse using an experimentally known duration of 0.1 sec, and a known pendulum mass and initial velocity of impact



Comparative Magnitudes of Impulses

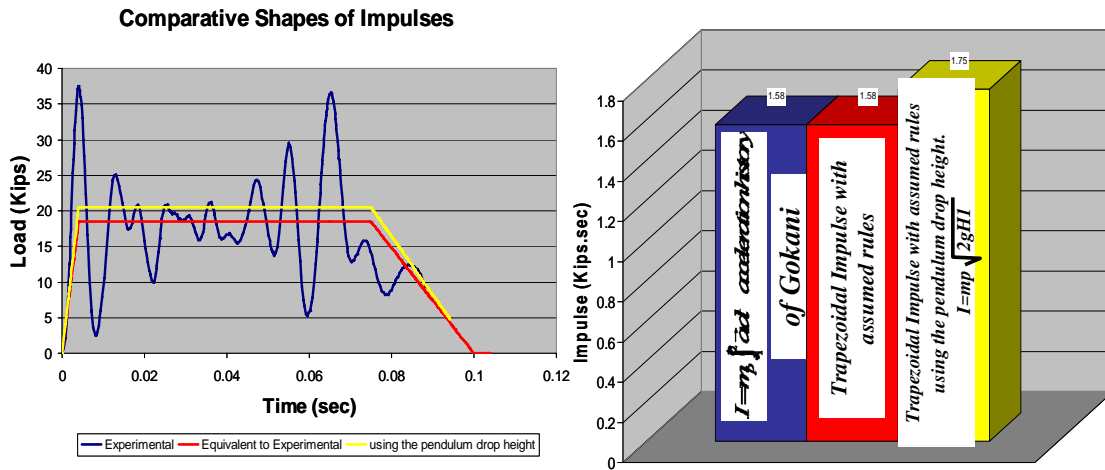


Why do all this?

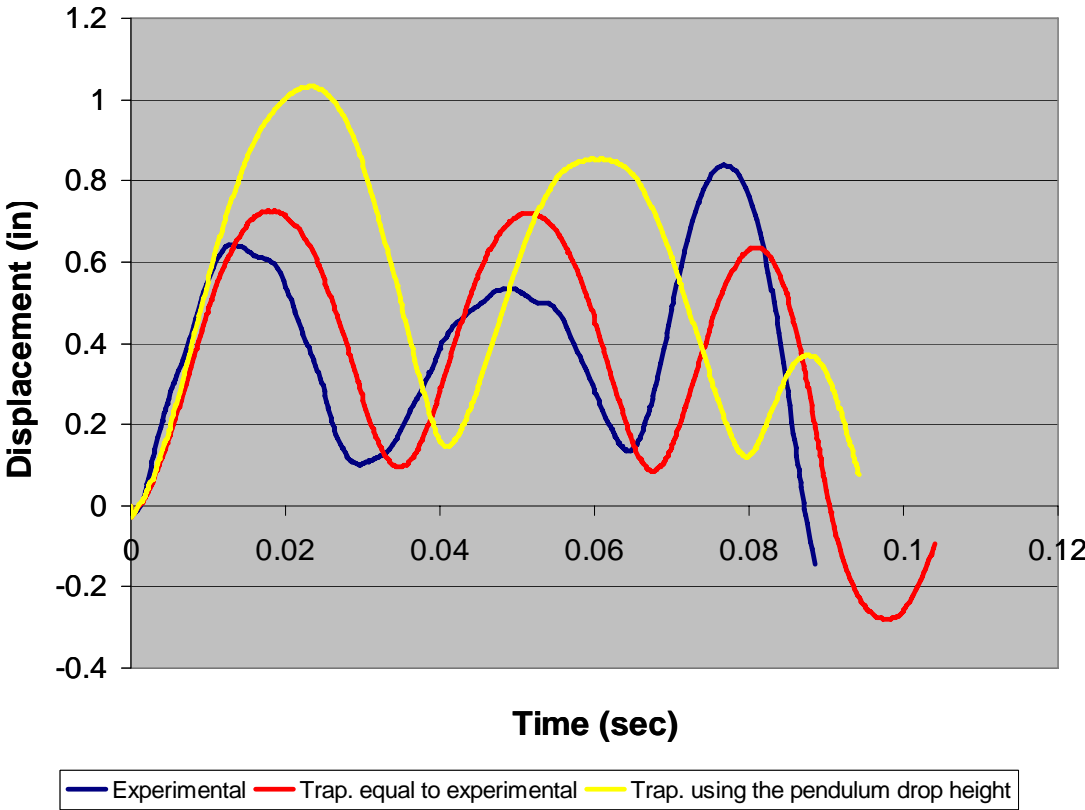
- It is possible to conduct fewer experimental tests and to obtain good results with numeric dynamic analysis using ABAQUS.
- Impact energy and initial impact velocity can be calculated using the pendulum drop height
- The magnitude of the impulse can be calculated assuming a final velocity of zero
- The corresponding history of impact force can be computed assuming a trapezoidal shape and an assumed typical impact duration of 0.1 sec.

Comparing the Magnitudes and Shapes of Impulses

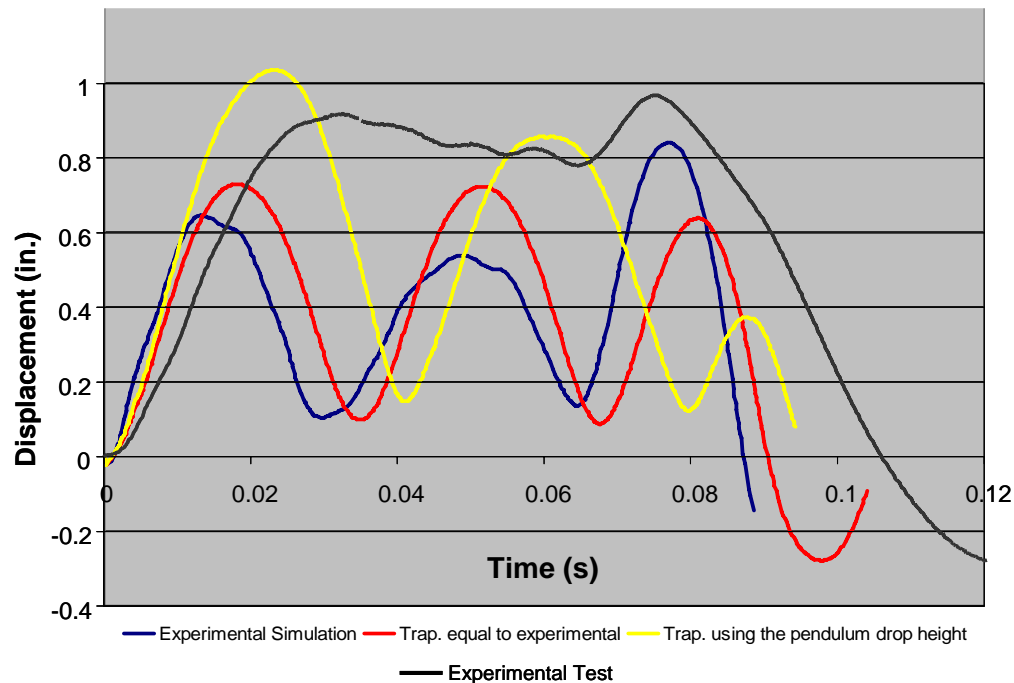
- Experimental Impulse.
- Trapezoidal Impulse equivalent to experimental with assumed rules.
- Trapezoidal Impulse using the pendulum drop height with assumed rules.



Comparative Displacement Responses from Different Impulses



Comparative Displacement vs. Time Responses from Pendulum Impact Test on Retrofit T203 Barrier



Conclusions and Recommendations

- The behavior of a vehicular barrier under impact can be reliably predicted using ABAQUS.
- The loading history required by ABAQUS can be approximated by an equivalent trapezoidal impulse of fixed shape and a duration of 0.1 sec, and whose magnitude is calculated from basic principles.
- Numerical simulations using ABAQUS are a useful and cost-effective complement to physical testing.